QUANTITATIVE INVESTIGATION OF THE MEMBRANE PROTEIN DEGRADATION MECHANISM BY MEMBRANE-INTEGRATED AAA PROTEASE FTSH UNDER NATIVE ENVIRONMENTS

By

Yiqing Yang

A DISSERTATION

Submitted to
Michigan state university
In partial fulfillment of the requirements
For the degree of

Chemistry—Doctor of philosophy

2019

ABSTRACT

QUANTITATIVE INVESTIGATION OF THE MEMBRANE PROTEIN DEGRADATION MECHANISM BY MEMBRANE-INTEGRATED AAA PROTEASE FTSH UNDER NATIVE ENVIRONMENTS

By

Yiqing Yang

Controlled degradation of misassembled and dispensable proteins is a crucial cellular process for maintaining the quality control of proteomes. In cells, one of the important carriers of this process is AAA+ (ATPases Associated with diverse cellular Activities) proteases, which mediate ATP-dependent proteolysis. The FtsH family proteins are the only membrane integrated AAA+ proteases, which critically contribute to membrane protein degradation. To investigate the mechanisms of membrane protein degradation mediated by FtsH, I successfully reconstituted the degradation process using FtsH of *E. coli* in a lipid bilayer environment (**Chapter 2**). I also developed a six-helical bundle intramembrane protease GlpG of *E. coli* into a model membrane substrate to study the quantitative relationship between folding and degradation (**Chapter 2**). I found that FtsH has a substantial ability to accelerate unfolding of membrane substrates up to 800 fold using ATP hydrolysis, and the intrinsic folding properties of the substrates such as local stability, spontaneous unfolding rates, and hydrophobicity also impact degradation rates. Finally, I quantified the total ATP cost that FtsH consumes to degrade membrane proteins (**Chapters 3** and **4**). To degrade membrane proteins, FtsH needs to overcome large energetic costs for unfolding substrates in the membranes and extracting them towards its protease domain located outside the membrane. I found that FtsH utilizes ATP hydrolysis in degrading membrane proteins with similar efficiency to other AAA+ proteases in degrading water-soluble substrates. This efficiency is achieved by

coupling multiple ATP hydrolysis events to degradation in a highly cooperative manner. These findings provide new insights into the physical principles of ATP-dependent degradation of membrane proteins, and the *in vitro* system developed will serve as a model for further refining the mechanisms of membrane protein degradation.

Dedicated to my beloved parents, Youyun Yang and Wenjing Chang.

ACKNOWLEDGEMENTS

I really enjoyed this journey of the past six years. I deeply thank everyone I have met. Professor Hong and my lab mates helped me so much, and I learned more than just about the experiments or the knowledge themselves. As I am writing down this page, I am experiencing the hardest moment in my life. I truly felt the love from everyone around me (special thanks to Zixuan Cang), and I could not thank more to express my sincere feelings. Every little help I received, I would carve them in my memory and wish to serve in return as much as I can.

Thank you all!

At last, I just want to share the poem ‘The Road Not Taken’ by Robert Frost here.

Two roads diverged in a yellow wood,
And sorry I could not travel both
And be one traveler, long I stood
And looked down one as far as I could
To where it bent in the undergrowth;

Then took the other, as just as fair,
And having perhaps the better claim,
Because it was grassy and wanted wear;
Though as for that the passing there
Had worn them really about the same,
And both that morning equally lay
In leaves no step had trodden black.
Oh, I kept the first for another day!
Yet knowing how way leads on to way,
I doubted if I should ever come back.

I shall be telling this with a sigh
Somewhere ages and ages hence:
Two roads diverged in a wood, and I—
I took the one less traveled by,
And that has made all the difference.

TABLE OF CONTENTS

LIST OF TABLES

LIST OF FIGURES

LIST OF ABBREVIATIONS

AAA+	ATPases Associated with diverse cellular Activities
ADEP	Acyldepsipeptide antibiotic
ATP	Adenosine Triphosphate
BME	β-mercaptoethanol
β -OG	n-octyl-β-D-glucoside
BSA	Bovine Serum Albumin
CHAPS	3-[(3-cholamidopropyl) dimethylammonio]-1-propanesulfonate
CHAPSO	3-[(3-cholamidopropyl) dimethylammonio]-2-hydroxy-1-propanesulfonate
CL	Cardiolipin
CP	Circular Permeated
DDM	n-dodecyl β-D-maltopyranoside
DGK	Diacyl Glycerol Kinase
DHFR	DiHydroxyFolate Reductase
DM	n-decyl β-D-maltopyranoside
DMPC	Dipalmitoylphosphatidylcholine
DMPG	1,2-Dimyristoyl-sn-glycero-3-phosphorylglycerol (sodium salt)
E. coli	*Escherichia coli*
EDTA	EthyleneDiamineTetraacetic Acid
EGFR	Epidermal Growth Factor Receptor
EM	Electron Microscopy
ER	Endoplasmic Reticulum
ERAD	Endoplasmic-Reticulum-Associated protein Degradation
GFP	Green Fluorescent Protein

HSP	Hereditary Spastic Paraplegia
IPTG	Isopropyl β-D-1-thiogalactopyranoside
LB media	Lysogeny Broth media
LDH	Lactate Dehydrogenase
LPS	Lipopolysaccharide
MBP	Maltose Binding Protein
MVB	MultiVesicular Bodies
NADH	Nicotinamide Adenine Dinucleotide Hydrogen
NP-40	Nonidet-40
Ni-NTA	Nickel-charged affinity resin (nitrilotriacetic acid)
PDB	Protein Data Bank
PEG	PolyEthylene Glycol
PEP	Phosphoenolpyruvic acid
PK	Pyruvate Kinase
PMSF	PhenylMethylSulfonyl Fluoride
SDS	Sodium Dodecyl Sulfate
SDS-PAGE	Sodium Dodecyl Sulfate -Polyacrylamide Gel Electrophoresis
SN	Staphylococcal Nuclease
SRH	Second Region Homology
TB media	Terrific Broth media
TCEP	Tris (2-carboxyethyl) phosphine
TEV	Tobacco Etch Virus
Tm	Melting Temperature
TM	Transmembrane
WT	Wild Type

Chapter 1 Introduction to membrane protein degradation

Membrane protein quality control

Cell membranes and membrane proteins

Our current understanding of cell membranes and membrane proteins is the legacy of a century's study that has concentrated on the membranes and their lipids and protein components. The cell membranes are permeability bilayer barriers separating a whole cell from the environment and various subcellular organelles from the cytosol (**Figure 1.1**).[1] The cell membranes are also not a static structure, but a dynamic entity undergoing cell division, the extension of neuronal arbors and vesicle trafficking.[2] Thus, the communications between membrane-encapsulated compartments through vesicle budding from donor compartments and fusion with others are elaborately regulated.[3]

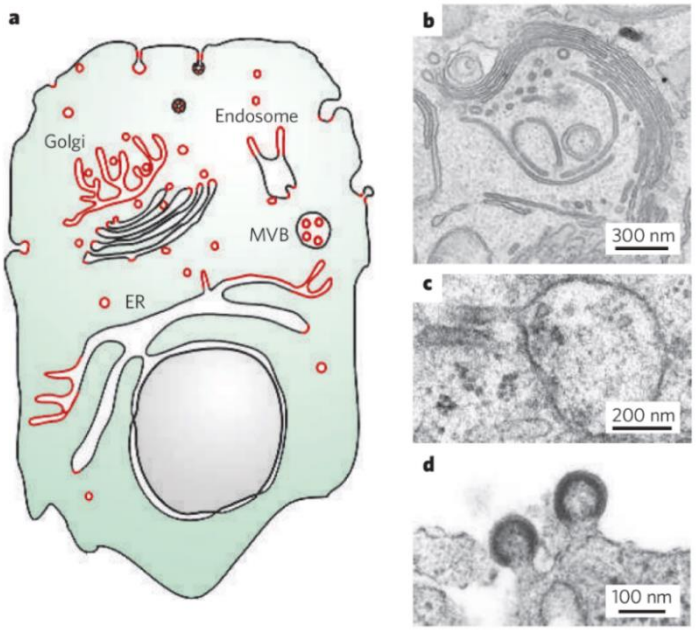

Figure 1.1 Cellular membranes visualized by electron microscopy.[1] a) A diagram of a eukaryotic cell; b) Golgi fenestrations; c) tubule on endosomes; d) HIV-1 viral budding.

The main components of cell membranes are phospholipids. The hydrophilic headgroups and two nonpolar fatty acid tails in lipid molecules allow them to

spontaneously form a double-layered lipid bilayer in aqueous solution.[4] Cell membranes also contain glycolipids and sterols, which regulates the fluidity of the membranes, cell signaling, and cell-cell communications.[5] Singer and Nicholson proposed the first molecular model of the cell membranes known as a 'fluid mosaic model' in 1972.[6] In the model, the lipids in cell membranes are free to diffuse in the plane of the fluidic bilayer leaflets, and the mosaic is also made of proteins that are inserted into the lipid bilayer.[7] Modern theories complete the model by including the concepts of the complex lipid dynamics caused by the formation of cholesterol- and sphingomyelin-rich lipid domains,[8] constant trafficking from and to the frontier,[9] and association of the cytoskeleton with the bilayer.[10, 11]

Proteins inserted in the cell membranes (i.e., membrane proteins, MPs) also occupy a substantial portion. In *E. coli*, they make up ~30% of the total membrane area fraction.[12] MPs have been observed only in two structural motifs in the membrane-spanning region: α-helix bundles and the β-barrels.[13] Compared to water-soluble proteins, MPs have similar general structural characteristics: (1) the traversing secondary structure elements of MPs are generally composed of 15-25 residues for α-helices and 10-12 residues for β-stands so that the 30 Å thick lipid bilayer hydrophobic core can be spanned;[13] (2) their amino acid distribution has a directionality in space along the membrane normal. For example, the positively charged arginine and lysine residues are more enriched in the cytoplasmic side rather than in the extracellular side, which is known as the 'positive-inside rule', and the positive residues are known to favorably interact with the negatively charged membranes stabilizing the topology of MPs;[14] (3) the water-bilayer interfacial regions are enriched with aromatic residues such as tyrosine and tryptophan in both sides.

These bulky residues possessing polar characters favorably interact with the lipid head groups through hydrogen bonds and π-cation interactions so that MPs can be stably anchored in the membrane.[15]

Constitutive MPs are assembled through a translocation/insertion process discovered by Blobel and Dobberstein.[16] During translation, nascent polypeptide chains from ribosomes, which possess an exposed signal sequence at the N-terminus, are targeted to the membrane-resident translocons, where the polypeptide chains are then inserted and released into the membrane depending on their hydrophobicity (**Figure 1.2**).[17] After this process, MPs fold in the membrane. Non-constitutive MPs spontaneously insert into the membrane from the aqueous phase.[18] They may exist as soluble forms in the aqueous phase, and bind to membranes then insert and fold.[19]

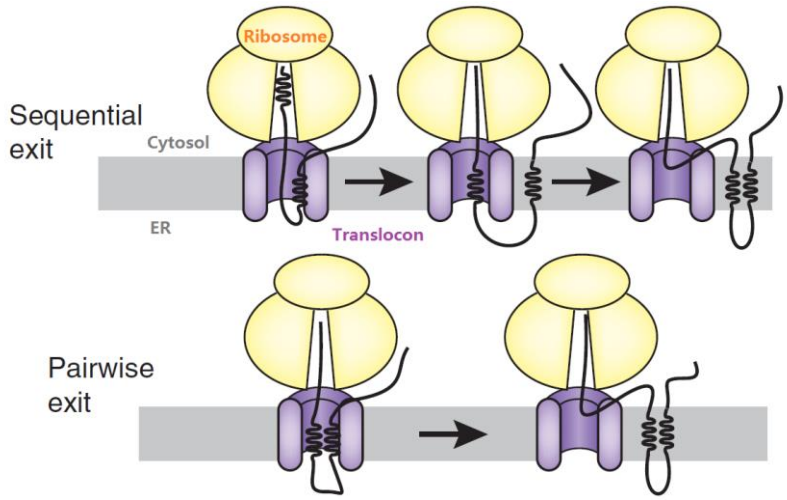

Figure 1.2 Membrane-integration mechanism of multi-spanning membrane proteins.[20] The transfer of transmembrane segments through a translocon may occur sequentially,[21] or pairwise.[22]

MPs carry out numerous critical functions such as transducing external stimuli into cellular signals by presenting antigens on the cell surface;[23] linking cells together;[24]

facilitating diffusion of specific ions and molecules;[25] catalyzing chemical reactions and transporting metabolites across the membranes against concentration gradients.[26]

The folding problem of membrane proteins

Protein folding is a fundamental molecular process in life. Proteins in the cell must correctly fold into their 3D structures for their biological functions. The native conformations of a majority of water-soluble proteins are known to be optimized at a free energy minimum structure under normal physiological conditions, as first proposed by Anfinsen.[27] The Classic Anfinsen experiment has demonstrated that the protein structure and biological activity of ribonuclease A are abolished under denaturing conditions but restored spontaneously upon returning to physiological conditions.[27]

Our current understanding of this process is that under physiological conditions, each protein molecule in the denatured state ensemble slides down an energy landscape to reach the conformation that optimizes its favorable interactions, i.e., the native state (**Figure 1.3**),[28] indicating that the amino acid sequence alone determines the native fold.[28] Although proteins with different sequences may adopt a similar fold.[29]

During water-soluble protein folding, the hydrophobic effect is the dominant driving force of this process.[30] Other forces such as electrostatic interactions between charged residues,[30] hydrogen bonding,[31] and van der Waals interaction[30] are affecting the protein stability.

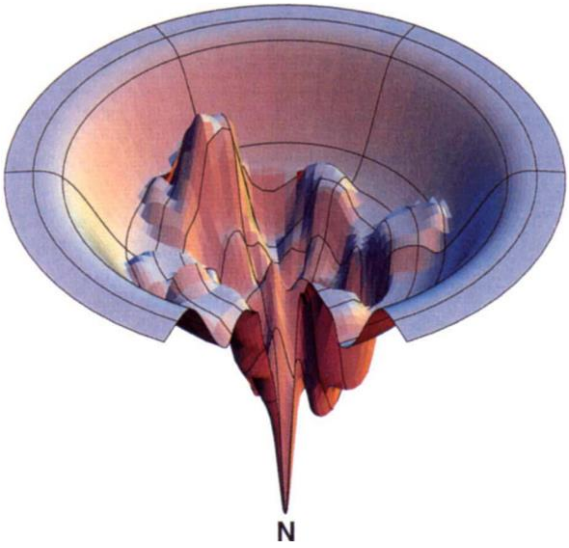

Figure 1.3 A model of the funnel-shaped rugged free energy landscape in protein folding.[32] N represents the native state.

The folding of a-helical MPs can be described by a two-stage model proposed by Popot and Engelman (**Figure 1.4**).[33] Because the lipid bilayer restricts the range of possible transmembrane protein conformations,[34] the folding process can be divided into two energetically distinct stages. In stage I, the independently stable hydrophobic-helices are formed across the lipid bilayer, in response to the hydrophobic effect, as well as the favorable backbone hydrogen-bonding in the non-aqueous environment.[35] In stage II, the helices interact to establish a tertiary fold with functional transmembrane structures.[33] The free energy gain of this process is contributed by packing and hydrogen bonding between transmembrane helices, loop structures, or cofactors if applicable, excluding lipid solvation.[36]

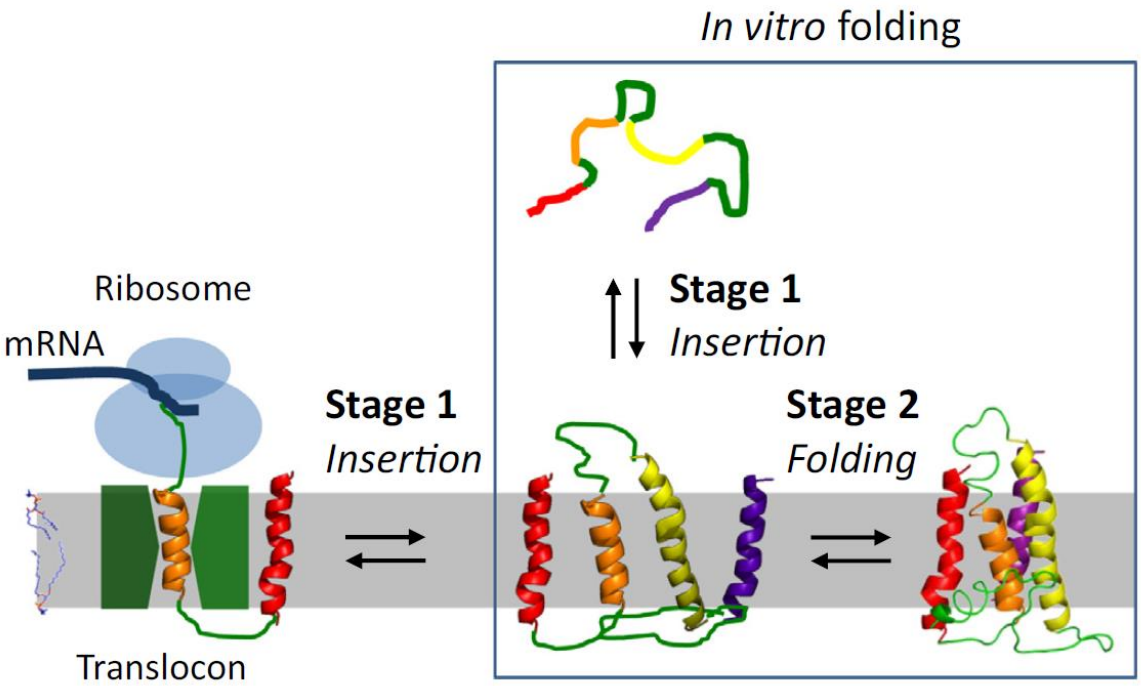

Figure 1.4 Folding of a membrane protein *in vivo* and *in vitro* within the framework of the two-stage model.[36] (PDB: 2HI7)

Protein quality control, an important process for normal cell function

Although many small globular proteins are thought to possess a funnel-shaped folding free energy landscape ensuring robust folding, the evolutionary pressure toward function may select the protein sequences that would fold into dynamic and marginally stable native states. However, this flexibility may mislead the polypeptide chain, subjecting it to misfolding and aggregation. Some of the misfolded polypeptides will be refolded by chaperones, or they all need to be degraded by proteases. Otherwise, misfolded proteins can accumulate, causing cytotoxic aggregation, such as amyloid fibrils, in the crowded cellular environment.[37]

Protein misfolding can be caused by missense mutations in the amino acid sequence, low protein stability, or environmental stresses.[38] Thus, the cells have

evolved with quality control mechanisms to maintain optimal levels of functional proteins. Protein homeostasis refers to the control of protein concentration, conformation, binding interaction (quaternary structure), and location of individual proteins making up the proteome.[38] Cells achieve this task mainly using two pathways, one is through molecular chaperones (often regulated by ATP) to assist correct folding (**Figure 1.5**);[39] and the other is through proteases to degrade misfolded or aggregated proteins and recycle them into amino acids.[40] Protein homeostasis thus influences general and specific cellular functions facing the constant intrinsic and environmental challenges to prevent disease development.[41] Since proteins are dynamic molecules, the surveillance by chaperones and proteases are required to operate constantly, and the two distinct activities need to be optimally balanced to influence protein synthesis, folding, trafficking, disaggregation, and degradation.[41]

MPs have been thought to share a similar quality control logic with water-soluble proteins.[42] Imbalance between MP folding and degradation causes many diseases, which occur via either excessive degradation of proteins that possess conformational defects (*e.g.,* cystic fibrosis is caused by excessive degradation of misfolded variant of cystic fibrosis transmembrane regulator protein)[43] or overwhelming deposition of protein aggregates beyond the normal degradation capacity of cells (*e,g.* Alzheimer's disease is caused by the aggregation of the truncated form of amyloid precursor protein).[44] To understand such disease mechanisms, it is crucial to understand the mechanisms of how misfolded proteins are selectively recognized and degraded by cellular proteases. This research project mainly focuses on dissecting the mechanism of MP degradation.

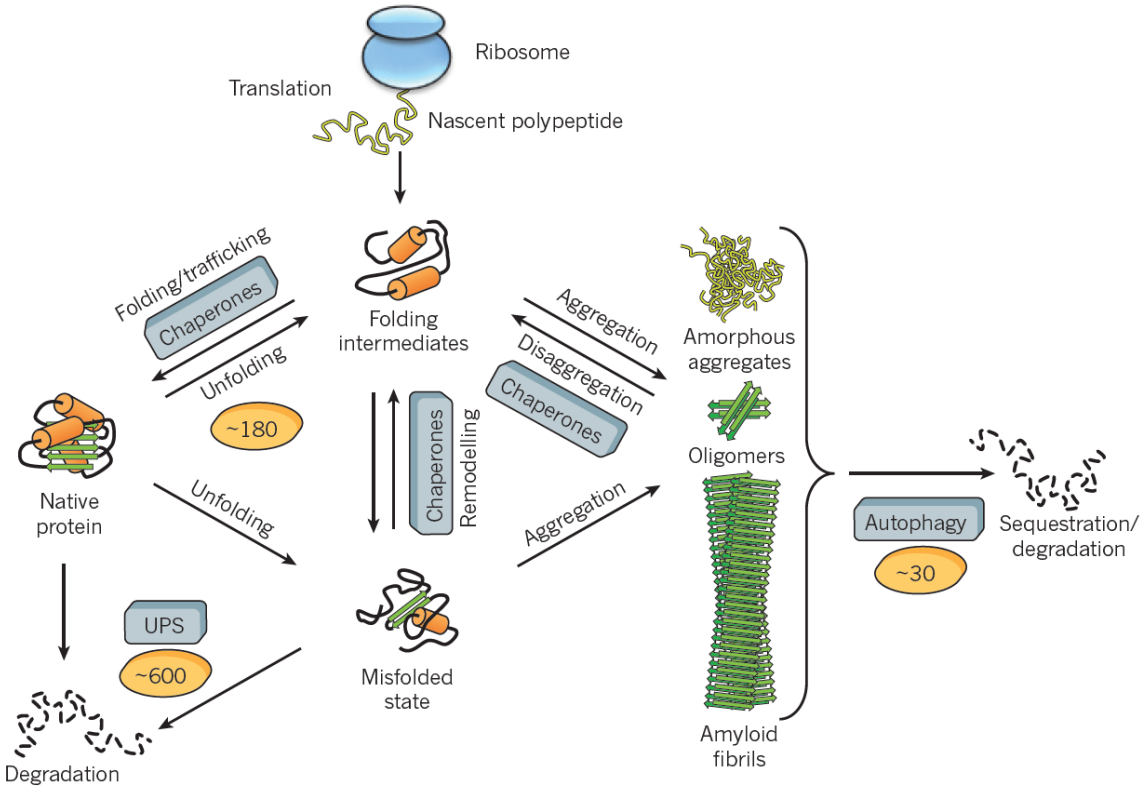

Figure 1.5 Protein homeostasis network.[38] The number in each yellow oval represents the number of cellular components involved in the process.

AAA+ protease family

Proteolysis itself is a free-energy downhill process not requiring ATP. Protein degradation in cells often involves the input of chemical energy generated by ATP hydrolysis.[45] ATP-dependent proteolysis, which is a focus of this study, is mediated by AAA+ proteases, which are generally composed of the ring-shaped hexameric AAA+ (ATPases associated with diverse cellular activities) ATPase and a compartmental protease. The AAA+ ATPase domain is a highly conserved protein module, which generally functions as a molecular motor that transduces chemical energy from ATP hydrolysis into mechanical energy.[46] The AAA+ domain can also be involved in various biological processes such as molecular chaperoning for protein refolding, DNA replication, membrane fusion, etc.[47] In the action of AAA+

proteases, the mechanical energy generated by AAA+ actively unravels misfolded or aggregated proteins and translocates the unraveled substrates into the compartmental proteases through a narrow pore which is excluded from bulk water. This highly regulated process allows selective degradation of proteins with abnormal conformations and precise quality control rather than massive degradation.

How are membrane proteins degraded?

Protein degradation pathways in eukaryotic cells have two major locations: lysosomes, containing a variety of hydrolases, and proteasomes, which are a type of ATP-dependent protease (**Figure 1.6**).[45]

Misfolded proteins on the cell surface or foreign proteins are delivered to lysosomes by endocytosis.[48] Damaged subcellular organelles are engulfed by autophagosomes and delivered to lysosomes as well.[45] On the other hand, the ubiquitin-proteasome system is in charge of the degradation of intracellular proteins.[45] In this case, substrates are conjugated to ubiquitin, which is then recognized by the proteasome. MPs share these main pathways on their fate of degradation.

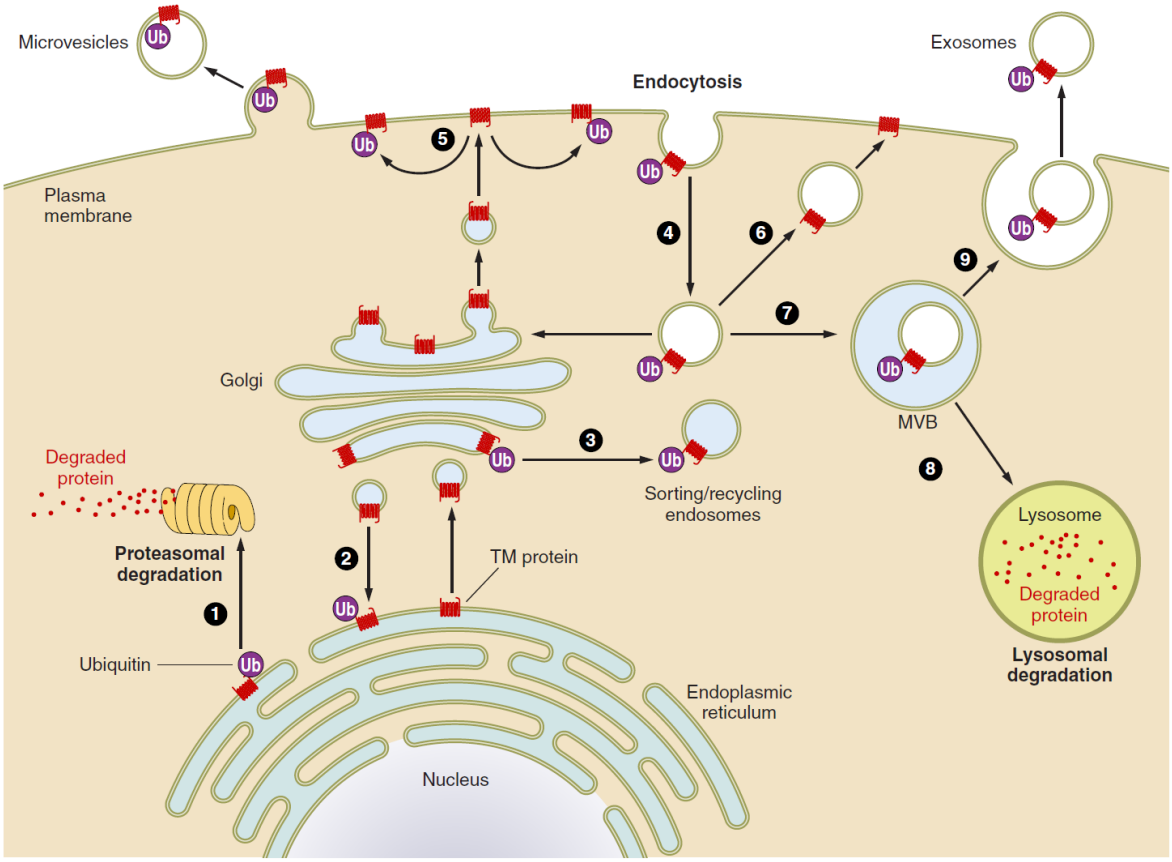

Figure 1.6 How membrane proteins are recognized and degraded in a eukaryotic cell.[49] Each numbered step is explained in the main text.

In eukaryotes, MPs are first synthesized on endoplasmic reticulum (ER) and then enter the ER quality control system called the Endoplasmic-Reticulum-Associated protein Degradation (ERAD) pathway (**Figure 1.6-①**), i.e., misfolded MPs are ubiquitinated by the membrane-bound ubiquitin ligase complex Hrd1/6 and extracted by the membrane-associated hexameric ring-shaped AAA+ ATPase Cdc48 to target the substrates to proteasomal degradation.[49, 50] The ubiquitinated proteins extracted from the ER membrane bind the regulatory particle of the 26S proteasome, where ubiquitin is then recognized and recycled by the 19S regulatory 'cap' of the 26S proteasome.[50] The AAA+ ATPase subunits within the regulatory particle utilize the free energy generated by ATP hydrolysis to unfold the substrate and translocate it

into the core particle, which forms a proteolytic chamber.[50] The substrate is then cleaved into small peptides. If MPs pass this first part of the quality test, they are then transported to the Golgi via vesicular trafficking. Here, misfolded MPs that have been missed by the previous quality control can be either recognized and sent back to the ER through retrograde transporting vesicles (**Figure 1.6-**②) or ubiquitinated at the Golgi and subjected to endosomes for lysosomal degradation (**Figure 1.6-**③).[51] If the MPs pass the Golgi quality test, they are trafficked to their designed destination, such as the plasma membrane, to fulfill their function. When the MPs are no longer needed, they can be ubiquitinated on the plasma membrane as well for internalization (**Figure 1.6-**④).[49] Another possible way is that the ubiquitin signal can direct the substrate to be released from the plasma membrane by forming microvesicles (**Figure 1.6-**⑤).[49] There are two options for the internalized MPs. One is that the MPs are deubiquitinated and travel back to either plasma membrane or Golgi (**Figure 1.6-**⑥).[49] The other is that the MPs are sent to multivesicular bodies (MVB) (**Figure 1.6-**⑦).[49] Once the MPs are in MVB, ubiquitinated proteins can either be sent for lysosomal degradation (**Figure 1.6-**⑧) or expelled as exosomes into the extracellular space (**Figure 1.6-**⑨).[49]

In prokaryotes and subcellular organelles of eukaryotes and archaea, misfolded proteins are recognized through solvent-exposed degradation markers or degrons, which are typically a short stretch of hydrophobic amino acids (**Figure 1.7**). Environmental stresses, including heat shock and endoproteolytic processing, can cause denaturation of cellular proteins and expose the cryptic degrons. Degrons are recognized either directly at the substrate entry pore of the ring AAA+ ATPase or by an adaptor protein that delivers bound substrates to the AAA+ pore. Substrates bound to the AAA+ ATPase are actively unfolded and translocated by ATP hydrolysis, and then to a compartmental peptidase.[52] The AAA+ protease superfamily includes various subfamilies, including Lon, ClpXP, ClpAP, ClpCP, HslUV, FtsH, 20S proteasome and PAN.

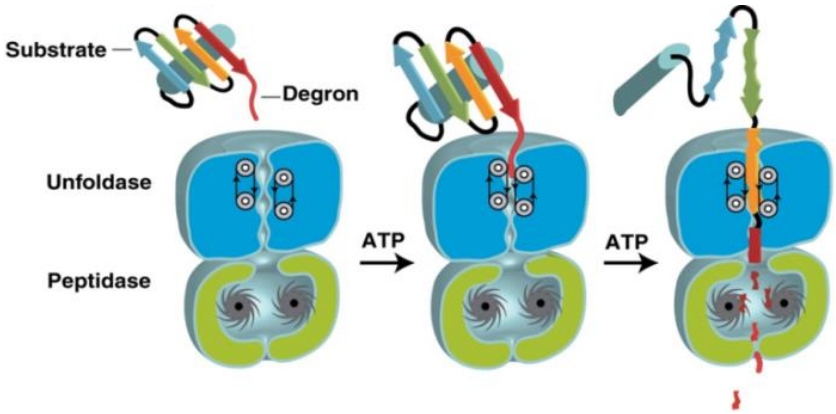

Figure 1.7 Schematic illustration of proteolysis mediated by AAA+ protease.[52]

Protein degradation in bacteria with AAA+ proteases

In *E. coli*, protein degradation is mainly carried out by AAA+ proteases, Lon, ClpXP including ClpAP. HslUV and FtsH.[53] For FtsH and Lon, the AAA+ ATPase and protease domains are covalently linked in one polypeptide chain. For all the others, two domains are synthesized as distinct polypeptide chains and assembled into a

large oligomeric functional unit.[52] Here I describe features of each AAA+ protease in *E. coli*.

Lon Lon protease was the first ATP-dependent protease which was isolated and reported by Chung, Goldberg and co-workers from *E. coli* in 1981.[54] Forming a functional hexamer, each monomer possesses a Lysine-Serine dyad in the active site.[55] In *E. coli*, Lon is the primary AAA+ protease responsible for ~50% of protein turnover in the cytosol. It recognizes aromatic and hydrophobic residues which would be normally buried in the hydrophobic core of native fold proteins but exposed in misfolded or denatured forms.[56] Degradation efficiency of Lon is also affected by the sequence of degrons.[57] *Mycoplasma*, which has a small genome, encodes only two types of AAA+ proteases: Lon and FtsH.[58]

One distinguishing feature of Lon is that in *E. coli*, it is co-purified with chromosomal DNA fragments.[59] Although there are no apparent sequence specificity and similarity, this high affinity for DNA of Lon suggests the protease function towards the rapid degradation of regulatory polypeptides or misfolded proteins associated with bacterial chromosomes.[60] Another interesting feature is that for HIV-1 enhancer, Lon favors binding to a GT-rich sequence. For both light and heavy chain promoters of the human mitochondrial genomes, Lon binds a specifically similar site,[60] suggesting that Lon participates in the regulation of DNA replication as well as in specific gene expression.[60]

ClpX/ClpA ClpP ClpXP and ClpAP are proteolytic enzymes sharing the same protease component, ClpP, and two different ATPases, ClpX and ClpA. ClpX has a significant sequence similarity to ClpA, but ClpX has only one AAA+ module,

whereas ClpA has two.[61] There is also a universal symmetry mismatch in the structure of Clp proteases, i.e., a hexameric AAA+ binds to a heptameric protease.[62] ClpP itself favors degradation of peptides with the length of ~10 residues and has minimal peptidase activity on longer and structurally folded polypeptides.[63] Stable proteins and long polypeptide substrates can be degraded when ClpP forms a complex with the ATPases ClpX and ClpA.[63, 64] It has been reported that Acyldepsipeptide antibiotic (ADEP) from *Streptococcus hawaiiensis* enhances the protease activity of isolated ClpP to degrade unfolded proteins, yet still not folded substrates.[65] ADEP binds to ClpA at a docking site similar to ClpX and ClpA, according to the crystal structures.[65] Bound ADEP changes the conformation of ClpP heptamer to open up the degradation passageway.[65] In summary, ClpP degrades stable proteins only when bound to ATP unfoldase, and ClpP itself degrades short peptides or unfolded proteins if stimulated by ADEP.

ClpXP and ClpAP usually have the highest degradation ability among all AAA+ proteases in *E. coli*.[66] Other than degrading unfolded proteins, ClpAP also prefers the substrates with abnormal N-termini (Phe, Leu, Trp, or Tyr).[52] ClpXP and ClpAP can rapidly degrade polypeptides tagged with the C-terminal degron called SsrA-tag (-AAXXXXXALAA), which is installed to incompletely translated polypeptides to rescue the stalled ribosomes.[67]

Interestingly, ClpP shares a remarkable structural similarity, but not a sequence similarity, with the inner core of β-subunits of the 20S proteasome. This suggests that cytosolic proteases evolutionarily select the conformation to restrict the access of the proteolytic active site from the cytosol. This substrate exclusion protects well-

folded and functional cellular proteins from degradation since substrates can only be proteolyzed after the interaction with ATP-dependent regulators.[68]

HslUV HslUV is a protein complex composed of the ATPase HslU and protease HslV, both of which form hexameric rings.[69] From sequence analysis, HslV displays homology to the β-subunit of the 20S proteasome particles suggesting that they share a common evolutionary precursor.[70] The biological role of HslUV remains unclear. It has been reported that HslUV targets unfolded protein for degradation.[71] When the HslU ring is bound to the HslV ring, only ATP-bound HslU sticks its C-terminal ~10 residue peptide into HslV to activate the proteolytic active site,[71] or a synthetic peptide can also activate HslV.[72] In other cases, HslV cannot degrade small peptides or interact with covalent inhibitors.[73]

FtsH The main subject of this study focuses on the degradation mechanism mediated by FtsH. The following section will describe FtsH in details.

FtsH: a membrane bound ATP-driven proteolytic machine

FtsH plays a crucial role in the protein quality control with its proteolytic and chaperoning ability in all life of forms except for archaea.

m-AAA and i-AAA proteases in mitochondria

FtsH homologs in mitochondria are classified into m-AAA protease and i-AAA protease. The m-AAA protease has two transmembrane segments, and the catalytic AAA+ and protease domains are oriented toward the matrix. The i-AAA protease has one transmembrane segment, and the catalytic domains are facing the mitochondrial intermembrane space. There are many kinds of m/i -AAA proteases in mitochondria

(**Table 1.1**). While FtsH in *E. coli* forms a homo-hexamer, m-AAA and i-AAA can form either a homo- or hetero-hexamer depending on the subclass. It has been proposed that the loss of one kind of functional m/i- AAA proteases can be compensated by another.[74] As a membrane associated AAA+ metalloprotease, it degrades proteins that have been transported across the mitochondrial membranes and end up misfolded.[75]

Organism /mitochondria	Localization		Nature of complex	Molecular mass of complex (kDa)
Saccharomyces cerevisiae	i-AAA	Yme1p (Yta11p)	Homo-oligomer	~850
	m-AAA	Yta10p (Afg3p) Yta12p (Rca1p)	Hetero-oligomer	~900 2000
Mouse	m-AAA	Paraplegin AFG3L2 AFG3L1	Hetero-oligomer Homo- and hetero-oligomer	~900
Homo sapiens	i-AAA	YME1L	Homo-oligomer	~900
	m-AAA	Paraplegin AFG3L2	Hetero-oligomer Homo- and hetero-oligomer	
Arabidopsis thaliana	i-AAA	AtFtsH4	Homo-oligomer	~1500
		AtFtsH11	Homo-oligomer	~1500
	m-AAA	AtFtsH3 AtFtsH10	Homo- and hetero-oligomer	~1000 2000

Table 1.1 Experimentally characterized m-/i-AAA proteases.[74]

The m-AAA protease first identified in human cells is Paraplegin. This name originates from the mutations of this protein from the patients of a genetically inherited autosomal neurodegenerative disease, *hereditary spastic paraplegia* (HSP).[76] Mutations in another m-AAA protease, AFG3L2, are thought to be a cause of another neurodegenerative disease *spinocerebellar ataxia*, which is often presented together with HSP.[77] Most of biochemical studies regarding the assembly

and function of eukaryotic FtsH homologs have been carried out with yeast orthologs.

Mitochondria lacking m/i-AAA proteases display a disruption in the assembly of respiratory complexes.[77, 78] In yeast, m/i-AAA proteases are in charge of the quality control of many MPs in subcellular organelles. i-AAA selectively degrades the unassembled cytochrome c oxidase subunit II[79], and external NADH dehydrogenase (Nde1).[80] Yeast i-AAA proteases are also involved in regulating the synthesis of cardiolipin (CL), a mitochondria specific phospholipid, by rapid degradation of the protein complexes that supply phosphatidic acid.[81] On the other hand, defects in m-AAA impair mitochondrial translation, and thus the assembly of mitochondria-encoded proteins can be inhibited. Loss of i-AAA from plant mitochondria delays both seed germination and the transition between the vegetative and the reproductive stage.[82] It also changes leaf morphology of aging rosettes and lowers the plant's fertility.[83] i-AAA from plant mitochondria prevents the accumulation of hyper-oxidized proteins via dual mechanisms: (1) degrading them directly and/or (2) decreasing the pool of unassembled subunits which would easily undergo oxidation.[84, 85]

FtsH in chloroplasts

FtsH in chloroplasts is localized in the thylakoid membranes with its catalytic domains exposed to the soluble stroma.[86] FtsH was reported as the protease which protects the structural and functional integrity of the photosynthetic reaction centers from environmental stresses at all stages of development.[74] It degrades unassembled chloroplast proteins on the stromal surface of the thylakoid

membrane.[87] One most studied example is the degradation of the core protein D1 protein in the photosystem II reaction center. It is anchored to the thylakoid membrane by five TM helices and is highly susceptible to oxidative damage induced by excess light.[88] This photoinhibition process is described as the conformational changes of the loops in the D1 protein upon excess irradiation, making the loops accessible for cleavage by the soluble stromal and luminal ATP-independent Deg proteases.[88, 89] Then the TM helices are subject to degradation by ATP-dependent FtsH.[89, 90]

FtsH in bacteria

The name FtsH originates from the temperature-sensitive mutation gene related to a cell division defect at 42 °C (**f**ilamentation **t**emperature-**s**ensitive) first detected in *E.coli*.[91] Although there are five different ATP-dependent proteases, FtsH is unique among them because only FtsH is membrane-integrated and growth essential.[92] Membrane localization reveals the feature that FtsH plays an important role in membrane protein degradation. FtsH of *E. coli* is the major focus of this research and described in details as follows.

E. coli FtsH structures

E. coli FtsH has 644 amino acids and a molecular weight of 70.7 kDa.[92] FtsH and its homologs are commonly composed of three domains (**Figure 1.8**). One is the TM domain with a folded periplasmic loop at the N terminus. Integration of the TM into the membrane is known to facilitate oligomerization of FtsH by increasing the effective concentration of FtsH and be essential to degradation of MPs.[93] The next part is the AAA+ domain with ~240 amino acid residues, required for binding,

unfolding, and translocation of substrates into the protease.[94] As a common feature of AAA+ enzymes, the AAA+ domain of FtsH contains the Walker A and B motifs, as well as the 'second region of homology (SRH)' motif, responsible for ATPase activity of FtsH.[94] The highly conserved residues in Walker A is important for ATP binding, while the Walker B and the SRH catalyze ATP hydrolysis.[95] The aromatic and nonpolar FVG (Phe, Val, and Gly) motif from each subunit of FtsH hexamer are aligned, forming the substrate recognition and entry pore in the hexameric ring.[96] The protease domain contains the HEXXH motif (His-Glu-X-X-His, where X designates any residues), which is responsible for the binding of the catalytic Zn^{2+} ion.[97]

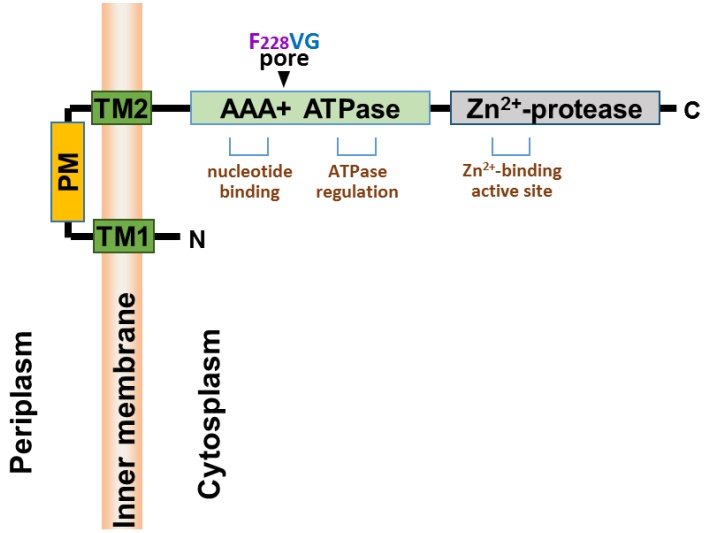

Figure 1.8 The domain structure and topology of *E. coli* FtsH.

X-ray crystal structures of cytosolic catalytic domains of bacterial FtsH The crystal structures of FtsH were determined for the whole cytosolic region containing both the AAA+ and protease domains in ADP-bound forms isolated from thermophilic bacteria *Aquifex aeolicus*[98, 99] and *Thermotoga maritima*,[100] and apo form from *Thermotoga maritima*.[101] The crystal structures of the isolated ATPase domain with

different nucleotide-bound states was obtained from FtsH from *E. coli*,[102] *Helicobacter pylori*,[103] *T. thermophilius*[104] and human mitochondrial homolog paraplegin (SPG7).[105] The crystal structure of the protease domain was obtained from FtsH of *Aquifex aeolicus*.[98]

The ATPase domain is composed of two subdomains (**Figure 1.9**). The large subdomain contains Walker motifs, entry pore motif and SRH. The small subdomain in the C-terminal region contains mostly α-helices. The ATP catalytic site lies at the interface between the two subdomains.[98-101] The conserved Arginine in SRH, known as an 'arginine finger' stabilizes the intersubunit contacts and senses the γ-phosphate of ATP.[95] The ATPase domain with these structural features forms a hexameric cylinder shape adapting 2, 3 or 6-fold symmetry, depending on the nucleotide bound state.[98-101] Nucleotide binding induces conformational changes of the ATPase domain. From the crystal structure of the cytosolic portion of FtsH from *Aquifex aeolicus*, it has been proposed that 'open' and 'closed' conformations of the ATPase domain are arranged alternatively within a hexamer.[98, 106] The closed conformation performs the ATP hydrolysis as the Arg finger R313 lies in the proper position, while the 6-fold symmetric apo form of FtsH from *T. maritima*[101] is in 'open' conformation for all subunits. The subunit switches between the two states with different pore-loop positions, leading to pulling of the substrate into the proteolytic chamber (**Figure 1.9**). From the study of ClpX, this conformational change is hypothesized to drive the rigid body movement of the entire AAA+ ring that generates a pulling force on bound substrates and induces active unfolding and translocation of the unfolded polypeptide chain[107].

The protease domain also forms a hexameric disk with 6-fold symmetry. Interestingly, the structure of the active sites in hexameric FtsH is very similar to those of other monomeric Zn^{2+} proteases, including 'zincin'.[98] Based on the study of zincin (e.g., tricorn interacting factor),[108] the peptide hydrolysis occurs by a nucleophilic attack of the carbonyl carbon by water molecules polarized by zinc ion and glutamic acid (aspartic acid in FtsH *E. coli*). The crystal structure of the hexameric periplasmic domain was also solved for FtsH of *E. coli*,[106] leaving only the TM domain unsolved.

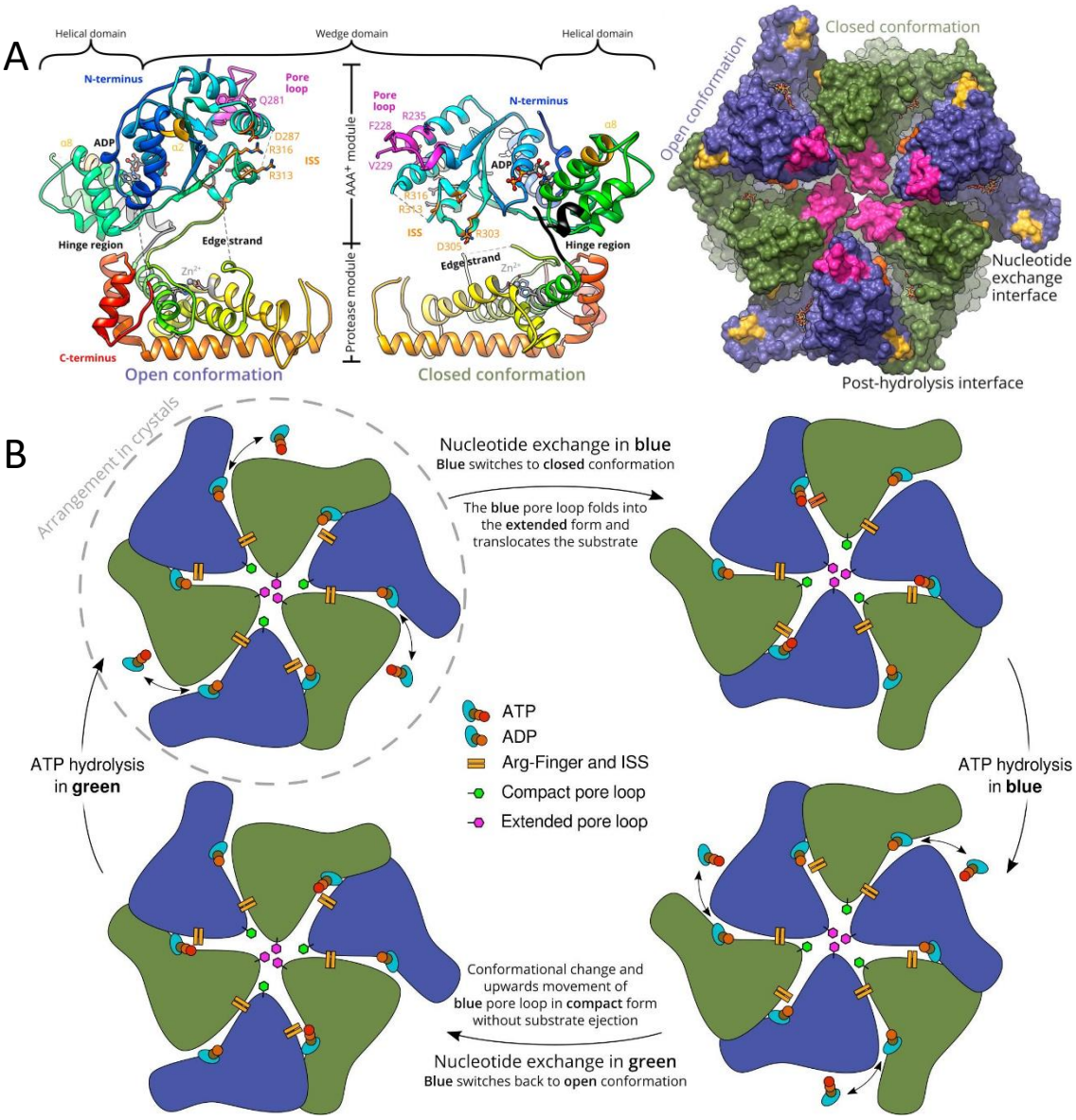

Figure 1.9 Crystal structure of FtsH cytosolic domains from *Aquifex aeolicus*.[99] (A) Side view of FtsH monomer with 'open' and 'closed' conformations (*left*). Top view of FtsH hexamer with the color codes- 'closed': green; 'open': blue (*right*). The pore loops in the subunits (pink) are very near in space sealing the pore in the 'closed' conformation, whereas they are apart in space in the 'open' conformation. (B) Schematic overview of the ATP hydrolysis cycle of FtsH. The same color code was used as in (A).

Cryo-Electron Microscopy (EM) structure of full-length FtsH In 2011, the first structure of a full-length FtsH homolog (an m-AAA protease of yeast) has been revealed as 12 Å resolution using cryo-EM (**Figure 1.10**). Although this protease is hetero-oligomeric in a naturally occurring form, only two mutations on one kind of subunit (Yta 12) lead to the formation of homo-oligomeric complexes. Despite the low resolution, this structure has unveiled an important characteristic of FtsH that there is an intermembrane space between the TM domain and the cytosolic domains, leaving a possible passage that is wide enough for unfolded but not folded substrates.[109]

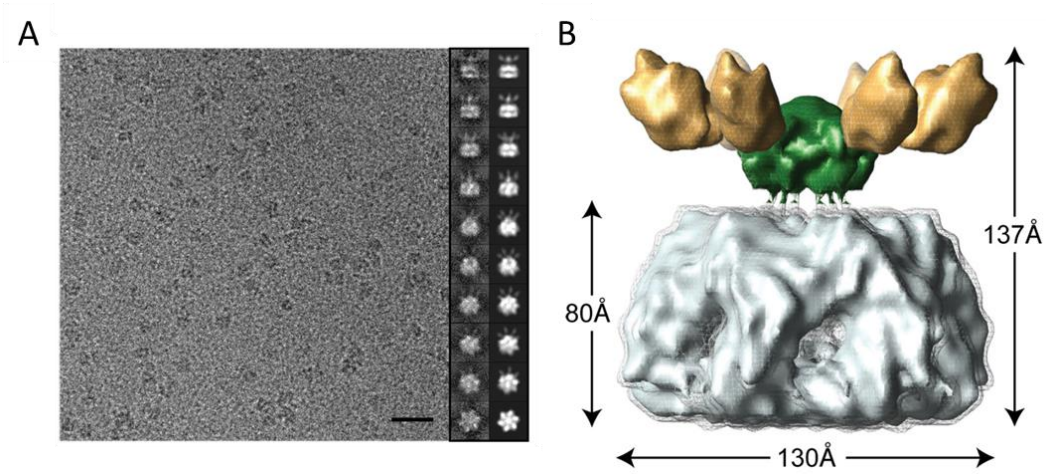

Figure 1.10 Cryo-EM analysis of an intact yeast *m*-AAA protease.[109] (A) Representative area of a digital micrograph of m-AAA hexamer embedded in vitreous ice. Selected projection views and their corresponding class averages (*right*) are also shown with 300 Å scale bar. (B) Side view of the structure of the m-AAA hexamer is shown as isosurface representation with the transmembrane domain colored *green*, the intermembrane space domain *gold*, and the matrix domain *gray*.

In 2017, the water-soluble portion of a human i-AAA was published with a 3.4 Å resolution using cryo-EM, elucidating the molecular mechanisms of ATP hydrolysis

and substrate translocation (**Figure 1.11**). This structure displays an asymmetric AAA+ ring with the spiral-staircase shape, which is stacked on the planar symmetric protease hexamer. A 10-residue peptide substrate was visualized in the AAA+ channel making close contacts with two Tyr residues from the entry pore loop. Individual AAA+ subunits undergo a tightly-coordinated ATP hydrolysis cycle with three different nucleotide-bound states, allosterically inducing the unfolded substrate circling to the protease chamber. This mechanism positions the interaction between the substrate and the central channel aligned with Tyr residues from all subunits in a stepwise manner, which links an inter-subunit signaling motif to the γ-phosphate sensitive Arginine fingers.[110]

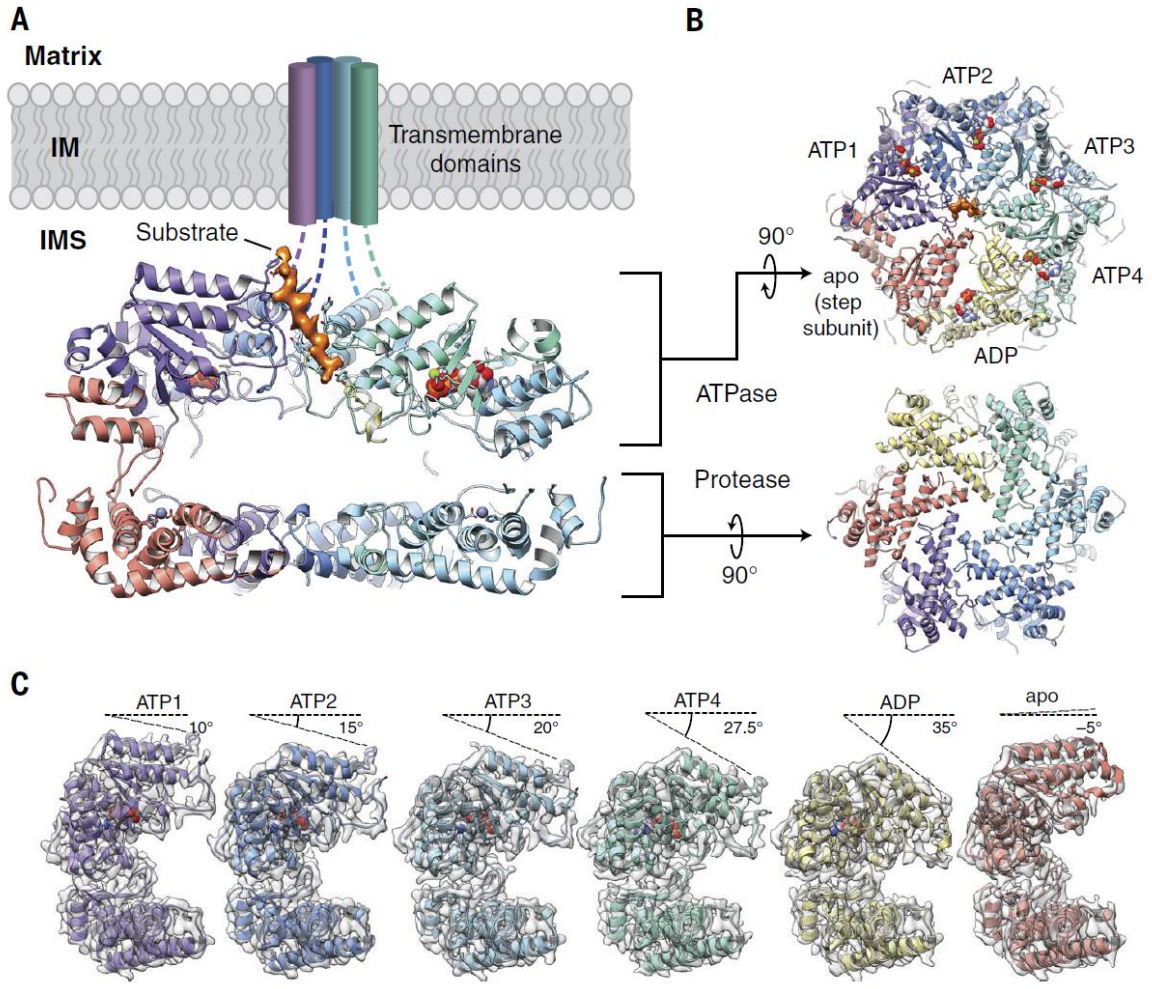

Figure 1.11 Cryo-EM analysis of the substrate-bound homo-hexameric YME1 AAA+ protease.[110] (A) The YME1 model with a bound substrate in cutaway view. The substrate is color-coded *orange* showing cryo-EM density. The nucleic acids are shown in sphere representation. (B) ATPase and protease rings are in orthogonal views. (C) Each subunit of the hexamer cytosolic domain is shown side-by-side with the transparent gray isosurface of the cryo-EM density. The relative movement of the ATPase domain to the protease domain is shown by the dashed-lined angle above each ATPase domain, sequentially. The tilt of the pore loop and pore loop tyrosine are also visible.

Features of FtsH substrates

FtsH degrades both water-soluble and MPs. It degrades intrinsically unstable folded and functional proteins, and thus regulates their functions by controlling their concentration. Known water-soluble substrates for FtsH include regulatory proteins such as a heat shock factor σ^{32} and the C-terminal domain of transcription factor cII which is critical for lysogenization of bacteriophage λ.[111,112] On the other hand, as a quality control center, FtsH degrades misfolded and excessively expressed MPs lacking their binding partners, such as uncomplexed subunits F_0a in ATP synthetase and SecY in SecYEG translocase.[113,114]

FtsH is known to have a weak sequence-specificity in recognition of degrons on protein substrates but requires certain features. Often degron sequences possess non-polar residues and sometimes a length requirement (>20 residues).[115] FtsH can recognize the C-terminal degradation tag SsrA, a universal degron targeted by all AAA+ proteases in *E. coli*, or a non-polar tag called “108” (SLLWS).[116] The recognition of SsrA tag indicates the sensitivity of FtsH to water-soluble proteins. One example is the regulation of the lipopolysaccharide (LPS) synthesis in bacteria by FtsH. The outer leaflet of the outer membrane of gram-negative bacterial cells is majorly composed of LPS to help the formation of a permeability barrier against external chemicals. The synthesis of LPS starts from lipid A catalyzed by a short-lived LpxC deacetylase (half-life, ~4 min).[117] The non-polar C terminal tail (20 amino acids, non-conserved) of LpxC can be recognized by FtsH, and the inactivating mutation of FtsH causes the lethal overaccumulation of LPS.[117] Besides, the N-terminal cytosolic tail of certain proteins can also be recognized by FtsH for degradation. Such an example is YccA, which is an *E. coli* MP unknown function.[118]

The previous quantitative studies of FtsH activity

The main goal of this dissertation was to elucidate the mechanism of membrane protein degradation by FtsH quantitatively. Hence, it is important to review the degradation measurements of FtsH reported in the field. Quantitative studies of FtsH activity have been mainly carried out with FtsH from *E. coli* and water-soluble substrates. The Ogura group has reported that FtsH hydrolyzes 196 ATP molecules min^{-1} $FtsH_6^{-1}$ at 37 °C with an apparent K_m value at [ATP] = 83 μM, in the absence of substrates.[104] FtsH can also hydrolyze CTP, GTP, and UTP.[104] It has also been reported that globular protein substrates such as water-soluble σ^{32} [111] and MP SecY[114] can be degraded *in vitro* in the presence of ATP but not non-hydrolyzable ATP analogs. Short peptides can be cleaved under both circumstances.[119] The proteolytic and ATPase activity of FtsH can be stimulated by the addition of 20% dimethyl sulfoxide.[120] As a Zn^{2+} metalloprotease, degradation of σ^{32} can be stimulated by Zn^{2+} and Mn^{2+} while inhibited by metal ion chelators such as Ethylenediaminetetraacetic acid (EDTA).[111] On the other hand, FtsH does not respond to the serine protease inhibitor Phenylmethylsulfonyl fluoride (PMSF).[111]

FtsH hexamer can degrade ~0.5 molecules min^{-1} of an unstable water-soluble protein σ^{32} and at 42 °C and consume ~140 ATP molecules to degrade one copy of the same protein.[121] Although AAA+ protease ClpXP and ClpAP can degrade thermodynamically or kinetically stable globular proteins such as green fluorescent protein (GFP), barnase and dihydrofolate reductase (DHFR), the Gross group found that FtsH degrades only proteins with low intrinsic thermodynamic stability.[122] The Matouschek group suggested that the weak unfoldase activity of FtsH originates from its weak ATPase activity (**Figure 1.12**).[66] Therefore, it has been widely

accepted that FtsH does not have a strong activity to unfold protein substrates, and this lack of robust unfoldase activity confers FtsH with an ability to selectively degrade abnormal proteins that have already been denatured (**Figure 1.13**).

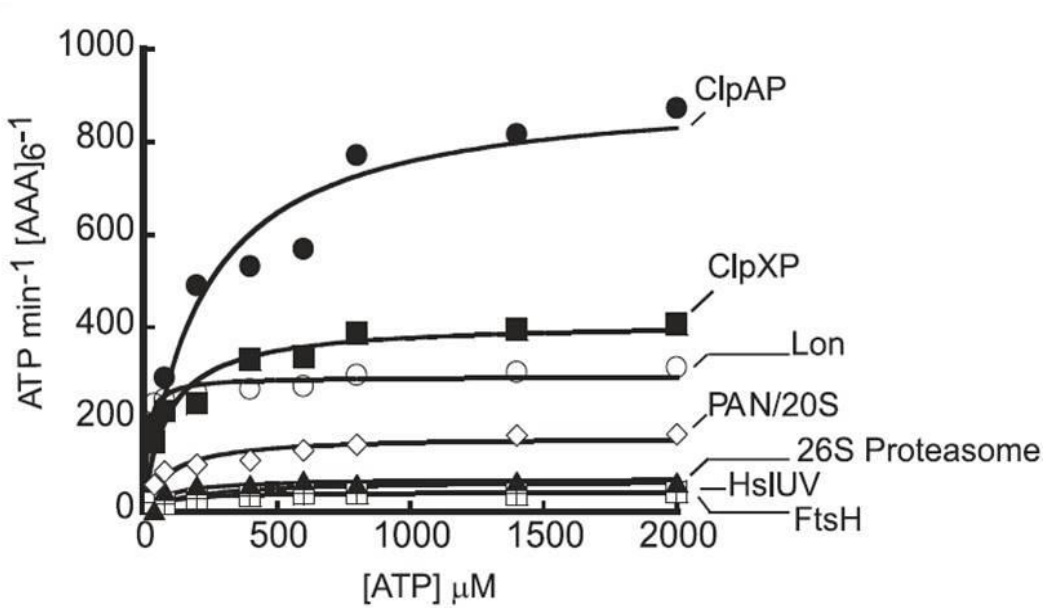

Figure 1.12 ATPase activity of FtsH in comparison to various AAA+ proteases.[66]

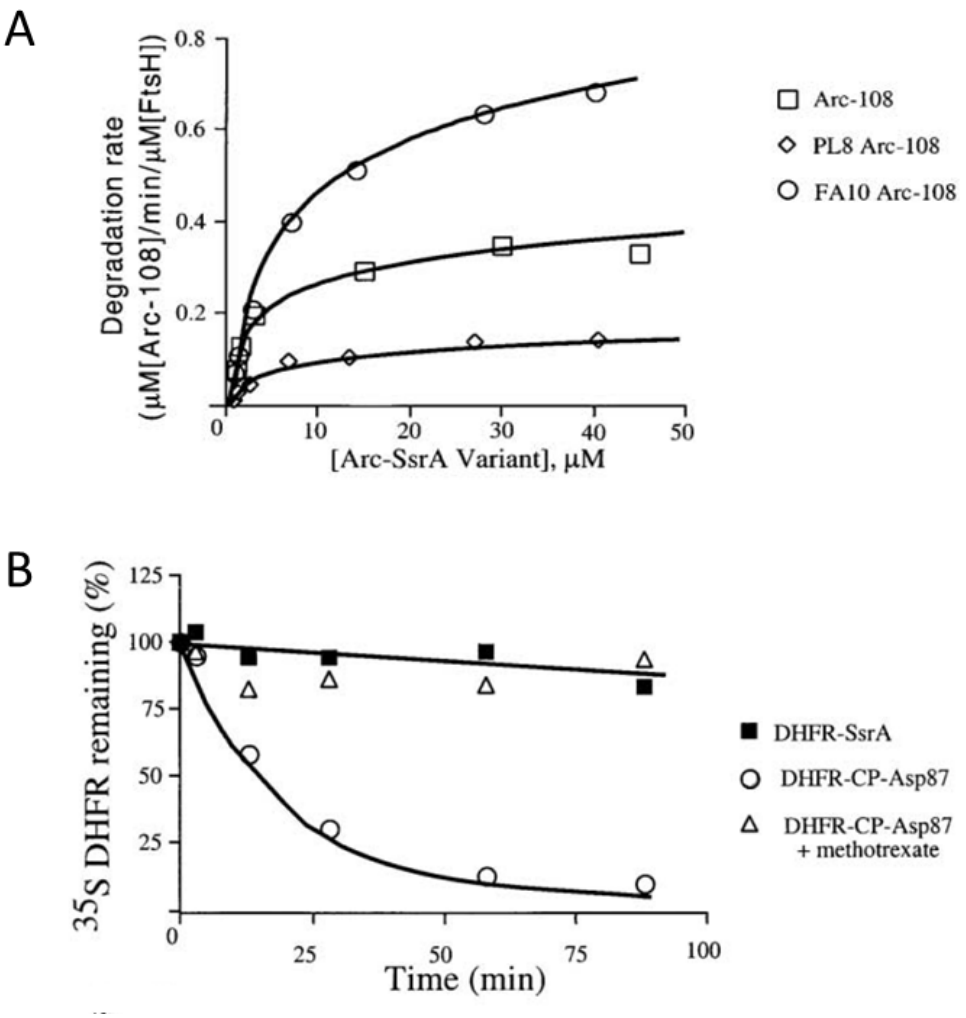

Figure 1.13 FtsH has a selectivity for intrinsically unstable proteins.[122] (A) FtsH degradation favors thermodynamically unstable mutant FA10 of Arc repressor. Degradation rates are lower for wild type and hyper stable mutant PL8. (B) FtsH can degrade the circular permeated (CP) dihydrofolate reductase (DHFR) Asp 87 mutant that has faster unfolding rate but not structurally or enzymatically altered. However, the degradation of DHFR wild type or DHFR-CP-Asp87 with stabilizing cofactor methotrexate is not successful.

Model membrane substrate GlpG

The proposed 'weak unfoldase' feature of FtsH served as a dogma in the field for more than a decade. As the studies were mainly carried out with the degradation of water-soluble substrates of FtsH, the knowledge gap remained for quantitative research of the degradation of membrane protein. To study FtsH-mediated degradation of MPs, I chose the rhomboid protease GlpG as a model. Rhomboid proteases are serine proteases and harbor the Ser-His catalytic dyad embedded in the bilayer core. They proteolyze a specific peptide bond connecting the soluble domains and TM domains near the membrane surface.[123] One of the most characterized rhomboid proteases is Rhomboid-1 from *Drosophila*.[124] It participates in the regulation of the epidermal growth factor receptor (EGFR) signaling by releasing the EGF from its membrane-tethered precursor[125] and activating the signaling pathway.[126,127] The rhomboid protease family is conserved in all kingdom of life, yet the only rhomboid, the function of which is known for bacteria, is AarA from the Gram-negative *Providencia stuartii*. AarA cleaves a precursor of the translocase channel formed by the multimerization of a single-pass TM protein, thereby allowing the transport of an unknown quorum-sensing signaling molecule.[128]

GlpG is a rhomboid protease from *E. coli*, but little is known about its function. GlpG is composed of six TM helices with both N- and C-termini facing the cytoplasm (**Figure 1.14**). Shorter TM4 is surrounded by the other TMs, forming an aqueous cavity under the surface of membrane contacting the Ser201-His254 catalytic dyad. The Ha group proposed that the membrane-embedded loop between TM1 and TM2 may serve as a gate towards the active site controlling the access of substrates,[129]

whereas subsequent mutagenesis and biochemical studies indicates that flexible TM5 serves as a substrate gate.[130, 131]

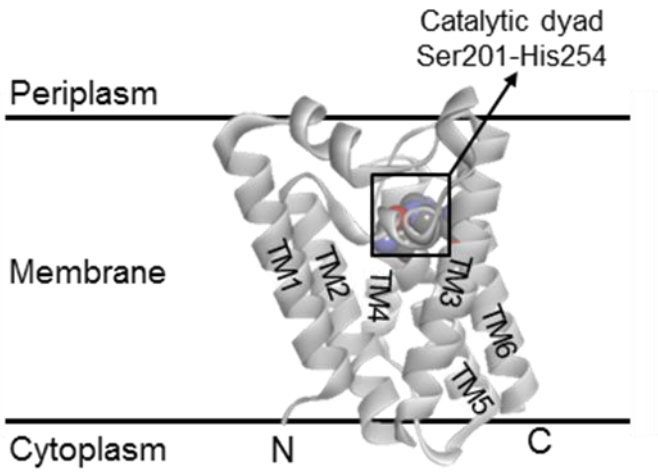

Figure 1.14 Structure of GlpG TM domain. (residues 87−276, PDB code: 3B45)[132]

GlpG has emerged as an important model system to study the folding of helical MPs. In 2014, the Otzen group reported that GlpG has the thermodynamic stability (ΔG) of 8.2 kcal/mole using a sodium dodecyl sulfate (SDS) denaturation method.[133] They have proposed that the unfolding of GlpG is 'two-state' within the detergent micellar phase since SDS perturbs the tertiary structure but not the secondary structure,[133] Therefore, ΔG here would be determined for the second stage within the context of the two-stage model for MP folding. This suggestion was further consolidated by the MD simulation studies by the Wolynes group.[131] Using the novel steric trapping strategy, our group has shown that GlpG is composed of two subdomains, the folding of which are partially coupled. Steric trapping has an advantage because of its ability to measure the thermodynamic stability directly under native conditions without using chemical denaturants. Using this method, we have determined that the global stability of GlpG is ΔG = ~6 kcal/mol.[134] Our group is now capable of manipulating its global and local stability by mutations. Thus, GlpG is an ideal model

system to study how intrinsic folding properties of MPs determine the susceptibility to degradation.

Table 1.2 shows the folding parameters of GlpG and other water-soluble model substrates that have been used for AAA+ proteases. GlpG has moderate stability with ΔG of 4-6 kcal/mol. Other folding properties of GlpG such as melting temperature and unfolding rate are comparable to several water-soluble proteins that are widely used as model substrates for other AAA+ proteases.

	ΔG_U (kcal/mol)	k_U (min^{-1})	T_m (°C)
DHFR	6.1[a]	5×10^{-2} [b]	54[c]
GFP	N/A[d]	~years[e]	76[f]
barnase	8.8[g]	~10^{-4} [h]	70[i]
Arc	10.9[j]	6[k]	59[l]
PhoA	N/A	N/A	~70[m]
DGK	16[n]	< ~10^{-5} [o]	~80[p]
GlpG	~4[q], 4.7[r], 5.8 [s]	3.4×10^{-3} [q] $2 – 3 \times 10^{-4}$ [t]	>85[u], 71[v]

ΔG_U: thermodynamic stability
k_U: spontaneous unfolding rate
T_m: thermal melting temperature
[a] measured at room temperature[135]
[b] measured at 15°C[136]
[c] from reference[137]
[d] No available data
[e] from reference[138]
[f] from reference[139]
[g] measured at room temperature[140]
[h] measured at room temperature[141]
[i] from reference[142]
[j] measured at room temperature[143]
[k] measured at room temperature [144]
[l] from reference[145]
[m] from reference[146]
[n] DGK (diacylglycerol kinase) measured in SDS/decylmaltoside mixed micelles[147]
[o] measured in *n*-octylglucoside by steric trapping[148]
[p] measured in dodecylmaltoside[149]
[q] measured by single-molecule force spectroscopy in neutral DMPC/CHAPS bicelles at room temperature[150]
[r] C-subdomain, measured by steric trapping at room temperature[134]
[s] N-subdomain, measured by steric trapping at room temperature[134]
[t] measured in DMPC/DMPG/CHAPS bicelles at 37°C[151]
[u] measured in DMPC/DMPG/CHAPS bicelles and *E. coli* lipids[151]
[v] measured in dodecylmaltoside[152]

Table 1.2 Comparison of folding parameters of GlpG and water-soluble model substrates for AAA+ proteases.

Crowding effect on protein activity

One of the most striking features of cells is that the biochemical and biophysical processes are carried out in the presence of enormously high concentrations of biomacromolecules. For example, the concentration of the biomacromolecules such as proteins, nucleic acids, and carbohydrates in an *E. coli* cell is up to ~300 mg/ml (www.bioNumbers.hms.harvard.edu). Therefore, it would be highly relevant to study biological processes in the presence of high concentrations of biomacromolecules.

When macromolecules are dissolved in solution at a high concentration, their physical properties such as size and concentration may affect kinetic and equilibrium behaviors of co-dissolved molecules, the situation of which is referred to 'macromolecular crowding.'[153] If the macromolecules do not interact with each other as well as with co-solutes, the major effect on the behavior of co-solutes would be reducing the free volume of the system. This is called the 'excluded volume' effect.

In case of a protein folding reaction (*U* represents the unfolded state, and *F* represents the folded state):

$$U \rightleftarrows F$$

This equilibrium can be characterized as the free energy change, which can be obtained from the corresponding equilibrium constant, where *R* is the molar gas constant, and *T* is the absolute temperature:

$$\Delta G_{UF} = -RT \ln K_{UF}$$

When we consider the crowding effect, the thermodynamic equilibrium of protein folding can be reconstructed as in **Figure 1.15**. The standard free energy change

and equilibrium constants in a dilute solution are denoted with superscript ‘o.’ Then, the free energy of protein folding in a crowded environment can be described as:

$$\Delta\Delta G_{UF} = \Delta G_{UF} - \Delta G^{0}_{UF} = \Delta G_{F}^{crowded} - \Delta G_{U}^{crowded}$$

And the corresponding equilibrium constant would be:

$$K_{UF} = K^{0}_{UF} \exp(-\Delta\Delta G_{UF} / RT)$$

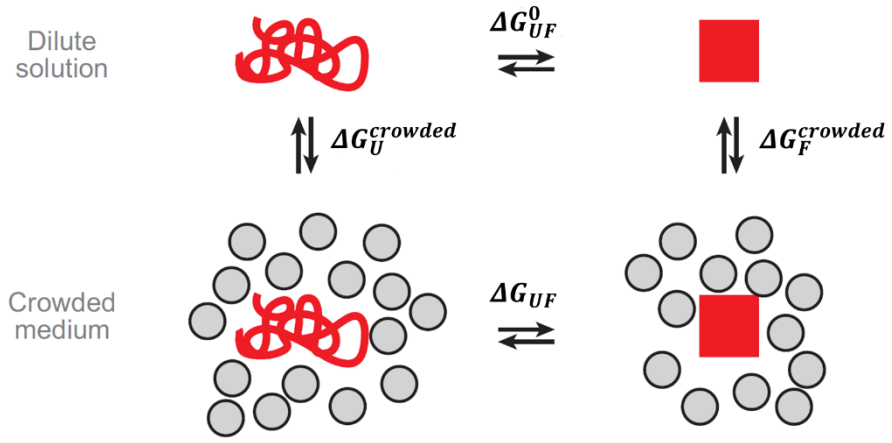

Figure 1.15 Thermodynamic equilibrium of protein folding in dilution and crowded medium.[153]

If it is assumed that macromolecules do not interact with protein molecules of interest, the excluded volume effect that reduces the free volume of each protein nonspecifically enhances compaction of the conformations of both folded and unfolded conformation. By the mass action law, the net outcome would be the stabilization of the folded state, which is more compact (see **Table 1.3** ‘protein stability’). If the reaction involves protein-protein interactions, the excluded volume effect will enhance the complex formation. In general, the macromolecular crowding is known to decrease the apparent thermodynamic stability, enhance the formation of macromolecular complexes in solution, increase the binding of macromolecules to surface sites and induce the formation of insoluble aggregates. The expected

magnitude of these effects strongly depends on the relative sizes and shapes of concentrated crowding reagents as well as the sizes of macromolecular reactants and products.

Also, macromolecular crowding is generally expected to increase the rate of slow transition state-limited association reactions and to decrease the rate of fast diffusion-limited association reactions. The various effects are shown in **Table 1.3**. Part of my project is to study the effects of macromolecular crowding on ATP hydrolysis and degradation activities mediated by FtsH. This study will provide an insight into how the physical environment mimicking the crowded cellular environment influences the function of FtsH.

	Protein	Macromolecule added	Effects
Association rates	*α*-synuclein[154]	Ficoll 70K 150 g/L	10 fold acceleration on amyloid fibrillation rate
		PEG 3.3K 150 g/L	3 fold acceleration on amyloid fibrillation rate
		BSA 50 g/L	5~6 fold acceleration on amyloid fibrillation rate
	HIV capsid protein[155]	Ficoll 70K 100 g/L	10 fold decrease on the half-time of protein self-assembly
Association equilibria	Bovine pancreatic trypsin inhibitor[156]	Dextran 10K 200 g/L	~5×10^5 fold increase in the association constant of decamer formation
	Replication protein RepA-DNA complex[157]	BSA 150 g/L	10 fold increase in the equilibrium association constant for complex formation
Conformational isomerization	RNase A[158]	PEG 20K 30 wt-%	Partially restores the enzymatic activity of RNase A in 2.4 M urea
	Adenylate kinase[159]	Dextran 270 g/L	Mean distance between residues 169 and 203 reduced in 1 M GuHCl
Protein stability with respect to denaturation	FK506-binding protein[160]	Dextran 160 g/L	The free energy of unfolding increase about *RT*
	DNase I[161]	PEG 4K 20 wt-%	T_m for thermal denaturation increases 15 °C
	Redesigned apocytochrome B562[162]	PEG 20K 85 g/L	Refolding rate increases by 30% at 30 °C and by 80% at 20 °C
Enzyme activity	DNase I[161]	PEG 4K~20K 20 wt-%	K_m was not affected, but V_{max} increased ~20-fold
	E. coli apoptosis stimulating protein[162]	PEG 6K 50 g/L	K_m decreased 4 fold, and V_{max} increased 6 fold.
	Urease[164]	Hemoglobin 30 wt-%	Urease activity increased 10-fold.

Abbreviations: BSA, bovine serum albumin; PEG, polyethylene glycol.

Table 1.3 Examples of macromolecular crowding effects on protein characteristics.

Projects description

Protein degradation is a key molecular process in protein quality control and regulation of functional networks in cells. While previous studies largely focused on the degradation of water-soluble proteins, numerous questions remain open how MPs are degraded. Using widely conserved FtsH as a model, I will provide answers to the questions, (1) How do the intrinsic folding properties of MPs determine their susceptibility of degradation? (2) How does FtsH utilize the free energy generated by ATP hydrolysis to degrade MPs? (3) What are the mechanisms of FtsH-mediated degradation of membrane proteins?

To answer these questions, I first reconstituted the MP degradation mediated by FtsH in the lipid bilayer environment (**Chapter 2**). Using the stable membrane protein GlpG as a model substrate, I quantitatively defined the ATP-driven unfoldase activity of FtsH and elucidated the quantitative relationship between intrinsic folding properties and degradation rates (**Chapter 3**). I also found that FtsH coupled multiple ATP hydrolysis events to degradation in a highly cooperative and efficient manner (**Chapter 2**). This mechanism explains how FtsH overcomes high energetic costs in unfolding substrates in membranes and extracts them towards its protease domain located outside the membrane.

This work represents the first study reporting the kinetics of MPs degradation by specific degradation machinery and will provide useful knowledge for generating new hypotheses to elucidate the challenging biological problem of MP degradation in eukaryotic cells.

REFERENCES

REFERENCES

(1) McMahon, H. T.; Gallop, J. L., Membrane curvature and mechanisms of dynamic cell membrane remodeling. *Nature* **2005,** *438* (7068), 590.

(2) Rothman, J. E.; Orci, L., Budding vesicles in living cells. *Scientific American* **1996,** *274* (3), 70-75.

(3) Bright, N. A.; Gratian, M. J.; Luzio, J. P., Endocytic delivery to lysosomes mediated by concurrent fusion and kissing events in living cells. *Current Biology* **2005,** *15* (4), 360-365.

(4) Robertson, J. D. In *The ultrastructure of cell membranes and their derivatives*, Biochemical Society Symposium, 1959; pp 3-43.

(5) Brown, D. A.; Rose, J. K., Sorting of GPI-anchored proteins to glycolipid-enriched membrane subdomains during transport to the apical cell surface. *Cell* **1992,** *68* (3), 533-544.

(6) Singer, S. J.; Nicolson, G. L., The fluid mosaic model of the structure of cell membranes. *Science* **1972,** *175* (4023), 720-731.

(7) Killian, J. A.; von Heijne, G., How proteins adapt to a membrane–water interface. *Trends in biochemical sciences* **2000,** *25* (9), 429-434.

(8) Saxton, M. J.; Jacobson, K., Single-particle tracking: applications to membrane dynamics. *Annual review of biophysics and biomolecular structure* **1997,** *26* (1), 373-399.

(9) Gheber, L. A.; Edidin, M., A model for membrane patchiness: lateral diffusion in the presence of barriers and vesicle traffic. *Biophysical Journal* **1999,** *77* (6), 3163-3175.

(10) Itoh, T.; Erdmann, K. S.; Roux, A.; Habermann, B.; Werner, H.; De Camilli, P., Dynamin and the actin cytoskeleton cooperatively regulate plasma membrane invagination by BAR and F-BAR proteins. *Developmental cell* **2005,** *9* (6), 791-804.

(11) Marieb, E. N.; Hoehn, K., *Human anatomy & physiology*. Pearson Education: 2007.

(12) Zimmerman, S. B.; Trach, S. O., Estimation of macromolecule concentrations and excluded volume effects for the cytoplasm of Escherichia coli. *Journal of molecular biology* **1991,** *222* (3), 599-620.

(13) White, S. H.; Wimley, W. C., Membrane protein folding and stability: physical principles. *Annual review of biophysics and biomolecular structure* **1999**, *28* (1), 319-365.

(14) Von Heijne, G., Membrane protein structure prediction: hydrophobicity analysis and the positive-inside rule. *Journal of molecular biology* **1992**, *225* (2), 487-494.

(15) Von Heijne, G., Membrane proteins: from sequence to structure. *Annual review of biophysics and biomolecular structure* **1994**, 23 (1), 167-192.

(16) Blobel, G., Intracellular protein topogenesis. *Proceedings of the National Academy of Sciences* **1980,** *77* (3), 1496-1500.

(17) von Heijne, G., Membrane-protein topology. *Nature reviews Molecular cell biology* **2006,** *7* (12), 909.

(18) Cramer, W.; Heymann, J.; Schendel, S.; Deriy, B.; Cohen, F.; Elkins, P.; Stauffacher, C., Structure-function of the channel-forming colicins. *Annual review of biophysics and biomolecular structure* **1995,** *24* (1), 611-641.

(19) Zhan, H.; Oh, K. J.; Shin, Y.-K.; Hubbell, W. L.; Collier, R. J., Interaction of the isolated transmembrane domain of diphtheria toxin with membranes. *Biochemistry* **1995,** *34* (14), 4856-4863.

(20) Skach, W. R., Cellular mechanisms of membrane protein folding. *Nature structural & molecular biology* **2009,** *16* (16), 606.

(21) Sadlish, H.; Pitonzo, D.; Johnson, A. E.; Skach, W. R., Sequential triage of transmembrane segments by Sec61α during biogenesis of a native multispanning membrane protein. *Nature structural & molecular biology* **2005,** *12* (10), 870.

(22) Skach, W. R.; Lingappa, V. R., Amino-terminal assembly of human P-glycoprotein at the endoplasmic reticulum is directed by cooperative actions of two internal sequences. *Journal of Biological Chemistry* **1993,** *268* (31), 23552-23561.

(23) Ervasti, J. M.; Campbell, K. P., Membrane organization of the dystrophin-glycoprotein complex. *Cell* **1991,** *66* (6), 1121-1131.

(24) Johnston, G. I.; Cook, R. G.; McEver, R. P., Cloning of GMP-140, a granule membrane protein of platelets and endothelium: sequence similarity to proteins involved in cell adhesion and inflammation. *Cell* **1989,** *56* (6), 1033-1044.

(25) Balda, M. S.; Whitney, J. A.; Flores, C.; González, S.; Cereijido, M.; Matter, K., Functional dissociation of paracellular permeability and transepithelial electrical resistance and disruption of the apical-basolateral intramembrane diffusion barrier by expression of a mutant tight junction membrane protein. *Journal of cell biology* **1996,** *134* (4), 1031-1049.

(26) Foster, D. L.; Boublik, M.; Kaback, H., Structure of the lac carrier protein of Escherichia coli. *Journal of Biological Chemistry* **1983,** *258* (1), 31-34.

(27) Anfinsen, C. B., Principles that govern the folding of protein chains. *Science* **1973,** *181* (4096), 223-230.

(28) Rose, G. D.; Fleming, P. J.; Banavar, J. R.; Maritan, A., A backbone-based theory of protein folding. *Proceedings of the National Academy of Sciences* **2006,** *103* (45), 16623-16633.

(29) Chan, H. S.; Dill, K. A., Protein folding in the landscape perspective: Chevron plots and non-Arrhenius kinetics. *Proteins: Structure, Function and Bioinformatics* **1998,** *30* (1), 2-33.

(30) Dill, K. A., Dominant forces in protein folding. *Biochemistry* **1990,** *29* (31), 7133-7155.

(31) Pauling, L.; Corey, R. B.; Branson, H. R., The structure of proteins: two hydrogen-bonded helical configurations of the polypeptide chain. *Proceedings of the National Academy of Sciences* **1951,** *37* (4), 205-211.

(32) Dill, K. A.; Chan, H. S., From Levinthal to pathways to funnels. *Nature structural & molecular biology* **1997,** *4* (1), 10.

(33) Popot, J.-L.; Engelman, D. M., Membrane protein folding and oligomerization: the two-stage model. *Biochemistry* **1990,** *29* (17), 4031-4037.

(34) Popot, J.-L.; Engelman, D. M., Helical membrane protein folding, stability, and evolution. *Annual review of biochemistry* **2000,** *69* (1), 881-922.

(35) Engelman, D.; Steitz, T., The spontaneous insertion of proteins into and across membranes: the helical hairpin hypothesis. *Cell* **1981,** *23* (2), 411-422.

(36) Hong, H., Toward understanding driving forces in membrane protein folding. *Archives of biochemistry and biophysics* **2014,** *564*, 297-313.

(37) Sipe, J. D.; Cohen, A. S., Review: history of the amyloid fibril. *Journal of structural biology* **2000,** *130* (2), 88-98.

(38) Hartl, F. U.; Bracher, A.; Hayer-Hartl, M., Molecular chaperones in protein folding and proteostasis. *Nature* **2011,** *475* (7356), 324-332.

(39) Hartl, F. U., Molecular chaperones in cellular protein folding. *Nature* **1996,** *381* (6583), 571.

(40) Kim, Y. E.; Hipp, M. S.; Bracher, A.; Hayer-Hartl, M.; Ulrich Hartl, F., Molecular chaperone functions in protein folding and proteostasis. *Annual review of biochemistry* **2013,** *82*, 323-355.

(41) Balch, W. E.; Morimoto, R. I.; Dillin, A.; Kelly, J. W., Adapting proteostasis for disease intervention. *Science* **2008,** *319* (5865), 916-919.

(42) Dobson, C. M., Protein folding and misfolding. *Nature* **2003,** *426* (6968), 884.

(43) Mattson, M. P.; Barger, S. W.; Cheng, B.; Lieberburg, I.; Smith-Swintosky, V. L.; Rydel, R. E., β-Amyloid precursor protein metabolites and loss of neuronal Ca 2+ homeostasis in Alzheimer's disease. *Trends in neurosciences* **1993,** *16* (10), 409-414.

(44) Douglas, P. M.; Dillin, A., Protein homeostasis and aging in neurodegeneration. *The Journal of cell biology* **2010,** *190* (5), 719-729.

(45) Clague, M. J.; Urbé, S., Ubiquitin: same molecule, different degradation pathways. *Cell* **2010,** *143* (5), 682-685.

(46) Vale, R. D., Aaa proteins lords of the ring. *The Journal of cell biology* **2000,** *150* (1), F13-F20.

(47) Snider, J.; Thibault, G.; Houry, W. A., The AAA+ superfamily of functionally diverse proteins. *Genome biology* **2008,** *9* (4), 216.

(48) Clague, M. J.; Urbé, S., Endocytosis: the DUB version. *Trends in cell biology* **2006,** *16* (11), 551-559.

(49) Foot, N.; Henshall, T.; Kumar, S., Ubiquitination and the regulation of membrane proteins. *Physiological reviews* **2016,** *97* (1), 253-281.

(50) Christianson, J.C. and Ye, Y., Cleaning up in the endoplasmic reticulum: ubiquitin in charge. *Nature structural & molecular biology* **2014**, *21*(4), 325.

(51) Henne, W.M., Buchkovich, N.J. and Emr, S.D., 2011. The ESCRT pathway. *Developmental cell* **2011**, *21*(1), 77-91.

(52) Sauer, R. T.; Baker, T. A., AAA+ proteases: ATP-fueled machines of protein destruction. *Annual review of biochemistry* **2011,** *80*, 587-612.

(53) Mogk, A.; Huber, D.; Bukau, B., Integrating protein homeostasis strategies in prokaryotes. *Cold Spring Harbor perspectives in biology* **2011,** *3* (4), a004366.

(54) Swamy, K. S.; Goldberg, A. L., *E. coli* contains eight soluble proteolytic activities, one being ATP dependent. *Nature* **1981,** *292* (5824), 652.

(55) Birghan, C.; Mundt, E.; Gorbalenya, A. E., A non-canonical Lon proteinase lacking the ATPase domain employs the Ser–Lys catalytic dyad to exercise broad control over the life cycle of a double-stranded RNA virus. *The EMBO journal* **2000,** *19* (1), 114-123.

(56) Maurizi, M. R.; Trisler, P.; Gottesman, S., Insertional mutagenesis of the lon gene in Escherichia coli: lon is dispensable. *Journal of bacteriology* **1985,** *164* (3), 1124-1135.

(57) Gur, E.; Sauer, R. T., Degrons in protein substrates program the speed and operating efficiency of the AAA+ Lon proteolytic machine. *Proceedings of the National Academy of Sciences* **2009**, pnas. 0910392106.

(58) Wong, P.; Houry, W. A., Chaperone networks in bacteria: analysis of protein homeostasis in minimal cells. *Journal of structural biology* **2004,** *146* (1-2), 79-89.

(59) Nomura, K.; Kato, J.; Takiguchi, N.; Ohtake, H.; Kuroda, A. J. J. o. B. C., Effects of inorganic polyphosphate on the proteolytic and DNA-binding activities of Lon in Escherichia coli. *Journal of Biological Chemistry* **2004,** *279* (33), 34406-34410.

(60) Fu, G. K.; Smith, M. J.; Markovitz, D. M., Bacterial protease Lon is a site-specific DNA-binding protein. *Journal of Biological Chemistry* **1997,** *272* (1), 534-538.

(61) Gottesman, S.; Clark, W. P.; de Crecy-Lagard, V.; Maurizi, M. R., ClpX, an alternative subunit for the ATP-dependent Clp protease of Escherichia coli. Sequence and *in vivo* activities. *Journal of Biological Chemistry* **1993,** *268* (30), 22618-22626.

(62) Grimaud, R.; Kessel, M.; Beuron, F.; Steven, A. C.; Maurizi, M. R., Enzymatic and Structural Similarities between theEscherichia coli ATP-dependent Proteases, ClpXP and ClpAP. *Journal of Biological Chemistry* **1998,** *273* (20), 12476-12481.

(63) Woo, K. M.; Chung, W. J.; Ha, D. B.; Goldberg, A.; Chung, C. H., Protease Ti from Escherichia coli requires ATP hydrolysis for protein breakdown but not for hydrolysis of small peptides. *Journal of Biological Chemistry* **1989,** *264* (4), 2088-2091.

(64) Kang, S. G.; Ortega, J.; Singh, S. K.; Wang, N.; Huang, N.-n.; Steven, A. C.; Maurizi, M. R., Functional proteolytic complexes of the human mitochondrial ATP-dependent protease, hClpXP. *Journal of Biological Chemistry* **2002,** *277* (23), 21095-21102.

(65) Li, D. H. S.; Chung, Y. S.; Gloyd, M.; Joseph, E.; Ghirlando, R.; Wright, G. D.; Cheng, Y.-Q.; Maurizi, M. R.; Guarne, A.; Ortega, J., Acyldepsipeptide antibiotics induce the formation of a structured axial channel in ClpP: a model for the ClpX/ClpA-bound state of ClpP. *Chemistry & Biology* **2010,** *17* (9), 959-969.

(66) Koodathingal, P.; Jaffe, N. E.; Kraut, D. A.; Prakash, S.; Fishbain, S.; Herman, C.; Matouschek, A., ATP-dependent proteases differ substantially in their ability to unfold globular proteins. *Journal of Biological Chemistry* **2009,** *284* (28), 18674-18684.

(67) Gottesman, S.; Roche, E.; Zhou, Y.; Sauer, R. T., The ClpXP and ClpAP proteases degrade proteins with carboxy-terminal peptide tails added by the SsrA-tagging system. *Genes & development* **1998,** *12* (9), 1338-1347.

(68) Pickart, C. M.; Cohen, R. E., Proteasomes and their kin: proteases in the machine age. *Nature Reviews Molecular Cell Biology* **2004,** *5* (3), 177.

(69) Sousa, M. C.; Trame, C. B.; Tsuruta, H.; Wilbanks, S. M.; Reddy, V. S.; McKay, D. B., Crystal and solution structures of an HslUV protease–chaperone complex. *Cell* **2000,** *103* (4), 633-643.

(70) Lupas, A.; Zwickl, P.; Baumeister, W., Proteasome sequences in eubacteria. *Trends in biochemical sciences* **1994,** *19* (12), 533-534.

(71) Rohrwild, M.; Coux, O.; Huang, H.; Moerschell, R. P.; Yoo, S. J.; Seol, J. H.; Chung, C. H.; Goldberg, A. L., HslV-HslU: A novel ATP-dependent protease complex in Escherichia coli related to the eukaryotic proteasome. *Proceedings of the National Academy of Sciences* **1996,** *93* (12), 5808-5813.

(72) Seong, I. S.; Kang, M. S.; Choi, M. K.; Lee, J. W.; Koh, O. J.; Wang, J.; Eom, S. H.; Chung, C. H., The C-terminal tails of HslU ATPase act as a molecular switch for activation of HslV peptidase. *Journal of Biological Chemistry* **2002,** *277* (29), 25976-25982.

(73) Sousa, M. C.; Kessler, B. M.; Overkleeft, H. S.; McKay, D. B., Crystal structure of HslUV complexed with a vinyl sulfone inhibitor: corroboration of a proposed mechanism of allosteric activation of HslV by HslU. *Journal of molecular biology* **2002,** *318* (3), 779-785.

(74) Janska, H.; Kwasniak, M.; Szczepanowska, J., Protein quality control in organelles—AAA/FtsH story. *Biochimica Et Biophysica Acta (BBA)-Molecular Cell Research* **2013,** *1833* (2), 381-387.

(75) Leonhard, K.; Herrmann, J.; Stuart, R.; Mannhaupt, G.; Neupert, W.; Langer, T., AAA proteases with catalytic sites on opposite membrane surfaces comprise a proteolytic system for the ATP-dependent degradation of inner membrane proteins in mitochondria. *The EMBO journal* **1996,** *15* (16), 4218-4229.

(76) Casari, G.; De Fusco, M.; Ciarmatori, S.; Zeviani, M.; Mora, M.; Fernandez, P.; De Michele, G.; Filla, A.; Cocozza, S.; Marconi, R., Spastic paraplegia and OXPHOS impairment caused by mutations in paraplegin, a nuclear-encoded mitochondrial metalloprotease. *Cell* **1998,** *93* (6), 973-983.

(77) Arlt, H.; Tauer, R.; Feldmann, H.; Neupert, W.; Langer, T., The YTA10–12 complex, an AAA protease with chaperone-like activity in the inner membrane of mitochondria. *Cell* **1996,** *85* (6), 875-885.

(78) Nakai, T.; Yasuhara, T.; Fujiki, Y.; Ohashi, A., Multiple genes, including a member of the AAA family, are essential for degradation of unassembled subunit 2 of cytochrome c oxidase in yeast mitochondria. *Molecular and Cellular Biology* **1995,** *15* (8), 4441-4452.

(79) Pearce, D. A.; Sherman, F., Degradation of cytochrome oxidase subunits in mutants of yeast lacking cytochrome c and suppression of the degradation by mutation of yme1. *Journal of Biological Chemistry* **1995,** *270* (36), 20879-20882.

(80) Augustin, S.; Nolden, M.; Müller, S.; Hardt, O.; Arnold, I.; Langer, T., Characterization of peptides released from mitochondria evidence for constant proteolysis and peptide efflux. *Journal of Biological Chemistry* **2005,** *280* (4), 2691-2699.

(81) Potting, C.; Wilmes, C.; Engmann, T.; Osman, C.; Langer, T., Regulation of mitochondrial phospholipids by Ups1/PRELI-like proteins depends on proteolysis and Mdm35. *The EMBO journal* **2010,** *29* (17), 2888-2898.

(82) Janska, H.; Piechota, J.; Kwasniak, M., ATP-dependent proteases in biogenesis and maintenance of plant mitochondria. *Biochimica et Biophysica Acta (BBA)-Bioenergetics* **2010,** *1797* (6-7), 1071-1075.

(83) Marta, K.; Marta, G.; Adam, U.; Hanna, J., The significance of Arabidopsis AAA proteases for activity and assembly/stability of mitochondrial OXPHOS complexes. *Physiologia plantarum* **2007,** *129* (1), 135-142.

(84) Gibala, M.; Kicia, M.; Sakamoto, W.; Gola, E. M.; Kubrakiewicz, J.; Smakowska, E.; Janska, H., The lack of mitochondrial AtFtsH4 protease alters Arabidopsis leaf morphology at the late stage of rosette development under short-day photoperiod. *The Plant Journal* **2009,** *59* (5), 685-699.

(85) Kicia, M.; Gola, E. M.; Janska, H., Mitochondrial protease AtFtsH4 protects ageing Arabidopsis rosettes against oxidative damage under short-day photoperiod. *Plant signaling & behavior* **2010,** *5* (2), 126-128.

(86) Lindahl, M.; Tabak, S.; Cseke, L.; Pichersky, E.; Andersson, B.; Adam, Z., Identification, characterization, and molecular cloning of a homologue of the bacterial FtsH protease in chloroplasts of higher plants. *Journal of Biological Chemistry* **1996,** *271* (46), 29329-29334.

(87) Ostersetzer, O.; Adam, Z., Light-stimulated degradation of an unassembled Rieske FeS protein by a thylakoid-bound protease: the possible role of the FtsH protease. *The plant Cell* **1997,** *9* (6), 957-965.

(88) Haußühl, K.; Andersson, B.; Adamska, I., A chloroplast DegP2 protease performs the primary cleavage of the photodamaged D1 protein in plant photosystem II. *The EMBO journal* **2001,** *20* (4), 713-722.

(89) Kato, Y.; Sakamoto, W., Protein quality control in chloroplasts: a current model of D1 protein degradation in the photosystem II repair cycle. *Journal of Biological Chemistry* **2009,** *146* (4), 463-469.

(90) Bailey, S.; Thompson, E.; Nixon, P. J.; Horton, P.; Mullineaux, C. W.; Robinson, C.; Mann, N. H., A critical role for the Var2 FtsH homologue of Arabidopsis thaliana in the photosystem II repair cycle *in vivo*. *Journal of Biological Chemistry* **2002,** *277* (3), 2006-2011.

(91) Begg, K.; Tomoyasu, T.; Donachie, W.; Khattar, M.; Niki, H.; Yamanaka, K.; Hiraga, S.; Ogura, T., Escherichia coli mutant Y16 is a double mutant

carrying thermosensitive ftsH and ftsI mutations. *Journal of bacteriology* **1992,** *174* (7), 2416-2417.

(92) Wang, R.-f.; O'Hara, E. B.; Aldea, M.; Bargmann, C. I.; Gromley, H.; Kushner, S. R., Escherichia coli mrsC Is an Allele ofhflB, Encoding a Membrane-Associated ATPase and Protease That Is Required for mRNA Decay. *Journal of bacteriology* **1998,** *180* (7), 1929-1938.

(93) Akiyama, Y.; Ito, K., Roles of multimerization and membrane association in the proteolytic functions of FtsH (HflB). *The EMBO journal* **2000,** *19* (15), 3888-3895.

(94) Ito, K.; Akiyama, Y., Cellular functions, mechanism of action, and regulation of FtsH protease. *Annu. Rev. Microbiol.* **2005,** *59*, 211-231.

(95) Karata, K.; Inagawa, T.; Wilkinson, A. J.; Tatsuta, T.; Ogura, T., Dissecting the role of a conserved motif (the second region of homology) in the AAA family of ATPases Site-directed mutagenesis of the ATP-dependent protease FtsH. *Journal of Biological Chemistry* **1999,** *274* (37), 26225-26232.

(96) Yamada-Inagawa, T.; Okuno, T.; Karata, K.; Yamanaka, K.; Ogura, T., Conserved pore residues in the AAA protease, FtsH, are important for proteolysis and its coupling to ATP hydrolysis. *Journal of Biological Chemistry* **2003,** 50182-50187.

(97) Tomoyasu, T.; Yuki, T.; Morimura, S.; Mori, H.; Yamanaka, K.; Niki, H.; Hiraga, S.; Ogura, T., The Escherichia coli FtsH protein is a prokaryotic member of a protein family of putative ATPases involved in membrane functions, cell cycle control, and gene expression. *Journal of bacteriology* **1993,** *175* (5), 1344-1351.

(98) Suno, R.; Niwa, H.; Tsuchiya, D.; Zhang, X.; Yoshida, M.; Morikawa, K., Structure of the whole cytosolic region of ATP-dependent protease FtsH. *Molecular cell* **2006,** *22* (5), 575-585.

(99) Uthoff, M.; Baumann, U., Conformational flexibility of pore loop-1 gives insights into substrate translocation by the AAA+ protease FtsH. *Journal of structural biology* **2018,** *204* (2), 199-206.

(100) Bieniossek, C.; Schalch, T.; Bumann, M.; Meister, M.; Meier, R.; Baumann, U., The molecular architecture of the metalloprotease FtsH. *Proceedings of the National Academy of Sciences* **2006,** *103* (9), 3066-3071.

(101) Bieniossek, C.; Niederhauser, B.; Baumann, U. M., The crystal structure of apo-FtsH reveals domain movements necessary for substrate unfolding and translocation. *Proceedings of the National Academy of Sciences* **2009**, 21579-21584.

(102) Krzywda, S.; Brzozowski, A. M.; Verma, C.; Karata, K.; Ogura, T.; Wilkinson, A. J., The crystal structure of the AAA domain of the ATP-dependent protease FtsH of Escherichia coli at 1.5 Å resolution. *Structure* **2002,** *10* (8), 1073-1083.

(103) Kim, S. H.; Kang, G. B.; Song, H.-E.; Park, S. J.; Bea, M.-H.; Eom, S. H., Structural studies on Helicobacter pylori ATP-dependent protease, FtsH. *Journal of synchrotron radiation* **2008,** *15* (3), 208-210.

(104) Niwa, H.; Tsuchiya, D.; Makyio, H.; Yoshida, M.; Morikawa, K., Hexameric ring structure of the ATPase domain of the membrane-integrated metalloprotease FtsH from Thermus thermophilus HB8. *Structure* **2002,** *10* (10), 1415-1424.

(105) Karlberg, T.; van den Berg, S.; Hammarström, M.; Sagemark, J.; Johansson, I.; Holmberg-Schiavone, L.; Schüler, H., Crystal structure of the ATPase domain of the human AAA+ protein paraplegin/SPG7. *PLoS One* **2009,** *4* (10), e6975.

(106) Scharfenberg, F.; Serek-Heuberger, J.; Coles, M.; Hartmann, M. D.; Habeck, M.; Martin, J.; Lupas, A. N.; Alva, V., Structure and evolution of N-domains in AAA metalloproteases. *Journal of molecular biology* **2015,** *427* (4), 910-923.

(107) Baker, T. A.; Sauer, R. T., ClpXP, an ATP-powered unfolding and protein-degradation machine. *Biochimica et Biophysica Acta -Molecular Cell Research* **2012,** *1823* (1), 15-28.

(108) Kyrieleis, O. J.; Goettig, P.; Kiefersauer, R.; Huber, R.; Brandstetter, H., Crystal structures of the tricorn interacting factor F3 from Thermoplasma acidophilum, a zinc aminopeptidase in three different conformations. *Journal of molecular biology* **2005,** *349* (4), 787-800.

(109) Lee, S.; Augustin, S.; Tatsuta, T.; Gerdes, F.; Langer, T.; Tsai, F. T., Electron cryomicroscopy structure of a membrane-anchored mitochondrial AAA protease. *Journal of Biological Chemistry* **2011,** *286* (6), 4404-4411.

(110) Puchades, C.; Rampello, A. J.; Shin, M.; Giuliano, C. J.; Wiseman, R. L.; Glynn, S. E.; Lander, G. C., Structure of the mitochondrial inner membrane AAA+ protease YME1 gives insight into substrate processing. *Science* **2017,** *358* (6363), eaao0464.

(111) Tomoyasu, T.; Gamer, J.; Bukau, B.; Kanemori, M.; Mori, H.; Rutman, A.; Oppenheim, A.; Yura, T.; Yamanaka, K.; Niki, H., Escherichia coli FtsH is a membrane-bound, ATP-dependent protease which degrades the heat-shock transcription factor sigma 32. *The EMBO Journal* **1995,** *14* (11), 2551-2560.

(112) Herman, C., Ogura, T., Tomoyasu, T., Hiraga, S., Akiyama, Y., Ito, K., Thomas, R., D'Ari, R. and Bouloc, P., Cell growth and lambda phage development controlled by the same essential Escherichia coli gene, ftsH/hflB. *Proceedings of the National Academy of Sciences* **1993**, *90*(22), 10861-10865.

(113) Akiyama, Y., Kihara, A. and Ito, K., Subunit a of proton ATPase F0 sector is a substrate of the FtsH protease in Escherichia coli. *FEBS letters* **1996**, *399*(1-2), 26-28.

(114) Akiyama, Y.; Kihara, A.; Tokuda, H.; Ito, K., FtsH (HflB) is an ATP-dependent protease selectively acting on SecY and some other membrane proteins. *Journal of Biological Chemistry* **1996,** *271* (49), 31196-31201.

(115) Chiba, S.; Akiyama, Y.; Mori, H.; Matsuo, E. i.; Ito, K., Length recognition at the N-terminal tail for the initiation of FtsH-mediated proteolysis. *EMBO reports* **2000,** *1* (1), 47-52.

(116) Herman, C.; Thévenet, D.; Bouloc, P.; Walker, G. C.; D'Ari, R., Degradation of carboxy-terminal-tagged cytoplasmic proteins by the Escherichia coli protease HflB (FtsH). *Genes & developmental* **1998,** *12* (9), 1348-1355.

(117) Ogura, T.; Inoue, K.; Tatsuta, T.; Suzaki, T.; Karata, K.; Young, K.; Su, L. H.; Fierke, C. A.; Jackman, J. E.; Raetz, C. R., Balanced biosynthesis of major membrane components through regulated degradation of the committed enzyme of lipid A biosynthesis by the AAA protease FtsH (HflB) in Escherichia coli. *Molecular microbiology* **1999,** *31* (3), 833-844.

(118) Kihara, A., Akiyama, Y., and Ito, K., Different pathways for protein degradation by the FtsH/HflKC membrane-embedded protease complex: an implication from the interference by a mutant form of a new substrate protein, YccA. *Journal of Molecular Biology* **1998,** *279* (1), 175-188.

(119) Karata, K.; Verma, C. S.; Wilkinson, A. J.; Ogura, T., Probing the mechanism of ATP hydrolysis and substrate translocation in the AAA protease FtsH by modeling and mutagenesis. *Molecular microbiology* **2001,** *39* (4), 890-903.

(120) Akiyama, Y.; Ito, K., Roles of homooligomerization and membrane association in ATPase and proteolytic activities of FtsH *in vitro*. *Biochemistry* **2001,** *40* (25), 7687-7693.

(121) Okuno, T.; Yamada-Inagawa, T.; Karata, K.; Yamanaka, K.; Ogura, T., Spectrometric analysis of degradation of a physiological substrate σ32 by Escherichia coli AAA protease FtsH. *Journal of structural biology* **2004,** *146* (1-2), 148-154.

(122) Herman, C.; Prakash, S.; Lu, C. Z.; Matouschek, A.; Gross, C. A., Lack of a robust unfoldase activity confers a unique level of substrate specificity to the universal AAA protease FtsH. *Molecular cell* **2003,** *11* (3), 659-669.

(123) Freeman, M., Rhomboid proteases and their biological functions. *Annual review of genetics* **2008,** *42*, 191-210.

(124) Mayer, U.; Nüsslein-Volhard, C., A group of genes required for pattern formation in the ventral ectoderm of the Drosophila embryo. *Genes & development* **1988,** *2* (11), 1496-1511.

(125) Urban, S.; Lee, J. R.; Freeman, M., Drosophila rhomboid-1 defines a family of putative intramembrane serine proteases. *Cell* **2001,** *107* (2), 173-182.

(126) Wasserman, J. D.; Urban, S.; Freeman, M., A family of rhomboid-like genes: Drosophila rhomboid-1 and roughoid/rhomboid-3 cooperate to activate EGF receptor signaling. *Genes & development* **2000,** *14* (13), 1651-1663.

(127) Shilo, B.-Z., Signaling by the Drosophila epidermal growth factor receptor pathway during development. In *The EGF Receptor Family*, Elsevier: 2003; pp 147-156.

(128) Stevenson, L. G.; Strisovsky, K.; Clemmer, K. M.; Bhatt, S.; Freeman, M.; Rather, P. N., Rhomboid protease AarA mediates quorum-sensing in Providencia stuartii by activating TatA of the twin-arginine translocase. *Proceedings of the National Academy of Sciences* **2007,** *104* (3), 1003-1008.

(129) Wang, Y.; Maegawa, S.; Akiyama, Y.; Ha, Y., The role of L1 loop in the mechanism of rhomboid intramembrane protease GlpG. *Journal of molecular biology* **2007,** *374* (4), 1104-1113.

(130) Wu, Z.; Yan, N.; Feng, L.; Oberstein, A.; Yan, H.; Baker, R. P.; Gu, L.; Jeffrey, P. D.; Urban, S.; Shi, Y., Structural analysis of a rhomboid family intramembrane protease reveals a gating mechanism for substrate entry. *Nature Structural Molecular biology of the cell* **2006,** *13* (12), 1084.

(131) Schafer, N. P.; Truong, H. H.; Otzen, D. E.; Lindorff-Larsen, K.; Wolynes, P. G., Topological constraints and modular structure in the folding and functional motions of GlpG, an intramembrane protease. *Proceedings of the National Academy of Sciences* **2016,** *113* (8), 2098-2103.

(132) Wang, Y.; Zhang, Y.; Ha, Y., Crystal structure of a rhomboid family intramembrane protease. *Nature* **2006,** *444* (7116), 179.

(133) Paslawski, W.; Lillelund, O. K.; Kristensen, J. V.; Schafer, N. P.; Baker, R. P.; Urban, S.; Otzen, D. E., Cooperative folding of a polytopic α-helical membrane protein involves a compact N-terminal nucleus and nonnative loops. *Proceedings of the National Academy of Sciences* **2015,** *112* (26), 7978-7983.

(134) Guo, R.; Gaffney, K.; Yang, Z.; Kim, M.; Sungsuwan, S.; Huang, X.; Hubbell, W. L.; Hong, H., Steric trapping reveals a cooperativity network in the intramembrane protease GlpG. *Nat Chem Biol* **2016,** *12* (5), 353-360.

(135) Iwakura, M.; Nakamura, T.; Yamane, C.; Maki, K., Systematic circular permutation of an entire protein reveals essential folding elements. *Nat Struct Biol* **2000,** *7* (7), 580-5.

(136) Touchette, N. A.; Perry, K. M.; Matthews, C. R., Folding of dihydrofolate reductase from Escherichia coli. *Biochemistry* **1986,** *25* (19), 5445-52.

(137) Tian, J.; Woodard, J. C.; Whitney, A.; Shakhnovich, E. I., Thermal stabilization of dihydrofolate reductase using monte carlo unfolding

simulations and its functional consequences. *PLoS Comput Biol* **2015,** *11* (4), e1004207.

(138) Kim, Y. I.; Burton, R. E.; Burton, B. M.; Sauer, R. T.; Baker, T. A., Dynamics of substrate denaturation and translocation by the ClpXP degradation machine. *Mol Cell* **2000,** *5* (4), 639-48.

(139) Nicholls, S. B.; Hardy, J. A., Structural basis of fluorescence quenching in caspase activatable-GFP. *Protein Sci* **2013,** *22* (3), 247-57.

(140) Clarke, J.; Fersht, A. R., Engineered disulfide bonds as probes of the folding pathway of barnase: increasing the stability of proteins against the rate of denaturation. *Biochemistry* **1993,** *32* (16), 4322-9.

(141) Fersht, A. R., A kinetically significant intermediate in the folding of barnase. *Proc Natl Acad Sci U S A* **2000,** *97* (26), 14121-6.

(142) Makarov, A. A.; Protasevich, II; Lobachov, V. M.; Kirpichnikov, M. P.; Yakovlev, G. I.; Gilli, R. M.; Briand, C. M.; Hartley, R. W., Thermostability of the barnase-barstar complex. *FEBS Lett* **1994,** *354* (3), 251-4.

(143) Waldburger, C. D.; Schildbach, J. F.; Sauer, R. T., Are buried salt bridges important for protein stability and conformational specificity? *Nature structural biology* **1995,** *2* (2), 122-8.

(144) Sauer, R. T.; Milla, M. E.; Waldburger, C. D.; Brown, B. M.; Schildbach, J. F., Sequence determinants of folding and stability for the P22 Arc repressor dimer. *FASEB J* **1996,** *10* (1), 42-8.

(145) Robinson, C. R.; Rentzeperis, D.; Silva, J. L.; Sauer, R. T., Formation of a denatured dimer limits the thermal stability of Arc repressor. *J Mol Biol* **1997,** *273* (3), 692-700.

(146) Brennan, C. A.; Christianson, K.; La Fleur, M. A.; Mandecki, W., A molecular sensor system based on genetically engineered alkaline phosphatase. *Proc Natl Acad Sci U S A* **1995,** *92* (13), 5783-7.

(147) Lau, F. W.; Bowie, J. U., A method for assessing the stability of a membrane protein. *Biochemistry* **1997,** *36* (19), 5884-92.

(148) Jefferson, R. E.; Blois, T. M.; Bowie, J. U., Membrane proteins can have high kinetic stability. *J Am Chem Soc* **2013,** *135* (40), 15183-90.

(149) Zhou, Y.; Bowie, J. U., Building a thermostable membrane protein. *J Biol Chem* **2000,** *275* (10), 6975-9.

(150) Min, D.; Jefferson, R. E.; Bowie, J. U.; Yoon, T. Y., Mapping the energy landscape for second-stage folding of a single membrane protein. *Nat Chem Biol* **2015,** *11* (12), 981-7.

(151) Yang, Y.; Guo, R.; Gaffney, K.; Kim, M.; Muhammednazaar, S.; Tian, W.; Wang, B.; Liang, J.; Hong, H., Folding-Degradation Relationship of a

Membrane Protein Mediated by the Universally Conserved ATP-Dependent Protease FtsH. *Journal of the American Chemical Society* **2018,** *140* (13), 4656-4665.

(152) Baker, R. P.; Urban, S., Architectural and thermodynamic principles underlying intramembrane protease function. *Nature chemical biology* **2012,** *8* (9), 759-68.

(153) Zhou, H.-X.; Rivas, G.; Minton, A. P. J. A. R. B., Macromolecular crowding and confinement: biochemical, biophysical, and potential physiological consequences. *Annual Review of Biophysics* **2008,** *37*, 375-397.

(154) Munishkina, L. A.; Cooper, E. M.; Uversky, V. N.; Fink, A. L., The effect of macromolecular crowding on protein aggregation and amyloid fibril formation. *Journal of Molecular Recognition* **2004,** *17* (5), 456-464.

(155) del Álamo, M.; Rivas, G.; Mateu, M. G., Effect of macromolecular crowding agents on human immunodeficiency virus type 1 capsid protein assembly *in vitro*. *Journal of virology* **2005,** *79* (22), 14271-14281.

(156) Snoussi, K.; Halle, B., Protein self-association induced by macromolecular crowding: a quantitative analysis by magnetic relaxation dispersion. *Biophysical journal* **2005,** *88* (4), 2855-2866.

(157) Díaz-López, T.; Dávila-Fajardo, C.; Blaesing, F.; Lillo, M. P.; Giraldo, R., Early events in the binding of the pPS10 replication protein RepA to single iteron and operator DNA sequences. *Journal of molecular biology* **2006,** *364* (5), 909-920.

(158) Tokuriki, N.; Kinjo, M.; Negi, S.; Hoshino, M.; Goto, Y.; Urabe, I.; Yomo, T., Protein folding by the effects of macromolecular crowding. *Protein Science* **2004,** *13* (1), 125-133.

(159) Ittah, V.; Kahana, E.; Amir, D.; Haas, E., Applications of time-resolved resonance energy transfer measurements in studies of the molecular crowding effect. *Journal of Molecular Recognition* **2004,** *17* (5), 448-455.

(160) Spencer, D. S.; Xu, K.; Logan, T. M.; Zhou, H.-X., Effects of pH, salt, and macromolecular crowding on the stability of FK506-binding protein: an integrated experimental and theoretical study. *Journal of molecular biology* **2005,** *351* (1), 219-232.

(161) Sasaki, Y.; Miyoshi, D.; Sugimoto, N., Regulation of DNA nucleases by molecular crowding. *Nucleic acids research* **2007,** *35* (12), 4086-4093.

(162) Ai, X.; Zhou, Z.; Bai, Y.; Choy, W.-Y., 15N NMR spin relaxation dispersion study of the molecular crowding effects on protein folding under native conditions. *Journal of the American Chemical Society* **2006,** *128* (12), 3916-3917.

(163) Morán-Zorzano, M. T.; Viale, A. M.; Muñoz, F. J.; Alonso-Casajús, N.; Eydallín, G. G.; Zugasti, B.; Baroja-Fernández, E.; Pozueta-Romero, J.,

Escherichia coli AspP activity is enhanced by macromolecular crowding and by both glucose-1, 6-bisphosphate and nucleotide-sugars. *FEBS letters* **2007,** *581* (5), 1035-1040.

(164) Derham, B. K.; Harding, J. J., The effect of the presence of globular proteins and elongated polymers on enzyme activity. *Biochimica et Biophysica Acta - Proteins and Proteomics* **2006,** *1764* (6), 1000-1006.

Chapter 2 Innovative methods to study membrane protein degradation

Yiqing Yang, Ruiqiong Guo, Kristen Gaffney, Miyeon Kim, Shaima Muhammednazaar,
Wei Tian, Boshen Wang, Jie Liang, and Heedeok Hong

The experimental content of this chapter was published in J. Am. Chem. Soc. 2018, 140, 4656−4665.

Previous work of MP degradation has mostly focused on qualitative *in vivo* study or semi-quantitative *in vitro* study.[1-5] Also, the environmental conditions of *in vitro* degradation study have been mainly detergent micelles rather than native lipid bilayers.[4,5] Therefore, the field is in need of a new model system for the quantitative understanding of detailed degradation mechanisms. There have been two challenges in achieving this goal: (1) it has been difficult to reconstitute a large amount of the protein complexes of MP degradation machinery in the lipid bilayers for biochemical and biophysical analysis; (2) Although it is widely accepted that the degradation machinery for MPs recognizes their folding features as major criteria for substrate selection, the characterization of the folding properties of MPs is still a daunting task. In this chapter, I will describe the detailed procedures towards developing an *in vitro* system for quantitative kinetic analysis of MP degradation on the basis of understanding of the folding of MP substrates.

First, for functional reconstitution of MP degradation, I chose the membrane-integrated AAA+ protease FtsH of *E. coli* as a model degradation machine. The overexpression and purification of FtsH in high yield was achieved by using the pET-based expression vector equipped with a C-terminal His_6-tag and a T7-promotor as well as by screening of various BL21(DE)-based *E. coli* strains, the concentrations of inducer Isopropyl β-d-1-thiogalactopyranoside (IPTG), and induction times and temperatures. An optimal detergent condition for the purification of FtsH in a functional form has been screened for the two major activities of FtsH, i.e., ATPase activity and proteolysis activity in various detergent (micelles) and bilayer (bicelles and liposomes) environments.

Second, to study the folding-degradation relationship of FtsH-mediated MP degradation, I chose the TM domain of GlpG as a model substrate because the Hong lab has a capability to investigate the folding properties of GlpG (i.e., thermodynamic stability and unfolding kinetics) directly under native conditions, as well as has tested a variety of mutants with modified folding properties. To convert stable MP GlpG into a substrate for FtsH, I fused various degradation markers that are known to be specifically recognized by FtsH or universally recognized by *E. coli* AAA+ proteases.

Finally, I established the assays that can test the degradation *in vivo* and *in vitro*. To monitor the degradation of GlpG *in vivo*, I employed Western blotting to track the amount of GlpG tagged with an epitope after blocking protein synthesis with the antibiotic spectinomycin. To monitor the degradation *in vitro*, a fluorescence-based degradation assay was developed by conjugating an environment-sensitive fluorophore to GlpG. In this way, I was able to determine degradation rates of the MP substrate in real-time precisely.

Equipped with an ATP-regeneration system, the model system established in this way turned out to be the simplest one for investigating MP degradation so that the detailed chemical and physical principles of the degradation process can be studied.

FtsH expression and purification

Obtaining an active form of FtsH with efficient expression and purification methods were one main obstacle in this research project. After many trials with expression cell line, induction condition, purification buffer and detergent screening, a mature expression and purification method with repeatable FtsH yield and activity was discovered.

The coding region for full-length FtsH was PCR-amplified from genomic DNA of the *E. coli* strain MG1655 and subcloned into pET21a expression vector encoding C-terminal His_6-tag.

For FtsH expression, *E. coli* C43 (DE3) pLysS cells containing plasmids encoding FtsH were grown on selection plates (100 mg/L ampicillin) at 37°C. The liquid culture was inoculated with a single colony and grown in LB media (100 mg/L ampicillin) overnight at 37°C until the cells reach the stationary phase. The overnight culture was used to inoculate a fresh LB media (100 mg/L ampicillin) and cultivated to the mid-exponential phase (OD_{600nm} = 1.2) at 37°C. The culture was induced with 1 mM isopropyl β-D-thiogalactopyranoside (IPTG) and was grown at 37°C for an additional 3 hr.

Harvested cells were resuspended in 1/40 culture volume of resuspension buffer of 25 mM Tris-HCl (pH 8.0), 0.1% β-mercaptoethanol (BME) (v/v), 15% glycerol (v/v) and 0.5 mM phenylmethylsulfonyl fluoride (PMSF). Cells were lysed five times using EmulsiFlex-C5 pressure homogenizer (Avestin). After removal of cell debris by centrifugation in F21 rotor using a Sorvall RC6+ centrifuge (Thermo Fisher Scientific)

at 6,000 rpm for 30 min, the total membrane fraction was obtained by ultracentrifugation (Beckman Coulter, Type 45 Ti rotor) at 28,000 rpm for 2 hr. The total membrane pellets were resuspended in 1/50 culture volume Base Buffer (25 mM Tris-HCl pH 8.0, 200 mM KCl, 15% glycerol) using a tissue homogenizer. The membrane resuspension was solubilized by addition of Triton X-100 to a final concentration of 2% (w/v). Aggregation was removed by centrifugation at 12,000 rpm for 1 hr. FtsH was purified from resulting supernatant using Ni^{2+}-NTA affinity chromatography (Qiagen, 1 mL resin volume per liter culture). After washing the resin with a 10-resin volume of wash buffer (Base Buffer with 0.1% Triton X-100, 20 mM imidazole), bound FtsH was eluted with a 10-resin volume of Elution Buffer (Base Buffer with 0.1% Triton X-100, 0.1% BME, 200 mM imidazole). The eluent was concentrated using a centrifugal filtration unit (Millipore, 50 kDa MWCO). After removal of excess imidazole in a desalting column (Bio-Rad) equilibrated with Base Buffer with 0.1% Triton X-100 and 0.1% BME, FtsH was concentrated to the final volume of 0.5~1.0 mL per liter culture (typically, 60~150 μM). All purification procedures were carried out at 4°C. The protein concentration was determined by 660 nm protein assay (Bio-Rad), which was compatible with Triton X-100.

The highest yield of FtsH in a detergent-solubilized form was obtained in the order, DDM > DM > NP-40 ≈ TritonX^{TM}-100 > CHAPSO ≈ β-OG. The protease activity was not fully supported on high concentrations of all other detergents, except for NP-40 and TritonX-100, and eventually, the TritonX-100 was chosen based on its supportive performance on FtsH activity. **Figure 2.1** (right) is the comparison of ATPase activity in detergent NP-40 and Triton X^{TM}-100. Here, TritonX^{TM}-100

supported ATP hydrolysis slightly better. ATP hydrolysis was measured by an enzyme-coupled assay[6] (**Figure 2.1** left) in the presence of 5 mM ATP at 37°C.

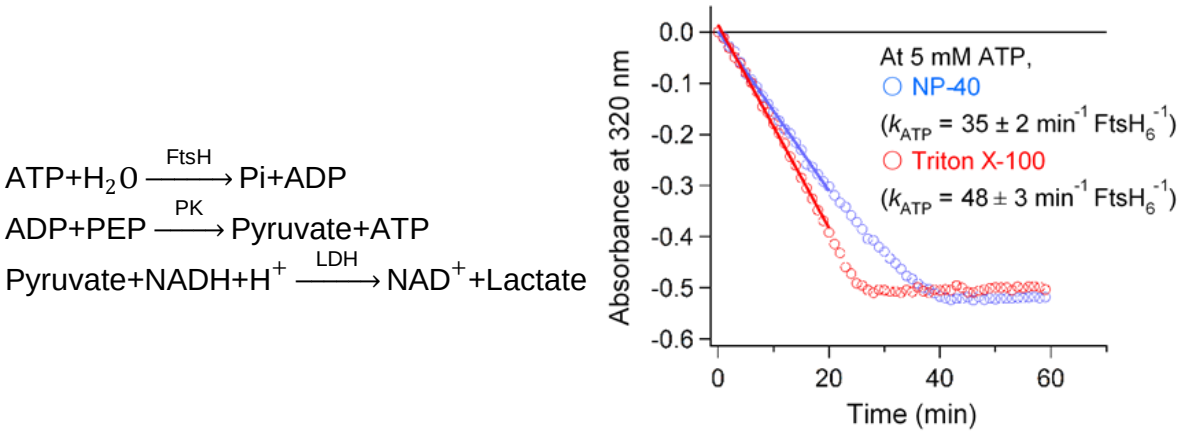

Figure 2.1 ATPase activity of FtsH measured in different detergent. The Y-axis represents the relative ATP consumption by the time as the NADH absorption signal decrease. PEP, phosphoenolpyruvic acid; PK, pyruvate kinase; LDH, lactate dehydrogenase. Same trend was observed in repeated experiments (n>3).

Design of a model membrane substrate using GlpG for *in vitro* degradation

The substrates for an *in vitro* assay of GlpG degradation were designed as in **Figure 2.2**. GlpG variants fused to the C-terminus of maltose binding protein (MBP) followed by a Tobacco Etch Virus (TEV) cleavage site were cloned into pET30a vector. The resulting plasmids encoded the proteins with an N (or C)-terminal His_6-tag. The MBP was to increase the yield of expression, and the TEV protease cleavage site was to let the fusion protein be site-specifically cleaved off from GlpG without disturbing other degradation markers.

FtsH is known to processively degrade a substrate starting from either N- or C-terminus by binding an unstructured tail (>20 residues) with diverse sequences as a

degradation marker.[7, 8] To establish GlpG as the model substrate, we chose four well-characterized degradation markers which are preferentially recognized by FtsH or other AAA+ proteases and examined their ability to induce GlpG degradation *in vivo* (in the following section). Here we chose “108” and “SsrA” for C-terminal. ‘108’ (-SLLWS) is an artificial FtsH-specific degradation marker.[9] “SsrA” (-AANDENYALAA) is a universal degradation marker can be recognized by all other AAA+ proteases.[10] For N-terminal, we employed the N-terminal tails (residues 1−23) of *E. coli* proteins YccA and Dps as degradation markers (**Figure 2.2**), which are known to be specifically recognized by FtsH and ClpXP, respectively.[7, 11]

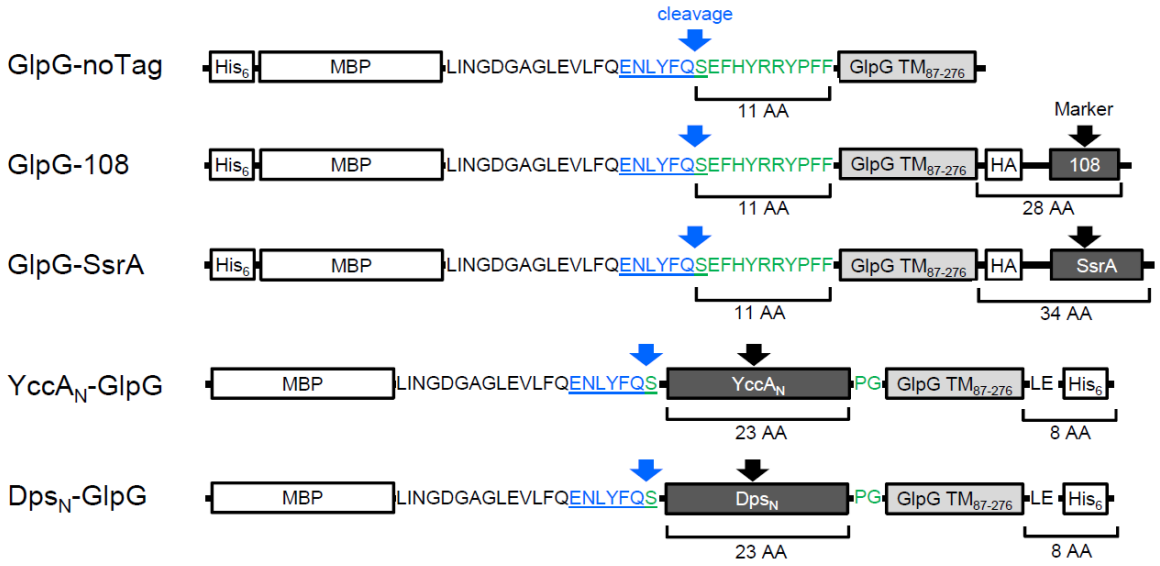

Figure 2.2 Substrate membrane protein GlpG design scheme and naming for *in vitro* degradation. Residues in blue are the TEV protease recognition sequence, and residues in green are the linkage peptides.

GlpG with a degradation marker was then tested by its proteolytic activity to confirm the active conformation was not affected by the marker. We use the second TM domain of lactose permease of *E. coli* fused to the staphylococcal nuclease (SN-LacYTM2: 25.7 kD) as a model substrate (**Figure 2.3**). GlpG cleaves the scissile peptide bond near the water-membrane interface of LacYTM2. This cleavage reaction can be measured by SDS-PAGE or fluorescence-based assay developed by the Hong group.[12] Here the SDS-PAGE data (**Figure 2.4**) show that all tested GlpG variants are fully functional and in the native conformation.

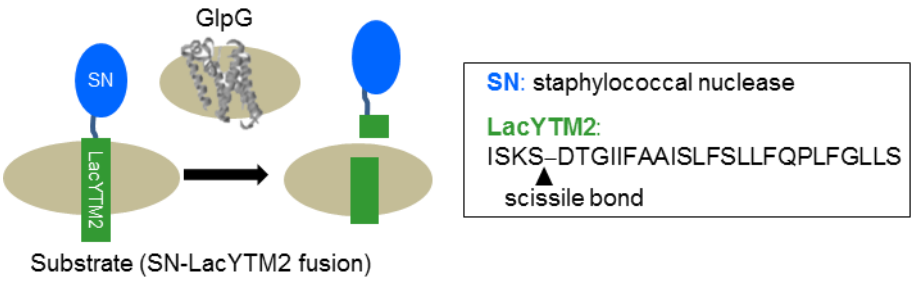

Figure 2.3 Activity assay of the model membrane substrate GlpG.

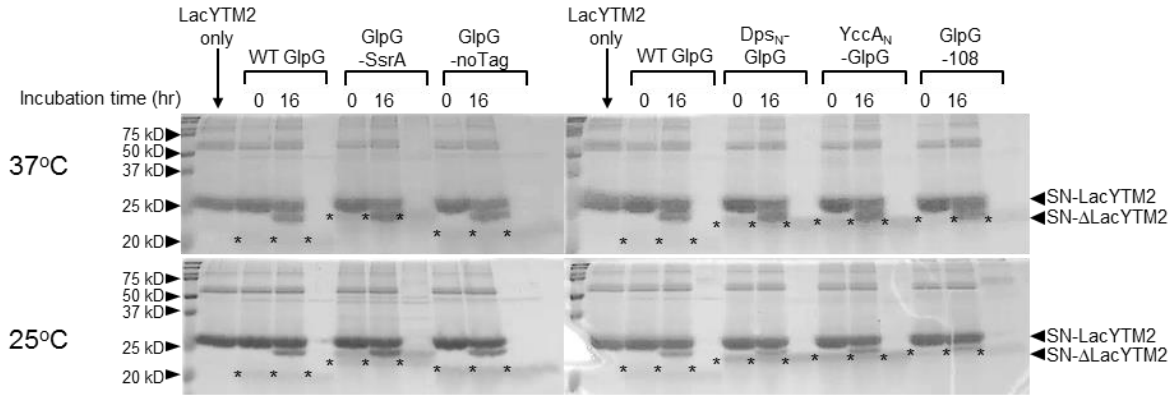

Figure 2.4 Activity of GlpG variants with various degradation markers measured by SDS-PAGE. The activity was measured under the same solution condition used for the degradation assay in 3% DMPC/DMPG/CHAPS bicelles. Briefly, GlpG (2 μM) and SN-LacYTM2 (10 μM), which were separately reconstituted in bicelles, were mixed and incubated for 16 hr at each temperature. This reaction yielded the cleavage product SN-ΔLacYTM2. The asterisk marks (*) on the gel indicate the location of GlpG variants.

Design of a model membrane substrate using GlpG for *in vivo* degradation

To validate the membrane protein GlpG substrate constructs can be degraded by FtsH in the cell, we design a similar set of constructs that can be tested *in vivo*. All *in vivo* constructs contain the TM domain of GlpG (residues 87−276) with N- or C-terminal degradation marker and FLAG or HA epitope, which were cloned into

pBAD/HisA vector (**Figure 2.5**). To test specific degradation by FtsH, we employed the E. coli strain with intact chromosomal ftsH (+*ftsH*) and the strain with disrupted ftsH (−*ftsH*).[13] *E. coli* AR3289 (+*ftsH*) and AR3291 (−*ftsH*) strains were transformed with each GlpG plasmid. Samples were then incubated at 37 °C, and an aliquot of each sample was taken at subsequent time points. Spun-down cells were resuspended with protein sample buffer and run on SDS-PAGE. GlpG degradation was monitored by Western blotting against HA or FLAG epitope. Then, the HA epitope was fused to the C-terminus of GlpG to investigate the effect of the N-terminal markers on GlpG degradation. However, it was found that the C-terminal HA tag can be recognized for degradation *in vivo*, and then two tandem Asp residues (DD)[14] were added after the epitope to suppress unwanted degradation from the C terminus (**Figure 2.6**). Thus, using this as a control, the specific effect of the N-terminal markers was studied.

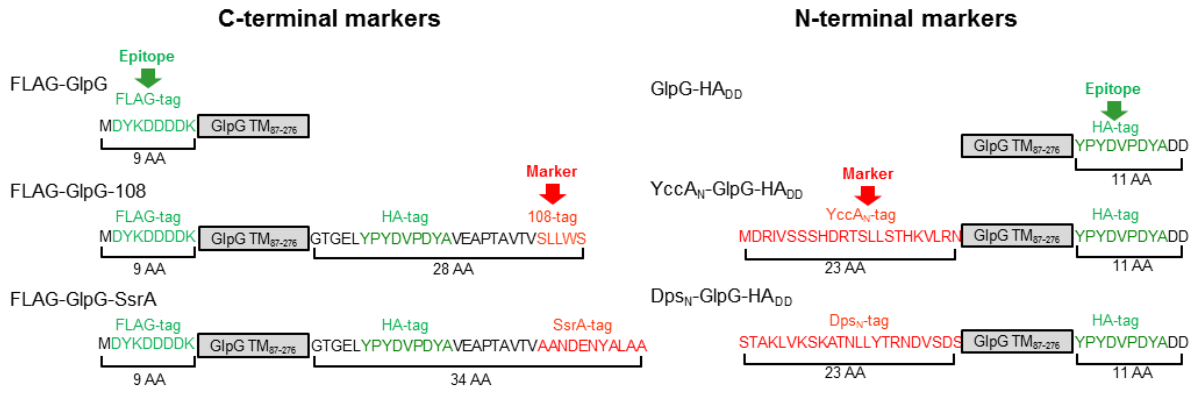

Figure 2.5 The constructs for measuring time-dependent degradation of GlpG. Possessing the (*left*)C-terminal degradation markers, the 108-tag, and the SsrA-tag and (*right*) the N-terminal markers, in the *+ftsH E. coli* strain, GlpG were then monitored by SDS-PAGE and Western blotting.

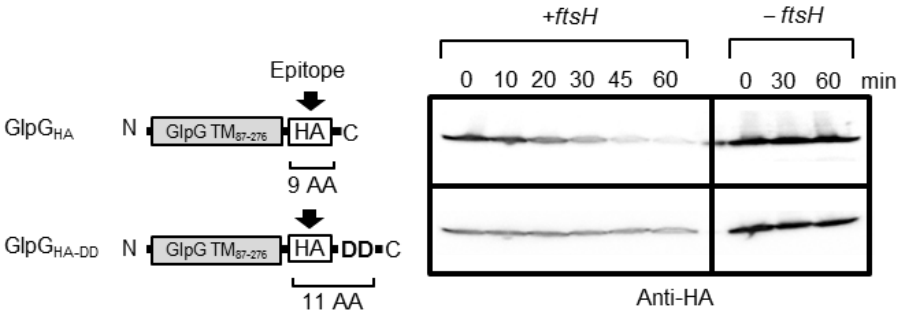

Figure 2.6 Modification of the N-terminal epitope on GlpG for FtsH degradation *in vivo*. (*Top*) The HA epitope induced unwanted degradation by FtsH, even in the absence of a specific marker. (*Bottom*) Addition of two Asp residues (DD) to the C-terminus suppressed the unwanted degradation.

Quantitative measurement of FtsH protease activity in *vitro*

We developed a fluorescence-based high-throughput *in vitro* assay that can precisely monitor the degradation of membrane proteins (**Figure 2.7**). GlpG with an engineered Cys residue was labeled with the thiol-reactive environment-sensitive

fluorophore NBD. Upon degradation, NBD fluorescence is quenched due to the transfer of the NBD label from the more hydrophobic bicellar phase to the aqueous phase.

First, I optimized the position for NBD labeling on GlpG. Three positions tested for single cysteine mutation (P95C, G172C, and V267C) are located at the membrane-water interface on TM1, TM3 and TM6 helices to achieve both efficient labeling and partition of NBD to the nonpolar lipid environment (**Figure 2.8a**). The sensitivity of each NBD label and its influence on the degradation rates were then tested. Time-dependent degradation of single-NBD labeled GlpG variants with the C-terminal 108 tag was measured using NBD-fluorescence and SDS-PAGE (**Figure 2.8b**). $GlpG_{172C\text{-}NBD}$-108 was chosen because it exhibited the largest fluorescence change upon degradation among these variants and was degraded at a similar rate to wild-type GlpG-108 lacking Cys mutation ($GlpG_{WT}$-108) as seen from SDS-PAGE.

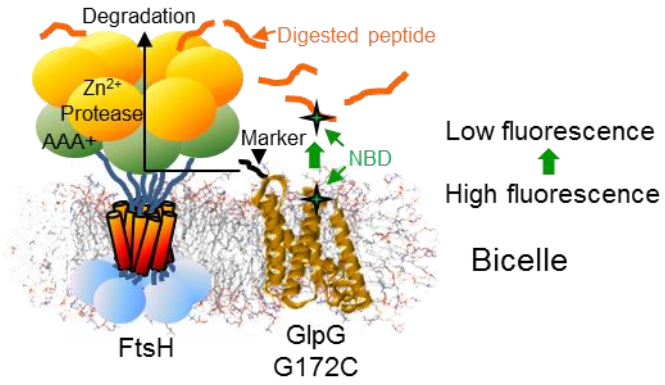

Figure 2.7 Fluorescence-based degradation assay to monitor membrane protein degradation.

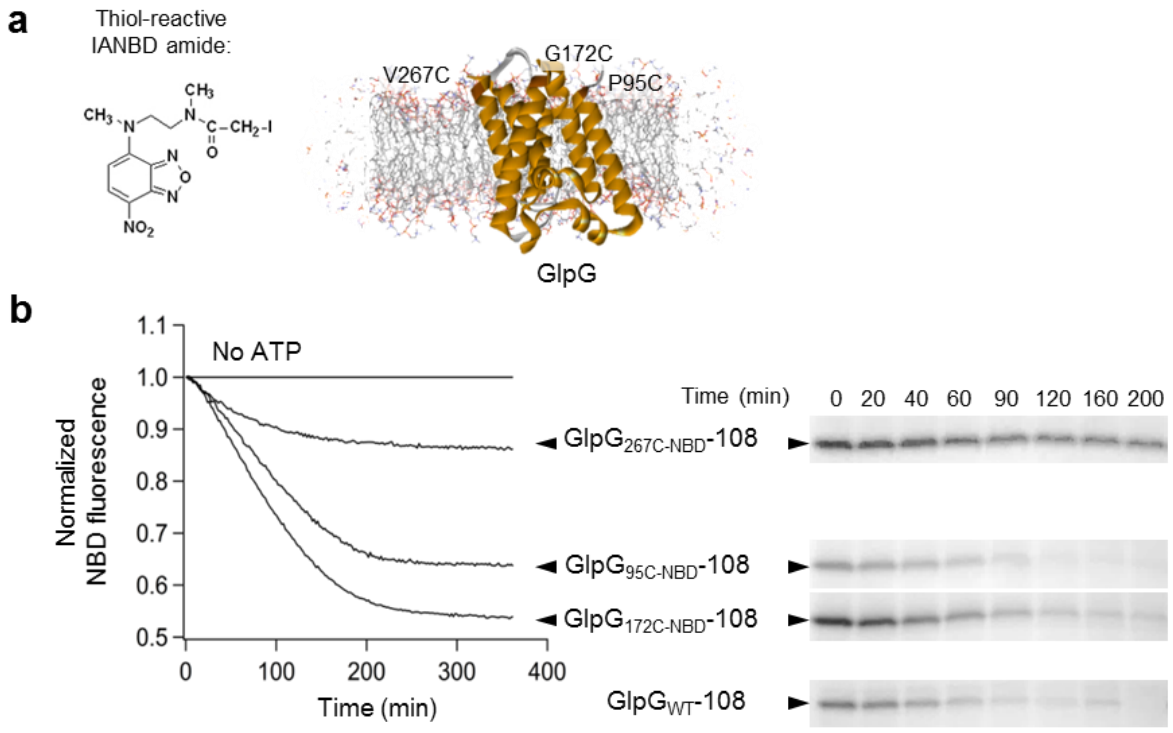

Figure 2.8 Optimization of NBD labeling position on GlpG for the fluorescence-based membrane protein degradation assay. (a) Display of Cysteine positions tested relative to the position of GlpG TM (residues 87−276) terminal. (b) The relative degradation rate of each GlpG mutant compared to wildtype in fluorescence-based assay and SDS-PAGE. Same trend was observed in repeating experiments(n=3).

On the basis of the optimized construct, GlpG variants with a degradation marker fused to the N-(Dps_N or $YccA_N$) or C-terminus (108 or SsrA) were prepared.

GlpG degradation by FtsH was measured in 3% DMPC/DMPG/CHAPS bicellar solution (q = 2.8; 2 μM FtsH; 20 mM HEPES, pH 7.5, 100 mM KCl, 15% glycerol, 0.1% BME, and 0.4 mM ZnCl2) with an ATP regeneration system (5 unit/mL pyruvate kinase and 10 mM PEP) at 37°C. The rationale of choosing the negatively

charged bicelles is described in **Chapter 3**. GlpG degradation was initiated by addition of 2 mM ATP (the final concentration) and monitored by quenching of NBD fluorescence at $\lambda_{emission}$ = 545 nm with $\lambda_{excitation}$ = 485 nm on a microplate reader over time. The net fluorescence change induced by GlpG degradation was obtained by subtracting NBD fluorescence with ATP from that without ATP.

Figure 2.9 shows an example of how the degradation rate of NBD-labeled GlpG-$108_{G172C\text{-}NBD}$ was determined using the fluorescence assay. First, NBD fluorescence at increasing concentrations of GlpG was measured in the absence and presence of ATP (**Figure 2.9a**). Then, the difference fluorescence (ΔF) indicates the time-dependent degradation of GlpG (**Figure 2.9b**). The initial linear slope of each trace (ΔF/min) in the early time range is related to the initial degradation rate (see below).

The plateaued region (**Figures 2.9a-b**) in the later period of time of each trace indicates that the degradation reaction was completed. If the plateaued fluorescence intensity in the absence and presence of ATP ($F_{\infty, -ATP}$ and $F_{\infty, +ATP}$, respectively: **Figure 2.10a**) and the difference fluorescence intensity in the plateaued region(i.e., $\Delta F_{\infty} = F_{\infty, -ATP} - F_{\infty, +ATP}$: **Figure 2.10a**) are linear as a function of GlpG concentration, it indicates that the total fluorescence intensity changes (ΔF_{∞}) are directly correlated with the changes in the molar concentrations of the substrate (i.e., the amount of degraded GlpG). From the slope($\Delta F_{\infty}/\Delta$[GlpG]) in **Figure 2.10b** and the slope in the trace of time-dependent fluorescence changes ($\Delta F/min$) in **Figure 2.9b**, we can determine the degradation rate of GlpG (Δ[GlpG]/min, **Equation 1**).

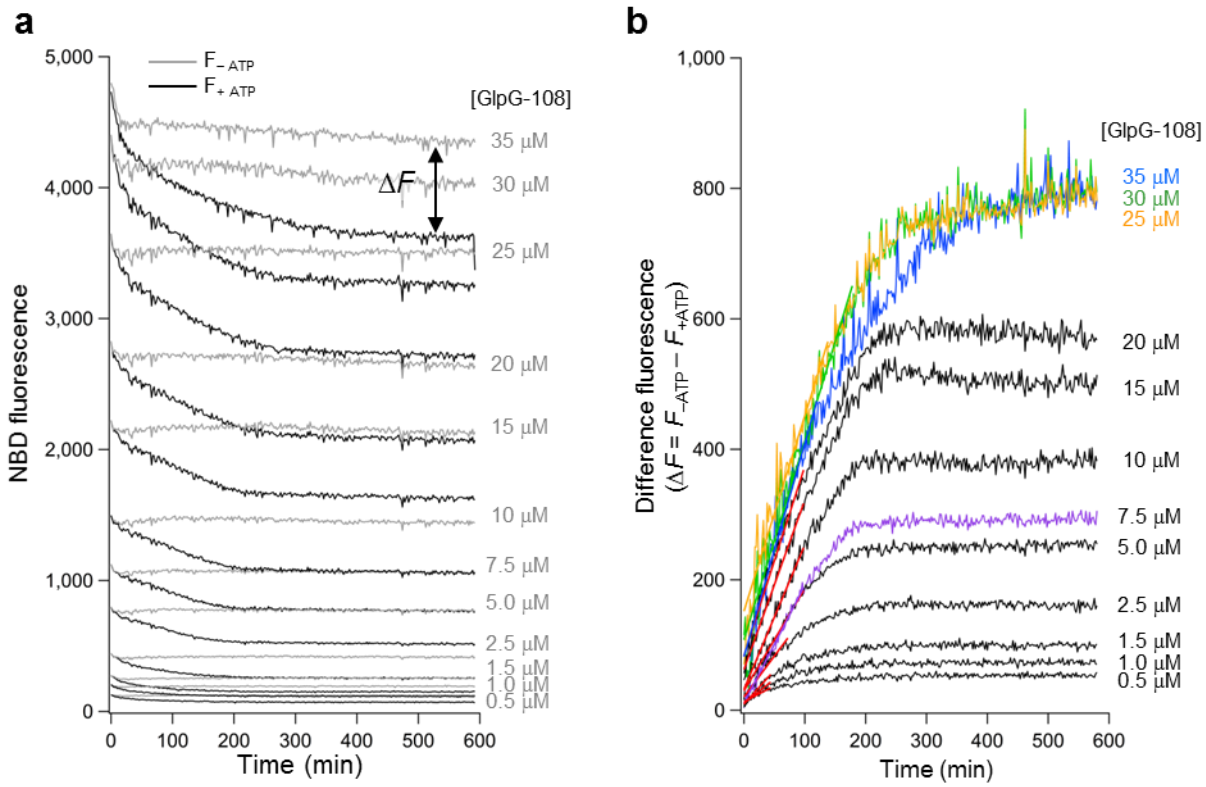

Figure 2.9 Example of GlpG-108$_{G172C\text{-}NBD\ deg}$ degradation with fluorescence assay. (a) Time-dependent NBD fluorescence was monitored at various concentrations of GlpG-108 in the absence ($F_{–ATP}$) and presence (F_{+ATP}) of ATP (original data). (b) Time-dependent change of the net fluorescence intensity indicates GlpG degradation. It was obtained by subtracting the fluorescence intensity without ATP from that with ATP at each GlpG concentration ($\Delta F = F_{–ATP} – F_{+ATP}$).

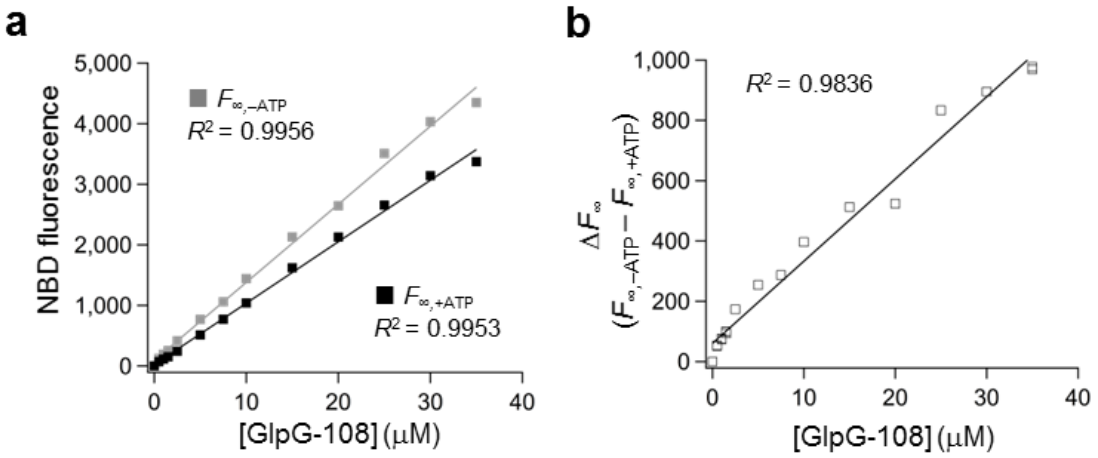

Figure 2.10 Correlation of the relative fluorescence intensity change to GlpG concentration change. (a) For each repeat of experiment (n>3), the average of the plateau region of the NBD fluorescence intensity in the absence ($F_{\infty, -ATP}$) or presence ($F_{\infty, +ATP}$) of ATP in a time range was obtained as Y-axis, which was then correlated to each protein concentration where the fluorescence intensity change measured. (b) The net intensity change ($\Delta F_\infty = F_{\infty, -ATP} - F_{\infty,+ATP}$) is linear as a function of GlpG concentration. ν_{deg}, GlpG degradation rate by each FtsH hexamer per minute, is defined as:

$$\nu_{\mathrm{deg}} = \frac{\dfrac{\Delta F}{\min}}{\dfrac{\Delta F_\infty}{[\mathrm{GlpG}]}} \times \frac{1}{[\mathrm{FtsH}_6]} \qquad \textbf{(Equation 1)},$$

where ΔF/min and ΔF_∞/[GlpG] were obtained from the slopes from Figures 2.9b and 2.10b and further normalized by FtsH hexamer concentration ([$FtsH_6$]), respectively.

Finally, the degradation rates of GlpG can be plotted as a function of the initial GlpG concentration (**Figure 2.11**). Here the concentration of GlpG was expressed as a mole fraction of GlpG out of the total concentration of the bicellar constituents, i.e., X_{GlpG} = [GlpG] / ([GlpG]+[DMPC]+[DMPG]+[CHAPS]+[FtsH]). Because both enzyme

(FtsH) and substrate (GlpG) are partitioned into bicelles so that it is more relevant to express the concentrations of those species out of the total amphiphile concentration.

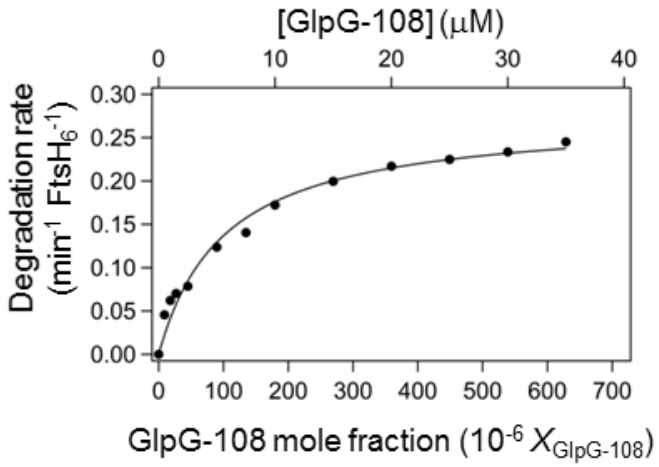

Figure 2.11 The final plot of degradation rate *vs.* GlpG concentration. This example plot was used for enzyme kinetic analysis using Michaelis-Menten and Hill equations. Full plot with error bars was shown in Chapter 3.

The plots of the degradation rates vs. GlpG concentrations were fitted to the Michaelis-Menten equation:

$$v_{\mathrm{deg}} = \frac{k_{\mathrm{cat,deg}} X_{\mathrm{GlpG}}}{K_{\mathrm{m,deg}} + X_{\mathrm{GlpG}}} \qquad \textbf{(Equation 2)},$$

where v_{deg} is GlpG degradation rate by each FtsH hexamer per min, $k_{\mathrm{cat,\,deg}}$ is maximal degradation turnover number of FtsH hexamer per min, and $K_{\mathrm{m,\,deg}}$ is the mole fraction of GlpG (see below) at which the degradation rate reaches a half maximum. Alternatively, the same plots were also fitted to the Hill equation:

$$v_{\mathrm{deg}} = \frac{X_{\mathrm{GlpG}}{}^{n_{\mathrm{H,deg}}}}{K_{\mathrm{m,deg}}{}^{n_{\mathrm{H,deg}}} + X_{\mathrm{GlpG}}{}^{n_{\mathrm{H,deg}}}} \qquad \textbf{(Equation 3)},$$

where $n_{\mathrm{H,\,deg}}$ is Hill constant of GlpG degradation by FtsH hexamer.

REFERENCES

REFERENCES

(1) Neal, S., Jaeger, P.A., Duttke, S.H., Benner, C., Glass, C.K., Ideker, T. and Hampton, R.Y., The Dfm1 Derlin is required for ERAD retrotranslocation of integral membrane proteins. *Molecular cell* **2018**, *69*(2), 306-320.

(2) Sun, Z. and Brodsky, J.L., The degradation pathway of a model misfolded protein is determined by aggregation propensity. *Molecular biology of the cell* **2018**, *29*(12), pp.1422-1434.

(3) Carvalho, P., Goder, V., and Rapoport, T. A., Distinct ubiquitin-ligase complexes define convergent pathways for the degradation of ER proteins. *Cell* **2006,** *126* (2), 361-373.

(4) Kihara, A., Akiyama, Y. and Ito, K., Dislocation of membrane proteins in FtsH-mediated proteolysis. *The EMBO Journal* **1999**, *18*(11), pp.2970-2981.

(5) Herman, C.; Prakash, S.; Lu, C. Z.; Matouschek, A.; Gross, C. A., Lack of a robust unfoldase activity confers a unique level of substrate specificity to the universal AAA protease FtsH. *Molecular cell* **2003,** *11* (3), 659-669.

(6) Nørby, J.G., Coupled assay of Na+, K+-ATPase activity. In *Methods in enzymology* **1988** 156, 116-119. Academic Press.

(7) Chiba, S.; Akiyama, Y.; Mori, H.; Matsuo, E. i.; Ito, K., Length recognition at the N-terminal tail for the initiation of FtsH-mediated proteolysis. *EMBO reports* **2000,** *1* (1), 47-52.

(8) Chiba, S.; Akiyama, Y.; Ito, K., Membrane protein degradation by FtsH can be initiated from either end. *Journal of bacteriology* **2002,** *184* (17), 4775-4782.

(9) Herman, C.; Thévenet, D.; Bouloc, P.; Walker, G. C.; D'Ari, R., Degradation of carboxy-terminal-tagged cytoplasmic proteins by the Escherichia coli protease HflB (FtsH). *Genes & developmental* **1998,** *12* (9), 1348-1355.

(10) Farrell, C. M.; Grossman, A. D.; Sauer, R. T., Cytoplasmic degradation of ssrA-tagged proteins. *Molecular microbiology* **2005,** *57* (6), 1750-1761.

(11) Flynn, J. M.; Neher, S. B.; Kim, Y.-I.; Sauer, R. T.; Baker, T. A., Proteomic discovery of cellular substrates of the ClpXP protease reveals five classes of ClpX-recognition signals. *Molecular cell* **2003,** *11* (3), 671-683.

(12) Guo, R.; Gaffney, K.; Yang, Z.; Kim, M.; Sungsuwan, S.; Huang, X.; Hubbell, W. L.; Hong, H., Steric trapping reveals a cooperativity network in the intramembrane protease GlpG. *Nature chemical biology* **2016,** *12* (5), 353.

(13) Ogura, T.; Inoue, K.; Tatsuta, T.; Suzaki, T.; Karata, K.; Young, K.; Su, L. H.; Fierke, C. A.; Jackman, J. E.; Raetz, C. R., Balanced biosynthesis of major membrane components through regulated degradation of the

committed enzyme of lipid A biosynthesis by the AAA protease FtsH (HflB) in Escherichia coli. *Molecular microbiology* **1999,** *31* (3), 833-844.

(14) Gottesman, S.; Roche, E.; Zhou, Y.; Sauer, R. T., The ClpXP and ClpAP proteases degrade proteins with carboxy-terminal peptide tails added by the SsrA-tagging system. *Genes & developmental* **1998,** *12* (9), 1338-1347.

Chapter 3 Folding-Degradation Relationship of a Membrane Protein Mediated by the Universally Conserved ATP-Dependent Protease FtsH

Yiqing Yang, Ruiqiong Guo, Kristen Gaffney, Miyeon Kim, Shaima Muhammednazaar,
Wei Tian, Boshen Wang, Jie Liang, and Heedeok Hong

The content of this chapter was published in J. Am. Chem. Soc. 2018, 140, 4656−4665.

Summary

ATP-dependent protein degradation mediated by AAA+ proteases is one of the major cellular pathways for protein quality control and regulation of functional networks. While a majority of studies of protein degradation have focused on water-soluble proteins, it is not well understood how membrane proteins with abnormal conformation are selectively degraded. The knowledge gap stems from the lack of an *in vitro* system in which detailed molecular mechanisms can be studied as well as difficulties in studying membrane protein folding in lipid bilayers. To quantitatively define the folding-degradation relationship of membrane proteins, we reconstituted the degradation using the conserved membrane-integrated AAA+ protease FtsH as a model degradation machine and the stable helical-bundle membrane protein GlpG as a model substrate in the lipid bilayer environment. We demonstrate that FtsH possesses a substantial ability to actively unfold GlpG, and the degradation significantly depends on the stability and hydrophobicity near the degradation marker. We find that FtsH hydrolyzes 380−550 ATP molecules to degrade one copy of GlpG. Remarkably, FtsH overcomes the dual energetic burden of substrate unfolding and membrane dislocation with the ATP cost comparable to that for water-soluble substrates by robust ClpAP/XP proteases. The physical principles elucidated in this study provide general insights into membrane protein degradation mediated by ATP-dependent proteolytic systems.

Introduction

ATP-dependent proteolysis is an essential cellular process to degrade damaged or misfolded proteins and to modulate the concentration of regulatory proteins.[1] This process is carried out by AAA+ proteases including ClpXP, ClpAP, Lon, HslUV,

FtsH, and 26S proteasomes, in which hexameric AAA+ ATPase binds substrates possessing degradation markers, and actively unfolds and translocates them into a protease chamber for degradation.[2] Current knowledge on ATP-dependent proteolysis is largely limited to degradation of water-soluble proteins with insufficient understanding for membrane proteins. This discrepancy is mainly due to the lack of a proper *in vitro* system for detailed analysis of degradation mechanisms. Also, inherent difficulties in studying membrane protein folding have hindered investigation of the quantitative relationship between folding and degradation.

FtsH family proteins are widely conserved AAA+ proteases localized in the inner membranes of bacteria and mitochondria, and in the thylakoid membranes of chloroplasts.[3] They generally consist of an N-terminal transmembrane (TM) domain, and aqueous C-terminal AAA+ and Zn^{2+}-metalloprotease domains, which assemble into a hexamer for function.[4, 5] In their respective membranes, FtsH proteases serve as major protein quality inspectors by degrading misassembled or damaged membrane proteins, as well as short-lived water-soluble enzymes and transcription factors.[6] In *E. coli*, disruption of the gene encoding FtsH induces the envelope stress response and leads to a severe growth defect.[6] In yeast, defects in FtsH orthologs cause impaired assembly of the respiratory chain and alter mitochondrial morphology.[7, 8] In plant, FtsH in chloroplasts mediates turnover of the photo oxidized core proteins of the photosynthetic reaction center and unassembled subunits in the electron transfer chain.[9, 10] In human mitochondria, mutations in FtsH orthologs paraplegin and AFG3L2 are implicated in severe neurological disorders such as spastic paraplegia and spinocerebellar ataxia.[11, 12] Compared to other AAA+ proteases, FtsH is known to possess unique features in recognition of substrates.

FtsH is the weakest at hydrolyzing ATP and unfolding water-soluble model proteins.[13] While ClpXP and ClpAP rapidly unfold and degrade stable water-soluble proteins,[14-16] FtsH cannot degrade them.[17, 18] FtsH degrades a misfolded variant of the membrane protein diacylglycerol kinase (DGK), but cannot degrade wildtype or a thermostable variant *in vivo*.[18] Therefore, it has been proposed that FtsH lacks robust unfoldase activity, which allows for selective degradation of unstable or misfolded proteins. These findings also suggest that FtsH degrades proteins depending on their spontaneous unfolding, and ATP hydrolysis is mainly used to translocate unfolded substrates.[18]

To understand how FtsH degrades membrane proteins, several key questions need to be answered. First, although FtsH is known to lack the ability to actively unfold water-soluble substrates, the relationship between the intrinsic folding properties of a membrane substrate (e.g., stability and unfolding rate) and its degradation has not been quantitatively studied. To define the folding-degradation relationship, it is necessary to establish a model membrane substrate with defined structure and folding properties that can be quantitatively characterized. Second, to degrade membrane substrates, FtsH dislocates their hydrophobic TM segments from the bilayer to the proteolytic active site in the cytosol using ATP hydrolysis.[17] Single-molecule force spectroscopy and thermodynamic analysis indicate that dislocating a single TM helix from the bilayer to water in an unfolded form requires an enormous free energy cost (50−100 kcal/mol).[19,20] With the proposed weak unfoldase activity, how can FtsH drive such a vastly unfavorable process? Third, the proposed weak ATPase and unfoldase activities have been mainly derived from *in vitro* studies in

micellar solution.[13, 18] However, does the micellar condition fully support native FtsH activity?

To answer these questions, we reconstituted membrane protein degradation mediated by *E. coli* FtsH using the stable helical-bundle membrane protein GlpG of *E. coli* as a model substrate in the bilayer environment provided by bicelles. Bicelles are aqueous lipid-detergent assemblies in which bilayer fragments are edge-stabilized by certain detergents.[21] Measuring the stability and unfolding rate of GlpG directly under native conditions was enabled by steric trapping,[22] a novel method for studying membrane protein folding. We demonstrate that contrary to the previous proposals, FtsH can actively unfold the thermodynamically and kinetically stable membrane protein GlpG and the degradation is significantly influenced by the unfolding energy landscape and the hydrophobicity of the substrate. FtsH efficiently utilizes ATP hydrolysis to degrade membrane proteins, overcoming the dual energetic burden of substrate unfolding and membrane dislocation.

Results

Bicelles enhance ATPase activity of FtsH and allow facile protein diffusion.

To establish an ideal *in vitro* system for quantitative investigation of FtsH function, we first optimized its ATPase activity by testing various lipid conditions, i.e., micelles, bicelles and liposomes (**Figure 3.1** and **Table 3.1**).

In detergent Triton X-100, the maximal ATP hydrolysis rate per FtsH hexamer ($k_{cat,ATP}$) was 51 ± 2 min^{-1} $FtsH_6^{-1}$, and the ATP concentration required for half-maximal velocity ($K_{m,ATP}$) was 400 ± 50 μM from Michaelis−Menten kinetics. Surprisingly, in

the large neutral (DMPC/CHAPS) and negatively charged (DMPC/DMPG/CHAPS) bicelles (disk diameter ≈ 30 nm [23]), $k_{cat,ATP}$ substantially increased by 3.3 and 2.5 fold, respectively, relative to that in Triton X-100, and $K_{m,\ ATP}$ decreased by half. FtsH reconstituted in liposomes composed of *E. coli,* or DMPC/DMPG lipids displayed higher overall ATPase activity than in Triton X-100 (**Figure 3.1**). To quantify ATP hydrolysis rate in the liposomes, we analyzed the orientation distribution of FtsH inserted in the liposomes using limited proteolysis (**Figure 3.2**). > 90% of FtsH was oriented with the AAA+, and protease domains outside, accessible to ATP added to the outside of the liposomes. ATPase activity was negligible in detergent CHAPS. Thus, enhanced ATP hydrolysis in bicelles appears mainly due to the interaction of FtsH with the bilayered lipid region rather than with detergents. Notably, $k_{cat,ATP}$ in native *E. coli* lipids was similar to that in DMPC/DMPG/CHAPS bicelles. Many AAA+ proteases exhibit moderate positive cooperativity in ATP hydrolysis with Hill coefficients ($n_{H,\ ATP}$) of 1.4−2.0.[24, 25, 26, 27] In contrast, FtsH lacked cooperativity ($n_{H,ATP}$ = 0.9−1.0) in all tested lipid environments, implying either negligible coupling among the AAA+ subunits or a 1:1 binding stoichiometry between ATP and FtsH hexamer.

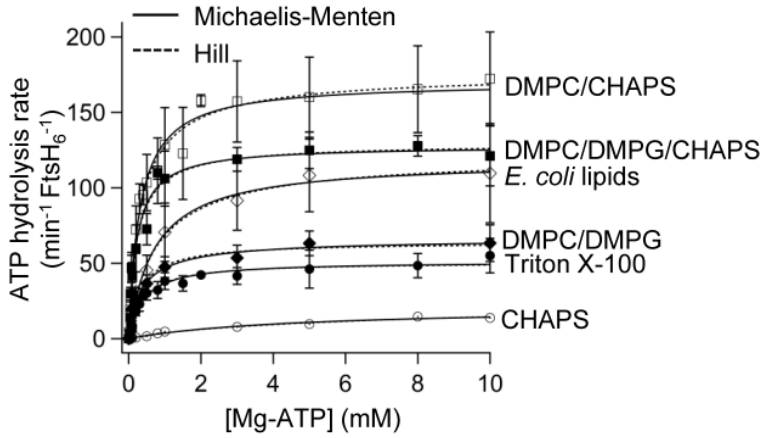

Figure 3.1 ATPase activity of FtsH in various lipid environments. Measured in 3% (w/v) Triton X-100, bicelles (DMPC/CHAPS, q = 2.8; DMPC/DMPG/ CHAPS, molar ratio = 3:1:1.4), liposomes (*E. coli* phospholipids; DMPC/DMPG, [DMPC]/[DMPG] = 3:1) and 3% (w/v) CHAPS. Data are represented as mean ± SEM (n = 3).

	Michaelis-Menten		Hill coefficient
	$k_{cat,ATP}$[a] (min^{-1} $FtsH_6^{-1}$)	$K_{m,ATP}$[a] (μM)	$n_{H,ATP}$[b]
DMPC/CHAPS	170 ± 4	310 ± 30	0.9 ± 0.1
DMPC/DMPG/CHAPS	128 ± 4	220 ± 30	1.0 ± 0.1
Triton X-100	51 ± 2	400 ± 50	1.0 ± 0.1
E. coli lipids	118 ± 3	700 ± 70	0.9 ± 0.1
DMPC/DMPG	64 ± 2	330 ± 50	0.9 ± 0.1
CHAPS	21 ± 2	4,700 ± 1,000	0.8 ± 0.2

All measurements were performed with [FtsH] = 2μM in 3% (w/v) total amphiphile concentration at 37ºC.
[a] $k_{cat,ATP}$ and $K_{m,ATP}$ values are from nonlinear least square fits of data in Figure 3.1 to the Michaelis-Menten equation (See Methods Equation 2).
[b] $n_{H,ATP}$ was obtained from nonlinear least squares fits of data in Figure 3.1 to the Hill equation (See Methods Equation 3).

Table 3.1 Kinetic parameters of ATPase activity of FtsH in various lipid environments.

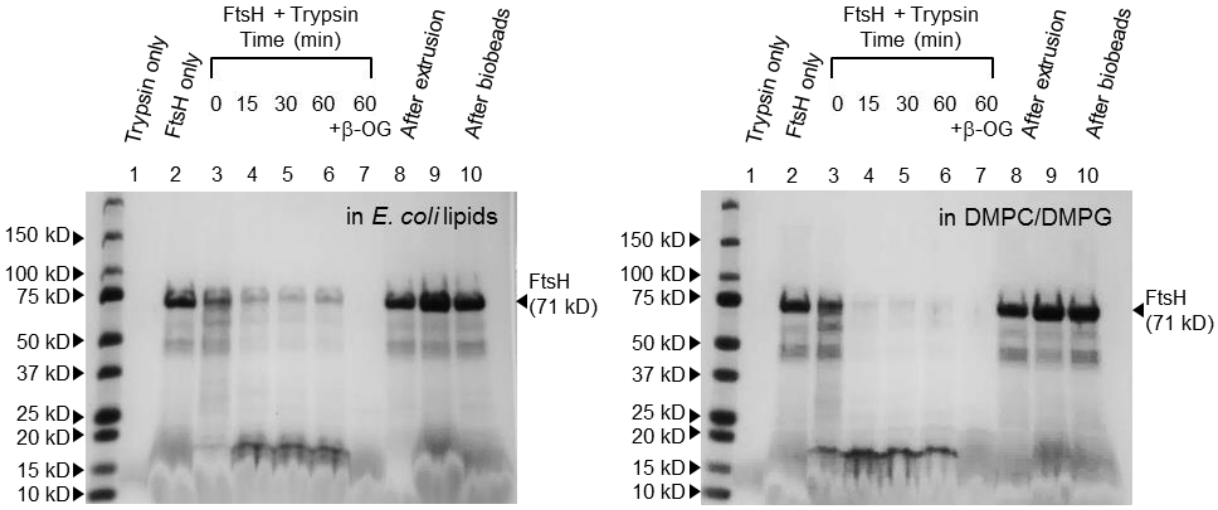

Figure 3.2 Analysis of the orientation distribution of FtsH in liposomes and tracking the protein loss during the reconstitution. FtsH purified in Triton X-100 (lanes 2) was reconstituted in (*left*) *E. coli* phospholipids or (*right*) DMPC/DMPG lipids for ATPase assay. For reconstitution, extruded liposomes (58 mM) were soaked with 0.5 mM (2 × CMC) Triton X-100, and detergent-solubilized FtsH was added to the lipid-detergent mixture ([FtsH] = 10 μM, lanes 9). Detergents were gradually removed using biobeads at 25 °C for 4 hr. The resulting proteoliposomes (lanes 10) were extruded again to remove protein aggregation. After these steps, ~60% of FtsH was lost (compare lanes 8 and 10). The orientation distribution of FtsH was analyzed by limited trypsin digestion (FtsH-to-trypsin mass ratio = 50), which proteolyzed its large cytoplasmic portion containing AAA+ and Zn^{2+} protease domains (52 kD; lanes 3-6). Solubilization of proteoliposomes with b-octylglucoside (β-OG) led to complete digestion of FtsH (lanes 7). Overall, >90% of FtsH was inserted into liposomes with its cytoplasmic portion pointing outside.

We further tested bicelles for the ability to mediate facile diffusion and mixing of the lipid and protein components (**Figure 3.3**), which is crucial for quantitative analysis of

enzyme function. We employed a FRET-based mixing assay developed for studying membrane fusion.[28] First, to test lipid diffusion, bicelles containing NBD (donor)- and rhodamine (acceptor)-labeled lipids were prepared, in which NBD fluorescence was highly quenched by rhodamine due to FRET. Upon mixing of the fluorescent bicelles with the bicelles without fluorescent labels, NBD fluorescence rapidly increased within a minute to the level of the homogeneously mixed state. We similarly tested protein diffusion. The model substrate GlpG labeled with either NBD or rhodamine was incorporated together in bicelles, and then mixing of the fluorescent protein-bicelle complex with the bicelles without fluorescent labels was monitored by FRET. We observed rapid protein diffusion in a similar time scale to that of lipid diffusion. This result demonstrates that a bicelle is not a discrete lipid assembly but subject to spontaneous fusion and dissociation, enabling facile mixing of lipid and protein components throughout the entire hydrophobic phase in solution.

It would be ideal to study FtsH function in pure lipid bilayers. However, in liposomes, each of which is regarded as a discrete assembly, it is inherently difficult to control substrate-to-enzyme ratio, and their relative orientation and mixing. Thus, we chose the negatively charged DMPC/DMPG/CHAPS bicelles as a lipid medium because of their ability to support ATPase activity similar to native *E. coli* lipids as well as to allow rapid protein mixing.

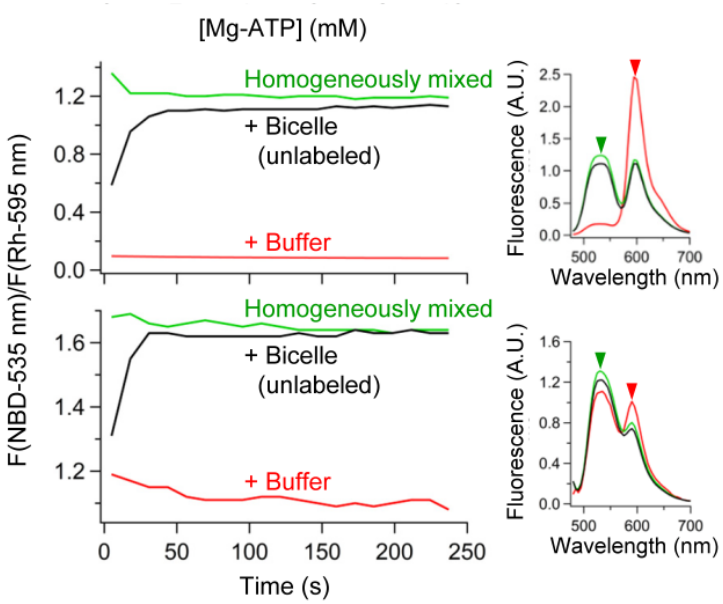

Figure 3.3 Diffusion of NBD- and rhodamine-labeled (*top*) lipids and (*bottom*) GlpG. In 3% DMPC/DMPG/CHAPS bicelles at 37 ºC monitored by FRET, i.e., the intensity ratio of NBD fluorescence at 535 nm to rhodamine fluorescence at 595 nm. (*Right*) NBD and rhodamine fluorescence spectra at the end of each mixing reaction.

Model substrate GlpG is highly thermostable in bilayers.

To quantitatively study the folding-degradation relationship of membrane proteins mediated by FtsH, we chose the TM domain of the site-specific intramembrane protease GlpG of *E. coli*[29] as a model substrate. We chose GlpG because (1) it is a monomeric six-helical bundle membrane protein with structural information available from >25 PDB entries (www.rcsb.org); (2) its folding has been extensively studied using various methods including thermal and SDS denaturation, single-molecule force spectroscopy and steric trapping in dodecylmaltoside (DDM) micelles and DMPC/CHAPS bicelles (**Table 1.2**). [22, 30, 31, 32]

We tested thermostability of GlpG in DMPC/DMPG/CHAPS bicelles and *E. coli* lipids employed in this study. GlpG was resistant to thermal inactivation and aggregation up to 85 °C (**Figure 3.4**). As a control, we measured the thermostability in DDM. The onset temperature of thermal denaturation (65−70 °C) agreed well with the reported value.[30] Taken together, GlpG is a highly thermostable membrane protein in bilayer environments.

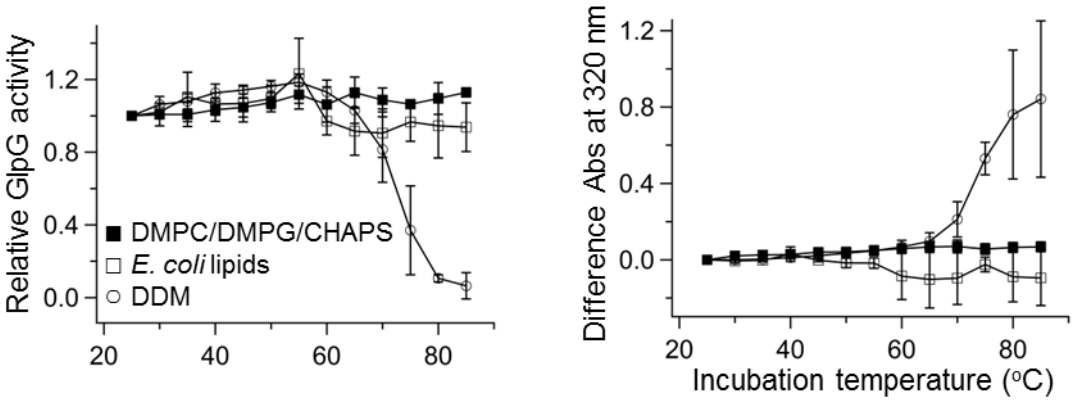

Figure 3.4 Thermostability of GlpG in various lipid environments.

Thermostability of GlpG measured by thermal (*top*) inactivation and (*bottom*) aggregation in DDM micelles, DMPC/DMPG/CHAPS bicelles, and liposomes composed of *E. coli* phospholipids. The activity and absorbance measured at various temperatures were normalized to those at 25°C. Data are represented as mean ± SEM (*n* = 3).

FtsH efficiently degrades stable GlpG in vivo.

FtsH is known to processively degrade a substrate starting from either N- or C-terminus by binding an unstructured tail (>20 residues) with diverse sequences as a degradation marker.[33, 34] To establish GlpG as a model substrate, we chose four well-characterized degradation markers which are preferentially recognized by FtsH or other AAA+ proteases and examined their ability to induce GlpG degradation *in*

vivo. To test specific degradation by FtsH, we employed the *E. coli* strain with intact chromosomal *ftsH* (+*ftsH*) and the strain with disrupted *ftsH* (−*ftsH*).[35]

As C-terminal degradation markers (**Figure 3.5a**), we tested the FtsH-specific 108 tag (GlpG-108) and the universal SsrA tag (GlpG-SsrA).[36, 37] Time-dependent degradation of the whole protein was monitored by Western blotting using FLAG epitope at the N-terminus. GlpG-108 was efficiently degraded in +*ftsH* (half-life, $T_{1/2} \approx$ 25 min) but not in −*ftsH*. Degradation of GlpG lacking a marker was negligible. Thus, FtsH degraded GlpG by recognizing the 108 tag. GlpG-SsrA was degraded in +*ftsH* at a similar rate to GlpG-108. However, GlpG-SsrA was also slowly degraded in –*ftsH* generating two large fragments (~22 and ~14 kDa; MW of the full length = 26 kDa), implying the involvement of other proteases in recognition of the SsrA tag. To test GlpG degradation by N-terminal markers, we employed the N-terminal tails (residues 1−23) of *E. coli* proteins YccA ($YccA_N$-GlpG) and Dps (Dps_N-GlpG) as degradation markers (**Figure 3.5b**), which are known to be specifically recognized by FtsH and ClpXP, respectively.[33, 38] Degradation of GlpG was monitored using HA epitope at the C-terminus. GlpG variants with the N-terminal markers were gradually degraded in +*ftsH* ($T_{1/2} \approx$ 35 min for $YccA_N$-GlpG and $T_{1/2} \approx$ 1 h for Dps_N-GlpG), while stable in −*ftsH*. Although FtsH had been thought to degrade only unstable proteins because of its proposed weak unfoldase activity,[18] the thermostable membrane protein GlpG was efficiently degraded by FtsH *in vivo*. It should be noted that GlpG with the Dps_N tag, which is known as a ClpXP-specific marker, was degraded depending on FtsH.

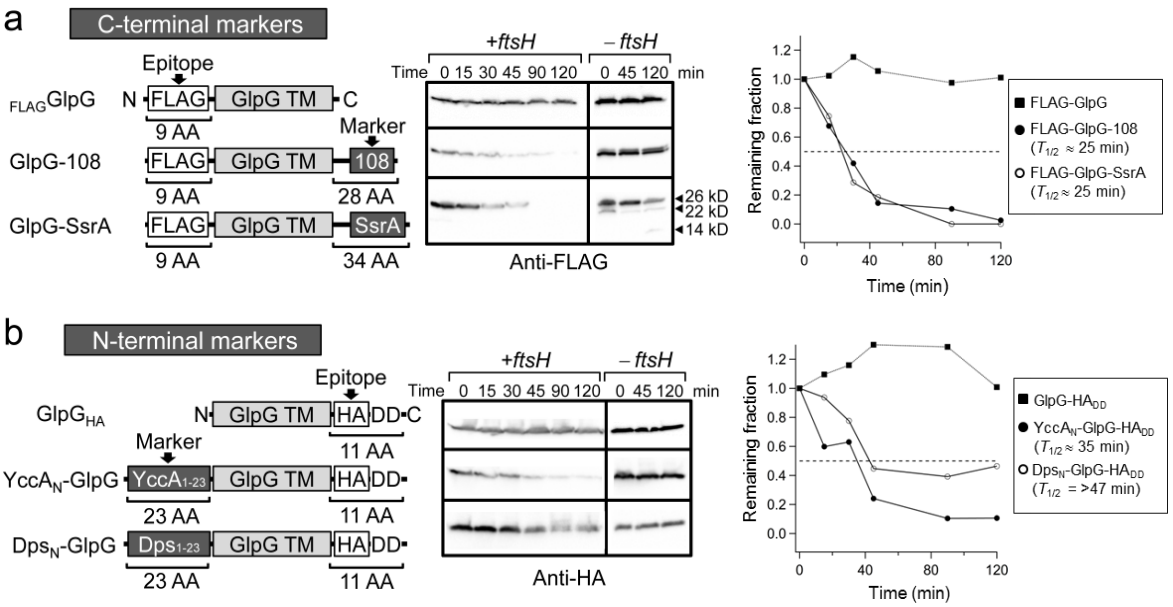

Figure 3.5 Degradation of GlpG *in vivo*. (a–b) (*Left*) GlpG constructs for testing the effect of the C- or N-terminal degradation markers on GlpG degradation. (*Middle*) Time-dependent degradation of GlpG variants monitored by Western blotting in the *E. coli –ftsH* and *+ftsH* strains. (Right) Quantification of time-dependent degradation of GlpG variants with the C- or N-terminal markers in the *+ftsH E. coli* strain monitored by SDS-PAGE and Western blotting (see also Figure 2.5).

Reconstitution of FtsH-mediated degradation of GlpG in bicelles.

To quantitatively study the mechanism of FtsH-mediated degradation of membrane proteins without the involvement of unknown cellular factors, we reconstituted the degradation using purified FtsH and GlpG in the bicelles optimized for ATPase activity and protein diffusion. GlpG variants with the fused degradation markers retained the activity level of wild-type (WT), indicating that the markers did not affect the native conformation. For precise and efficient measurement of degradation rates, we developed a fluorescence-based assay using the environment-sensitive fluorophore NBD conjugated to GlpG (See detail in Chapter 2). In bicelles, we

successfully recapitulated FtsH-mediated degradation of GlpG (**Figures 3.6**) observed *in vivo*. At the substrate-to-enzyme molar ratio of 10, FtsH degraded GlpG with the C-terminal 108- and SsrA-tags ($T_{1/2} \approx 50$ min) in a comparable time scale as *in vivo* ($T_{1/2} \approx 25$ min) in the presence of ATP. GlpG lacking a marker was not degraded, indicating that the degradation was specifically induced by the markers. Interestingly, GlpG with the N-terminal markers ($YccA_N$- and Dps_N-tag) were degraded significantly slower than those with the C-terminal markers. There was no noticeable cleavage of FtsH by GlpG, which is a site-specific protease (**Figure 3.7**). The degradation rate of GlpG-108 was enhanced in bicelles by ~3 fold relative to that in micelles (**Figure 3.8**), demonstrating that bicelles support not only ATP hydrolysis but also substrate degradation superior to micelles.

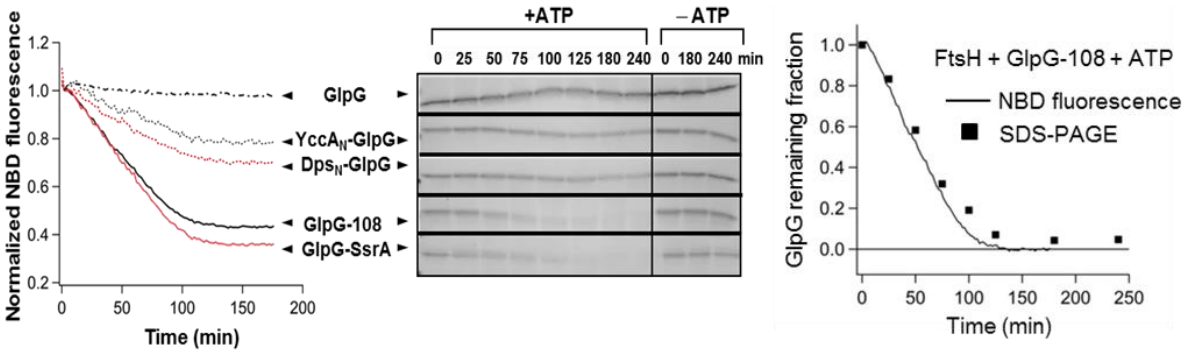

Figure 3.6 GlpG degradation by FtsH in bicelles. (*Left*) Time-dependent degradation of GlpG variants (5 μM) by FtsH ([$FtsH_6$] = 0.5 μM) monitored by NBD fluorescence in 3% DMPC/DMPG/CHAPS bicelles at 37 °C. Fluorescence intensity with 5 mM ATP at each time point was normalized to the intensity without ATP. (*Middle*) Degradation of GlpG variants monitored by SDS-PAGE and Coomassie blue staining. (*Right*) Comparison of degradation of GlpG-108 monitored by NBD fluorescence and SDS-PAGE shown in *left* and *middle*.

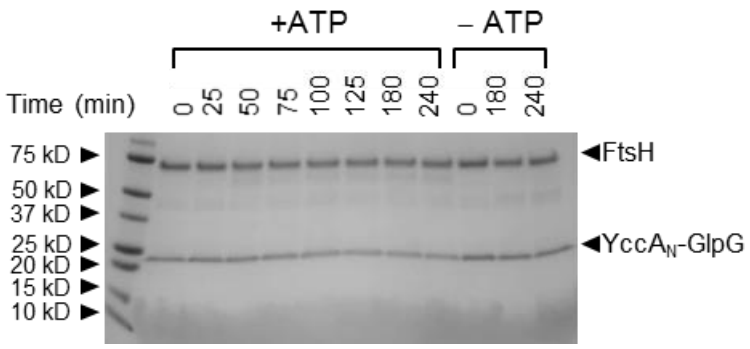

Figure 3.7 The whole-gel image of SDS-PAGE monitoring time-dependent degradation of GlpG variant in bicelles. This result indicated the site-specific protease GlpG did not significantly cleave FtsH over prolonged incubation.

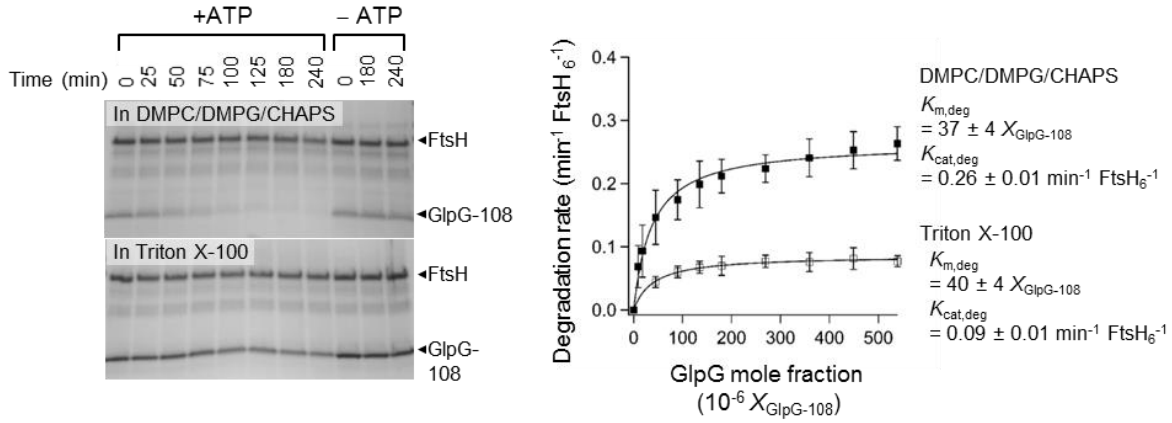

Figure 3.8 Comparison of GlpG degradation kinetics in bicelles and micelles. (*Left*) Comparison of time-dependent degradation of GlpG-108 (5 μM) by FtsH (3 μM) in 3% DMPC/DMPG/CHAPS bicelles and 3% Triton X-100 micelles monitored by SDS-PAGE. (*Right*) Michaelis-Menten plot of GlpG degradation measured at an increasing concentration of GlpG-108 (0.5–30 μM) and a fixed concentration of FtsH (2 μM) in 3% DMPC/DMPG/CHAPS bicelles and 3% Triton X-100. The reactions were performed in the presence of 5 mM ATP at 37oC. Data are represented as mean ± SEM (*n* = 3). The detailed procedures to obtain degradation rates are described in Chapter 2.

The degradation rate of GlpG is determined by the location of the marker, not by its sequence.

Next, we carried out kinetic analysis of GlpG degradation in bicelles by measuring the degradation rate as a function of substrate concentration (**Figure 3.9**). Because both enzyme and substrate were constrained in bicelles, the substrate concentration was expressed as a mole fraction in the protein-bicelle complex (X_{GlpG}). Fitting of degradation rates to a Michaelis−Menten equation yielded $K_{m,\,deg} = 3.0{-}3.7 \times 10^{-5}$ X_{GlpG} for GlpG-108 and GlpG-SsrA, and $K_{m,deg} = 6.3{-}9.0 \times 10^{-5}$ X_{GlpG} for $YccA_N$-GlpG and Dps_N-GlpG (**Table 3.2**), indicating that the C-terminal markers bound FtsH slightly tighter than the N-terminal markers. Remarkably, the degradation rate was largely determined by the position of the marker rather than by its amino acid sequence. We observed a similar maximum degradation rate, $k_{cat,\,deg} \approx 2.5{-}2.7 \times 10^{-1}$ min^{-1} $FtsH_6^{-1}$ for GlpG-108 and GlpG-SsrA while $k_{cat,deg} \approx 1.6 \times 10^{-1}$ min^{-1} $FtsH_6^{-1}$ for $YccA_N$-GlpG and Dps_NGlpG. GlpG with the C-terminal markers were degraded more rapidly than that with the N-terminal markers by ~1.7 fold. The strong dependence of the degradation rate on the position of the marker may have stemmed from the different efficiency of FtsH to process GlpG variants that are engaged in opposite directions. However, previous *in vivo* studies indicate that membrane substrates lacking stable tertiary or quaternary interactions (e.g., YccA, the SecY subunit and the TM fragment of proW) are rapidly degraded by FtsH with $T_{1/2} < 8$ min regardless of the position of the marker, much faster than GlpG ($T_{1/2} \approx$ 25−60 min).[34, 39, 40] Also for other AAA+ proteases including ClpXP, ClpAP, and proteasomes, the translocation rates of substrates are not significantly affected by the direction of pulling.[41, 42] Therefore, our result raises a possibility that certain

differences in the folding properties between the N- and C-terminal regions of GlpG may have caused the difference in the degradation rate.

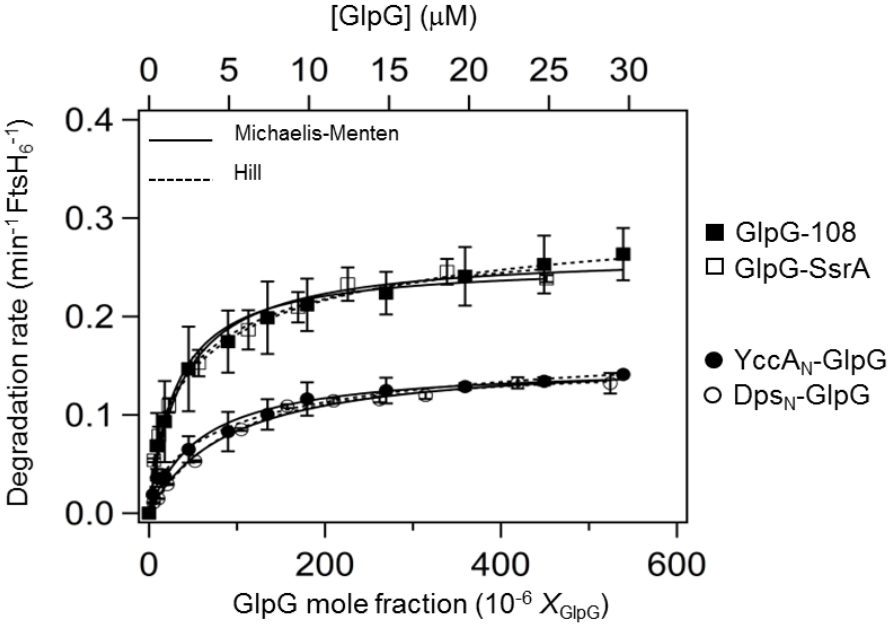

Figure 3.9 GlpG degradation by FtsH in bicelles with various degradation markers. Kinetic analysis of FtsH-mediated degradation of GlpG with various degradation markers. Data are represented as mean ± SEM (n = 3).

	Michaelis-Menten		Hill coefficient
	$k_{cat,deg}$[a] (min^{-1} $FtsH_6^{-1}$)	$K_{m,deg}$[a] (X_{GlpG})	$n_{H,deg}$[b]
GlpG-108	$2.7 \pm 0.1 \times 10^{-1}$	$3.7 \pm 0.5 \times 10^{-5}$	0.6 ± 0.1
GlpG-SsrA	$2.5 \pm 0.1 \times 10^{-1}$	$3.0 \pm 0.4 \times 10^{-5}$	0.7 ± 0.1
$YccA_N$-GlpG	$1.6 \pm 0.1 \times 10^{-1}$	$6.3 \pm 0.7 \times 10^{-5}$	0.8 ± 0.1
Dps_N-GlpG	$1.6 \pm 0.1 \times 10^{-1}$	$9.0 \pm 0.8 \times 10^{-5}$	1.1 ± 0.1

All measurements were performed with [FtsH] = 2 μM in 3% (w/v) DMPC/DMPG/CHAPS bicelles at 37°C.
[a] $k_{cat, deg}$, and $K_{m, deg}$ values are from nonlinear least square fits of data in Figures 3.9 to the Michaelis-Menten equation (See Chapter 2 Equation 2).
[b] $n_{H, deg}$ was obtained from nonlinear least squares fits of data in Figures 3.9 to the Hill equation (See Chapter 2 Equation 2).

Table 3.2 Kinetic parameters of GlpG degradation by FtsH.

Steric trapping to measure the spontaneous unfolding rate of GlpG.

Our findings that FtsH efficiently degrades stable GlpG and that the degradation rate strongly depends on the location of the marker raise important mechanistic questions regarding the folding-degradation relationship of membrane proteins: (1) Can FtsH actively unfold a membrane substrate? (2) How do the intrinsic folding properties of the membrane substrate influence its degradation?

To determine if FtsH can actively unfold membrane substrates, it is necessary to measure the spontaneous unfolding rate (k_U) of GlpG under the same bicellar condition for measuring degradation and compare the measured k_U to the ATP-driven unfolding rate. Here we employed the novel steric trapping strategy developed for studying membrane protein folding.[22, 43] Steric trapping couples unfolding of a doubly-biotinylated protein to competitive binding of bulky monovalent streptavidin (mSA) (**Figure 3.10**). This method is advantageous because: (1) k_U and thermodynamic stability (ΔG^o_U) can be measured directly under native bilayer conditions without using perturbants such as chemical denaturants and pulling force; (2) trapping of the unfolded state depends on transient unfolding of the region between two specific biotin labels separated at a close distance in the folded state. Thus, it allows for measuring the local unfolding rate depending on the position of the biotin pair.

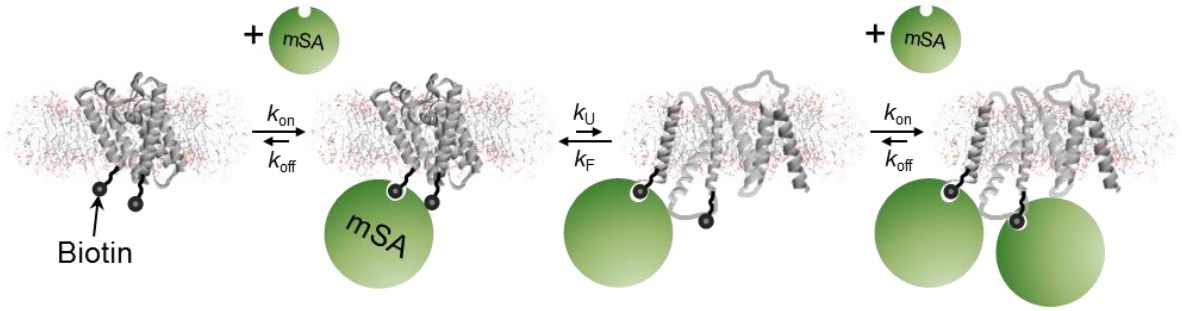

Figure 3.10 Principle of steric trapping. When biotin tags are conjugated to two specific residues that are spatially close in the folded state but distant in the amino acid sequence, the first mSA binds either biotin label with intrinsic binding affinity, but due to steric hindrance, the second mSA binds only when native tertiary contacts are unraveled by transient unfolding. k_{on}: on-rate constant of mSA binding to biotin label; k_{off}: off-rate constant of the mSA-biotin complex; k_U: spontaneous unfolding rate; k_F: folding rate.

Using steric trapping, k_U can be determined by shifting the reaction flux dominantly towards unfolding upon the addition of a molar excess of WT mSA with a high biotin-binding affinity (**Figure 3.11a**).[43-45] The apparent unfolding rate ($k_{U,\,app}$) is asymptotic as a function of mSA concentration, the maximum value of which corresponds to k_U (**Figure 3.11b**).

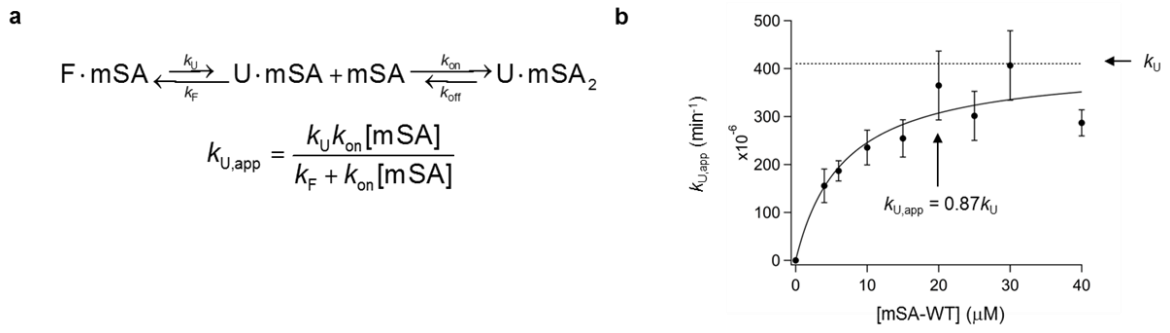

Figure 3.11 Steric trapping of GlpG scheme to measure the spontaneous unfolding rate k_U. (a) Steric trapping for measuring k_U was achieved by shifting the reaction flux towards the unfolding direction using wild type monovalent streptavidin (mSA-WT) possessing high-affinity to biotin (mSA-WT; $K_{d,\ biotin} \approx 10^{-14}$ M; $k_{on,biotin} \approx 10^7$ M^{-1} s^{-1}; $k_{off,biotin} \approx$ weeks)[44, 45]. Under the steady-state condition, in which k_U (unfolding rate) << k_F (folding rate) and $k_{off,\ biotin}$ (off-rate of mSA from biotin) << $k_{on,\ biotin}$· [mSA-WT] (on-rate of mSA to biotin), the apparent unfolding rate ($k_{U,app}$) can be approximated to an asymptotic equation shown in Figure 3.11b. At high mSA-WT concentration, $k_{U,\ app}$ approaches k_U. **(b)** Dependence of the apparent unfolding rate ($k_{U,\ app}$) on the concentration of mSA-WT. The unfolding rates were measured for the double-biotin variant of GlpG, 95/172$_N$-BtnPyr$_2$ (1 mM) [22] at different mSA concentrations in 20 mM sodium phosphate (pH7.5), 200 mM NaCl and 5 mM dodecylmaltoside (DDM). GlpG activity was used as an unfolding readout in the unfolding kinetic measurement at each mSA-WT concentration (see also Figure 2.3). The data were fit to the steady-state kinetic equation shown in Figure 3.11a. In the subsequent unfolding kinetic study (Figures 3.12 – 3.18), the mSA-to-GlpG molar ratio of 20 was used, at which $k_{U,app}$ was close to k_U (upward arrow). Errors designate ± STD from fitting.

We have identified two pairs of optimal biotinylation sites, 95C/172C, and 172C/267C[22] (**Figure 3.12**). After biotinylation, each biotin pair approximately covers the N-terminal (N-subdomain, probed with the biotin pair $95/172_N$-$biotin_2$) or C-terminal half (C-subdomain, probed with the biotin pair $172/267_C$-$biotin_2$) of GlpG.[22]

FtsH actively unfolds GlpG for degradation.

To test if FtsH can actively unfold GlpG during degradation, we determined k_U in bicelles using GlpG activity as an unfolding readout at a 20-times molar excess of mSA-WT (**Figure 3.12** and **3.13**). The C-subdomain unfolded slow with $k_{U,app}$ = 2.7 ± 0.7 × 10^{-4} min^{-1}. The N-subdomain unfolded even slower by ~1.5 fold ($k_{U,app}$ = 1.8 ± 0.5 × 10^{-4} min^{-1}). Increase of mSA concentration up to a 30-times molar excess did not significantly change $k_{U,\,app}$, indicating $k_{U,app} \approx k_U$ (**Figure 3.14**).

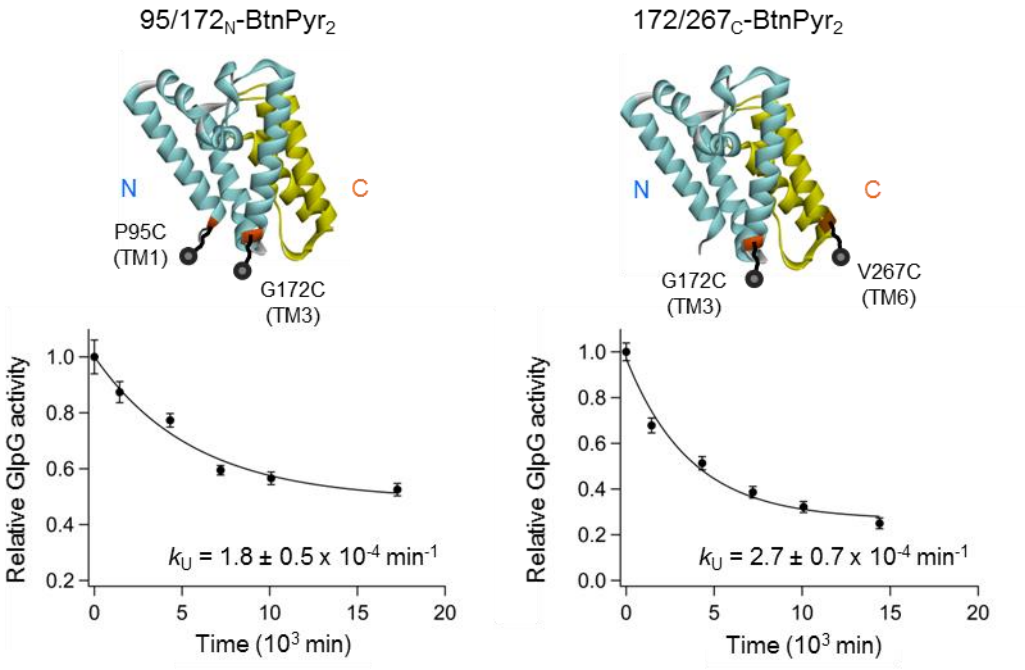

Figure 3.12 Unfolding kinetics of double biotin variants of GlpG measured by steric trapping. In 3% DMPC/DMPG/CHAPS bicelles at 37 °C. The N- and C-subdomains[22] were color-coded in cyan and orange, respectively. GlpG activity with mSA relative to that without mSA was used as an unfolding readout. Errors designate ± STD from fitting.

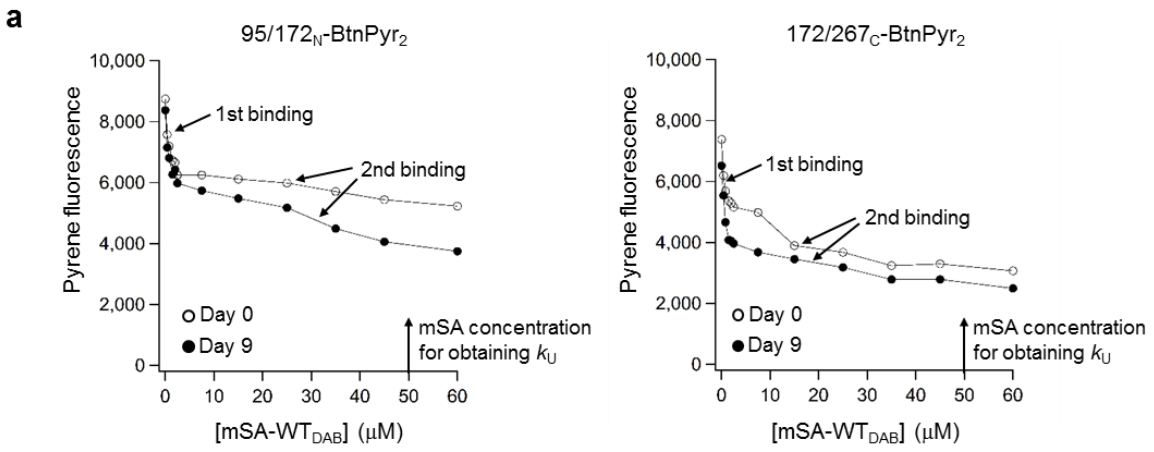

Figure 3.13 Unfolding kinetics measurements of GlpG by steric trapping. (a) Binding isotherm between a double-biotin GlpG variant (95/172$_N$ or 172/267$_C$, 2.5 mM) and mSA-WT$_{DAB}$ in DMPC/DMPG/CHAPS bicelles, 20 mM HEPES (pH 7.5) and 100 mM NaCl. The unhindered first binding is tight (1st binding) while the second binding coupled with unfolding is weak (2nd binding). The 2nd binding phase was slowly developed as the population of the trapped unfolded state increased over time (Day 0 vs. Day 9). In the unfolding kinetic assay (Figure 3.12) for measuring the spontaneous unfolding rate (k_U), the [mSA]/[GlpG] ratio of 20 (upward arrows) was used to ensure double binding of mSA to the double-biotin variants of GlpG.

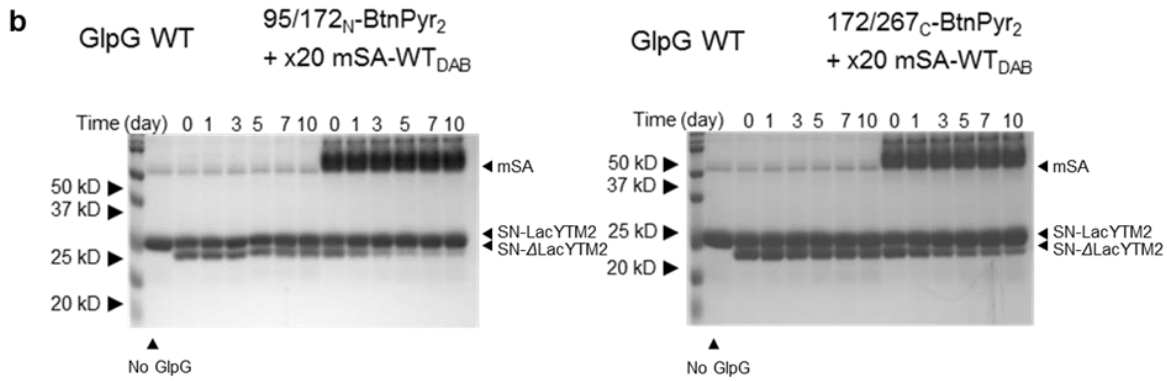

Figure 3.13 Continued. (b) The spontaneous unfolding rates of GlpG WT was determined by steric trapping using GlpG activity as an unfolding readout. GlpG was incubated in the absence or presence of 50 μM mSA-WT at 37°C in 3% DMPC/DMPG/CHAPS bicelles, 40 mM HEPES (pH 7.5) and 100 mM NaCl. Steric trapping was carried out for both double-biotin variants, (*left*) 95/172C-BtnPyr2 and (*right*) 172/267C-BtnPyr2 at a 20-times molar excess of [mSA-WT_{DAB}]. The apparent unfolding rate ($k_{U,\,app}$) was determined by applying the first-order reaction kinetics. GlpG activity was measured by quantifying the amount of cleavage product of the model substrate SN-LacYTM2 on SDS-PAGE.

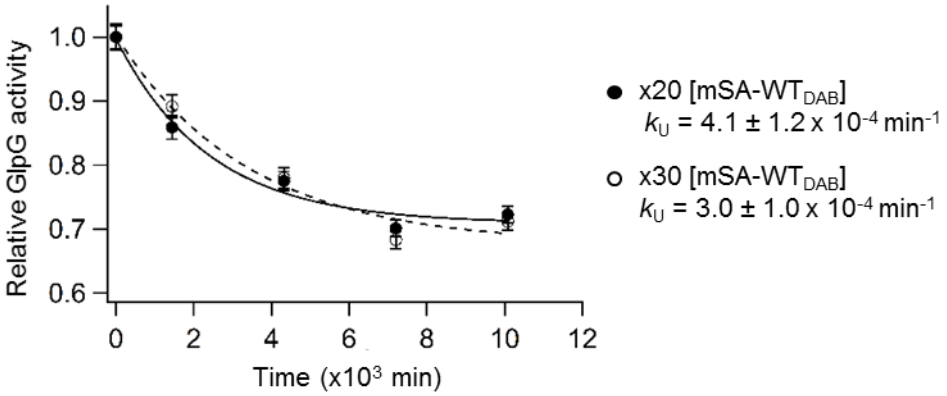

Figure 3.14 Comparison of the unfolding rates of GlpG measured at 20-times and 30-times molar excess of mSA-WT$_{DAB}$. $k_{U,\ app}$'s obtained at a different molar excess of mSA-WT$_{DAB}$ agreed reasonably well, indicating that $k_{U,\ app}$'s that we determined (**Figure 3.12**) are close to k_U. Errors designate ± STD from fitting.

To quantify the degree of acceleration of GlpG unfolding by FtsH, we decomposed the degradation process represented by $\tau_{cat,\ deg}$ (substrate lifetime, $1/k_{cat,\ deg}$) into three sequential sub-processes[17, 46]: ATP-driven unfolding ($\tau_{cat,\ U}$) and membrane dislocation ($\tau_{cat,\ dislocation}$) by the AAA+ domain, and proteolysis ($\tau_{cat,\ proteolysis}$) by the protease domain (i.e., $\tau_{cat,\ deg} = \tau_{cat,\ U} + \tau_{cat,\ dislocation} + \tau_{cat,\ proteolysis}$). Although we were not able to determine the lifetime of each sub-process, it is evident that $\tau_{cat,\ deg} > \tau_{cat,\ U}$. Next, we compared $\tau_{cat,\ deg}$ obtained with the N-terminal marker to τ_U (lifetime of spontaneous unfolding, $1/k_U$) obtained from steric trapping at the N-terminal biotin pair, and $\tau_{cat,\ deg}$ with the C-terminal marker to τ_U from steric trapping at the C-terminal biotin pair (**Figures 3.9** and **3.12, Table 3.2**). By this comparison, $\tau_U/\tau_{cat,\ deg} \approx$ 800–900 regardless of the position of the degradation marker. Because $\tau_{cat,\ deg} > \tau_{cat,\ U}$, we conclude that FtsH accelerated GlpG unfolding at least 800 fold (i.e., $\tau_U/\tau_{cat,\ U} >$800), clearly demonstrating the substantial ability of FtsH to actively unfold GlpG.

This finding is contrary to the previous proposal that FtsH degrades substrates depending on spontaneous unfolding.[17]

Substrate stability and hydrophobicity contribute to degradation rate.

To determine how intrinsic folding properties of a membrane substrate influence its degradation, it is necessary to obtain ΔG^{o}_{U}, k_U and activation energy of unfolding ($E_{a,U}$) (i.e. the unfolding energy landscape) of the substrate, and examine the correlation between each folding property and the degradation rate. Due to slow unfolding, however, it was difficult to measure ΔG^{o}_{U} of GlpG using steric trapping under the same bicellar condition for measuring degradation. Instead, because GlpG unfolded faster in micelles by 40–100 fold, we were able to describe the unfolding energy landscape in DDM micelles using ΔG^{o}_{U} that has been previously determined[22], and k_U and $E_{a,U}$ obtained in this study (**Figure 3.15** and **3.16**). Notably, we obtained a highly asymmetric unfolding energy landscape in micelles (**Figure 3.15**), i.e., the N-subdomain possessed higher kinetic ($\Delta E_{a,U} \approx 8$ kcal/mol) and thermodynamic ($\Delta\Delta G^{o}_{U} \approx 1$ kcal/mol) stability than the C-subdomain.

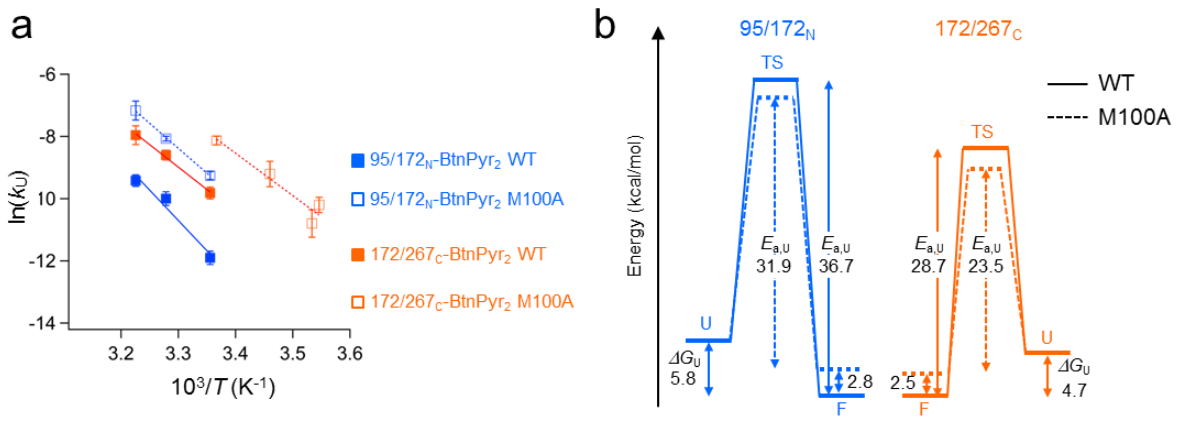

Figure 3.15 Unfolding energy landscape of GlpG. (a) Arrhenius plot for obtaining activation energy of unfolding ($E_{a,U}$) of GlpG WT and M100A variant. Spontaneous unfolding rates (k_U) were measured using steric trapping in DDM at various temperatures (see Figure 3.16). (b) Unfolding energy landscape of GlpG WT and M100A variants in DDM including the thermodynamic stability[31] (ΔG_U) and $E_{a,U}$. F, U, and TS denote the folded state, unfolded state and transition state, respectively.

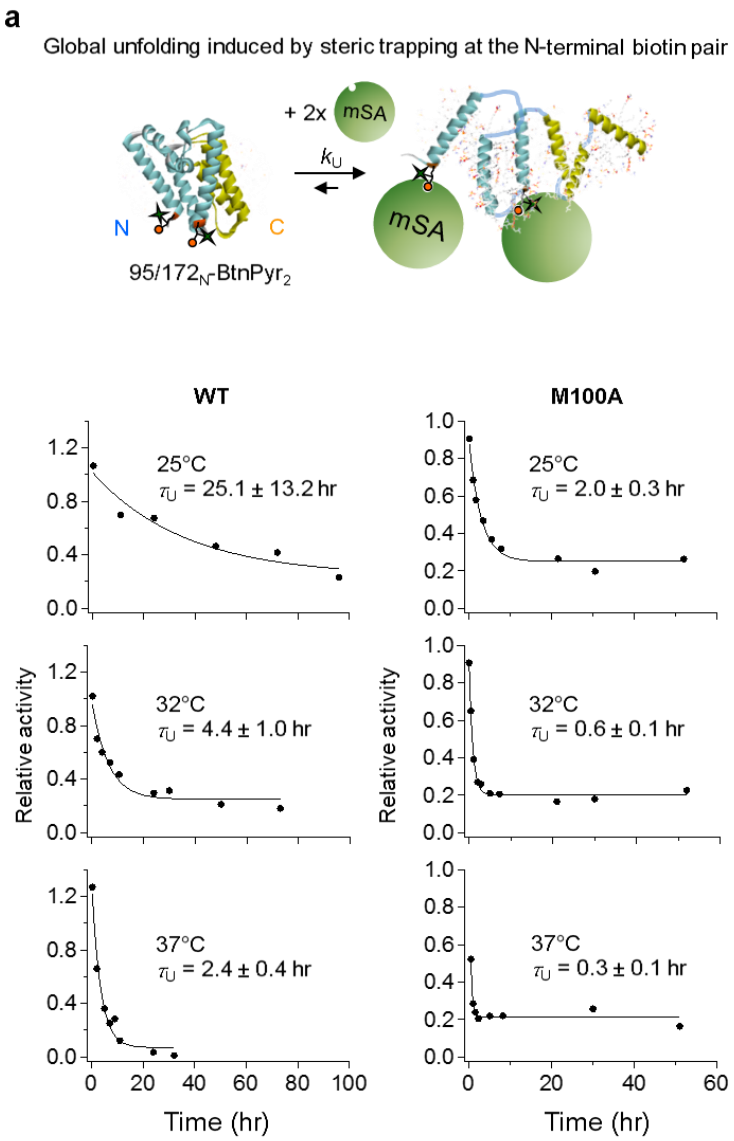

Figure 3.16 Unfolding energy landscape of GlpG in DDM micelles revealed by steric trapping. Temperature-dependence of the unfolding kinetics (unfolding lifetime, $t_U = 1/k_U$) of GlpG WT and M100A variant in DDM micelles. (a) GlpG unfolding was induced by steric trapping at the biotin labels located at the N-subdomain of GlpG (95/172$_N$-BtnPyr$_2$). The unfolding of the subdomain leads to global unfolding.[1] Unfolding of GlpG (1 mM) was measured by monitoring activity of GlpG cleaving the TM model substrate SN-LacYTM2 upon addition of excess mSA-WT (20 mM).

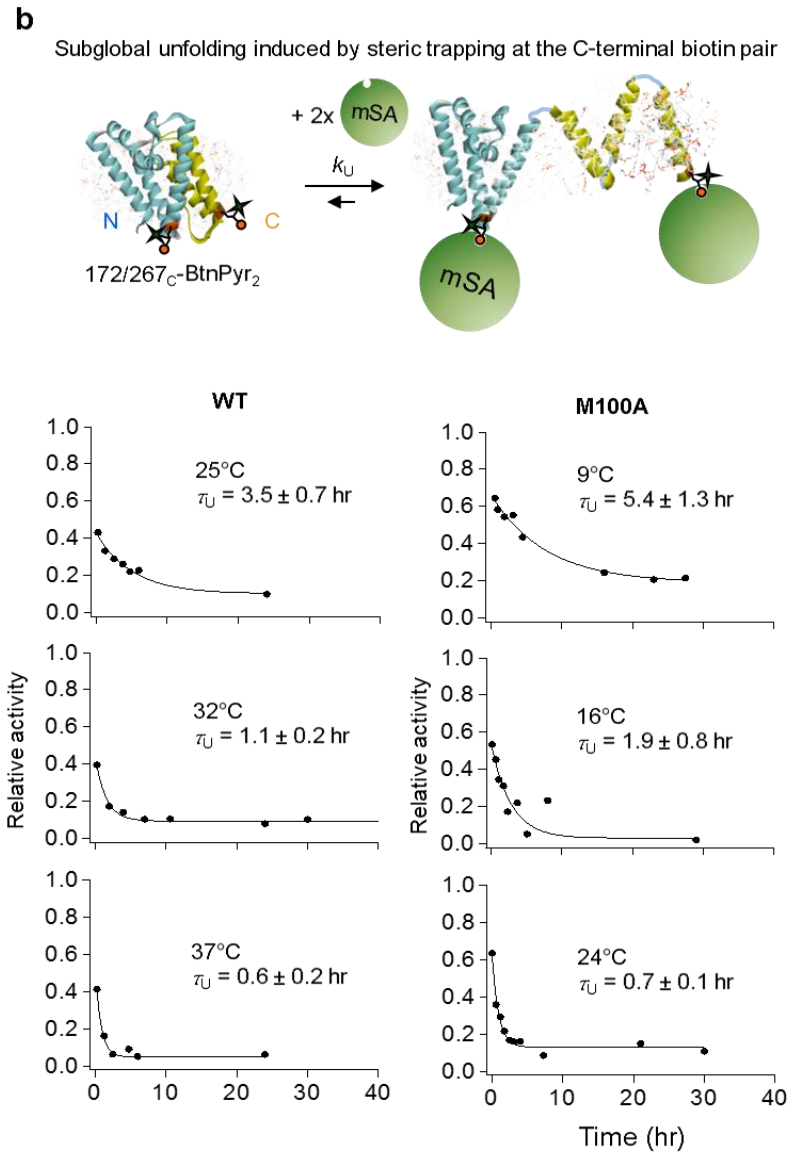

Figure 3.16 Continued. (b) Unfolding was induced by steric trapping at the biotin labels located at the C-subdomain of GlpG (172/267$_N$-BtnPyr$_2$). The unfolding of the C-subdomain leads to subglobal unfolding.[1] Unfolding of GlpG (1 mM) was measured by monitoring activity of GlpG cleaving SN-LacYTM2 upon addition of mSA-WT (20 mM).

Having the tools to analyze the unfolding energy landscape and degradation in hand, we hypothesized that the degradation rate of GlpG depends on the unfolding kinetic

barrier and stability of the region to which a degradation marker is attached, analogous to the suggestion from degradation studies of water-soluble proteins by ClpAP and ClpXP.[14] To test this, we made an amino acid substitution on GlpG to modify the unfolding energy landscape and investigated how the modification would change the degradation rate. We chose M100A substitution in the internal packing region (**Figure 3.17**), which destabilizes the N- and C-subdomains by $\Delta\Delta G^{o}_{U,\ WT\text{-}M100A}$ = 2.5 and 2.8 kcal/mol, respectively, in micelles.[22] $E_{a,\ U}$ of the two subdomains similarly decreased by ~5 kcal/mol (5–10 fold increase in k_U) (**Figure 3.15**). Also, in bicelles, the substitution accelerated unfolding by 35–50 fold relative to WT for both subdomains (**Figure 3.18**). Although the residue M100 is located at the N-terminal TM1 helix, the structural perturbation by the substitution was propagated throughout the protein. Indeed, the substitution increased $k_{cat,\ deg}$'s of both variants with the N- and C-terminal markers ($GlpG_{M100A}$-108 and $YccA_N$-$GlpG_{M100A}$) by ~1.5 fold (**Figure 3.19, Table 3.2 and 3.3**).

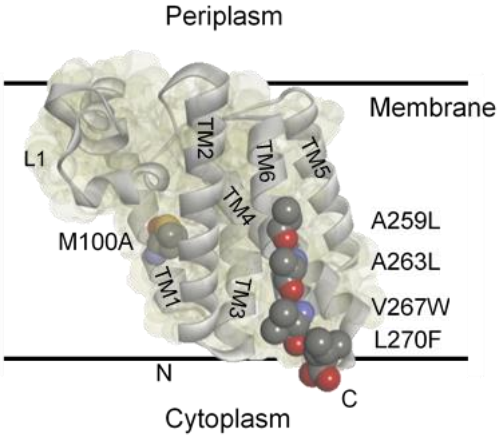

Figure 3.17 GlpG conformation. The residues for amino acid substitutions to decrease the conformational stability (M100A) or increase the hydrophobicity of the C-terminal TM6 helix (A259L/A263L/V267W/L270F, designated as "LLWF").

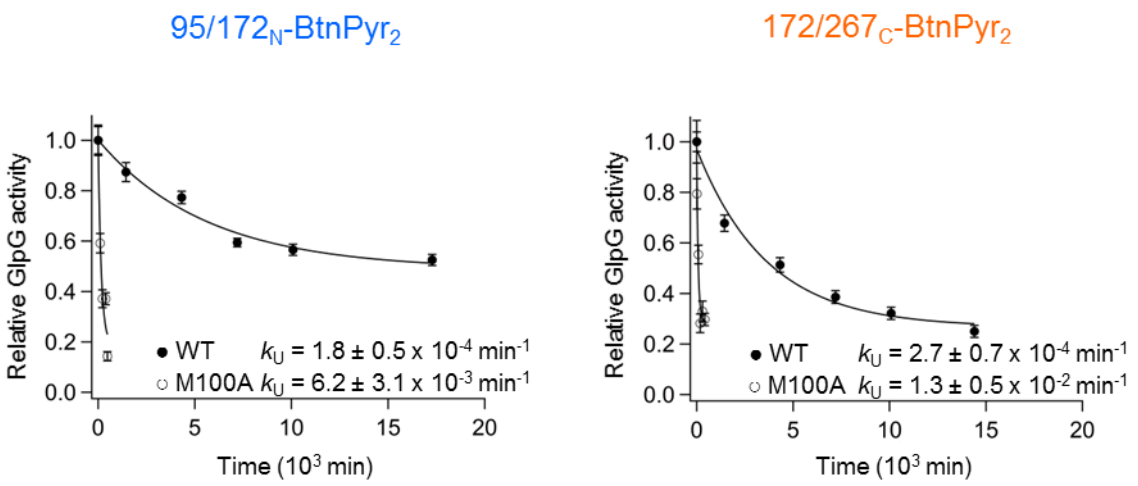

Figure 3.18 The effect of M100A substitution on k_U of double biotin variants of GlpG. 2.5 μM of GlpG was tested in 3% DMPC/DMPG/CHAPS bicelles at 37ºC. Errors designate ± STD from fitting.

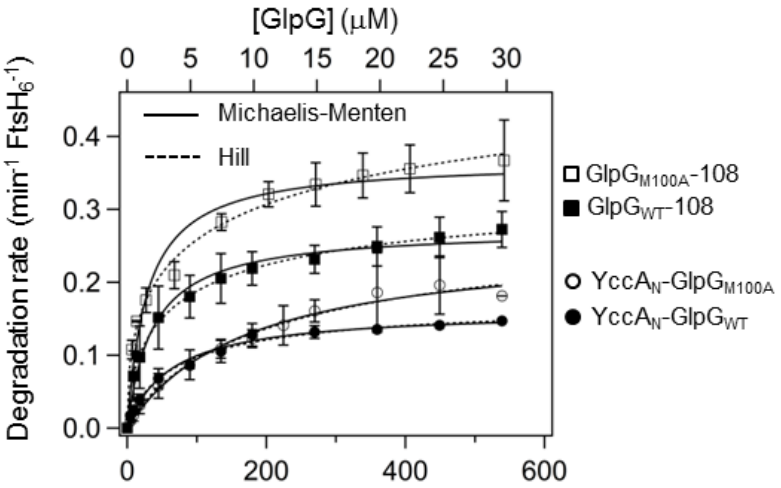

Figure 3.19 The effect of M100A substitution on the degradation rates of GlpG with the C-terminal (the 108 tag) or N-terminal (the $YccA_N$ tag) marker. Data are represented as mean ± SEM (*n* = 3–6).

	Michaelis-Menten		Hill coefficient
	$k_{cat,deg}$[a] (min^{-1} $FtsH_6^{-1}$)	$K_{m,deg}$[a] (X_{GlpG})	$n_{H,deg}$[b]
$GlpG_{M100A}$-108	3.7 ± 0.1 ×10^{-1}	2.8 ± 0.6 ×10^{-5}	0.5 ± 0.1
$YccA_N$-$GlpG_{M100A}$	2.6 ± 0.1 ×10^{-1}	17.3 ± 2.4 ×10^{-5}	0.9 ± 0.1
$GlpG_{LLWF}$-108	2.2 ± 0.1 ×10^{-1}	2.3 ± 0.3 ×10^{-5}	1.2 ± 0.2

All measurements were performed with [FtsH] = 2μM in 3% (w/v) DMPC/DMPG/CHAPS bicelles at 37°C.
[a] $k_{cat,\ deg,}$ and $K_{m,\ deg}$ values are from nonlinear least square fits of data in **Figures 3.19** and **3.20** to the Michaelis-Menten equation (See **Chapter 2** Equation 2).
[b] $n_{H,\ deg}$ was obtained from nonlinear least squares fits of data in **Figures 3.19** and **3.20** to the Hill equation (See **Chapter 2** Equation 3).

Table 3.3 Kinetic parameters of GlpG varients degradation by FtsH.

On the basis of the asymmetric unfolding energy landscape and the sensitivity of the degradation rate to the stability change, we reasoned that the slow degradation of GlpG with the N-terminal degradation markers (**Figure 3.9**) was caused by the higher conformational stability of the N-subdomain. However, from the hydrophobicity analysis of GlpG using the membrane depth-dependent hydrophobicity scale,[47] and Hessa-von Heijne and Wimley-White scales determined near the center of the bilayer (**Figure 3.20**),[48, 49] we noticed that the N-terminal TM1 helix was much more hydrophobic than the C-terminal TM6 helix by 4−10 kcal/mol. This fact raises a possibility that, in addition to the conformational stability that resists unfolding, the hydrophobicity of the TM segment near the marker that would resist membrane dislocation may also control degradation. To test this possibility, we designed a quadruple substitution on the lipid-exposed residues in TM6 (A259L/A263L/V267W/L270F) near the C-terminal 108 tag ($GlpG_{LLWF}$-108 hereafter) to increase its hydrophobicity to the comparable level to that of TM1 (**Figures 3.17** and **3.20**). This variant possessed the activity and stability similar to WT (**Figures**

3.21). If the hydrophobicity dominantly determines the degradation rate, $GlpG_{LLWF}$-108 would be degraded slower than $GlpG_{WT}$-108 but at a similar rate to GlpG with the N-terminal marker ($YccA_N$-$GlpG_{WT}$). Indeed, $k_{cat,\ deg}$ of $GlpG_{LLWF}$-108 decreased but only halfway to the level of $YccA_N$-GlpG (**Figure 3.22**). Thus, the dependence of the degradation rate on the position of the degradation marker appears to be caused by the combined effect of the stability and hydrophobicity of the substrate region near the marker.

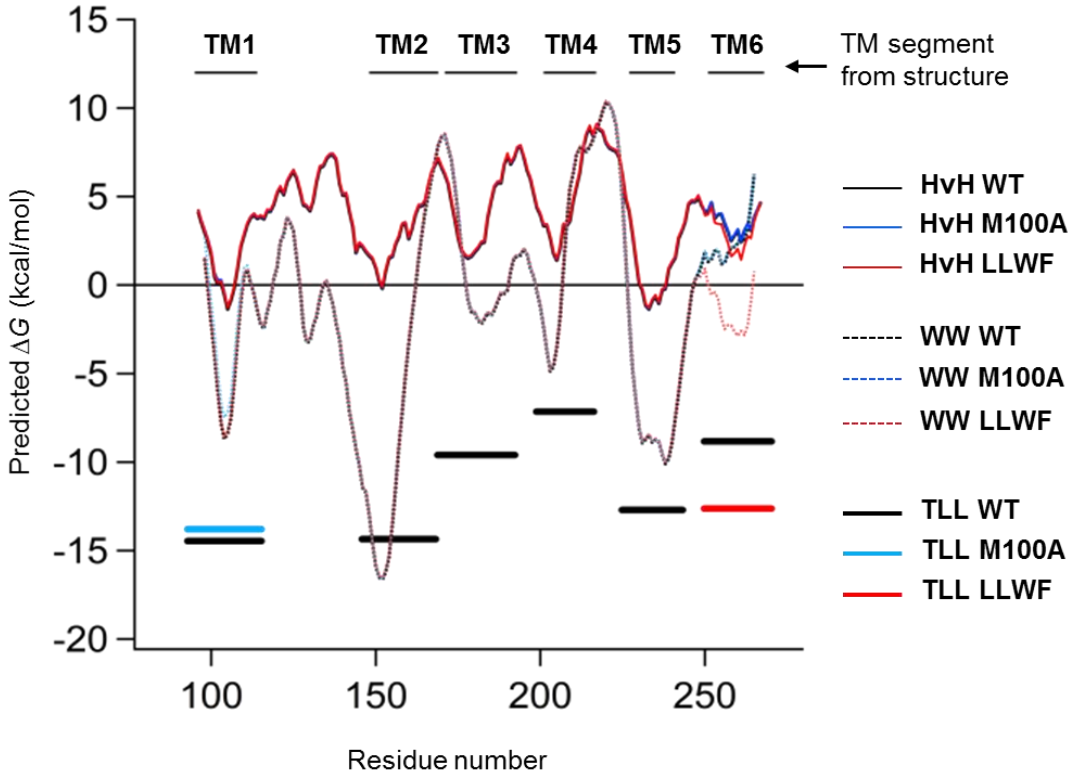

Figure 3.20 The whole-residue hydropathy plot of GlpG WT, M100A, and LLWF variants. Hessa-von Heijne (HvH), Wimley-White (WW) octanol and Tian-Lin-Liang (TLL) depth-dependent scales were used.

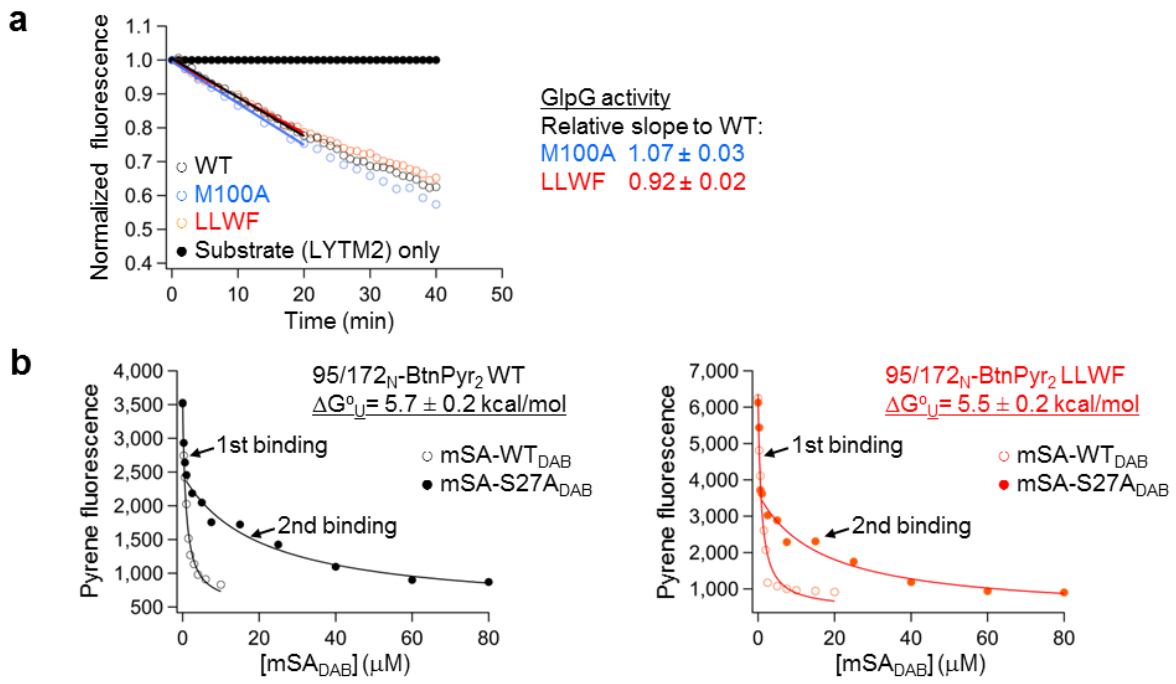

Figure 3.21 Characterization of M100A and LLWF variants *in vitro*.

(a) Comparison of the activity of GlpG WT, M100A, and LLWF variants. Proteolytic activity was measured by a fluorescence-based assay[1] using NBD-labeled SNLacYTM2 (10 mM) as a substrate in the presence of 1 mM GlpG in 20 mM HEPES (pH7.5), 100 mM NaCl, 0.5 mM TCEP and 5 mM DDM (see Figure S2a). The initial slope of each trace is directly related to the activity. (b) Comparison of thermodynamic stability (DG^0_U) of GlpG WT (95/172$_N$-BtnPyr$_2$) and its LLWF variant measured by steric trapping in 5 mM DDM. A detailed description of the steric trapping principle for measuring GlpG stability is described in Figure S5c and the literature.[1] Briefly, the binding isotherm was obtained using weaker mSA variant mSA-S27A ($K_{d,\ biotin}$ = 1.4 nM) labeled with dabcyl quencher (mSA-S27A$_{DAB}$). The degree of attenuation of the second mSA binding phase relative to the first binding is correlated with the stability.

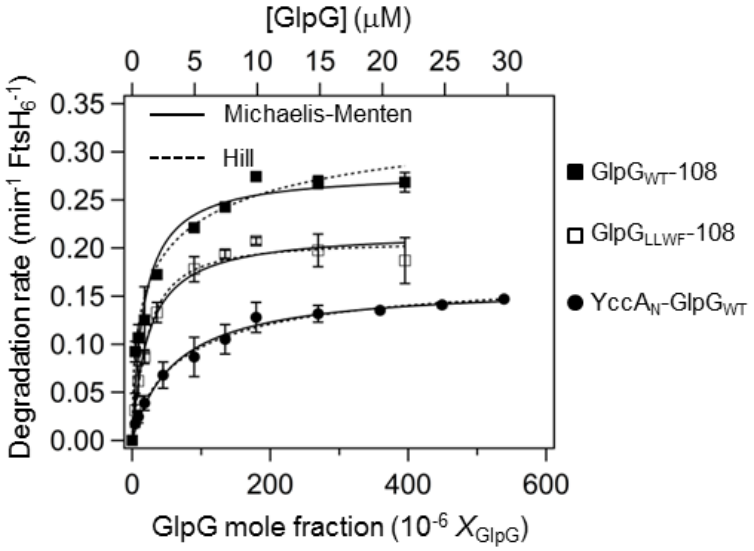

Figure 3.22 The effect of the LLWF substitution on the degradation rates of GlpG with the 108 tag. The degradation rates of $GlpG_{WT}$-108 and $YccA_N$-$GlpG_{WT}$ were also plotted for comparison. Data are represented as mean ± SEM (*n* = 3).

In summary, we found that the conformational stability and hydrophobicity of membrane substrates are important factors that control degradation. Nonetheless, the large changes in the unfolding rate (30−50 fold in bicelles) and the hydrophobicity (~4 kcal/mol) led to only moderate changes in the degradation rate. Probably, substantial unfoldase activity of FtsH elucidated in this study dampened the sensitivity of the degradation rate to the changes in these folding properties. *In vivo*, M100A and LLWF substitutions induced similar changes in the degradation rate to those observed *in vitro* (**Figure 3.23**).

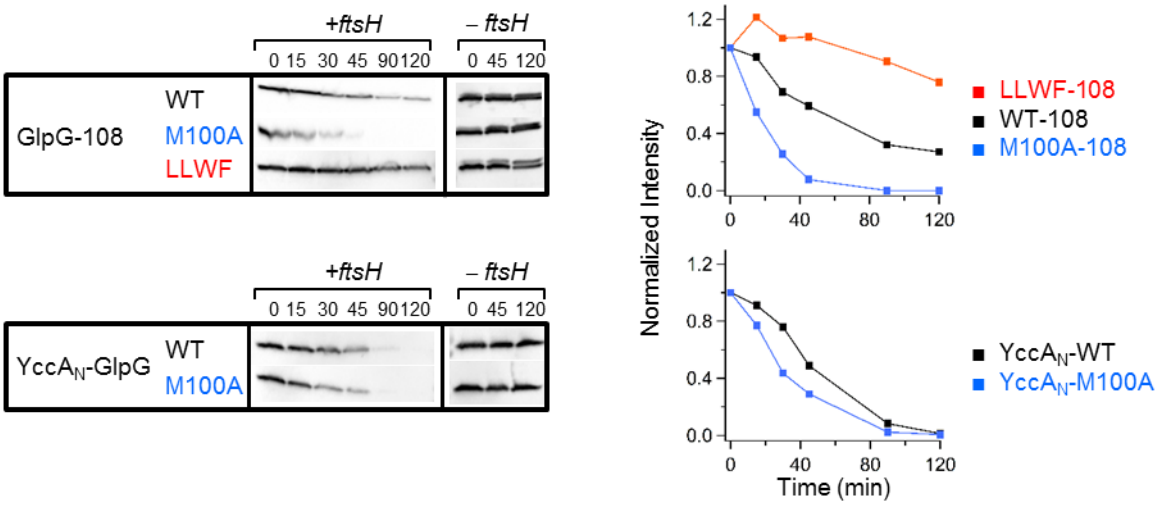

Figure 3.23 Characterization of M100A and LLWF variants *in vivo*. Comparison of degradation of GlpG WT, M100A, and LLWF variants *in vivo* measured by Western blotting. The intensities of GlpG bands were quantified using the ImageJ program.

Free energy cost to dislocate GlpG.

To obtain a quantitative measure of the hydrophobic nature of GlpG and the energetic cost of its membrane dislocation, we calculated the total free energy of dislocation ($\Delta G_{dislocation}$) using the depth-dependent hydrophobicity scale (**Figure 3.24**, **Table 3.4**). We assumed that the tertiary structure of GlpG is completely unraveled in the bilayer before dislocation, while the helical content of each TM segment is maintained. $\Delta G_{dislocation}$ was defined as the free energy change from GlpG whose tertiary structures are unraveled in the bilayer to its random coil form in water. The calculated $\Delta G_{dislocation}$ was +360 kcal/mol, indicating that FtsH overcomes an enormous free energy cost to dislocate GlpG. Studies using single-molecule force spectroscopy report that $\Delta G_{dislocation}$ for a single TM helix ranges from 50 to 100

kcal/mol.[20] Our calculated $\Delta G_{dislocation}$ (~60 kcal/mol/TM helix) reasonably agrees with this result.

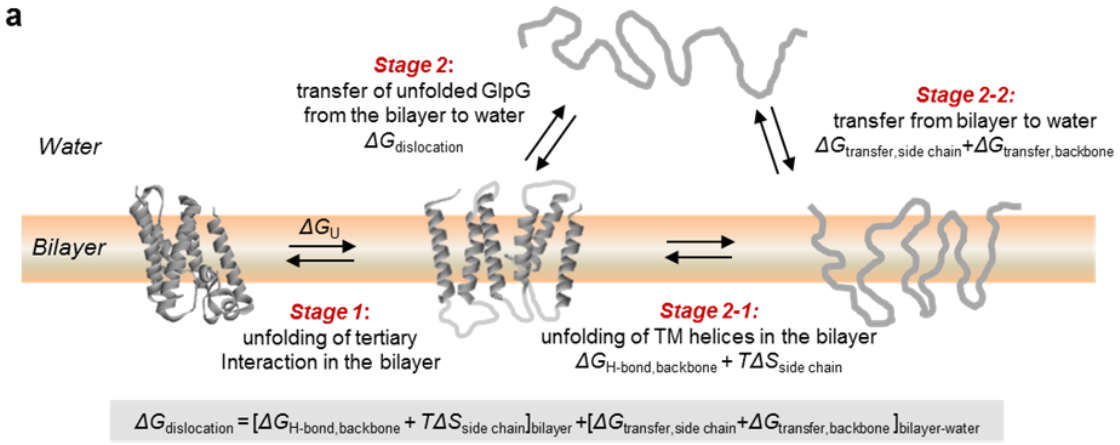

Figure 3.24 Calculation of the free energy of dislocation ($\Delta G_{dislocation}$) using the depth-dependent hydrophobicity scale. Dissection of thermodynamics of FtsH-mediated degradation of helical membrane proteins. (a) Overall, degradation of a helical membrane protein can be divided into two ATP-driven steps, unfolding of tertiary interactions within the bilayer (*Stage 1*) and dislocation of the unfolded state from the bilayer to the aqueous phase for proteolysis (*Stage 2*) (see also Figure 3.27). *Stage 2* can be further decomposed into *Stage 2-1* (backbone unfolding of TM helices in the bilayer) and *Stage 2-2* (transfer of fully unfolded GlpG from the bilayer to water) for thermodynamic analysis of dislocation free energy ($\Delta G_{dislocation}$).

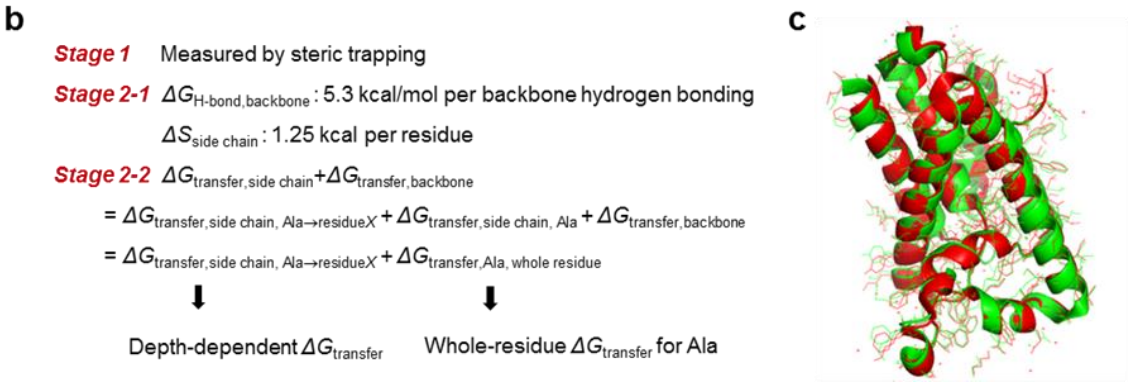

Figure 3. 24 Continued. (b) Thermodynamic stability in *Stage 1* can be experimentally determined using steric trapping. In *Stage 2-1*, the free energy change (5.3 kcal/mol) for breaking a backbone hydrogen bond (NH – CO) within the nonpolar hydrocarbon phase ($\Delta G_{\text{H-bond, backbone}}$) was obtained from the rigorous computational study using the density-functional theory.[50] This value falls into the range of experimentally determined $\Delta G_{\text{H-bond, backbone}}$ (4–8 kcal/mol).[51] The average side-chain entropy change (1.25 kcal/mol) per residue ($T\Delta S_{\text{side chain}}$) was obtained from the study by Privalov.[52] In *Stage 2-2*, the membrane depth-dependent transfer free energy change of a certain residue (X) relative to Ala ($\Delta G_{\text{transfer, side chain, Ala}\rightarrow\text{residue }X}$) was predicted using the computational method.[53, 47, 54] The transfer free energy of the whole Ala residue including a peptide group ($\Delta G_{\text{transfer, Ala, whole residue}}$= 0.16 kcal/mol) was obtained from the knowledge-based unified hydrophobicity scale.[55] Here it was assumed that the depth-dependence of $\Delta G_{\text{H-bond, backbone}}$, and $\Delta G_{\text{transfer, Ala, whole residue}}$ was not significant.[56] The total $\Delta G_{\text{dislocation}}$ of all TM residues are shown in Table 3.4. (c) Structural comparison of inhibitor-bound GlpG (2XOW) and apo-GlpG (3B45). The structure of inhibitor-bound GlpG was used to obtain the depth of each side chain in the TM helices using the OPM database because the apo-structure was not included in the database.[57] The two structures are highly similar (RMSD = 0.6 Å).

Helix ID	Helix Segment	*Stage 2-1*		*Stage 2-2*	Total
		$\Delta G_{\text{H-bond,backbone}}$[a]	$T\Delta S_{\text{side chain}}$[b]	$\Delta G_{\text{transfer,side chain, Ala→residue}X}$[c] + $\Delta G_{\text{transfer,Ala, whole residue}}$[d]	
TM1	95-113	79.50	-23.75	14.46	70.21
TM2	148-166	79.50	-23.75	14.36	70.11
TM3	171-190	84.80	-25.00	9.60	69.40
TM4	201-214	53.00	-17.50	7.15	42.65
TM5	227-241	58.30	-18.75	12.70	52.25
TM6	252-267	68.90	-21.25	8.83	56.48
All TM helices		424.00	-130.00	67.10	**361.11**

[a] $\Delta G_{\text{H-bond,backbone}}$ = Number of H bond per TM helix × 5.3 kcal/mol = (Number of TM residues – 4) × 5.3 kcal/mol[66]. This value falls into the range of stronger backbone hydrogen bonds (ΔG^{HB} = 4–8 kcal/mol) experimentally determined in detergent micelles.[67]

[b] $T\Delta S_{\text{side chain}}$: Because one peptide bond is shared by two resides, one residue contributes -1.25 kcal/mol of $T\Delta S_{\text{side chain}}$.[68]

[c] $\Delta G_{\text{transfer, side chain, Ala→residue}X}$: computationally derived depth-dependent hydrophobicity scale relative to Ala residue.[69]

[d] $\Delta G_{\text{transfer, Ala, whole residue}}$ = 0.16 kcal/mol, knowledge-based unified hydrophobicity scale for the whole Ala residue.[71]

Table 3.4 $\Delta G_{\text{dislocation}}$ of individual TM helices of GlpG using membrane-depth dependent transfer free energy.

Total ATP Cost to Degrade GlpG.

Finally, to understand how efficiently FtsH utilizes ATP hydrolysis to degrade membrane substrates, we quantified the total number of ATP molecules hydrolyzed during GlpG degradation in bicelles using the equation: [46]

$$\text{total ATP cost} = k_{\text{cat,ATP}} \times \tau_{\text{cat,deg}}$$

$k_{\text{cat, ATP}}$ denotes the maximal ATP hydrolysis rate per $FtsH_6$ with a bound substrate, and $\tau_{\text{cat, deg}}$ indicates the substrate lifetime (1/ $k_{\text{cat, deg}}$). These parameters were obtained from Michaelis−Menten analysis of ATP hydrolysis and degradation of

GlpG-108 and YccA$_N$-GlpG (**Figure 3.25, Tables 3.2** and **3.5**). The total number of ATP molecules hydrolyzed by FtsH hexamer to degrade a single copy of GlpG was 380 ± 30 for GlpG-108 and 550 ± 60 for YccAN-GlpG.

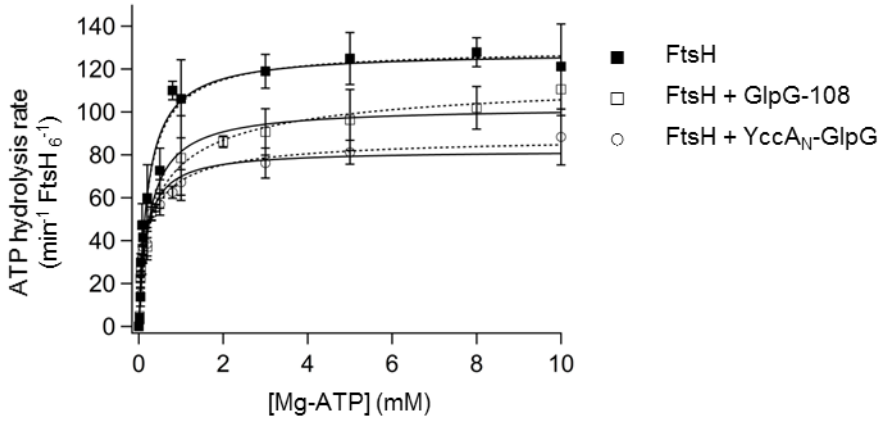

Figure 3.25 ATPase activity of FtsH in the presence of bound substrate.

ATPase activity of FtsH was measured in the presence of saturating concentrations of the membrane protein substrate GlpG-108 and YccA$_N$-GlpG. ATP hydrolysis by FtsH (2 μM) was measured in DMPC/DMPG/CHAPS bicelles at 37ºC using the enzyme-coupled assay. Data are represented as mean ± SEM (n = 3).

	Michaelis-Menten		Hill coefficient
	$k_{cat,ATP}$[a] (min^{-1} FtsH$_6$$^{-1}$)	$K_{m,ATP}$[a] (X_{GlpG})	$n_{H,ATP}$[b]
No substrate	109 ± 2	0.17 ± 0.02	1.0 ± 0.1
+ GlpG-108	99 ± 3	0.20 ± 0.03	0.7 ± 0.1
+ YccA$_N$-GlpG	82 ± 3	0.17 ± 0.02	0.8 ± 0.1

All measurements were performed with [FtsH] = 2 μM in 3% (w/v) DMPC/DMPG/CHAPS bicelles at 37ºC.
[a]$k_{cat, ATP,}$ and $K_{m, ATP}$ values are from nonlinear least square fits of data in Figure 3.25 to the Michaelis-Menten equation (See Method Equation 2).
[b]$n_{H, ATP}$ was obtained from nonlinear least squares fits of data in Figure 3.25 to the Hill equation (See Method Equation 3).

Table 3.5 The effects of bound substrates on the ATPase activity of FtsH.

Discussion

Here, we present the first quantitative study that defines the folding-degradation relationship of a membrane protein mediated by a specific cellular degradation machine. A striking finding of this work is that FtsH substantially accelerates unfolding of a stable membrane protein (>800 fold) and carries out its membrane dislocation overcoming enormous free energy cost (~360 kcal/mol). This result redefines the unfolding capability of FtsH, shifting the long-standing paradigm that FtsH passively selects substrates depending on spontaneous unfolding. We also showed that the degradation of the membrane substrate is significantly influenced by conformational stability and hydrophobicity. Hydrophobicity is a unique determining factor in the degradation of membrane proteins, which may provide another layer of complexity in the degradation mechanism.

FtsH Degrades Membrane Substrates More Efficiently than Water-Soluble Substrates.

The weak unfoldase activity, which has long been regarded as a distinctive feature of FtsH,[18] is based on the observation that FtsH cannot degrade stable globular proteins such as DHFR, GFP, and barnase which unfold slowly, whereas degrading fast unfolding Arc and its variants depends on their stability. Also, the correlation between the degradation rates of Arc variants by FtsH and their proteolysis rates by the energy-independent proteinase Arg-C suggested that FtsH cannot actively unfold a substrate.[18, 58] Thus, it is surprising that FtsH degrades GlpG via active unfolding although its conformational stability is comparable to or exceeds that of water-soluble proteins which cannot be degraded by FtsH (**Table 1.2**).

How can this discrepancy be explained? Structural and single-molecule studies of AAA+ enzymes suggest that during the cycles of ATP hydrolysis, AAA+ subunits undergo power stroke motions applying pulling forces on the bound substrate to induce its unfolding and translocation.[59, 60] A similar principle has been suggested for FtsH.[61] The cryo-EM image of Yta12, an FtsH ortholog in yeast, shows that the substrate entry pore formed by the AAA+ domains faces the membrane plane with a narrow gap of ~13 Å (**Figure 1.11B**).[5] Under this spatial constraint, water-soluble and membrane proteins will be engaged with FtsH in very different geometric arrangements through the flexible tails containing a degradation marker (**Figure 3.26**). For water-soluble proteins, only the unfolded polypeptide chain, not a globular domain, can approach the gap. Thus, the tail bound to the entry pore will align the excluded globular domain at ~90° relative to the pore axis. For membrane proteins with known structure, TM helices are tilted from the bilayer normal at ~20° on average.[62] Thus, the TM helices can be closely aligned along the pore axis. Although the pulling forces along the pore axis exert the same tension on the tails of the two types of proteins, a larger opposing frictional force would be generated at the deflection point near the pore for the water-soluble proteins aligned at ~90° than for the membrane proteins aligned at a smaller angle. Thus, the pulling forces would be more effectively applied to the membrane proteins than on the water-soluble proteins.

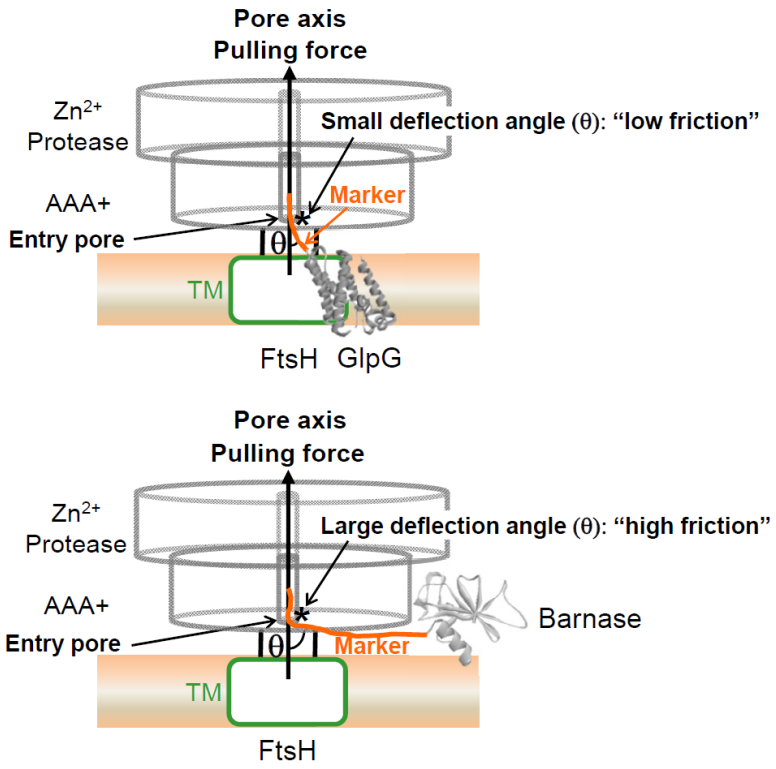

Figure 3.26 A mechanical model to explain why FtsH more efficiently degrades membrane proteins than water-soluble proteins. (up) When a membrane-protein (GlpG here) with a flexible tail as a degradation marker binds to FtsH, the bound tail will align the TM helices of GlpG at a small deflection angle[62] relative to the direction of the pulling force. In this case, a less frictional force is generated at the deflection point (*) near the substrate entry pore and the pulling forces will be efficiently applied to the membrane protein. Despite the presence of the PM (periplasmic) domain, probably GlpG can approach close to the pore axis because of the large gap between neighboring PM domains. (down) When a water-soluble protein (barnase here) with a flexible tail binds to FtsH, the bound tail aligns barnase at a large deflection angle (~90°) relative to the direction of the pulling force. In this case, more frictional force is exerted at the deflection point, reducing the effective pulling force.

Another possible reason for the discrepancy is the difference in the spontaneous refolding rate (k_F) between the two types of proteins. Previous studies indicate that GFP that has been transiently unfolded by ClpXP can fold back to the native state when the ATP hydrolysis rate is low.[63, 64] The k_F's of Barnase and DHFR in water, which cannot be degraded by FtsH, are ~300 and ~8 fold higher ($k_F \approx 12\ s^{-1}$ and $0.25\ s^{-1}$), respectively, than that of GlpG in neutral bicelles ($k_F \approx 0.04\ s^{-1}$). [32, 65, 66] Notably, unfolded DHFR can rapidly refold to a compact intermediate with $k_{F,\,U-I} \approx 6.7\ s^{-1}$.[65] The k_F's of these water-soluble proteins are comparable or higher than the rate of ATP hydrolysis on FtsH (~$2\ s^{-1}$, **Figure 3.1**), whereas that of GlpG is much lower. Therefore, even if barnase and DHFR can be unfolded by FtsH in a certain round of ATP hydrolysis, they could possibly refold to the compact intermediate or native state before the next round of ATP hydrolysis. In contrast, once GlpG unfolds, it is likely to remain unfolded until the next ATP hydrolysis occurs, entering the subsequent dislocation and degradation stages.

Our result seems hard to reconcile with the result that FtsH cannot degrade the membrane protein DGK *in vivo*.[18] DGK forms a tightly packed trimer with high kinetic stability.[67, 68] It does not unfold by steric trapping up to 30 days in micelles,[43] much slower than GlpG ($\tau_U \approx 2$ days). Thus, it is likely that the kinetic barrier of DGK unfolding is beyond the unfolding capability of FtsH.

Folding-Degradation Relationship of Membrane Proteins.

Previous studies on the degradation of water-soluble proteins by ClpXP and ClpAP have shown that the pulling forces generated by ATP hydrolysis act primarily on the local structure adjacent to a degradation marker.[14, 42, 69] Thus, degradation strongly

depends on local conformational stability as well as unfolding cooperativity of the whole structure.[64] Here we demonstrate that the same principle can be applied to the degradation of membrane proteins. For GlpG, we observed a strong correlation between the degradation rate and the local stability of the region to which a degradation marker was attached (**Figure 3.9**). Then, if one subdomain is unraveled by FtsH, what will happen in the other? Previously, we have shown that the perturbation of the native tertiary interactions near the N- or C-terminus is readily propagated throughout the protein.[22] Thus, once FtsH actively unravels either subdomain with its substantial unfoldase activity, the subsequent unfolding of the rest would not experience much resistance.

Through analysis of various intrinsic folding properties of GlpG, we revealed the role of the conformational stability and hydrophobicity in determining the degradation of a membrane protein. Recently, the conformational stability has been shown to be a key determinant for the cellular trafficking efficiency of the human membrane protein PMP22.[70] In yeast, the presence of a mitochondrial FtsH ortholog increases the threshold hydrophobicity level of a TM helix for its retention in the inner membrane.[71] Our systematic study dissecting the effects of the two physical forces further supports these observations.

A Three-Step Model for Membrane Protein Degradation.

On the basis of our findings, we suggest a three-step model for FtsH-mediated membrane protein degradation (**Figure 3.27**). In the first “engagement” step, the degradation marker on a membrane substrate binds to the entry pore of the AAA+ hexamer. Although we only tested well-characterized markers, the substrate-enzyme

affinity does not seem to strongly depend on the detailed sequence of the marker (**Figure 3.9**). Thus, any flexible cytoplasmic tails on native membrane substrates or the tails that are exposed upon protein misfolding, chemical or enzymatic cleavage, subunit dissociation or premature truncation of the translation may serve as degradation markers.[2, 33, 34]

In the second “unfolding” step, FtsH actively unravels the tertiary structure of the bound substrate in the membrane using ATP hydrolysis. If the membrane substrate is highly stable, unfolding would require multiple power-stroke motions, during which the substrate may undergo “slippingrelease” events without unfolding.[46] Also, as noted earlier, the transiently unfolded substrate may refold before the next pulling occurs. Thus, it is likely that the engagement and unfolding steps are reversible. In the third “dislocation and degradation” step, FtsH dislocates the unfolded substrate from the membrane to the protease chamber for degradation using ATP hydrolysis. If the substrate is highly hydrophobic, partial dislocation-reinsertion of the TM segments may repeatedly occur during pulling events.

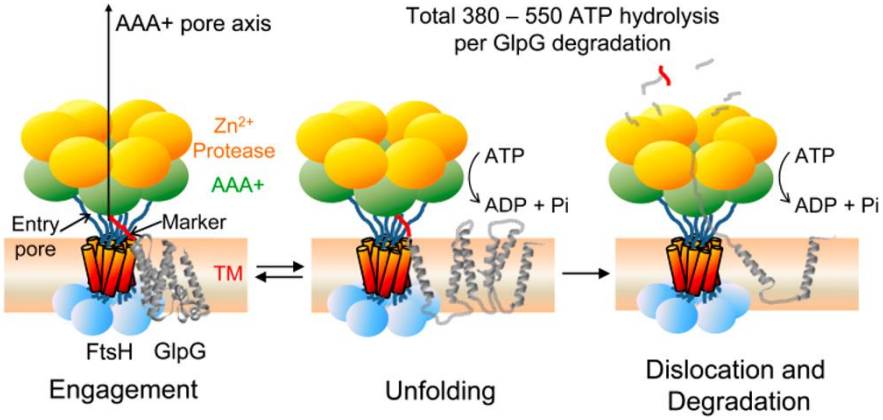

Figure 3.27 Three-step model of FtsH-mediated degradation of membrane proteins.

Degradation of GlpG requires the hydrolysis of a total of 380−550 ATP (1.7−2.5 ATP/residue). Although it appears energetically wasteful, the ATP cost per residue is comparable to that of other AAA+ proteases in the degradation of water-soluble substrates (0.2−6.6 ATP/residue, **Table 3.6**). To degrade water-soluble substrates, ATP hydrolysis is used to unfold them in water and translocate the unfolded chains into the similarly aqueous proteolytic chamber. Surprisingly, for membrane substrates, FtsH carries out the energetically expensive dislocation step (ΔG ≈ 360 kcal/mol) with a similar ATP cost.

AAA+ protease	Substrate	Substrate type	Number of ATP hydrolysis min^{-1} $substrate^{-1}$	Number of residues	Number of ATP hydrolysis/residue
FtsH[a]	GlpG-108	membrane	380 – 550	228	1.7–2.5
FtsH[b]	σ^{32}	water-soluble	140	289	0.5
ClpXP[c]	Titin-I27-SsrA	water-soluble	644	98	6.6
ClpXP[d]	GFP-SsrA	water-soluble	146	268	0.5
Lon[e]	β-galactosidase (3-93)	water-soluble	175	91	1.9
Lon[f]	cp6-sul20[g]/ cp7-sul20[g]	water-soluble	60/ 186	284	0.2/ 0.7
PAN[h]	casein	water-soluble	312	220	1.4

[a] from this work
[b] from reference[72]
[c] from reference[46]
[d] from reference[24]
[e] from reference[73]
[f] from reference[74]
[g] circular-permutated superfolder GFP variants
[h] from reference[75]

Table 3.6 Comparison of ATP costs during degradation of several model proteins by AAA+ proteases.

To further understand the mechanisms of membrane protein degradation, it is necessary to determine which step is rate-determining and how the total ATP cost is distributed between the unfolding and dislocation steps. Extensive mutational studies varying the stability and hydrophobicity in a wide range and assessing their correlation with degradation rates and ATP consumption are under progress.

Implications in Membrane Protein Quality Control.

Our findings have broad implications in the role of FtsH in membrane protein quality control. The substantial unfolding dislocation ability discovered in this study will expand the range of potential substrates to membrane proteins which are misfolded or aggregated with stable non-native interactions, membrane proteins which are folded but need to be degraded for regulatory purpose or toxicity, and prematurely truncated translation products which need to be immediately degraded from the membrane. Several pieces of evidence support the need and existence of significant unfoldase activity of FtsH in bacteria, mitochondria and chloroplasts: (1) FtsH rapidly degrades the whole SecYEG translocase complex jammed with an inefficiently secreted protein; [76] (2) FtsH in the thylakoid membranes mediates swift regeneration of the damaged photosynthetic reaction center by degrading the photo-oxidized core proteins;[9, 77] (3) Chaperone activity of FtsH has been reported which requires active unfolding.[78] These quality control processes can be better understood by the FtsH activity redefined in this study.

Methods

ATPase activity assay of FtsH.

ATP hydrolysis rate by FtsH was measured by an enzyme-coupled assay. The assay mixture (typically 100 µL) in a 96-well UV-compatible microplate (Greiner Bio-One) contained 2 µM FtsH, 20 mM HEPES (pH 7.8), 10 mM $MgCl_2$, 400 µM $ZnCl_2$, 0.1% BME, 100 mM KCl, 15% glycerol, 0.5 mM NADH, 10 mM phosphoenolpyruvic acid, 0.5 units of pyruvate kinase and 0.5 units of lactic dehydrogenase. The oxidation of NADH coupled to ATP hydrolysis was monitored at 37°C by continuous monitoring absorbance at 340 nm on a microplate reader (M5e, Molecular Devices). Data analysis and fitting equations to calculate ATP hydrolysis rate (ν_{ATP}) by FtsH hexamer per minute are shown as following:

$$v_{\mathrm{ATP}} = \frac{\frac{\Delta Abs}{\min}}{\frac{\Delta Abs}{[\mathrm{ATP}]}} \times \frac{1}{[\mathrm{FtsH_6}]} \qquad \textbf{(Equation 1)}$$

A fitting equation using Michaelis-Menten kinetics for ATPase activity of FtsH is given as:

$$v_{\mathrm{ATP}} = \frac{k_{\mathrm{cat,ATP}}[\mathrm{ATP}]}{K_{\mathrm{m,ATP}} + [\mathrm{ATP}]} \qquad \textbf{(Equation 2)}$$

where v_{ATP} is ATP hydrolysis rate, $k_{\mathrm{cat,\ ATP}}$ is a maximal ATP turnover number by FtsH hexamer per min, and $K_{\mathrm{m,\ ATP}}$ is Michaelis constant, the ATP concentration at which ATP hydrolysis rate reaches the half-maximum.

Hill equation to fit ATPase activity of FtsH is given as:

$$v_{\mathrm{ATP}} = \frac{[\mathrm{ATP}]^{n_{\mathrm{H,ATP}}}}{K_{\mathrm{m,ATP}}^{\ n_{\mathrm{H,ATP}}} + [\mathrm{ATP}]^{n_{\mathrm{H,ATP}}}} \qquad \textbf{(Equation 3)}$$

where $n_{\mathrm{H,\ ATP}}$ is Hill constant of FtsH hexamer ATPase activity.

Preparation of bicelles.

15% (w/v) stock of DMPC/DMPG/CHAPS (lipid-to-detergent molar ratio, q = 2.8) bicelles were prepared by hydrating DMPC/DMPG (molar ratio = 3:1) mixture with water and adding 20% (w/v) CHAPS to reach the desired q value. Lipid and Protein Diffusion Assays in Bicelles. To test lipid diffusion in bicelles, 3% bicelles containing fluorescently labeled lipids (NBD-DPPE and rhodamine-DPPE; a lipid mole fraction of 0.01 for each) were mixed with 3% unlabeled bicelles at a 1:35 volume ratio in 20 mM HEPES (pH 7.5), 15% glycerol (v/v), 80 mM KCl and 10 mM $MgCl_2$. FRET signal, i.e., the ratio of fluorescence intensity of NBD at 530 nm to that of rhodamine at 590 nm, was monitored over time at 37 °C. To test protein diffusion in bicelles, GlpG labeled with NBD or rhodamine was incorporated together into the bicelles by direct injection to the final concentration of each labeled proteins at 74 μM. GlpG diffusion in bicelles was measured in the same manner as in lipid diffusion.

Lipid and protein diffusion assays in bicelles.

3% (w/v) bicelles (DMPC/DMPG/CHAPS, *q* = 2.8) without fluorophores (hereafter, unlabeled bicelles) were prepared in 20 mM HEPES (pH 7.5), 15% glycerol (v/v), 80 mM KCl and 10 mM $MgCl_2$ buffer by diluting 15% bicelle stock solution described above. The bicelles containing fluorescently labeled lipids were prepared using the following procedures: First, DMPC and DMPG lipids (DMPC:DMPG molar ratio = 3:1) dissolved in chloroform were mixed with NBD (nitrobenzoxadiazole)-DPPE (1,2-dipalmitoyl-*sn*-glycerol-3-phosphoethanolamine) (FRET donor) and Rh (rhodamine)-DPPE (FRET acceptor) lipids which were also dissolved in chloroform at a lipid mole fraction of 0.01 for each. The lipid solution was dried under a stream of nitrogen gas and further in vacuum for 2 hours. The resultant lipid film was resuspended in 20 mM

HEPES (pH 7.5), 15% glycerol, 80 mM KCl, and 10 mM $MgCl_2$ buffer. The desired amount of CHAPS was added to a final lipid and detergent concentration of 3% (w/v) to form the fluorescent bicelles. Lipid diffusion in bicelles was tested by mixing the fluorescent bicelles with unlabeled bicelles at a 1:35 volume ratio and monitoring FRET signal, i.e., the ratio of fluorescence intensity of NBD at 530 nm to that of Rh at 590 nm, as a function of time. As a negative control that represents no diffusion, the fluorescent bicelles were mixed with buffer solution. As a positive control that represents a homogeneously mixed state, the bicelles containing NBD-DPPE and the bicelles containing Rh-DPPE were added separately to unlabeled bicelles and carefully mixed.

Diffusion of protein components in bicelles was also tested to evaluate the time scale of the interaction between FtsH and substrates, both of which are integrated into bicelles. The principle is similar to that of the lipid diffusion assay described above. Instead of using fluorescently labeled lipids, we incorporated the model membrane substrate GlpG labeled with NBD or Rh into DMPC/DMPG/CHAPS bicelles by direct injection of GlpG solubilized in *n*-dodecyl-*β*-D-maltoside (DDM, Anatrace) to bicelles. The fluorescent GlpG-bicelle complex contained 74 μM of NBD-GlpG and 74 μM of Rh-GlpG. GlpG diffusion in bicelles was tested by measuring the ratio of fluorescence intensity of NBD at 530 nm to that of Rh at 590 nm as a function of time. As a negative control that represents no diffusion of proteins, the bicelles containing NBD and Rh labeled GlpG were mixed with buffer solution without bicelles. As a positive control that represents a homogeneously mixed state, the bicelles containing NBD-GlpG and the bicelles containing Rh-GlpG were added separately to unlabeled bicelles without incorporated proteins. All fluorescence

measurements were performed on PTI QW4 fluorimeter at 37ºC with a final sample volume of 1,400 μL. For FRET, the excitation wavelength for NBD was 467 nm, and the emission wavelengths were 530 nm for NBD and 590 nm for Rh. Both excitation and emission slit-widths were set to 0.75 mm.

Thermostability of GlpG in lipid environments.

Thermostability of the model substrate GlpG was studied in bicelles, liposomes, and micelles by measuring resistance to irreversible thermal inactivation and aggregation. To measure the thermostability in bicelles, GlpG-108 (see below for cloning, expression and purification of GlpG variants for detailed information) in DDM was incorporated into 2 mL of 3% (w/v) DMPC/DMPG/CHAPS bicelle solution (20 mM HEPES, 15% glycerol, 100 mM NaCl, pH 7.5 buffer) to a final concentration of 5 μM by direct injection of concentrated GlpG-108 in DDM into preformed bicelles and incubating for 1hr on ice. The total volume was transferred to a quartz cuvette and heated from 25°C to 90°C with a 5°C interval in the cuvette holder on CARY 100 Series UV-Vis spectrophotometer connected to a temperature-controller. At each target temperature, the sample was incubated for 5 min, and then 100 μL sample was aliquoted from the cuvette and cooled down on ice for 1 hr. 70 μL from each aliquot was used for measuring thermal aggregation and 25 μL for thermal inactivation. Thermal aggregation was measured by absorbance at 320 nm at room temperature. Thermal inactivation was measured by fluorescence-based GlpG activity assay[22], which was carried out by the addition of 25 μL of SN-LacYTM2 labeled with NBD, the model GlpG substrate, to a final concentration of 10 μM at room temperature. The substrate was pre-incorporated in 3% bicelles.

To measure the thermostability in *E. coli* liposomes, GlpG-108 was first reconstituted in *E. coli* lipid vesicles. Dried *E. coli* lipid (Avanti Polar Lipids) film was hydrated with 20 mM HEPES (pH 7.5), 100 mM NaCl buffer to a final lipid concentration of 10 mM. The lipid suspension was homogenized by three cycles of freeze-thaw and then extruded through 0.2 μM pore size polycarbonate membrane (Whatman). DDM was added to the liposome suspension to a final concentration of 10 mM and incubated for 30 min, and GlpG protein stock was added to a final concentration of 5 μM. The lipid-protein-detergent mixture was incubated for 30 min. For detergent removal, three portions of Bio-Beads (Bio-Rad) were added (20 mg/mL for each) stepwise. In each step, the mixture was gently stirred for 1–2 hr at room temperature. The resulting proteoliposomes were extruded again using 0.2 μM pore size membrane. 2.0 mL of reconstituted GlpG in 20 mM HEPES (pH 7.5), 100 mM NaCl buffer at a concentration of 5 μM was added to a quartz cuvette. Sample heating and aliquoting were performed in the same way as in bicelles. For the samples to measure irreversible aggregation, one portion from each aliquoted sample was solubilized with a final concentration of 2% (w/v) octyl- β-glucoside (β-OG, Anatrace) and incubated overnight, and absorbance at 320 nm was measured at room temperature. For the samples to measure irreversible inactivation, the other portion from the aliquoted sample was solubilized in 20 mM DDM overnight and GlpG activity (1 μM at a final concentration) was measured by addition of NBD-labeled SN-LacYTM2 in DDM to a final concentration of 10 μM. As a control, thermostability of GlpG-108 was measured in DDM under the same condition used by Baker and Urban (2.5 μM GlpG in 50 mM Tris pH 7.4, 100 mM NaCl, 1 mM EDTA, 1 mM DTT and 0.1% (w/v) DDM)[30]. Sample heating, aliquoting, absorbance, and GlpG activity measurement were performed in the same way as in bicelles and liposomes.

In all measurements, absorbance at 320 nm and GlpG activity for the samples that had been incubated at each temperature were normalized relative to those at 25^{o}C, respectively.

GlpG degradation assay in vivo.

E. coli AR3289 (+*ftsH*) and AR3291 (–*ftsH*) strains were transformed with each GlpG variant plasmid. 7 mL of LB containing 100 μg/mL of ampicillin was inoculated with a single colony, and cells were grown for 18 hr at 37°C for AR3289 and 30°C for AR3291. $OD_{600\ nm}$ was measured to check growth. When $OD_{600\ nm}$ reached in 1.5–1.7 (AR3289) and 0.8–1.0 (AR3291), GlpG expression was induced by addition of 0.2% (w/v) arabinose at 37°C for 1 hour. Then protein synthesis was blocked by the addition of 300 μg/mL spectinomycin, immediately followed by a collection of the sample at time 0. To monitor degradation over time, samples were further incubated at 37°C in a shaker at 180 rpm. 600 μL of aliquot of each sample was taken at subsequent time points. All samples were frozen in liquid nitrogen immediately after collection. For immunodetection, thawed cells were spun down at 13,000 rpm for 3 minutes using a bench-top centrifuge (Eppendorf, 5424R). Depending on their absorbance, cell pellets were resuspended in TE Buffer (10 mM Tris-HCl, 1 mM EDTA, pH 8.0) and mixed with protein sample buffer (final concentration of 2% SDS (w/v), 0.1% (w/v) bromophenol blue, 10% glycerol (v/v), 1% (v/v) BME, 50 mM Tris-HCl, pH 6.8). The mixtures were sonicated for 10–30 seconds prior to SDS-PAGE. 4–20% Mini-PROTEAN TGX gels (Bio-Rad) were used in all electrophoresis. To monitor GlpG degradation by FtsH, Western blotting analysis against HA or FLAG epitopes was performed. Epitope-tagged proteins were transferred to a PVDF membrane (Bio-Rad). The following procedures were performed according to the

protocol provided by manufacturers. GlpG variants containing HA epitope were probed with HRP-conjugated anti-HA monoclonal antibody (Thermo Fisher Scientific, 1:1000 dilution). GlpG variants with FLAG epitope were detected using rabbit monoclonal anti-FLAG primary antibody (Cell Signaling Technology, 1:1000 dilution) and anti-rabbit IgG-HRP secondary antibody (Cell Signaling Technology, 1:2000 dilution). Chemiluminescent detection was performed using Clarity Western ECL substrate (Bio-Rad) and ChemiDoc Imager (Bio-Rad).

Cloning and mutagenesis of GlpG for in vitro degradation.

Variants of GlpG TM domain (residues 87–276) fused to N-terminal MBP followed by TEV cleavage site ($TEV_{cleavage}$) were cloned into pET30a vector using NdeI and XhoI restriction sites. The resulting expression plasmids encode the proteins with an N-terminal His_6-tag (His_6-MBP-$TEV_{cleavage}$-GlpG). Using this as a base construct, a degradation marker for FtsH was fused to the N-(Dps_N or $YccA_N$) or C-terminus (108 or SsrA) of GlpG. Cysteine mutant G172C was generated by QuickChange site-directed mutagenesis for thiol-reactive fluorophore labeling. *E. coli* BL21(DE3) RP cells transformed with a GlpG plasmid were cultivated on selection plates (50 mg/L kanamycin) at 37°C. The liquid culture was inoculated with a single colony and cultured in LB media (50 mg/L kanamycin) overnight at 37°C until reaching the stationary phase. The overnight culture was used to inoculate a fresh LB media (50 mg/L kanamycin), and the culture was grown at 37°C until an OD_{600nm} of 1.0, at which a final concentration of 0.5 mM IPTG was added. The culture was further grown 16 hours at 15°C.

Purification of GlpG variants for in vitro degradation assay.

His_6-MBP-$TEV_{cleavage}$-GlpG possessing a degradation marker was expressed in *E. coli* BL21(DE3) RP cells. Cells were harvested and resuspended in 1/50 culture volume of 50 mM Tris-HCl buffer solution (pH 8.0) containing 0.5 mM TCEP, 5 mM EDTA, and 0.5 mM PMSF. The resuspended cells were lysed five times using pressure homogenizer. The lysate was centrifuged at 6,000 rpm for 30 min in F21 rotor using a Sorvall RC6+ centrifuge. The supernatant was centrifuged to obtain the total membrane fraction at 28,000 rpm for 2 hours in Type 45 Ti rotor using ultracentrifuge (Beckman-Coulter). The membrane pellets were resuspended in 1/100 culture volume of 50 mM Tris-HCl buffer solution (pH 8.0) containing 200 mM NaCl and 0.5 mM TCEP using tissue homogenizer. The membrane resuspension was solubilized by addition of 1/100 culture volume of solubilization buffer (pH 8.0) containing 50 mM Tris-HCl, 2% (w/v) n-decyl-β-D-maltoside (DM, Anatrace), 200 mM NaCl, 0.5 mM TCEP, and 0.5 mM PMSF followed by ultracentrifugation at 12,000 rpm for 30 min in Type 45 Ti rotor. His_6-MBP-$TEV_{cleavage}$-GlpG in the supernatant was purified using Ni^{2+}-NTA affinity chromatography (1 mL resin per liter culture). After removal of excess imidazole in a desalting column (Bio-Rad), the linker between His_6-MBP and GlpG was cleaved using TEV protease with an N-terminal His_7-tag (His_7-TEV protease) ([GlpG] / [TEV protease] = 5) after 6 hours of gentle stirring at room temperature. 1 mL of Ni-NTA resin was added to the reaction mixture to bind His_7-TEV protease and His_6-MBP. GlpG portion was isolated in the flow-through and further concentrated using an Amicon centrifugal filter unit (Millipore Sigma, 10 kDa MWCO). The protein concentration was measured using absorbance at 280 nm (ε_{280nm} = 69,940 $M \cdot cm^{-1}$)

NBD-labeling of GlpG variants.

About 30 μM of purified single-cysteine mutant (G172C) of GlpG variants in 0.5% DM, 50 mM Tris-HCl and 200 mM NaCl (pH 8.0) was incubated with 10 times molar excess of TCEP for 1 hour at room temperature. 15 times molar excess of thiol-reactive, environment-sensitive fluorophore IA-NBD amide dissolved in DMSO (~10 mg/ml) was added to the mixture while vortexing. The labeling reaction was incubated at 4°C overnight in the dark. Excess free labels were removed by dialysis against buffer containing 0.2% DM, 50 mM Tris-HCl, and 200 mM NaCl (pH 8.0) and a desalting column. Typically, the labeling efficiency of NBD ranged from 1.0–1.2 as determined by comparing the concentration of NBD measured by UV-Vis absorbance (ε_{480nm} = 23,500 $M \cdot cm^{-1}$) to the concentration of GlpG measured by DC protein assay (Bio-Rad).

GlpG degradation assay in vitro using NBD fluorescence

Degradation of NBD-labeled GlpG variants by FtsH was measured in 3% (w/v) bicelles (DMPC/DMPG/CHAPS, q = 2.8). To ensure integration of the model substrate GlpG into bilayers, GlpG was first reconstituted in DMPC/DMPG liposomes with the following protocol: Mixed dried lipid ([DMPC]:[DMPG] = 3:1) was dispersed in 20 mM HEPES (pH 7.6) 100 mM KCl, 15% glycerol, 0.1% BME and 4% β-OG to a final lipid concentration of 3% (w/v). The NBD-labeled GlpG stock solution (100-300 μM) in DM was mixed with the solubilized lipids to a final concentration of 50-100 μM and incubated on ice for 1 hr. The mixture was dialyzed against ×350 sample volumes of 20 mM HEPES (pH 7.5), 100 mM KCl, 15% glycerol, 0.1% BME buffer solution, with four buffer exchanges over 48 hours at 4°C (10 kDa cutoff dialysis tubing, Thermo Fisher Scientific), followed by incubation with Bio-Beads (Bio-Rad,

0.2 mg/mL suspension) for 16 hr at room temperature for further removal of residual detergents. The resulting proteoliposomes were extruded through a 0.2 μM pore size polycarbonate membrane (Sigma). The total phospholipid concentration was determined by an organic phosphate assay. Based on the measured total lipid concentration, the desired amount of CHAPS was added to form bicelles with q = 2.8. The final concentration of NBD-labeled GlpG in bicelles was determined by the DC assay. Measurements of time-dependent degradation of GlpG were performed in 3% bicellar solution (20 mM HEPES, pH 7.5, 100 mM KCl, 15% glycerol, 0.1% BME, and 400 μM $ZnCl_2$) containing various concentrations of NBD-labeled GlpG and an ATP regeneration system (0.5 unit/100 μL pyruvate kinase and 10 mM phosphoenolpyruvic acid). FtsH was incorporated into bicelles by direct injection of FtsH stock solution in Triton X-100 (60-100 μM) to preformed bicelles at a final monomer concentration of 2 μM on ice. A total volume of 100 μL of each sample was transferred to a 96-well UV-compatible microplate (Greiner Bio-One) and sealed with a polyolefin film. Degradation of GlpG was initiated by addition of 2 mM ATP to each well and monitored by quenching of NBD fluorescence at 545 nm with an excitation wavelength of 485 nm on a SpectraMax M5 plate reader. The net change of NBD fluorescence induced by GlpG degradation was obtained by subtracting the time-dependent change of NBD fluorescence in the presence of ATP from that in the absence of ATP at each GlpG concentration. Data analysis and fitting equations are described in Chapter 2.

Computing dislocation free energy of GlpG.

Free energy of dislocation ($\Delta G_{dislocation}$) was defined as the free energy required to transfer the whole TM helices of fully unraveled GlpG from the lipid bilayer to water.

It can be approximated by summing up the free energy changes in Stage 2-1 (backbone unfolding of TM helices in the bilayer) and Stage 2-2 (transfer of the unfolded polypeptide from bilayer to water) (**Figure 3.24**) as follows:

$$\Delta G_{\text{dislocation}} = \sum_{\text{H-bonds}} \Delta G_{\text{H-bond,backbone}} + \sum_{\text{residues}} T\Delta S_{\text{side-chain}} + \sum_{\text{residues}} \Delta G_{\text{transfer,residueX}} \quad \textbf{(Equation 4)},$$

where $\Delta G_{\text{H-bond, backbone}}$ is the free energy change for breaking a backbone hydrogen bond in the TM α-helices inside the lipid bilayer[50], $T\Delta S_{\text{side-chain}}$ is the change in side-chain entropy for helix unfolding[52], and $\Delta G_{\text{transfer, residueX}}$ is the free energy change for transferring the whole residue X from the bilayer to water. Here $\Delta G_{\text{transfer, residueX}}$ can be computed as

$$\Delta G_{\text{transfer,residueX}} = \Delta G_{\text{transfer,Ala}} + \Delta G_{\text{transfer,Ala}\rightarrow\text{residueX}} \quad \textbf{(Equation 9)},$$

where $\Delta G_{\text{transfer, Ala}}$ is the transfer free energy of whole residue Ala[55], and $\Delta G_{\text{transfer, Ala}\rightarrow\text{residueX}}$ is the side-chain transfer free energy of residue X with respect to Ala. Here it was assumed that the depth-dependence of $\Delta G_{\text{H-bond, backbone}}$ and $\Delta G_{\text{transfer, Ala, whole residue}}$ was not significant[56].The side-chain transfer free energy $\Delta G_{\text{transfer, Ala}\rightarrow\text{residueX}}$ was determined using the depth-dependent general transfer free energy profile (GeTFEP)[53], which is obtained by computing the side-chain transfer free energies in β-barrel membrane proteins[47,54]. GlpG structure of PDB ID 2XOW was used, with the TM segments determined using the Orientations of Proteins in Membranes (OPM) database[57]. The C_α coordinates of each TM residue and the thickness of TM segments were used to determine the relative depth d of that residue, which is then used for calculating the side-chain transfer free energy $\Delta G_{\text{transfer, Ala}\rightarrow\text{residueX}}(d)$ using GeTFEP.

$$\Delta G_{\text{transfer,Ala}\rightarrow\text{residueX}}(d) = \sum_{i=0}^{3} p_{X,i} \cdot d^i$$ **(Equation 10)**,

where $p_{X,i}$ is the *i*-th coefficients of residue X in GeTFEP. The sequence of GlpG structure with a bound inhibitor (PDB ID 2XOW) is identical to that of the apo-structure (PDB ID) 3B45. The root-mean-square deviation (RMSD) between these two structures is 0.60Å.

Quantification and statistical analysis

Throughout the manuscript, the data are represented as the average ± SEM or ± STD of fit. All experiments were performed at least in triplicates unless specified. Quantitative band analysis of the resulting SDS-PAGE gel and Western blot was carried out using ImageJ (https://imagej.nih.gov/ij/index.html) software to determine the band intensity, the fraction of substrate cleaved at each time point.

REFERENCES

REFERENCES

(1) Gottesman, S., Proteases and their targets in Escherichia coli. *Annual review of genetics* **1996,** *30* (1), 465-506.

(2) Sauer, R. T.; Baker, T. A., AAA+ proteases: ATP-fueled machines of protein destruction. *Annual review of biochemistry* **2011,** *80*, 587-612.

(3) Langer, T., AAA proteases: cellular machines for degrading membrane proteins. *Trends in biochemical sciences* **2000,** *25* (5), 247-251.

(4) Ito, K.; Akiyama, Y., Cellular functions, mechanism of action, and regulation of FtsH protease. *Annu. Rev. Microbiol.* **2005,** *59*, 211-231.

(5) Lee, S.; Augustin, S.; Tatsuta, T.; Gerdes, F.; Langer, T.; Tsai, F., Electron cryomicroscopy structure of a membrane-anchored mitochondrial AAA protease. *Journal of Biological Chemistry* **2011,** *286* (6), 4404-4411.

(6) Shimohata, N.; Chiba, S.; Saikawa, N.; Ito, K.; Akiyama, Y., The Cpx stress response system of Escherichia coli senses plasma membrane proteins and controls HtpX, a membrane protease with a cytosolic active site. *Genes to Cells* **2002,** *7* (7), 653-662.

(7) Campbell, C. L.; Tanaka, N.; White, K. H.; Thorsness, P. E., Mitochondrial morphological and functional defects in yeast caused by yme1 are suppressed by mutation of a 26S protease subunit homologue. *Molecular biology of the cell* **1994,** *5* (8), 899-905.

(8) Arlt, H.; Steglich, G.; Perryman, R.; Guiard, B.; Neupert, W.; Langer, T., The formation of respiratory chain complexes in mitochondria is under the proteolytic control of the m-AAA protease. *The EMBO journal* **1998,** *17* (16), 4837-4847.

(9) Krynická, V.; Shao, S.; Nixon, P. J.; Komenda, J., Accessibility controls selective degradation of photosystem II subunits by FtsH protease. *Nature plants* **2015,** *1* (12), 15168.

(10) Ostersetzer, O.; Adam, Z., Light-stimulated degradation of an unassembled Rieske FeS protein by a thylakoid-bound protease: the possible role of the FtsH protease. *The Plant Cell* **1997,** *9* (6), 957-965.

(11) Di Bella, D.; Lazzaro, F.; Brusco, A.; Plumari, M.; Battaglia, G.; Pastore, A.; Finardi, A.; Cagnoli, C.; Tempia, F.; Frontali, M., Mutations in the mitochondrial protease gene AFG3L2 cause dominant hereditary ataxia SCA28. *Nature genetics* **2010,** *42* (4), 313.

(12) Nolden, M.; Ehses, S.; Koppen, M.; Bernacchia, A.; Rugarli, E. I.; Langer, T., The m-AAA protease defective in hereditary spastic paraplegia controls ribosome assembly in mitochondria. *Cell* **2005,** *123* (2), 277-289.

(13) Koodathingal, P.; Jaffe, N. E.; Kraut, D. A.; Prakash, S.; Fishbain, S.; Herman, C.; Matouschek, A., ATP-dependent proteases differ substantially in their ability to unfold globular proteins. *Journal of Biological Chemistry* **2009,** *284* (28), 18674-18684.

(14) Lee, C.; Schwartz, M. P.; Prakash, S.; Iwakura, M.; Matouschek, A., ATP-dependent proteases degrade their substrates by processively unraveling them from the degradation signal. *Molecular cell* **2001,** *7* (3), 627-637.

(15) Kim, Y.-I.; Burton, R. E.; Burton, B. M.; Sauer, R. T.; Baker, T. A., Dynamics of substrate denaturation and translocation by the ClpXP degradation machine. *Molecular cell* **2000,** *5* (4), 639-648.

(16) Hoskins, J. R.; Yanagihara, K.; Mizuuchi, K.; Wickner, S., ClpAP and ClpXP degrade proteins with tags located in the interior of the primary sequence. *Proceedings of the National Academy of Sciences* **2002,** *99* (17), 11037-11042.

(17) Kihara, A.; Akiyama, Y.; Ito, K., Dislocation of membrane proteins in FtsH-mediated proteolysis. *The EMBO Journal* **1999,** *18* (11), 2970-2981.

(18) Herman, C.; Prakash, S.; Lu, C. Z.; Matouschek, A.; Gross, C. A., Lack of a robust unfoldase activity confers a unique level of substrate specificity to the universal AAA protease FtsH. *Molecular cell* **2003,** *11* (3), 659-669.

(19) Heyden, M.; Freites, J. A.; Ulmschneider, M. B.; White, S. H.; Tobias, D. J., Assembly and stability of α-helical membrane proteins. *Soft matter* **2012,** *8* (30), 7742-7752.

(20) Preiner, J.; Janovjak, H.; Rankl, C.; Knaus, H.; Cisneros, D. A.; Kedrov, A.; Kienberger, F.; Muller, D. J.; Hinterdorfer, P., Free energy of membrane protein unfolding derived from single-molecule force measurements. *Biophysical journal* **2007,** *93* (3), 930-937.

(21) Sanders, C. R.; Landis, G. C., Reconstitution of membrane proteins into lipid-rich bilayered mixed micelles for NMR studies. *Biochemistry* **1995,** *34* (12), 4030-4040.

(22) Guo, R.; Gaffney, K.; Yang, Z.; Kim, M.; Sungsuwan, S.; Huang, X.; Hubbell, W. L.; Hong, H., Steric trapping reveals a cooperativity network in the intramembrane protease GlpG. *Nature chemical biology* **2016,** *12* (5), 353.

(23) Glover, K. J.; Whiles, J. A.; Wu, G.; Yu, N.-j.; Deems, R.; Struppe, J. O.; Stark, R. E.; Komives, E. A.; Vold, R. R., Structural evaluation of phospholipid bicelles for solution-state studies of membrane-associated biomolecules. *Biophysical journal* **2001,** *81* (4), 2163-2171.

(24) Hersch, G. L.; Burton, R. E.; Bolon, D. N.; Baker, T. A.; Sauer, R. T., Asymmetric interactions of ATP with the AAA+ ClpX6 unfoldase: allosteric control of a protein machine. *Cell* **2005,** *121* (7), 1017-1027.

(25) Maurizi, M. R., ATP-promoted interaction between Clp A and Clp P in activation of Clp protease from Escherichia coli. *Portland Press Limited: Biochemical society transactions* **1991**,19, 719-723.

(26) Wohlever, M. L.; Baker, T. A.; Sauer, R. T., A mutation in the N domain of *E. coli* Lon stabilizes dodecamers and selectively alters degradation of model substrates. *Journal of bacteriology* **2013**, 00886-13.

(27) Yakamavich, J. A.; Baker, T. A.; Sauer, R. T., Asymmetric nucleotide transactions of the HslUV protease. *Journal of molecular biology* **2008,** *380* (5), 946-957.

(28) Duzgunes, N.; Allen, T. M.; Fedor, J.; Papahadjopoulos, D., Lipid mixing during membrane aggregation and fusion: why fusion assays disagree. *Biochemistry* **1987,** *26* (25), 8435-8442.

(29) Lemberg, M. K.; Freeman, M., Functional and evolutionary implications of enhanced genomic analysis of rhomboid intramembrane proteases. *Genome research* **2007,** *17* (11), 000-000.

(30) Baker, R. P.; Urban, S., Architectural and thermodynamic principles underlying intramembrane protease function. *Nature chemical biology* **2012,** *8* (9), 759.

(31) Paslawski, W.; Lillelund, O. K.; Kristensen, J. V.; Schafer, N. P.; Baker, R. P.; Urban, S.; Otzen, D. E., Cooperative folding of a polytopic α-helical membrane protein involves a compact N-terminal nucleus and nonnative loops. *Proceedings of the National Academy of Sciences* **2015,** *112* (26), 7978-7983.

(32) Min, D.; Jefferson, R. E.; Bowie, J. U.; Yoon, T.-Y., Mapping the energy landscape for second-stage folding of a single membrane protein. *Nature chemical biology* **2015,** *11* (12), 981.

(33) Chiba, S.; Akiyama, Y.; Mori, H.; Matsuo, E. i.; Ito, K., Length recognition at the N-terminal tail for the initiation of FtsH-mediated proteolysis. *EMBO reports* **2000,** *1* (1), 47-52.

(34) Chiba, S.; Akiyama, Y.; Ito, K., Membrane protein degradation by FtsH can be initiated from either end. *Journal of bacteriology* **2002,** *184* (17), 4775-4782.

(35) Ogura, T.; Inoue, K.; Tatsuta, T.; Suzaki, T.; Karata, K.; Young, K.; Su, L. H.; Fierke, C. A.; Jackman, J. E.; Raetz, C. R., Balanced biosynthesis of major membrane components through regulated degradation of the committed enzyme of lipid A biosynthesis by the AAA protease FtsH (HflB) in Escherichia coli. *Molecular microbiology* **1999,** *31* (3), 833-844.

(36) Herman, C.; Thévenet, D.; Bouloc, P.; Walker, G. C.; D'Ari, R., Degradation of carboxy-terminal-tagged cytoplasmic proteins by the Escherichia coli protease HflB (FtsH). *Genes & developmental* **1998,** *12* (9), 1348-1355.

(37) Farrell, C. M.; Grossman, A. D.; Sauer, R. T., Cytoplasmic degradation of ssrA-tagged proteins. *Molecular microbiology* **2005,** *57* (6), 1750-1761.

(38) Flynn, J. M.; Neher, S. B.; Kim, Y.-I.; Sauer, R. T.; Baker, T. A., Proteomic discovery of cellular substrates of the ClpXP protease reveals five classes of ClpX-recognition signals. *Molecular cell* **2003,** *11* (3), 671-683.

(39) Akiyama, Y.; Kihara, A.; Tokuda, H.; Ito, K., FtsH (HflB) is an ATP-dependent protease selectively acting on SecY and some other membrane proteins. *Journal of Biological Chemistry* **1996,** *271* (49), 31196-31201.

(40) Hari, S. B.; Sauer, R. T., The AAA+ FtsH protease degrades an ssrA-tagged model protein in the inner membrane of Escherichia coli. *Biochemistry* **2016,** *55* (40), 5649-5652.

(41) Berko, D.; Tabachnick-Cherny, S.; Shental-Bechor, D.; Cascio, P.; Mioletti, S.; Levy, Y.; Admon, A.; Ziv, T.; Tirosh, B.; Goldberg, A. L., The direction of protein entry into the proteasome determines the variety of products and depends on the force needed to unfold its two termini. *Molecular cell* **2012,** *48* (4), 601-611.

(42) Olivares, A. O.; Kotamarthi, H. C.; Stein, B. J.; Sauer, R. T.; Baker, T. A., Effect of directional pulling on mechanical protein degradation by ATP-dependent proteolytic machines. *Proceedings of the National Academy of Sciences* **2017,** *114* (31), E6306-E6313.

(43) Robinson, C. R.; Rentzeperis, D.; Silva, J. L.; Sauer, R. T., Formation of a denatured dimer limits the thermal stability of Arc repressor. *J Mol Biol* **1997,** *273* (3), 692-700.

(44) Howarth, M., Chinnapen, D.J., Gerrow, K., Dorrestein, P.C., Grandy, M.R., Kelleher, N.L., El-Husseini, A. and Ting, A.Y., A monovalent streptavidin with a single femtomolar biotin binding site. *Nature methods* **2006**, *3*(4), 267.

(45) Srisa-Art, M., Dyson, E.C., deMello, A.J. and Edel, J.B., Monitoring of real-time streptavidin− biotin binding kinetics using droplet microfluidics. *Analytical chemistry* **2008**, *80*(18), 7063-7067.

(46) Kenniston, J. A.; Baker, T. A.; Fernandez, J. M.; Sauer, R. T., Linkage between ATP consumption and mechanical unfolding during the protein processing reactions of an AAA+ degradation machine. *Cell* **2003,** *114* (4), 511-520.

(47) Lin, M., Gessmann, D., Naveed, H. and Liang, J., Outer membrane protein folding and topology from a computational transfer free energy scale. *Journal of the American Chemical Society* **2016**, *138*(8), 2592-2601.

(48) Hessa, T., Kim, H., Bihlmaier, K., Lundin, C., Boekel, J., Andersson, H., Nilsson, I., White, S.H. and von Heijne, G., Recognition of transmembrane helices by the endoplasmic reticulum translocon. *Nature* **2005**, *433*(7024), 377.

(49) Wimley, W.C., Creamer, T.P. and White, S.H., Solvation energies of amino acid side chains and backbone in a family of host− guest pentapeptides. *Biochemistry* **1996**, *35*(16), 5109-5124.

(50) Ben-Tal, N., Sitkoff, D., Topol, I.A., Yang, A.S., Burt, S.K. and Honig, B., Free energy of amide hydrogen bond formation in vacuum, in water, and in liquid alkane solution. *The Journal of Physical Chemistry B* **1997**, *101*(3), 450-457.

(51) Cao, Z., Hutchison, J.M., Sanders, C.R. and Bowie, J.U., Backbone hydrogen bond strengths can vary widely in transmembrane helices. *Journal of the American Chemical Society* **2017**, *139*(31), 10742-10749.

(52) Privalov, P.L., Stability of proteins small globular proteins. In *Advances in protein chemistry* **1979**, 33, 167-241. Academic Press.

(53) Tian, W., Naveed, H., Lin, M., and Liang, J., GeTFEP: a general transfer free energy profile for transmembrane proteins. *BioRxiv* **2017**, 191650.

(54) Tian, W., Lin, M., Naveed, H., and Liang, J., Efficient computation of transfer free energies of amino acids in beta-barrel membrane proteins. *Bioinformatics* **2017**,33 (11), 1664-1671.

(55) Koehler, J., Woetzel, N., Staritzbichler, R., Sanders, C. R., and Meiler, J., A unified hydrophobicity scale for multispan membrane proteins. *Proteins* **2009**,76 (1), 13-29.

(56) Hessa, T., Meindl-Beinker, N. M., Bernsel, A., Kim, H., Sato, Y., Lerch-Bader, M., Nilsson, I., White, S. H., and von Heijne, G., Molecular code for transmembrane-helix recognition by the Sec61 translocon. *Nature* **2007**,450 (7172), 1026-1030.

(57) Lomize, M. A., Lomize, A. L., Pogozheva, I. D., and Mosberg, H. I., OPM: orientations of proteins in membranes database. *Bioinformatics* **2006**,22 (5), 623-625.

(58) Burton, R.E., Siddiqui, S.M., Kim, Y.I., Baker, T.A. and Sauer, R.T., Effects of protein stability and structure on substrate processing by the ClpXP unfolding and degradation machine. *The EMBO journal* **2001**, *20*(12), 3092-3100.

(59) Maillard, R. A., Chistol, G., Sen, M., Righini, M., Tan, J., Kaiser, C. M., Hodges, C., Martin, A., and Bustamante, C., ClpX(P) generates mechanical force to unfold and translocate its protein substrates. *Cell* **2011,** *145* (3), 459-469.

(60) Glynn, S.E., Martin, A., Nager, A.R., Baker, T.A. and Sauer, R.T., Structures of asymmetric ClpX hexamers reveal nucleotide-dependent motions in a AAA+ protein-unfolding machine. *Cell* **2009**, *139*(4), 744-756.

(61) Bieniossek, C.; Niederhauser, B.; Baumann, U. M., The crystal structure of apo-FtsH reveals domain movements necessary for substrate unfolding and translocation. *Proceedings of the National Academy of Sciences* **2009**, 21579-21584.

(62) Bowie, J.U., Helix packing in membrane proteins. *Journal of molecular biology* 1997, *272*(5), 780-789.

(63) Sen, M., Maillard, R.A., Nyquist, K., Rodriguez-Aliaga, P., Presse, S., Martin, A. and Bustamante, C., The ClpXP protease unfolds substrates using a constant rate of pulling but different gears. *Cell* **2013**, *155*(3), 636-646.

(64) Martin, A., Baker, T. A., and Sauer, R. T., Protein unfolding by a AAA+ protease is dependent on ATP-hydrolysis rates and substrate energy landscapes. *Nat Struct Mol Biol* **2008,** *15* (2), 139-145.

(65) Swanwick, R.S., Shrimpton, P.J. and Allemann, R.K., Pivotal role of Gly 121 in dihydrofolate reductase from Escherichia coli: the altered structure of a mutant enzyme may form the basis of its diminished catalytic performance. *Biochemistry* 2004, *43*(14), 4119-4127.

(66) Vu, N.D., Feng, H. and Bai, Y., The folding pathway of barnase: the rate-limiting transition state and a hidden intermediate under native conditions. *Biochemistry* **2004**, *43*(12), 3346-3356.

(67) Koehler, J., Sulistijo, E.S., Sakakura, M., Kim, H.J., Ellis, C.D. and Sanders, C.R., Lysophospholipid micelles sustain the stability and catalytic activity of diacylglycerol kinase in the absence of lipids. *Biochemistry* **2010**, *49*(33), 7089-7099.

(68) Li, D., Lyons, J.A., Pye, V.E., Vogeley, L., Aragão, D., Kenyon, C.P., Shah, S.T., Doherty, C., Aherne, M. and Caffrey, M., Crystal structure of the integral membrane diacylglycerol kinase. *Nature* **2013**, *497*(7450), 521.

(69) Cordova, J. C., Olivares, A. O., Shin, Y., Stinson, B. M., Calmat, S., Schmitz, K. R., Aubin-Tam, M. E., Baker, T. A., Lang, M. J., and Sauer, R. T., Stochastic but highly coordinated protein unfolding and translocation by the ClpXP proteolytic machine. *Cell* **2014,** *158* (3), 647-658.

(70) Schlebach, J.P., Narayan, M., Alford, C., Mittendorf, K.F., Carter, B.D., Li, J. and Sanders, C.R., Conformational stability and pathogenic misfolding of the integral membrane protein PMP22. *Journal of the American Chemical Society* **2015**, *137*(27), pp.8758-8768.

(71) Botelho, S.C., Tatsuta, T., von Heijne, G. and Kim, H., Dislocation by the m-AAA protease increases the threshold hydrophobicity for retention of transmembrane helices in the inner membrane of yeast mitochondria. *Journal of Biological Chemistry* **2013**, *288*(7), 4792-4798.

(72) Okuno, T.; Yamada-Inagawa, T.; Karata, K.; Yamanaka, K.; Ogura, T., Spectrometric analysis of degradation of a physiological substrate σ32 by Escherichia coli AAA protease FtsH. *Journal of structural biology* **2004,** *146* (1-2), 148-154.

(73) Gur, E. and Sauer, R. T., Recognition of misfolded proteins by Lon, a AAA(+) protease. *Genes Dev* **2008,** *22* (16), 2267-2277.

(74) Wohlever, M. L., Nager, A. R., Baker, T. A., and Sauer, R. T., Engineering fluorescent protein substrates for the AAA+ Lon protease. *Protein Eng Des Sel* **2013,** *26* (4), 299-305.

(75) Benaroudj, N. and Goldberg, A. L., PAN, the proteasome-activating nucleotidase from archaebacteria, is a protein-unfolding molecular chaperone. *Nature Cell Biology* **2000,** *2* (11), 833-839.

(76) Van Stelten, J., Silva, F., Belin, D. and Silhavy, T.J., Effects of antibiotics and a proto-oncogene homolog on destruction of protein translocator SecY. *Science* **2009**, *325*(5941), 753-756.

(77) Jarvi, S., Suorsa, M., Tadini, L., Ivanauskaite, A., Rantala, S., Allahverdiyeva, Y., Leister, D., and Aro, E. M., Thylakoid-Bound FtsH Proteins Facilitate Proper Biosynthesis of Photosystem I. *Plant Physioloy* **2016,** *171* (2), 1333-1343.

(78) Leonhard, K., Stiegler, A., Neupert, W., and Langer, T., Chaperone-like activity of the AAA domain of the yeast Yme1 AAA protease. *Nature* **1999,** *398* (6725), 348-351.

Chapter 4 Proteolysis mediated by the membrane-integrated ATP-dependent protease FtsH has a unique nonlinear dependence on ATP hydrolysis rates

Yiqing Yang, Mihiravi Gunasekara, Shaima Muhammednazaar, Zhen Li, and Heedeok Hong

The content of this chapter was published in Protein Science 2019.

Summary

AAA+ proteases utilize ATP hydrolysis to actively unfold native or misfolded proteins and translocate them into a protease chamber for degradation. This basic mechanism yields diverse cellular consequences, including the removal of misfolded proteins, control of regulatory circuits, and remodeling of protein conformation. Among various bacterial AAA+ proteases, FtsH is only membrane-integrated and plays a key role in membrane protein quality control. Previously, we have shown that FtsH has substantial unfoldase activity for degrading membrane proteins overcoming a dual energetic burden of substrate unfolding and membrane dislocation. Here we asked how efficiently FtsH utilizes ATP hydrolysis to degrade membrane proteins. To answer this question, we measured degradation rates of the model membrane substrate GlpG at various ATP hydrolysis rates in the lipid bilayers. We find that the dependence of degradation rates on ATP hydrolysis rates is highly nonlinear: (1) FtsH cannot degrade GlpG until it reaches a threshold ATP hydrolysis rate; (2) after exceeding the threshold, the degradation rates steeply increase and saturate at the ATP hydrolysis rates far below the maxima. During the steep increase, FtsH efficiently utilizes ATP hydrolysis for degradation, consuming only 40–60% of the total ATP cost measured at the maximal ATP hydrolysis rates. This behavior does not fundamentally change upon addition of the macromolecular crowding agent Ficoll70 as well as against water-soluble substrates. The Hill analysis shows that the nonlinearity stems from the coupling of 3–5 ATP hydrolysis events to degradation, which represents unique cooperativity compared to other AAA+ proteases including ClpXP, HslUV, Lon, and proteasomes.

Introduction

Unicellular organisms such as bacteria need to readily adjust an optimal level of functional proteins in response to the changing environment.[1,2] Therefore, rapid degradation of misfolded or damaged proteins as well as native regulatory proteins that are no longer needed, is critical to the viability of the cells.[3-5] In bacteria, this process is mainly mediated by ATP-dependent proteases including ClpXP, ClpAP, HslUV, Lon, and FtsH. They generally work as large protein complexes composed of hexameric AAA+ ring ATPases and multimeric compartmental peptidases.[6] For ClpXP, ClpAP, and HslUV, the AAA+ (ClpX, ClpA, and HslU) and peptidase (ClpP and HslV) domains are synthesized as separate polypeptide chains and post-translationally assemble with their partners. For Lon and FtsH, the two domains are encoded in a single polypeptide chain and form a hexamer as a functional unit.[7-11] For function, water-exposed degradation markers on the substrates, which are typically a peptide segment largely composed of nonpolar residues, bind to the AAA+ ring at a narrow entry pore.[6,12-15] Repetitive cycles of ATP hydrolysis on individual AAA+ subunits induce power stroke motions, applying vectorial pulling forces on the bound substrate and mechanically unfolding it. By the same force, the unfolded substrate is translocated through the axial pore into the peptidase chamber, in which the substrate is proteolyzed into small fragments and recycled.[16]

Since the coupling of ATP hydrolysis to substrate unfolding and translocation is the hallmark in the mechanisms of ATP-dependent proteolysis, considerable efforts have been made to quantify how efficiently ATP hydrolysis drives the subsequent energy-requiring steps.[17-21] Despite the shared mechanisms, each AAA+ protease possesses a substantially different ability to hydrolyze ATP and unfold substrates, the

two activities of which are not necessarily correlated.[22] ClpAP and ClpXP are robust ATPases (400–900 ATP hydrolysis min^{-1} $AAA+_6^{-1}$) and strong unfoldases that can degrade thermodynamically or kinetically stable globular proteins such as green fluorescent protein (GFP), DHFR, barnase, and titin I27.[19,22-24] Lon can hydrolyze ATP at a moderate speed (150–200 min^{-1} $AAA+_6^{-1}$) when stimulated by substrates but has weaker unfolding power to unfold stable globular proteins.[13,21,22] HslUV is a slow ATPase (~70 min^{-1} $AAA+_6^{-1}$) but can unfold stable substrates as well as ClpAP or ClpXP depending on the location of the degradation marker.[22,25] Lastly, FtsH, which is only membrane-integrated and growth-essential among *E. coli* AAA+ proteases, is a slow ATPase (50–100 min^{-1} $AAA+_6^{-1}$) and cannot actively unfold globular proteins.[22,26]

The total ATP costs required to degrade a single copy of substrate are widely varied (0.2–6.6 ATP/residue) depending on the stability of substrate and the type of AAA+ protease.[13,17-21,27] It has been shown that the rate-determining step that requires more ATP hydrolysis is the disruption of tertiary interactions, especially those that stabilize the local structure near the degradation marker.[19,24] Interestingly, a large portion of total hydrolyzed ATP molecules are futile, i.e., multiple power-stroke motions occur to induce a single mechanical unfolding event because the substrate undergoes frequent “slipping-release” motions without unfolding.[19,28,29]

While a majority of studies of ATP-dependent proteolysis have concerned globular proteins, it is poorly understood how membrane proteins are degraded in cells. Here, we investigated membrane protein degradation mediated by the membrane-integrated AAA+ protease FtsH of *E. coli* (**Figure 4.1a**), focusing on how efficiently

FtsH utilizes ATP hydrolysis for degradation. FtsH family proteins are widely conserved in the inner membranes of bacteria and mitochondria as well as in the thylakoid membranes of chloroplasts.[30,31] In these membranes, they are responsible for quality control of membrane proteins by degrading misassembled, intrinsically unstable or damaged proteins especially under stress conditions (*e.g.*, heat, oxidation, irradiation and starvation).[26,32-44] Previously, we have successfully reconstituted FtsH-mediated membrane protein degradation using the six-helical bundle intramembrane protease GlpG as a model membrane substrate in the large negatively charged phospholipid bicelles as a bilayer medium.[20] We also have demonstrated that FtsH can accelerate unfolding of GlpG up to ~800 fold in contrast to its poor unfoldase activity for globular proteins.[20]

Here we aim to answer three specific questions: (1) To degrade membrane proteins, FtsH needs to overcome two thermodynamically unfavorable steps, i.e., substrate unfolding in the membrane and dislocation of the hydrophobic transmembrane (TM) segments to the proteolytic active sites located in the cytosol (**Figure 4.1a**). Does the degradation linearly correlate with ATP hydrolysis rates or require a threshold? (2) The apparently large ATP costs in protein degradation by AAA+ proteases have been attributed to the resistance of substrates against unfolding and translocation, and stochastic fluctuations in the mechanical stability of substrates or in the unfolding power of AAA+ proteases.[19,28,45] Then, what is the effective ATP cost that is converted to actual “work” to degrade membrane proteins? (3) In cells, protein degradation occurs in the environment crowded with macromolecules, which can affect the conformational equilibria and diffusion of both AAA+ protease and substrate.[46] How does macromolecular crowding influence degradation of membrane

proteins?

To answer these questions, we measured FtsH-mediated degradation of the model membrane substrate GlpG over a wide range of ATP hydrolysis rates in bicelles. Unexpectedly, we found a sigmoidal dependence of the degradation rates on the ATP hydrolysis rates. We show that this nonlinearity originates from the cooperativity among multiple ATP hydrolysis events that efficiently converts the released free energy to substrate unfolding and membrane dislocation. Macromolecular crowding mildly impacts degradation activity. Our result provides new insights into how FtsH utilizes ATP hydrolysis for degrading membrane proteins overcoming the dual energetic burden of substrate unfolding and membrane dislocation.

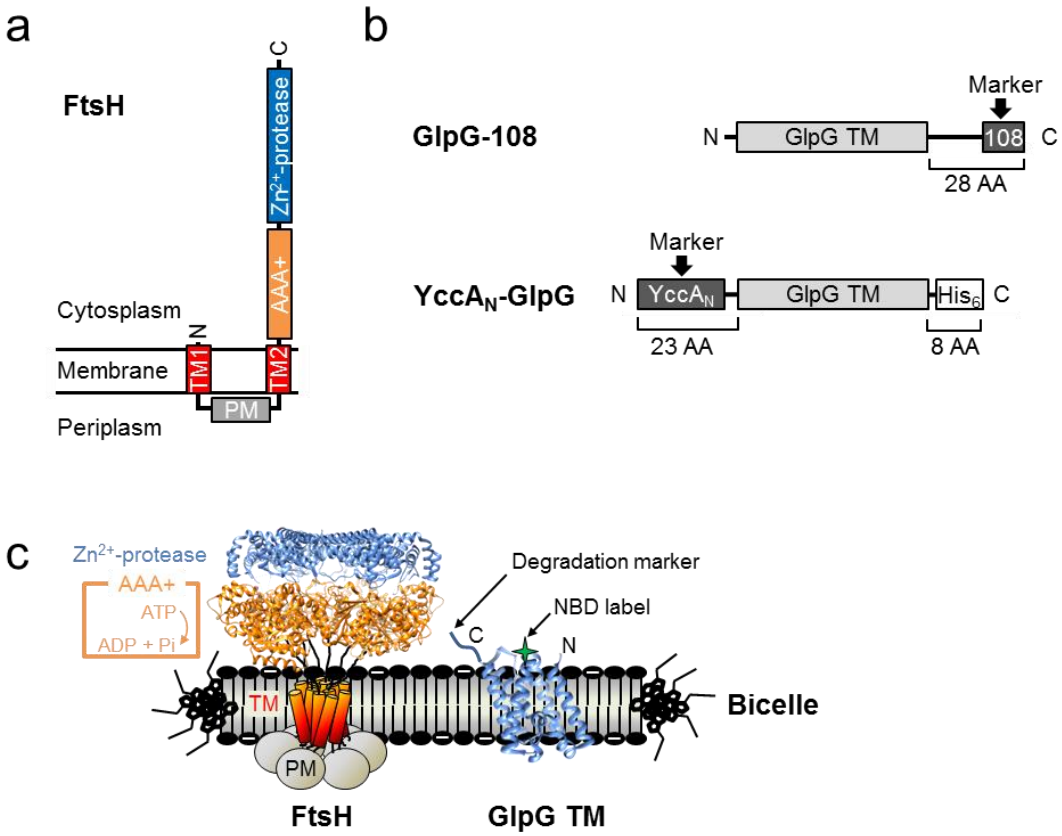

Figure 4.1 The membrane-integrated AAA+ protease FtsH and the model membrane substrate GlpG. (a) The domain structure and membrane topology of FtsH. TM: transmembrane segment; PM: periplasmic domain. (b) The model GlpG constructs with the C- and N-terminal degradation markers employed in this study. GlpG TM: the transmembrane domain of GlpG (residues 87–276); the 108 tag: -SLLWS; the $YccA_N$-tag: MDRIVSSSHDRTSLLSTHKVLRN-. (c) Reconstitution of FtsH-mediated degradation of GlpG in the negatively charged DMPC/DMPG/CHAPS bicelles (molar ratio, 3:1:1). The thiol-reactive fluorescent NBD label as a reporter group to monitor degradation was conjugated to the cytoplasmic interfacial region of the middle helix TM3 of GlpG variant G172C.

Results

Dependence of degradation rates on ATP hydrolysis rates has three distinct phases

FtsH is known to initiate degradation by binding to the flexible tail at either N- or C-terminus of a substrate as a degradation marker and processively proteolyze it towards the other end.[14,15,47] It has also been reported that FtsH can initiate proteolysis at an internal site of a substrate.[48] The model membrane substrate GlpG of *E. coli* is a site-specific intramembrane protease composed of a cytosolic N-terminal domain (residues 1–86) and a six-helical bundle catalytic TM domain (residues 87–276) (**Figure 4.1b–c**).[49] Here we chose the constructs possessing only the TM domain to exclude the possible involvement of the cytosolic portion in degradation and focus on protein interactions within the membrane. The isolated TM domain is not degraded by FtsH but becomes a good FtsH substrate when a degradation marker (>~20 residues) is fused to either terminus.[20] We used the N-terminal tail of an *E. coli* membrane protein YccA (the $YccA_N$-tag) as an N-terminal marker and the sequence 108 (the 108-tag) as a C-terminal marker (**Figure 4.1b**).[15,50] Both tags are known to be specifically recognized by FtsH.[47,51] To monitor degradation, we conjugated the environment-sensitive fluorophore NBD to an engineered cysteine (G172C) in GlpG.[20] NBD fluorescence is quenched when the fluorophore is transferred from the hydrophobic bicellar phase to the aqueous phase upon degradation (**Figure 4.1c** and **4.2**).

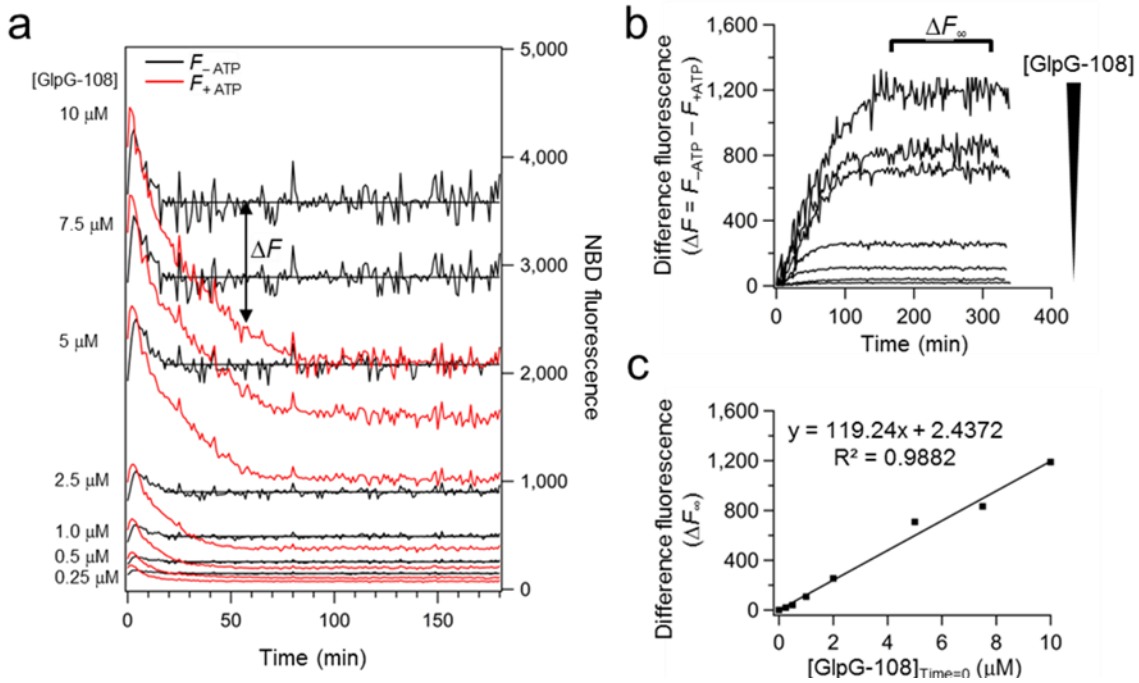

Figure 4.2 The procedures to determine FtsH-mediated degradation of GlpG using NBD fluorescence. This is an example for GlpG-108 labeled at the residue position G172C. The assay was performed at a fixed concentration of FtsH (2 μM) in 2% (w/v) DMPC/DMPG/CHAPS bicelles at 37°C in the presence of an ATP regeneration system (phosphoenol pyruvate/pyruvate kinase). (a)–(c)**:** The procedures to obtain the relationship between the concentration of degraded GlpG and the intensity change of NBD-fluorescence. (a) Time-dependent NBD fluorescence was measured at various concentrations of GlpG-108 in the absence (F_{-ATP}) and presence (F_{+ATP}) of ATP. (b) Time-dependent change of F_{+ATP} relative to F_{-ATP}($\Delta F = F_{-ATP} - F_{+ATP}$) indicates GlpG degradation. After the degradation is completed, ΔF reaches a plateau and ΔF's in the plateaued time range are averaged (designated as ΔF_∞). (c) ΔF_∞ is linear as a function of GlpG concentration. The slope of ΔF_∞ *vs* [GlpG] yields the intensity change per μM GlpG degraded (ΔF/ μM degraded GlpG).

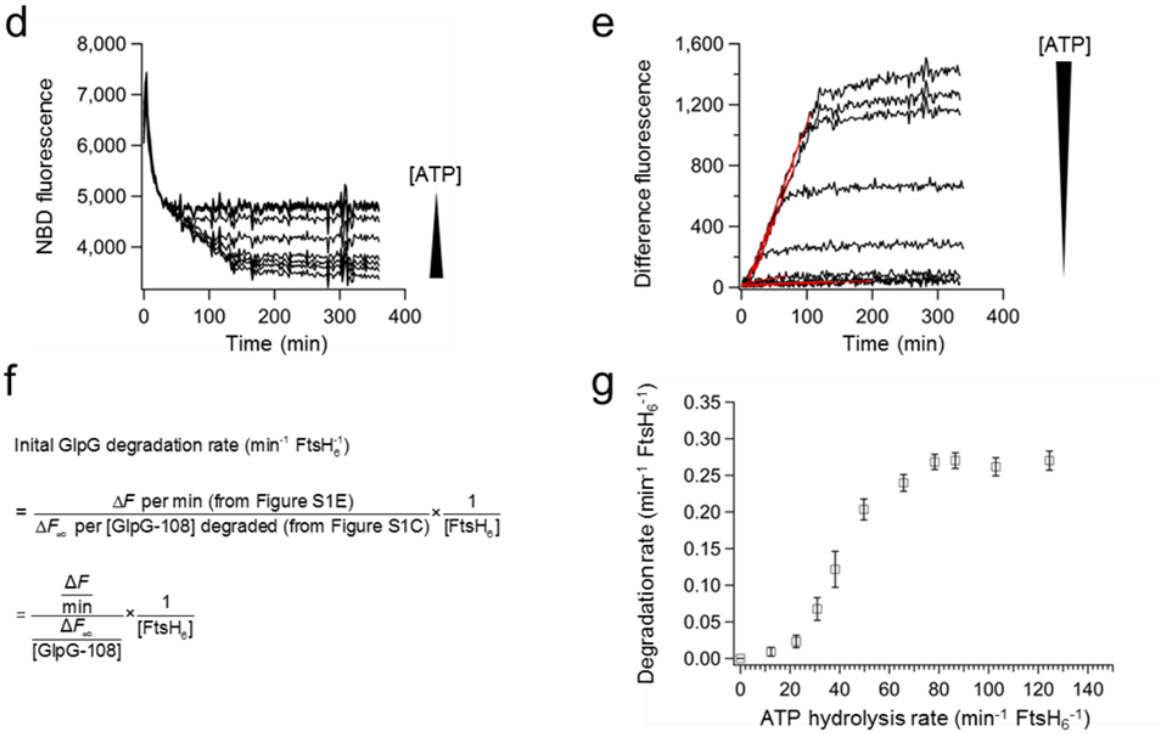

Figure 4.2 Continued. (d)–(g): The procedures to obtain the degradation rates of GlpG and its relationship with the ATP hydrolysis rates. (d) Time-dependent NBD fluorescence was measured at various concentrations of ATP including [ATP] = 0 in the presence of 15 μM GlpG. (e) For the intensity data at a certain ATP concentration other than 0, ΔF is calculated relative to that at [ATP] = 0 as a function of time. The linear slopes of fitted lines in the early time range (ΔF/min) is related to the initial rate of GlpG degradation. (f) The slopes from Figure 4.2c (ΔF/ μM degraded GlpG) and Figure 4.2e (ΔF/min) and is related to the degradation rate through the relationship, the initial degradation rate (μM/min) = (ΔF/min)/(ΔF_∞/μM degraded GlpG). This rate was further normalized by FtsH hexamer concentration ([$FtsH_6$]). (g) The final plot of the degradation rates *vs.* the ATP hydrolysis rates. The ATP hydrolysis rates at each ATP concentration were obtained from the Michaelis-Menten plots (ATP hydrolysis rates vs. ATP concentration, Figure 4.3 measured in the presence of 15 μM GlpG.

To investigate how ATP hydrolysis rates of FtsH influence degradation rates of GlpG, we controlled the ATP hydrolysis rate by varying the concentration of ATP (0–5,000 μM) and measured the degradation rate at each ATP concentration in the presence of an ATP regeneration system (see **Methods**). ATP hydrolysis rates measured as a function of ATP concentration in the presence of GlpG yielded the Michaelis-Menten parameters, $K_{M,\,ATP} \approx 45$ μM and $k_{cat,\,ATP} \approx 125$ min^{-1} FtsH$_6^{-1}$ (**Figure 4.3, Table 4.1**).[20] Thus, the ATP hydrolysis rates were varied in the range of 0–125 min^{-1} FtsH$_6^{-1}$.

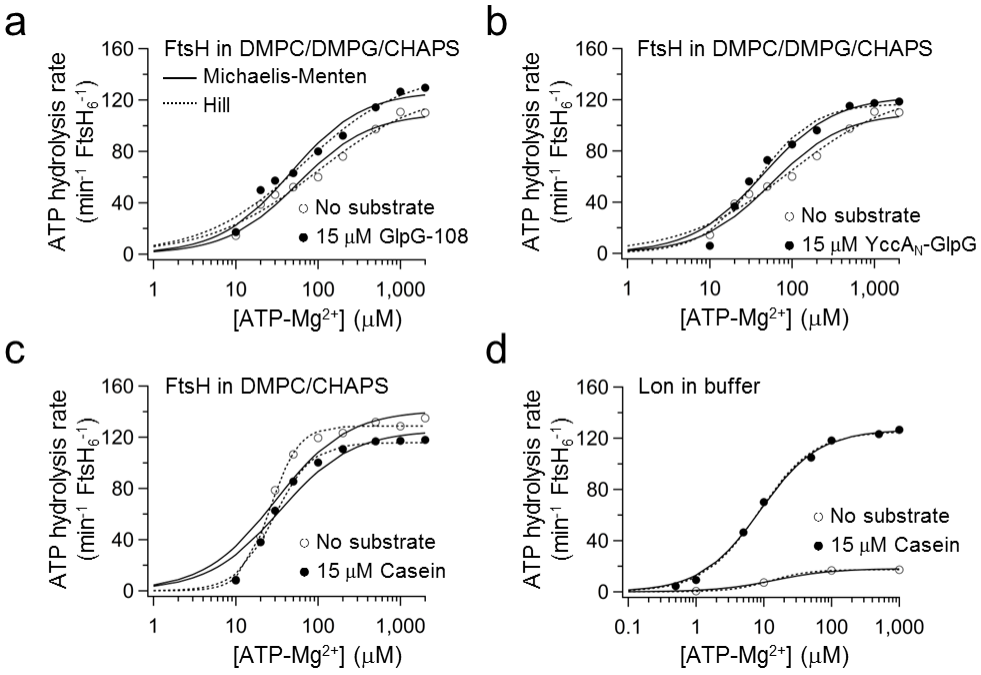

Figure 4.3 Measurement of ATP hydrolysis rate of FtsH as a function of ATP concentration. These data were used to investigate the relationship between substrate degradation rates vs. ATP hydrolysis rates. For GlpG degradation by FtsH (Figure 4.6) and casein degradation by Lon (Figure 4.10), the ATP hydrolysis rates obtained from the Michaelis Menten equations were used. For casein degradation by FtsH (Figure 4.7), those obtained from the Hill analysis were used.

	Michaelis-Menten		Hill		
	$K_{m,ATP}$ (min^{-1} $FtsH_6^{-1}$)	$k_{cat,deg}$ (min^{-1} $FtsH_6^{-1}$)	$K_{m,ATP}$ (min^{-1} $FtsH_6^{-1}$)	$k_{cat,deg}$ (min^{-1} $FtsH_6^{-1}$)	$n_{H,ATP}$
FtsH[a] DMPC/DMPG/CHAPS	56 ± 10	110 ± 5	96 ± 38	128 ± 13	0.7 ± 0.1
FtsH + GlpG-108 DMPC/DMPG/CHAPS	46 ± 7	127 ± 5	66 ± 20	141 ± 11	0.7 ± 0.1
FtsH + $YccA_N$-GlpG DMPC/DMPG/CHAPS	44 ± 7	123 ± 5	38 ± 5	117 ± 5	1.3 ± 0.2
FtsH DMPC/CHAPS	30 ± 8	141 ± 8	26 ± 1	129 ± 2	2.5 ± 0.2
FtsH + casein DMPC/CHAPS	34 ± 7	125 ± 6	29 ± 1	116 ± 2	1.9 ± 0.2
Lon[b]	14 ± 3	18 ± 1	12 ± 1	17 ± 1	1.5 ± 0.1
Lon + casein	9 ± 1	127 ± 2	8 ± 1	125 ± 2	1.1 ± 0.1

[a] For FtsH, all measurements were performed with [FtsH] = 2 mM in 2% (w/v) DMPC/DMPG/CHAPS or DMPC/CHAPS bicelles at 37 °C. The final concentrations of GlpG variants and casein were 15 mM or 0.45 mg/ml.
[b] For Lon, all measurements were performed with [Lon] = 1 mM in 20 mM HEPES (pH 7.4), 100 mM KCl, 1 mM DTT buffer solution. The final concentration of casein was 0.08 mg/ml.

Table 4.1 Kinetic parameters of FtsH and Lon ATP hydrolysis rate in different substrates and environments.

Overall, GlpG with the C-terminal degradation marker (GlpG-108) was degraded faster than that with the N-terminal marker ($YccA_N$-GlpG) at all ATP concentrations (**Figure 4.4**). The slower degradation of $YccA_N$-GlpG is due to the higher local conformational stability and hydrophobicity of the N-terminal region of GlpG, which resist active unfolding and membrane dislocation, respectively.[20] It should be noted that, despite the presence of the ATP regeneration system, GlpG degradation by FtsH continued only for 2–4 hours, leaving 20~70% of substrates not degraded after overnight. This is rather due to the inactivation of FtsH after prolonged enzyme turnover or sample incubation rather than the defects in the ATP regeneration system (**Figure 4.5**).

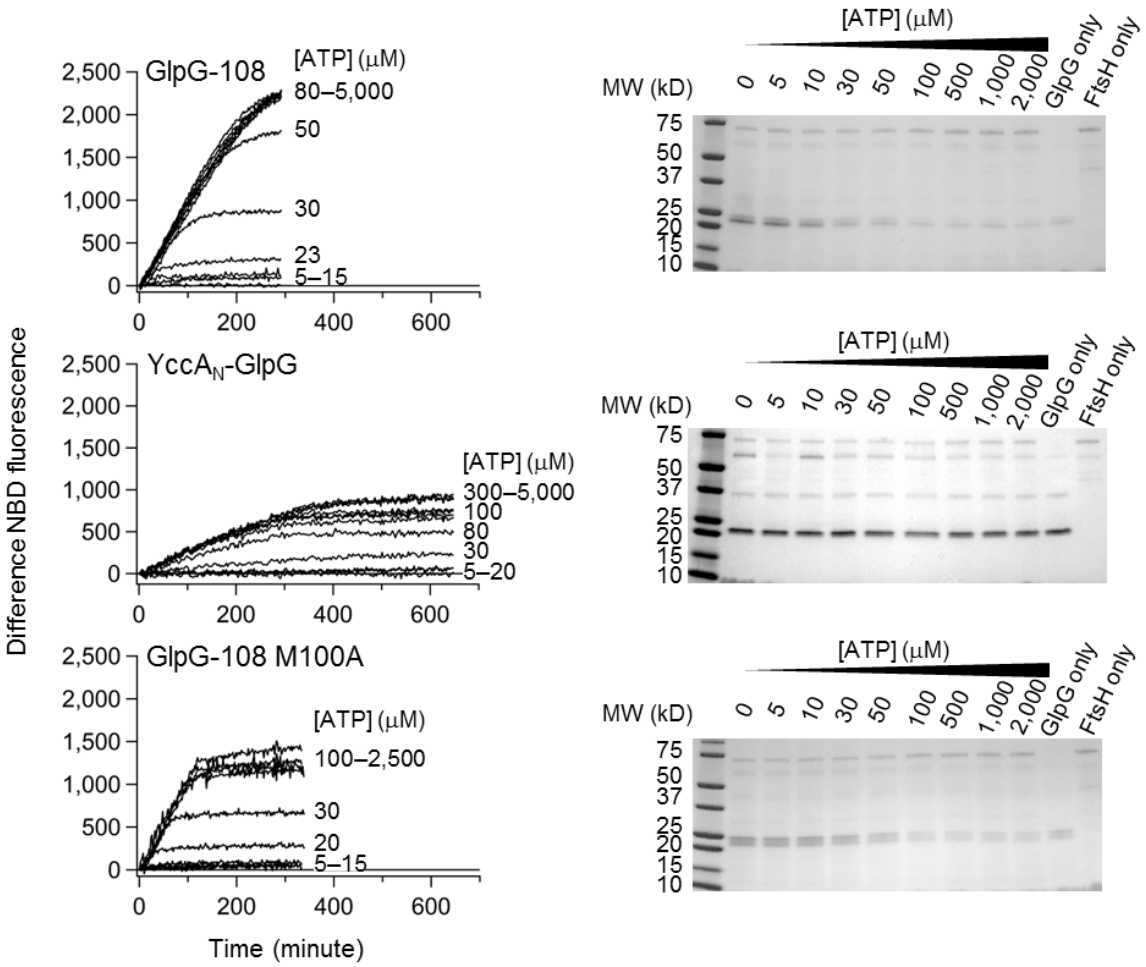

Figure 4.4 FtsH-mediated degradation of GlpG in bicelles at various ATP concentrations. (*Left*) Time-dependent degradation monitored by NBD-fluorescence and (*Right*) end-point degradation measured by SDS-PAGE after 16 hours. *Top*: Degradation of GlpG-108; *Middle*: Degradation of YccA$_N$-GlpG; *Bottom*: Degradation of the destabilized variant M100A of GlpG-108. All assays were performed at 37 ^oC with FtsH (2 μM) and GlpG (15 μM) in DMPC/ DMPG/CHAPS bicelles (pH 7.5).

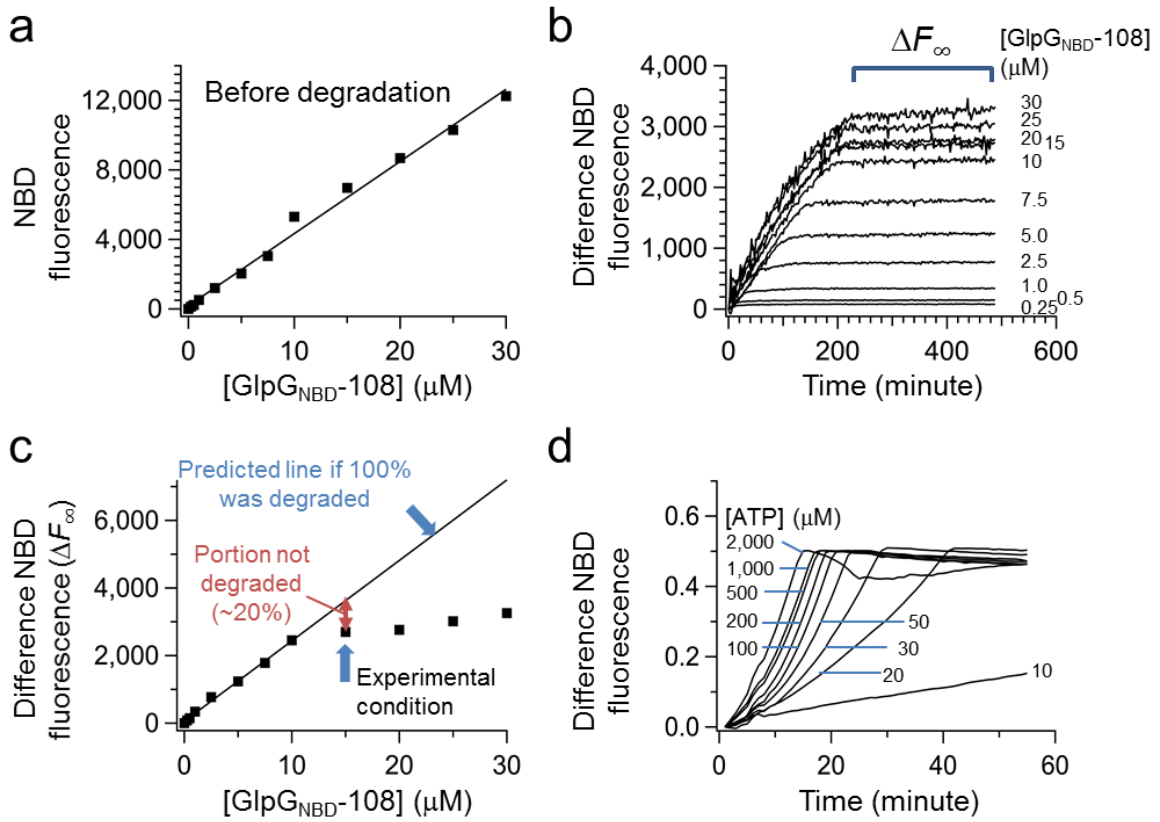

Figure 4.5 Incomplete degradation of GlpG by FtsH. (a) The linearity of NBD fluorescence as a function of the concentration of the model substrate NBD-labeled GlpG-108 (GlpG$_{NBD}$-108) in DMPC/DMPG/CHAPS bicelles. (b) Time-dependent changes of difference NBD fluorescence (ΔF) during degradation of GlpG$_{NBD}$-108 by FtsH at various GlpG$_{NBD}$-108 concentrations. The difference was obtained by subtracting NBD fluorescence of the sample (GlpG$_{NBD}$-108 and 2 μM FtsH in bicelles) in the presence of ATP (5 mM) from that in the absence of ATP. DF_∞ indicates the maximal fluorescence change after DF reaches a plateau. An ATP regeneration system was added to each sample. (c) ΔF_∞ as a function of GlpG$_{NBD}$-108 concentrations. (d) ATPase activity of FtsH (2 μM) in DMPC/DMPG/CHAPS bicelles using an enzyme-coupled assay containing the ATP regeneration system. The samples contain 15 μM casein.

Interestingly, the dependence of the degradation rates on the ATP hydrolysis rates displayed a sigmoidal behavior with three distinct phases for both GlpG variants (**Figure 4.6** *left*): (1) At lower ATP hydrolysis rates (0–20 min^{-1} $FtsH_6^{-1}$), the degradation rates were negligible; (2) As the ATP hydrolysis rate increased (20–80 min^{-1} $FtsH_6^{-1}$), the degradation rates steeply increased up to ~0.22 min^{-1} $FtsH_6^{-1}$ for GlpG-108 and 0.12 min^{-1} $FtsH_6^{-1}$ for $YccA_N$-GlpG; (3) At higher ATP hydrolysis rates (>80 min^{-1} $FtsH_6^{-1}$), the degradation rates were saturated without a further increase. Notably, the degradation rates were saturated at the ATP hydrolysis rates far lower than the maximal ATP hydrolysis rates ($k_{cat, ATP}$), even close to $k_{cat, ATP}/2$.

This result indicates that the degradation of GlpG requires a minimum threshold level of the ATP hydrolysis rate. Remarkably, the degradation rates are highly sensitive to a small change in ATP concentration (from ~20 to ~60 μM, **Figure 4.4** *right*) or ATP hydrolysis rate (from ~25 to ~70 min^{-1} $FtsH_6^{-1}$, **Figure 4.6** *left*) before reaching the maximal degradation rates.

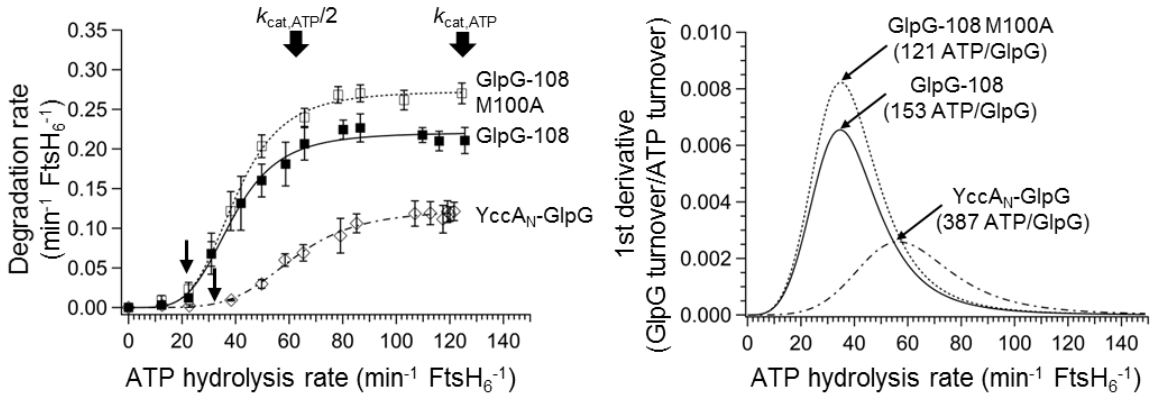

Figure 4.6 Dependence of the degradation rates of the membrane substrate GlpG on the ATP hydrolysis rates. (*Left*) Degradation rates of GlpG-108, YccA$_N$-GlpG, and GlpG-108 M100A as a function of ATP hydrolysis rate at 37 °C. The positions of the maximal ATP hydrolysis rates ($k_{cat, ATP}$) and the half maxima ($k_{cat, ATP}/2$) are marked with black arrows. The threshold ATP-hydrolysis rate is marked with a line arrow. (*Right*) The effective ATP cost for each GlpG variant (in parenthesis) was obtained by taking the inverse of the maximum value of the first derivative of the plot in *left*.

Sigmoidal behavior is intrinsic, not depending either on the conformational stability or membrane localization of substrates

To degrade membrane proteins, FtsH actively unfolds substrates in the membrane and dislocates them into the proteolytic active sites located in the aqueous phase. GlpG possesses moderate thermodynamic stability (ΔG^o_U = ~6 kcal/mol) and a high activation energy of unfolding ($E_{a,U}$ = ~30 kcal/mol) in mild detergent dodecylmaltoside.[20,52-56] Also, the free energy costs for transferring a single hydrophobic TM helix from the lipid bilayer to water in an unfolded form can be substantially large (50–100 kcal/mol).[20,57,58] We hypothesized that FtsH requires a

threshold ATP hydrolysis rate to overcome the conformational stability of GlpG and the large free energy cost for membrane dislocation. If this hypothesis is true, the threshold level will be reduced or disappear if the conformational stability of the substrate decreases or the substrate is not localized in the membrane.

To test this hypothesis, we first tested a destabilized GlpG variant M100A with the C-terminal 108 tag. This mutation disrupts core packing in the TM region of GlpG, lowering ΔG^{o}_{U} and $E_{a,U}$ by ~2.5 kcal/mol and ~5 kcal/mol relative to wild type, respectively.[20,52] This mutation also accelerates unfolding by 30–60 fold in bicelles.[20] Nonetheless, this mutation did not change the threshold ATP hydrolysis rate relative to wild type with the same marker, retaining the sigmoidal relationship between the degradation and ATP hydrolysis rates (**Figure 4.4** *bottom* and **4.6** *left*). The decrease of conformational stability only increased the maximal degradation rate by ~30% as observed in the previous study.[20] Next, we tested the influence of membrane localization using the water-soluble model substrate casein, which lacks both membrane localization and conformational stability (**Figure. 4.7**). Again, the sigmoidal relationship was retained with the clear appearance of a threshold at ~30 ATP hydrolysis min^{-1} $FtsH_6^{-1}$.

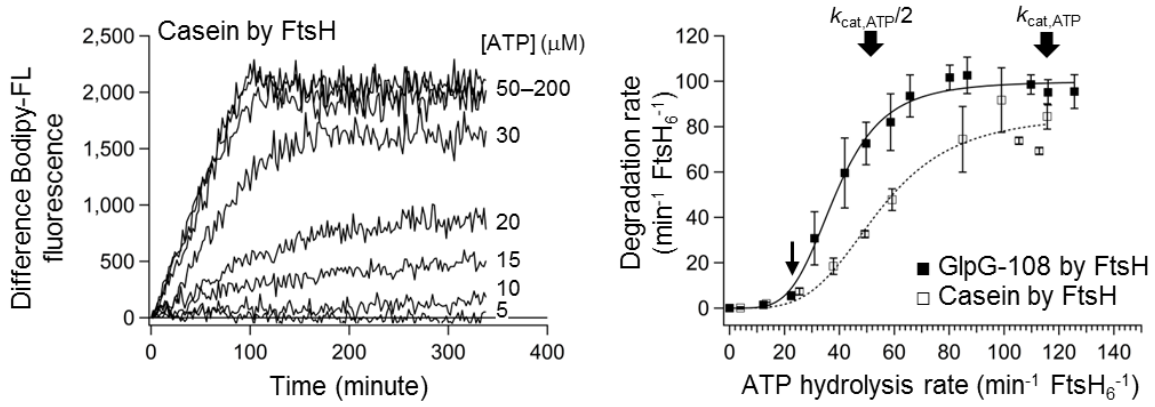

Figure 4.7 Dependence of the degradation rates of the water-soluble substrate casein on the ATP hydrolysis rates by FtsH. (*Left*) Time-dependent degradation of water-soluble Bodipy FL-labeled casein (0.45 mg/ml) by FtsH (2 μM) at various ATP concentrations in neutral DMPC/CHAPS bicelles. Degradation was monitored by dequenching of Bodipy FL fluorescence ($\lambda_{excitation}$ = 485 nm; $\lambda_{emission}$ = 525 nm) at 37 °C. (*Right*) Dependence of the degradation rates of Bodipy-FL casein on the ATP hydrolysis rates in comparison to that of GlpG-108. Values are means ± SEM (N = 2–5).

We also asked why the degradation rates of both membrane and water-soluble substrates are saturated far below the maximal ATP hydrolysis rates. We suspected that the hexameric Zn^{2+} protease domain may not be fully functional in our reconstituted system, limiting the flux of translocated substrates towards degradation. However, the addition of the protein stabilizer glycerol or the macromolecular crowding agent Ficoll70 for enhancing the assembly of FtsH hexamer did not noticeably improve the degradation rate in the absence of both (**Figure 4.8**). Reducing the substrate load by lowering the substrate concentration by 30 fold did not affect the sigmoidal nature (**Figure 4.9**).

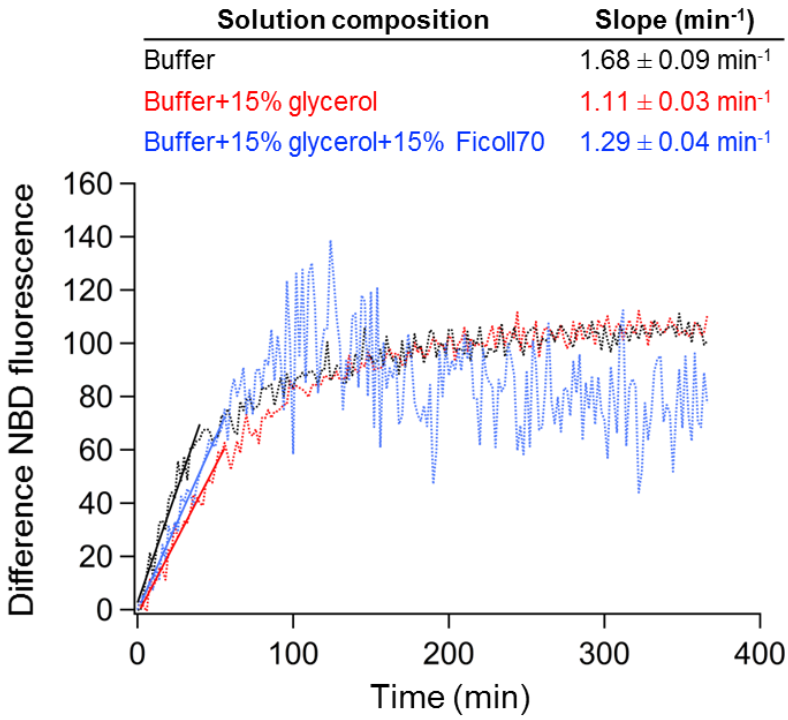

Figure 4.8 The addition of glycerol (protein stabilizer) or Ficoll70 (macromolecular crowding agent) does not significantly improve the degradation rate of GlpG. Time-dependent degradation of GlpG-108 (0.5 μM) by FtsH (2 μM) was measured at 5 mM ATP in DMPC/DMPG/CHAPS bicelles. The slope of the linear fitted line in each data represents the degradation rate.

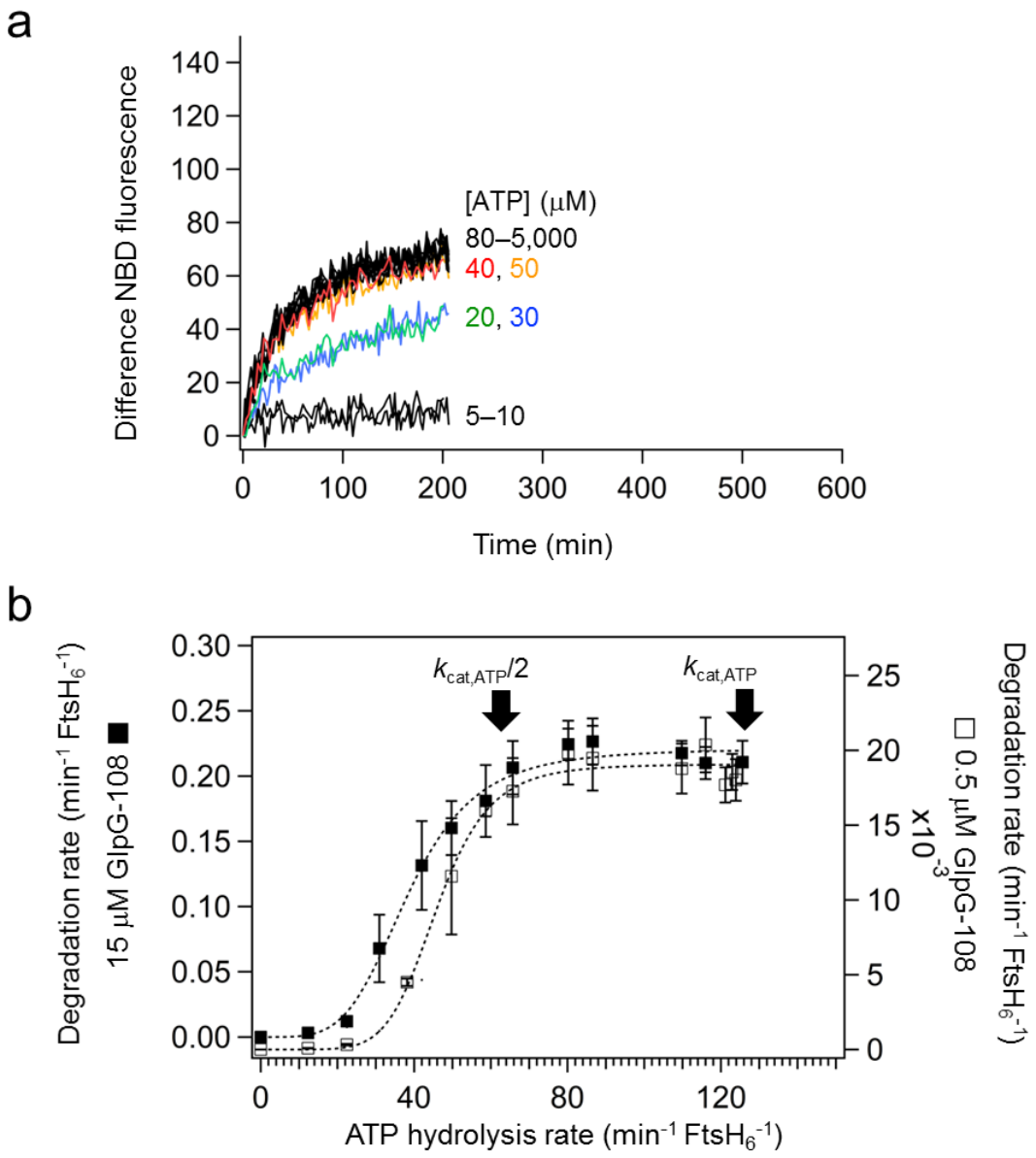

Figure 4.9 Reducing the substrate load to FtsH does not fundamentally change the relationship between the degradation rate and the ATP hydrolysis rate. (a) Time-dependent degradation of GlpG-108 (0.5 μM) by FtsH (2 μM) at various ATP concentrations in DMPC/DMPG/CHAPS bicelles. (b) Dependence of the degradation rates of 0.5 μM GlpG-108 on the ATP hydrolysis rates in comparison to that of 15 μM GlpG-108.

To further confirm the nonlinear relationship, we tested degradation of the same

model substrate casein by another *E. coli* AAA+ protease, Lon, by which the degradation rates are linearly increased proportionally to the ATP hydrolysis rates.[59] Indeed, the rates of casein degradation and ATP hydrolysis displayed an excellent linear relationship (R^2 = 0.97) (**Figure 4.10** and **4.3d**). Therefore, we conclude that the sigmoidal dependence of the degradation rates on the ATP hydrolysis rates is an intrinsic property of FtsH.

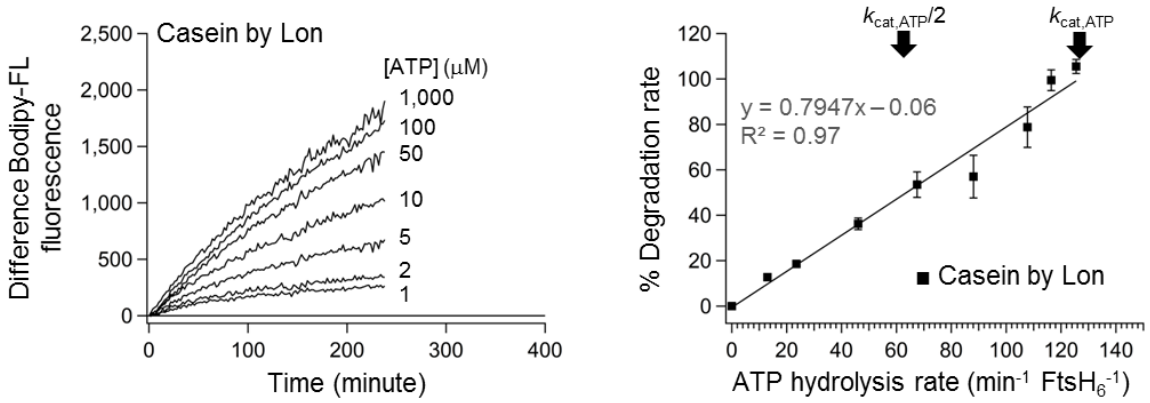

Figure 4.10 Dependence of the degradation rates of the water-soluble substrate casein on the ATP hydrolysis rates by Lon. (*Left*) Time-dependent degradation of Bodipy FL-labeled casein (0.08 mg/ml) by *E. coli* Lon in 20 mM HEPES (pH 7.5), 100 mM KCl, 1 mM DTT at 30 °C. (*Right*) The relationship between degradation and ATP hydrolysis rates mediated by Lon.

The Hill analysis suggests that the sigmoidal dependence stems from the cooperativity among ATP hydrolysis events

The sigmoidal relationship between the degradation and ATP hydrolysis rates strongly suggests cooperativity among multiple ATP hydrolysis events. To quantitatively understand the sigmoidal behavior, we employed the Hill analysis (**Figure 4.6** *left*). Surprisingly, although the relationship between ATP concentrations

and hydrolysis rates shows weak or no cooperativity (the Hill coefficients, $n_{H, ATP}$ = 0.7–1.3)[20] (**Figure 4.3**), we observed strong cooperativity between the degradation and ATP hydrolysis rates with n_H = 4.3–4.5 for GlpG-108 and GlpG-108 M100A, n_H = 5.0 for $YccA_N$-GlpG and n_H = 3.9 for casein (**Table 4.2**). $K_{m, ATP}$, the ATP hydrolysis rate at which the degradation rate reaches a half maximum, was only 60–80 min^{-1} $FtsH_6^{-1}$ (50–70% of the maximal ATP hydrolysis rates).

	$k_{cat,deg}$[a] (min^{-1} $FtsH_6^{-1}$)	$K_{m,ATP}$[b] (min^{-1} $FtsH_6^{-1}$)	$n_{H, ATP}$[c]
GlpG-108	0.22 ± 0.01	39 ± 1	4.3 ± 0.4
GlpG-108 M100A	0.27 ± 0.01	40 ± 1	4.4 ± 0.3
$YccA_N$-GlpG	0.12 ± 0.01	61 ± 1	5.0 ± 0.4
GlpG-108/Ficoll 70 (15%)	0.20 ± 0.01	50 ± 2	3.4 ± 0.4
Casein-Bodipy FL[d]	N/A[e]	54 ± 5	3.9 ± 1.2

All measurements were performed with [FtsH] = 2 μM in 2% (w/v) DMPC/DMPG/CHAPS bicelles at 37 °C.
The final concentrations of all GlpG variants were 15 μM.
[a] The maximal degradation rate.
[b] The ATP hydrolysis rate at which the degradation rate becomes $k_{cat,deg}/2$.
[c] The Hill coefficient.
[d] Measured in DMPC/CHAPS bicelles at 0.45 mg/ml of casein-Bodily FL.
[e] Not determined because of the uncertainty in molecular weight.

Table 4.2 Kinetic parameters describing the dependence of degradation rates of GlpG on ATP hydrolysis rates by FtsH. The data were Obtained by fitting to the Hill equation (Equation 4).

Our Hill analysis reveals a remarkable principle of how FtsH, which is known as weaker ATPase and unfoldase than other AAA+ proteases, utilizes ATP hydrolysis to carry out protein degradation. At low ATP hydrolysis rates (<20–30 min^{-1} $FtsH_6^{-1}$), FtsH cannot drive substrate unfolding and membrane dislocation. As the ATP hydrolysis rate increases, accumulated ATP hydrolysis events start to cooperate,

enabling substrate degradation that efficiently reaches the maximal rates. The steep increase of the degradation rates is an outcome of coupling of 4–5 ATP hydrolysis events which occur probably in an independent, stochastic manner on individual AAA+ subunits in FtsH. This cooperative behavior by FtsH is distinct from the degradation mediated by other robust AAA+ proteases such as ClpXP, HslUV, Lon, PAN and 26S proteasomes, which linearly increase degradation rates in response to an increase in ATP hydrolysis rates.[17,18,59-61]

Effective ATP cost for degrading GlpG

So far, the total ATP costs by AAA+ proteases for degrading substrates have been quantified under the steady-state conditions, where both ATP hydrolysis rates and degradation rates are maximal[19]:

$$\text{Total ATP cost} = k_{cat,ATP} \times \tau_{deg} = k_{cat,ATP} \times (1/k_{cat,deg}) \qquad \textbf{(Equation 1)}$$

Here, $k_{cat,\,ATP}$ designates the maximal ATP hydrolysis rate per FtsH hexamer at a saturating concentration of substrate, and τ_{deg} indicates the substrate lifetime, i.e., the inverse of the maximal substrate degradation rate, $k_{cat,deg}$. Using this method, we have determined the total ATP costs: 380 ATP for GlpG-108, 270 ATP for destabilized variant GlpG-108 M100A, and 550 ATP for $YccA_N$-GlpG.[20] Despite the relevance, however, this method will generally overestimate the ATP cost for FtsH-mediated degradation because the ATP hydrolysis rates at which degradation rates reach a maximum are much lower than the maximal ATP hydrolysis rates (**Figure 4.6** *left*, **4.7** *left* and **4.10** *left*).

Therefore, we suggest an alternative approach to quantify an “effective” ATP cost that actually leads to substrate degradation using the degradation rate *versus* ATP

hydrolysis rate plot (**Figure 4.6** *left*).[17] As shown in the plot, after the ATP hydrolysis rates exceed the threshold levels, the degradation rates increase until reaching a saturated level. In this increasing range, the inverse of the slope represents the excess number of ATP hydrolysis required to degrade one more unit of GlpG:

$$\text{Effective ATP cost} = \frac{1}{\text{Slope}}$$

$$= \frac{1}{\dfrac{\text{Degradation rate (number of GlpG degraded min}^{-1}\ [\text{FtsH}_6]^{-1})}{\text{ATP hydrolysis rate (number of ATP hydrolyzed min}^{-1}\ [\text{FtsH}_6]^{-1})}} = \frac{\text{Number of ATP hydrolyzed}}{\text{Number of GlpG degraded}}$$

(Equation 2)

The slope at each ATP hydrolysis rate was obtained by taking the first derivative of the functional form fitted to the Hill equation (**Figure 4.6** *right*). For each GlpG variant, we defined the effective ATP cost at the ATP hydrolysis rate, which yielded a maximal slope. The effective ATP costs were 153 ATP for GlpG-108, 121 ATP for GlpG-108 M100A and 387 ATP for $YccA_N$-GlpG. These values are only 40–45% (GlpG-108 WT and M100A) and ~70% ($YccA_N$-GlpG) of the total ATP costs measured under the steady-state conditions.[20] Thus, FtsH utilizes ATP hydrolysis more efficiently than previously thought, and the effective ATP cost is well correlated with the local stability of the region to which the degradation marker is fused.

Macromolecular crowding does not affect ATPase and protease activities of FtsH

Finally, we asked how the physical environment mimicking the crowded cellular environment influences ATPase and degradation activities of FtsH using the inert macromolecular crowding agent Ficoll70 (average molecular weight ≈ 70 kDa; hydrodynamic radius ≈ 4 nm).[62] Crowding agents at high concentrations in solution

place steric constraints on proteins because of the large excluded volume. The reduced free space can influence the equilibria of protein conformations and protein-protein interactions.[46,63] In general, macromolecular crowding is known to induce compaction of unfolded states and enhance protein-protein interactions.[64] We expected that Ficoll70, which has a molecular weight similar to FtsH, may influence ATPase and degradation activities of FtsH by enhancing the hexameric assembly of FtsH, facilitating the interaction between FtsH and substrate, or possibly decreasing the volume of unfolded GlpG.

We first measured the effect of Ficoll70 on ATPase activity in bicelles. In the range of 0–15% (w/v) Ficoll70, ATP hydrolysis rates did not change significantly (**Figure 4.11a** and **4.12**). Also, the Michaelis-Menten analysis at 15% Ficoll70 indicates a negligible influence of the crowding agent on ATPase activity (**Figure 4.11b**). Before assessing the effect of Ficoll70 on degradation activity of GlpG, we tested if the macromolecular crowding would impact the conformational stability of GlpG using the novel steric trapping method in mild dodecylmaltoside detergent. Steric trapping couples transient unfolding of a doubly biotinylated protein to double binding of bulky mSA (52 kD; **Figure 4.11c**).[52] This method is an advantageous tool for measuring protein stability directly under native solvent or lipid conditions. The thermodynamic stability (ΔG^{o}_{U}) of GlpG was determined from the binding isotherm between doubly-biotinylated GlpG and monovalent streptavidin variant with reduced biotin binding affinity (mSA-S27A) (**Figure 4.13)** for the schemes of biotinylation and binding assay). The attenuated second binding phase is correlated with the stability of GlpG. Addition of 15% Ficoll70 moderately decreased the stability by $\Delta\Delta G^{o}_{U} = 0.4 \pm 0.2$

kcal/mol (**Figure 4.11d**). Probably, the excluded volume by Ficoll70 mildly stabilized the unfolded state by inducing its compaction in the micellar phase.

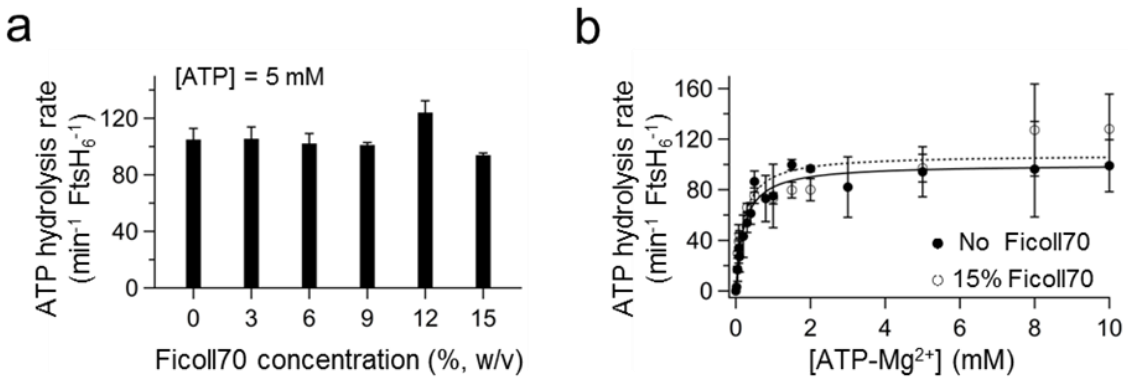

Figure 4.11 The effects of the macromolecular crowding agent Ficoll 70 on the ATPase activity of FtsH and thermodynamic stability of GlpG. (a) Dependence of ATP hydrolysis rates of FtsH (2 μM) on the concentration of Ficoll70 measured at a saturating concentration of ATP (5 mM) in DMPC/DMPG/CHAPS bicelles at 37 °C (see also Figure 4.12). (b) Michaelis-Menten analysis of ATPase activity in the presence and absence of 15% Ficoll70 (w/v) measured in DMPC/DMPG/CHAPS bicelles.

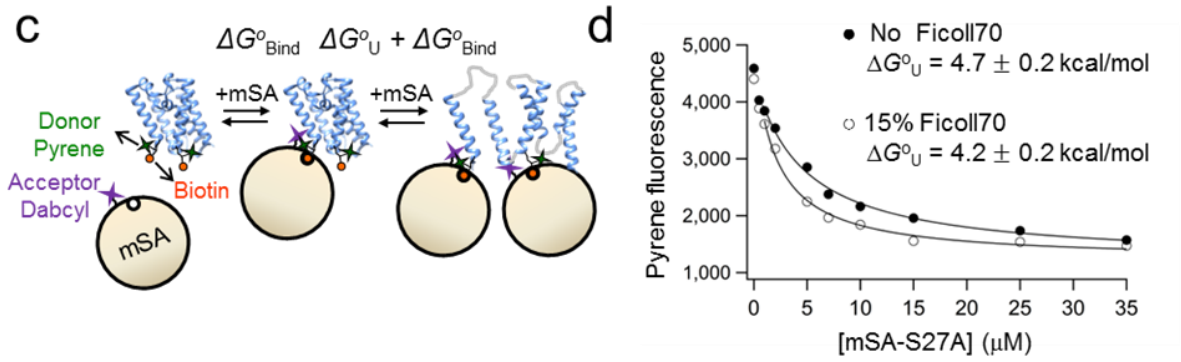

Figure 4.11 Continued. (c) The principle of steric trapping.[52] When biotin tags are conjugated to two specific residues that are spatially close in the folded state but distant in the amino acid sequence, the first monovalent streptavidin (mSA) binds either biotin label with the intrinsic binding affinity (ΔG^{o}_{Bind}). Because of steric hindrance, the second mSA binds only when native tertiary contacts are unraveled by transient unfolding. Hence, binding of the second mSA is attenuated depending on the stability of the target protein ($\Delta G^{o}_{Bind} + \Delta G^{o}_{U}$). By adjusting the biotin affinity of mSA by mutation, unfolding and binding reactions can be reversibly controlled, and ΔG^{o}_{U} of the target protein can be obtained by monitoring binding of the second mSA. Binding of mSA to biotin labels on GlpG was measured by FRET-based assay employing BtnPyr label (donor) and mSA labeled with nonfluorescent dabcyl quencher (acceptor) [52] (Figure 4.13a). (d) The effect of Ficoll70 on the stability of GlpG measured in dodecylmaltoside detergent (5 mM). Binding isotherms between double-biotin variants of GlpG (172/267-$BtnPyr_2$) and a mSA_{DAB} variant with a reduced biotin binding affinity (mSA_{DAB}-S27A, $K_{d,\ biotin}$ = 1.4 nM) monitored by quenching of pyrene fluorescence.[52] 15% Ficoll70 does not significantly affect the intrinsic biotin binding affinity of mSA to the biotin labels (Figure 4.13b). Values are means ± SEM (N = 2–3).

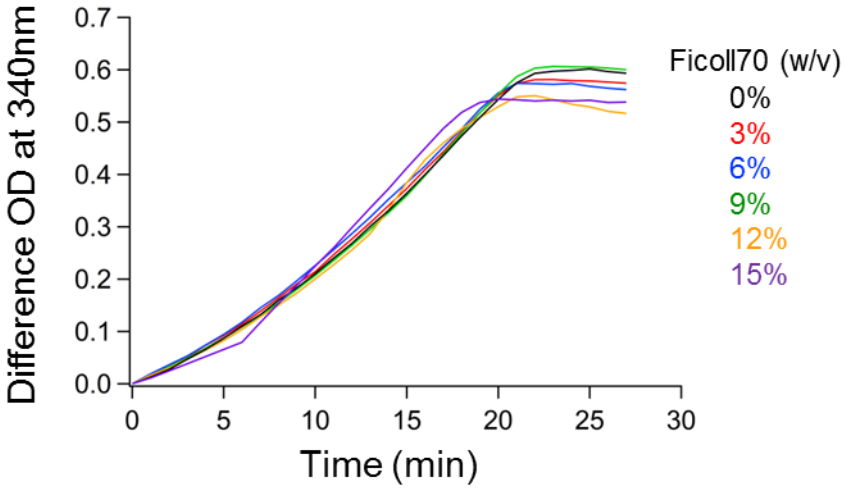

Figure 4.12 The macromolecular crowding agent Ficoll70 does not affect the ATP hydrolysis rate by FtsH. Time-dependent ATPase activity assay monitored by UV absorption of NADH using an enzyme-coupled assay (see Methods). Each data indicates the difference of absorbance of the samples in the absence and presence of 5 mM ATP at 2 μM FtsH in 2% DMPC/DMPG/CHAPS bicelles.

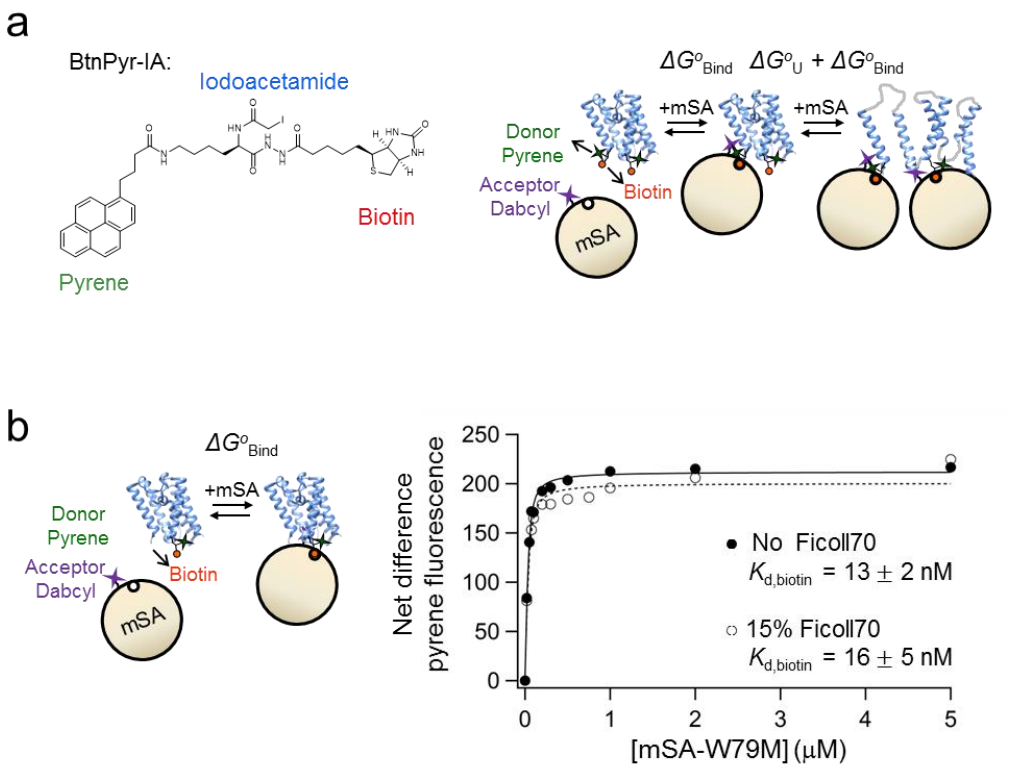

Figure 4.13 The macromolecular crowding agent Ficoll70 does not significantly affect the intrinsic binding affinity of monovalent streptavidin (mSA) to a single biotin label on GlpG-G172C. (a) Thiol-reactive biotin label possessing a fluorescent pyrene fluorophore. The pyrene fluorophore in the label serves as a FRET donor to detect binding of quencher labeled mSA. (b) The intrinsic binding affinity between a weaker biotin binding variant mSA-W79M and a single-biotin label on GlpG (75 nM) was measured at an increasing concentration of mSA-W79Q. The binding was monitored by FRET between fluorescent pyrene from the fluorescent biotin label (BtnPyr) and dabcyl quencher labeled near the biotin binding pocket of mSA. The resulting net difference pyrene fluorescence was obtained by subtracting the pyrene fluorescence intensity under binding equilibrium from that with added excess free biotin (2 mM) which induced complete dissociation of bound mSA.

Next, the degradation rates of GlpG-108 were measured as a function of ATP-hydrolysis rate in the presence of 15% Ficoll70 (**Figure 4.14a**). While the degradation rates overall decreased in the presence of Ficoll70, the threshold ATP hydrolysis and maximal degradation rates remained similar, and the degradation rate became less sensitive to the increase in ATP hydrolysis rate. As a result, the effective ATP cost increased by 40% relative to that without Ficoll70 (**Figure 4.14b**). Probably, the large increase in viscosity caused by Ficoll70 slowed down the dislocation of the unfolded substrate, making the ATP cost larger as shown for ClpXP.[65] Overall, the macromolecular crowding only had a mild impact on activities of FtsH.

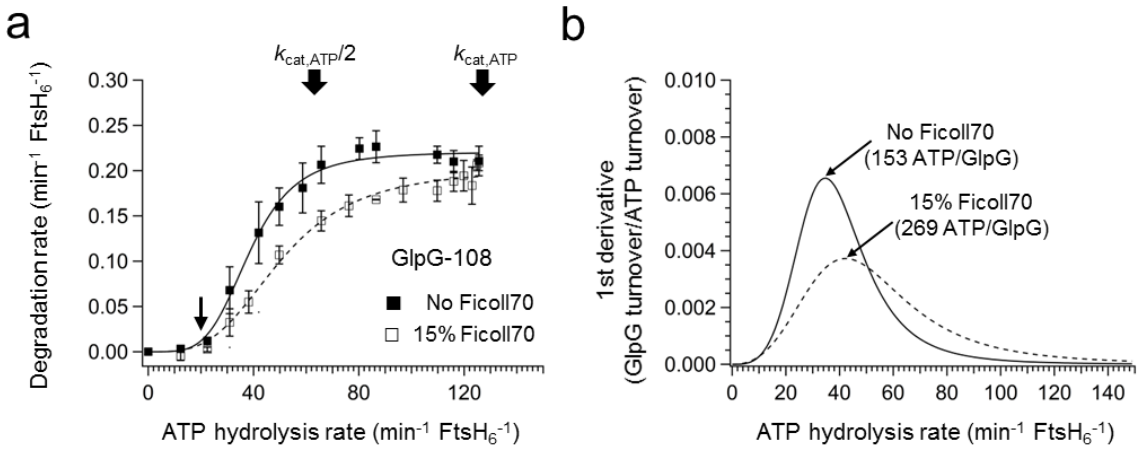

Figure 4.14 The effect of the macromolecular crowding agent Ficoll70 on the relationship between the degradation and ATP hydrolysis rates. (a) Degradation rates of GlpG-108 measured as a function of ATP hydrolysis rate in the presence of 15% Ficoll70. The data were compared with those in the absence of Ficoll70. Values are means ± SEM (N = 2). (b) The influence of Ficoll70 on the effective ATP cost (parentheses) obtained by taking the inverse of the first derivative of the plot in Figure 4.14 (a).

Discussion

The most striking finding of this study is that degradation rates by FtsH display nonlinear dependence on ATP hydrolysis rates. At least, ~20 ATP hydrolysis events need to be accumulated per minute for degradation to occur, but once exceeding the threshold, FtsH tightly couples ATP hydrolysis to degradation in a highly cooperative manner (n_H = 4–5). The degradation rates are saturated at remarkably low ATP hydrolysis rates, only 50–70% of the maximal ATP hydrolysis rates. It is surprising because in the cases of other relatively well-characterized AAA+ proteases such as *E. coli* ClpXP, *E. coli* HslUV, Lon, yeast 20S proteasomes and archaeal PAN, the rates of degradation and ATP hydrolysis are linearly correlated.[18,59-61,66] A notable exception is degradation of GFP by ClpXP, which requires ~20% of the maximal ATP hydrolysis rate to initiate degradation.[60] In that study, the existence of threshold has been attributed to a stable unfolding intermediate of GFP which is rapidly formed in-between low frequency bursts of ATP hydrolysis on ClpX.[28,60] However, after the ATP hydrolysis rate exceeds the threshold, the degradation rate of GFP keeps increasing until the ATP hydrolysis rate reaches a maximum. This is different from the unique cooperativity observed in FtsH-mediated degradation.

We also hypothesized that certain folding features of GlpG might have caused the appearance of the threshold. In comparison to water-soluble substrates, ATP-dependent degradation of membrane proteins poses a general thermodynamic challenge, i.e., dislocation of hydrophobic TM segments from the membrane to the proteolytic active sites located in the cytosol ($\Delta G_{dislocation}$ = 50–100 kcal/mol per TM),[20,57,58] as seen in the degradation by FtsH, the endoplasmic reticulum-associated degradation by the Hrd1 ubiquitin ligase complex/Cdc48 (an AAA+

enzyme)/26S proteasome system and dislocation of mislocalized tail-anchored membrane proteins by the membrane-anchored AAA+ enzyme Msp1 from the mitochondrial outer membranes.[43,67-69] The conformational stabilities of membrane proteins can also be substantial (ΔG^{o}_{U} = 3–12 kcal/mol).[52,70-73] However, we always observed the sigmoidal dependence with threshold regardless of substrate stability and membrane localization, indicating that the high degree of cooperativity among ATP hydrolysis events is an intrinsic feature of FtsH-mediated degradation. Probably, this cooperativity would be ideal for FtsH to efficiently overcome the large energetic cost of substrate unfolding and membrane dislocation.

Another interesting finding in this study is that while ATP hydrolysis on FtsH occurs independently ($n_H \approx 1$ for ATP hydrolysis rates *versus* ATP concentration), the independent events become cooperative in degrading substrates. Because the Hill coefficients in this process are 4–5, we can speculate that the cooperativity stems from the coordination of ATP hydrolysis throughout the subunits within the AAA+ hexamer ring of FtsH. Intringuingly, a recent cryo-electron microscopic (cryo-EM) study of FtsH orthologs, Yme1 of yeast, suggests a remarkable mechanism by which the Yme1 hexamer carries out substrate translocation by tightly coordinating ATP-bound, ADP-bound, and apo forms of the six AAA+ subunits with 4_{ATP}:1_{ADP}:1_{apo} stoichiometry.[9] However, the cryo-EM structures of substrate-bound 26S proteasomes that have a linear relationship between the degradation and ATP hydrolysis rates also show a similar number (4–6) of bound nucleotides 4_{ATP}:1_{ADP}:1_{apo}, 3_{ATP}:2_{ADP}:1_{apo} or 3_{ATP}:1_{ADP}:2_{apo}.[74] The structures of PAN proteasomes that have the linear relationship again suggest the coordination of five nucleotides' binding 4_{ATP}:1_{ADP}:1_{apo} on the PAN ATPase during substrate translocation.[75] These

results imply that the coordination of multiple nucleotides' binding itself may not explain the cooperativity between ATP hydrolysis events for degradation by FtsH. To better understand the mechanism, it is necessary to precisely determine the binding stoichiometry, affinity, and kinetics between FtsH and ATP or ADP as well as to track down the origin of cooperativity at each functional step during degradation.

Our study suggests that FtsH is a slow but highly efficient degradation machine for membrane proteins. The effective ATP costs for degrading GlpG (150–390 ATP, 0.6–1.9 ATP per residue) were only 40–70% of those measured at steady-state conditions (380–550 ATP, 1.8–2.6 ATP hydrolysis per residue).[20] Considering the reported range of ATP costs for various AAA+ proteases and substrates (0.2–6.6 ATP per residue),[13,17-21,27] the effective ATP costs by FtsH fall into the lower edge of the range. This finding demonstrates a remarkable ATP efficiency achieved by FtsH, which overcomes the large free energy costs to degrade membrane proteins. Our result reasonably agrees with recent single-molecule force spectroscopic studies showing that ClpXP spends 40~70% of the time working for unfolding and translocation with many futile ATP hydrolysis events over a wide range of dwell time (a few seconds–a hundred seconds) before inducing abrupt and cooperative substrate unfolding.[28,29]

What can we learn about membrane protein quality control in the cells from our *in vitro* studies? The macromolecular crowding agent Ficoll70 for mimicking the cellular environment has mild impacts on ATPase and degradation activities of FtsH. Therefore, it is likely that the features of FtsH discovered in this study will be maintained in the cells. The fact that the level of the saturated degradation rate

depends on the conformational stability suggests that the AAA+ ATPase of FtsH has a limited pulling power such that, as the ATP-hydrolysis rate increases, an equilibrium point is reached at which the resisting force (substrate stability, hydrophobicity and diffusive dissociation of substrates) and pulling force are balanced. This principle may explain the ability of FtsH as quality control machinery for membrane proteins, preferentially degrading misfolded, or intrinsically unstable membrane proteins.

We observed that, because of the high cooperativity, the maximal degradation rates by FtsH is reached at surprisingly low ATP concentrations (60–80 μM). For comparison, the degradation activity of ClpXP can be modulated in the range of 0–500 μM ATP because of the linearity between ATP hydrolysis and degradation rates.[22,60,76] Considering that ATP concentrations in a single *E. coli* cell vary from ~200 to ~5,000 μM under normal growth conditions,[77] ClpXP activity will respond sensitively to the changes in the availability of ATP. One clear example is the control of the cellular concentration of RspO (σ^s-factor) by ClpXP in *E. coli*. RspO is accumulated under nutrient-deprivation or in the stationary growth phase, inducing the transcription of various stress response genes.[1] Degradation of RspO by ClpXP is known to be directly controlled by the cellular level of ATP upon carbon starvation.[78] On the other hand, we expect that FtsH works at its full degradation capacity under broad stress conditions which compromise membrane protein quality and deplete the cellular levels of ATP.[79-81] This feature may also serve as a safety scheme at an elevated ATP level (*e.g.*, heat shock)[82] preventing excessive protein degradation in the cell membranes.

Methods

ATPase Activity Assay of FtsH.

ATP hydrolysis rate by FtsH was measured by an enzyme-coupled assay on a microplate reader (M5e, Molecular Devices) at 37°C. The assay solution contained 2 μM FtsH, 20 mM 4-(2-hydroxyethyl)-1-piperazineethanesulfonic acid (HEPES, pH 7.5), 10 mM $MgCl_2$, 400 μM $ZnCl_2$, 0.1% BME, 100 mM KCl, 15% glycerol, 0.5 mM NADH, 10 mM phosphoenolpyruvic acid, 0.5 units of pyruvate kinase and 0.5 units of lactic dehydrogenase. The oxidation of NADH coupled to ATP hydrolysis was monitored by $OD_{340\ nm}$.

Reconstitution of GlpG in Bicelles and Degradation Assay using NBD Fluorescence.

Degradation of NBD-labeled GlpG variants by FtsH was measured in 2% (w/v) negatively charged bicelles (DMPC/DMPG/CHAPS, q = 2.8). GlpG was first reconstituted in 3% (w/v) DMPC/DMPG liposomes ([DMPC]:[DMPG] = 3:1) in 20 mM HEPES (pH 7.6) 100 mM KCl, 15% glycerol, and 0.1% BME. The NBD-labeled GlpG stock in DM was mixed with the lipids solubilized with 4% *n*-octyl-β-D-glucoside to a final concentration of 50–100 μM and incubated on ice for 1 h. For removal of residual detergents, the mixture was dialyzed against 20 mM HEPES (pH 7.5), 100 mM KCl, and 0.1% BME at 4 °C overnight, followed by incubation with Bio-Beads (Bio-Rad) for 3 days at room temperature. The resulting proteoliposomes were extruded through a 0.2 μM pore size polycarbonate membrane (Waters) to remove aggregation. The total phospholipid concentration was determined by an organic phosphate assay. Based on the measured lipid concentration, the desired amount of CHAPS was added to form bicelles with q = 2.8. The final concentration of NBD-

labeled GlpG in bicelles was determined by 660 nm assay. Time-dependent degradation of GlpG was measured in 2% bicellar solution (20 mM HEPES, pH 7.5, 100 mM KCl, 15% glycerol, 0.1% BME, 5 mM $MgCl_2$ and 400 μM $ZnCl_2$) with an ATP regeneration system (0.5 unit/100 μL pyruvate kinase and 10 mM phosphoenolpyruvic acid). FtsH was incorporated into bicelles by direct injection of FtsH stock solution in Triton X-100 to preformed bicelles at a final monomer concentration of 2 μM on ice. A total volume of 100 μL of each sample was transferred to a 96-well UV-compatible microplate (Greiner Bio-One) and sealed with a polyolefin film. Degradation of GlpG was initiated by addition of ATP to each well and monitored by quenching of NBD fluorescence at 545 nm with an excitation wavelength of 485 nm on a plate reader. The change of NBD fluorescence induced by GlpG degradation was obtained by subtracting the time-dependent change of NBD fluorescence in the presence of ATP from that in the absence of ATP at each GlpG concentration. The degradation rate of GlpG by each FtsH hexamer per minute (v_{deg}) is defined as:

$$v_{\mathrm{deg}} = \frac{\frac{\Delta F}{\min}}{\frac{\Delta F_{\infty}}{[\mathrm{GlpG}]}} \times \frac{1}{[\mathrm{FtsH}_6]} \qquad \textbf{(Equation 3)},$$

where $\Delta F/\min$ and $\Delta F_{\infty}/[\mathrm{GlpG}]$ were obtained from the slopes from **Figure 4.2c and 4.2d**, respectively. For the assay of casein degradation, casein excessively labeled with Bodipy FL (Thermo Fisher Scientific) was used. Casein degradation was monitored by dequenching of Bodipy FL fluorescence at 525 nm ($\lambda_{emission}$ = 485 nm). The Hill equation to fit the degradation rate *vs.* ATP hydrolysis rate of FtsH is given as:

$$v_{Deg} = \frac{(\text{ATP-hydrolysis rate})^{n_H}}{K_{m,ATP}{}^{n_H} + (\text{ATP-hydrolysis rate})^{n_H}}$$ **(Equation 4)**,

where $n_{H,ATP}$ is Hill constant of FtsH hexamer ATPase activity.

Cloning, expression, and purification of E. coli Lon.

The gene of *lon* of *E. coli* strain K12 MG1655 was amplified by colony PCR with the primers containing *NheI* (5'-end) and *XhoI* (3'-end) restriction sites, and then inserted into the pET21a vector with a C-terminal His_6-tag. The Lon protein was expressed in *E. coli* C43 (DE3) pLysS cells. The cells transformed with the expression vector were cultivated in LB media (100 mg/L ampicillin) at 37°C until OD_{600nm} reached 0.6. Protein expression was induced with 0.2 mM IPTG, and the culture was further incubated at 24°C for an additional 16 h. Harvested cells were resuspended in resuspension buffer (20 mM HEPES pH 7.5, 400 mM NaCl, 100 mM KCl, 1mM TCEP). After cell lysis using C5 pressure homogenizer, the soluble fraction was obtained by ultracentrifugation (Beckman Coulter, Type 45 Ti rotor) at 18,000 rpm for 20 min. The supernatant containing Lon was purified using Ni^{2+}-NTA-affinity chromatography (Qiagen). The packed resin was washed with resuspension buffer containing 100 mM imidazole and eluted with 15 mL resuspension buffer containing 800 mM imidazole. Excess imidazole in the eluent was removed by dialysis against storage buffer (25mM HEPES pH7.5, 100mM KCl). Purified Lon was concentrated to the final concentration of 40–50 μM per liter culture (660 nm protein assay, Pierce). All purification procedures were carried out at 4°C.

Measuring thermodynamic stability of GlpG using steric trapping.

Detailed procedures of steric trapping have been previously reported.[52] Briefly, double-cysteine variant of GlpG (G172C/V267C) purified in DDM was labeled with the thiol-reactive biotin derivative possessing pyrene fluorophore, N-(5-(2-iodoacetamido)-6-oxo-6-(2-(+)-Biotin hydrazinyl)hexyl)-4-(pyren-1-yl)butanamide (BtnPyr-IA) to yield 172/267-$BtnPyr_2$.[52] Thermodynamic stability of GlpG in DDM micelles was determined by measuring the attenuated second binding of mSA labeled with dabcyl quencher (mSA_{DAB}) to 172/267-$BtnPyr_2$ at room temperature.[52] mSA_{DAB} binding was monitored by quenching of pyrene fluorescence from BtnPyr labels by Förster resonance energy transfer. 1 μM of $172/267_C$-$BtnPyr_2$ was titrated with a mSA_{DAB} variant possessing a reduced biotin binding affinity[52], mSA_{DAB}-S27A ($K_{d,biotin}$ = 1.4 ± 0.9 nM) in 20 mM DDM, 0.25 mM TCEP, 20 mM sodium phosphate and 200 mM NaCl (pH 7.5).[52] Quenching of pyrene-monomer fluorescence at 390 nm was monitored with an excitation wavelength of 345 nm on a plate reader. The attenuated second binding phase of a binding isotherm was fitted to the equation:

$$F = \frac{1}{[1+\left(K_{\mathrm{d,biotin}} + \frac{K_{\mathrm{d,biotin}}}{K_{\mathrm{U}}}\right)\frac{1}{[\mathrm{mSA}]}]}\left(F_{\infty} - F_{o}\right) + F_{o} \qquad \textbf{(Equation 5)},$$

where F is measured fluorescence intensity, and F_0 and F_∞ are the fluorescence intensities at [mSA] = 0 and at the saturated bound level, respectively. [mSA] is the total mSA concentration, $K_{d,\ biotin}$ is the dissociation constant for unhindered biotin binding affinity of mSA, and K_U is the equilibrium constant for unfolding of GlpG. After obtaining the fitted K_U, the thermodynamic stability was calculated using the equation $\Delta G^{o}_{U} = -RT\ln K_U$.

REFERENCES

REFERENCES

(1) Battesti, A., Majdalani, N., and Gottesman, S., The RpoS-mediated general stress response in Escherichia coli. *Annual Review of Microbiology* **2011,** *65*, 189-213.

(2) Gottesman, S., Proteases and their targets in Escherichia coli. *Annu Rev Genet* **1996,** *30*, 465-506.

(3) Mogk, A., Huber, D., and Bukau, B., Integrating protein homeostasis strategies in prokaryotes. *Cold Spring Harb Perspect Biol* **2011,** *3* (4).

(4) Wickner, S., Maurizi, M. R., and Gottesman, S., Posttranslational quality control: folding, refolding, and degrading proteins. *Science* **1999,** *286* (5446), 1888-1893.

(5) Gottesman, S., Wickner, S., and Maurizi, M. R., Protein quality control: triage by chaperones and proteases. *Genes Dev* **1997,** *11* (7), 815-823.

(6) Sauer, R. T. and Baker, T. A., AAA+ proteases: ATP-fueled machines of protein destruction. *Annu Rev Biochem* **2011,** *80*, 587-612.

(7) Vieux, E. F., Wohlever, M. L., Chen, J. Z., Sauer, R. T., and Baker, T. A., Distinct quaternary structures of the AAA plus Lon protease control substrate degradation. *Proceedings of the National Academy of Sciences of the United States of America* **2013,** *110* (22), E2002-E2008.

(8) Bieniossek, C., Niederhauser, B., and Baumann, U. M., The crystal structure of apo-FtsH reveals domain movements necessary for substrate unfolding and translocation. *Proc. Natl. Acad. Sci. USA* **2009,** *106* (51), 21579-21584.

(9) Puchades, C., Rampello, A. J., Shin, M., Giuliano, C. J., Wiseman, R. L., Glynn, S. E., and Lander, G. C., Structure of the mitochondrial inner membrane AAA plus protease YME1 gives insight into substrate processing. *Science* **2017,** *358* (6363), 609-+.

(10) Lee, S., Augustin, S., Tatsuta, T., Gerdes, F., Langer, T., and Tsai, F. T., Electron cryomicroscopy structure of a membrane-anchored mitochondrial AAA protease. *J Biol Chem* **2011,** *286* (6), 4404-4411.

(11) Suno, R., Niwa, H., Tsuchiya, D., Zhang, X. D., Yoshida, M., and Morikawa, K., Structure of the whole cytosolic region of ATP-dependent protease FtsH. *Molecular Cell* **2006,** *22* (5), 575-585.

(12) Gottesman, S., Roche, E., Zhou, Y., and Sauer, R. T., The ClpXP and ClpAP proteases degrade proteins with carboxy-terminal peptide tails added by the SsrA-tagging system. *Genes Dev* **1998,** *12* (9), 1338-1347.

(13) Gur, E. and Sauer, R. T., Recognition of misfolded proteins by Lon, a AAA(+) protease. *Genes Dev* **2008,** *22* (16), 2267-2277.

(14) Chiba, S., Akiyama, Y., and Ito, K., Membrane protein degradation by FtsH can be initiated from either end. *J Bacteriol* **2002,** *184* (17), 4775-4782.

(15) Chiba, S., Akiyama, Y., Mori, H., Matsuo, E., and Ito, K., Length recognition at the N-terminal tail for the initiation of FtsH-mediated proteolysis. *EMBO Rep* **2000,** *1* (1), 47-52.

(16) Olivares, A. O., Baker, T. A., and Sauer, R. T., Mechanical Protein Unfolding and Degradation. *Annu Rev Physiol* **2018,** *80*, 413-429.

(17) Benaroudj, N., Zwickl, P., Seemuller, E., Baumeister, W., and Goldberg, A. L., ATP hydrolysis by the proteasome regulatory complex PAN serves multiple functions in protein degradation. *Mol Cell* **2003,** *11* (1), 69-78.

(18) Peth, A., Nathan, J. A., and Goldberg, A. L., The ATP costs and time required to degrade ubiquitinated proteins by the 26 S proteasome. *J Biol Chem* **2013,** *288* (40), 29215-29222.

(19) Kenniston, J. A., Baker, T. A., Fernandez, J. M., and Sauer, R. T., Linkage between ATP consumption and mechanical unfolding during the protein processing reactions of an AAA(+) degradation machine. *Cell* **2003,** *114* (4), 511-520.

(20) Yang, Y., Guo, R., Gaffney, K., Kim, M., Muhammednazaar, S., Tian, W., Wang, B., Liang, J., and Hong, H., Folding-Degradation Relationship of a Membrane Protein Mediated by the Universally Conserved ATP-Dependent Protease FtsH. *J Am Chem Soc* **2018,** *140* (13), 4656-4665.

(21) Wohlever, M. L., Nager, A. R., Baker, T. A., and Sauer, R. T., Engineering fluorescent protein substrates for the AAA+ Lon protease. *Protein Eng Des Sel* **2013,** *26* (4), 299-305.

(22) Koodathingal, P., Jaffe, N. E., Kraut, D. A., Prakash, S., Fishbain, S., Herman, C., and Matouschek, A., ATP-dependent proteases differ substantially in their ability to unfold globular proteins. *J Biol Chem* **2009,** *284* (28), 18674-18684.

(23) Kim, Y. I., Burton, R. E., Burton, B. M., Sauer, R. T., and Baker, T. A., Dynamics of substrate denaturation and translocation by the ClpXP degradation machine. *Mol Cell* **2000,** *5* (4), 639-648.

(24) Lee, C., Schwartz, M. P., Prakash, S., Iwakura, M., and Matouschek, A., ATP-dependent proteases degrade their substrates by processively unraveling them from the degradation signal. *Mol Cell* **2001,** *7* (3), 627-637.

(25) Yakamavich, J. A., Baker, T. A., and Sauer, R. T., Asymmetric nucleotide transactions of the HslUV protease. *J Mol Biol* **2008,** *380* (5), 946-957.

(26) Herman, C., Prakash, S., Lu, C. Z., Matouschek, A., and Gross, C. A., Lack of a robust unfoldase activity confers a unique level of substrate specificity to the universal AAA protease FtsH. *Mol Cell* **2003,** *11* (3), 659-669.

(27) Okuno, T., Yamada-Inagawa, T., Karata, K., Yamanaka, K., and Ogura, T., Spectrometric analysis of degradation of a physiological substrate sigma32 by Escherichia coli AAA protease FtsH. *J Struct Biol* **2004,** *146* (1-2), 148-154.

(28) Maillard, R. A., Chistol, G., Sen, M., Righini, M., Tan, J., Kaiser, C. M., Hodges, C., Martin, A., and Bustamante, C., ClpX(P) generates mechanical force to unfold and translocate its protein substrates. *Cell* **2011,** *145* (3), 459-469.

(29) Aubin-Tam, M. E., Olivares, A. O., Sauer, R. T., Baker, T. A., and Lang, M. J., Single-molecule protein unfolding and translocation by an ATP-fueled proteolytic machine. *Cell* **2011,** *145* (2), 257-267.

(30) Langer, T., AAA proteases: cellular machines for degrading membrane proteins. *Trends Biochem Sci* **2000,** *25* (5), 247-251.

(31) Ito, K. and Akiyama, Y., Cellular functions, mechanism of action, and regulation of FtsH protease. *Annu Rev Microbiol* **2005,** *59*, 211-231.

(32) Akiyama, Y., Kihara, A., Tokuda, H., and Ito, K., FtsH (HflB) is an ATP-dependent protease selectively acting on SecY and some other membrane proteins. *J. Biol. Chem.* **1996,** *271* (49), 31196-31201.

(33) Hari, S. B. and Sauer, R. T., The AAA plus FtsH Protease Degrades an ssrA-Tagged Model Protein in the Inner Membrane of Escherichia coli. *Biochemistry* **2016,** *55* (40), 5649-5652.

(34) Jarvi, S., Suorsa, M., Tadini, L., Ivanauskaite, A., Rantala, S., Allahverdiyeva, Y., Leister, D., and Aro, E. M., Thylakoid-Bound FtsH Proteins Facilitate Proper Biosynthesis of Photosystem I. *Plant Physiol* **2016,** *171* (2), 1333-1343.

(35) Krynicka, V., Shao, S., Nixon, P. J., and Komenda, J., Accessibility controls selective degradation of photosystem II subunits by FtsH protease. *Nat Plants* **2015,** *1*, 15168.

(36) Ostersetzer, O. and Adam, Z., Light-stimulated degradation of an unassembled Rieske FeS protein by a thylakoid-bound protease: the possible role of the FtsH protease. *Plant Cell* **1997,** *9* (6), 957-965.

(37) Arlt, H., Steglich, G., Perryman, R., Guiard, B., Neupert, W., and Langer, T., The formation of respiratory chain complexes in mitochondria is under the proteolytic control of the m-AAA protease. *EMBO J.* **1998,** *17* (16), 4837-4847.

(38) Leonhard, K., Stiegler, A., Neupert, W., and Langer, T., Chaperone-like activity of the AAA domain of the yeast Yme1 AAA protease. *Nature* **1999,** *398* (6725), 348-351.

(39) Nolden, M., Ehses, S., Koppen, M., Bernacchia, A., Rugarli, E. I., and Langer, T., The m-AAA protease defective in hereditary spastic paraplegia controls ribosome assembly in mitochondria. *Cell* **2005,** *123* (2), 277-289.

(40) Janska, H., Kwasniak, M., and Szczepanowska, J., Protein quality control in organelles - AAA/FtsH story. *Biochim Biophys Acta* **2013,** *1833* (2), 381-387.

(41) Janska, H., Piechota, J., and Kwasniak, M., ATP-dependent proteases in biogenesis and maintenance of plant mitochondria. *Biochim Biophys Acta* **2010,** *1797* (6-7), 1071-1075.

(42) Langer, T., Kaser, M., Klanner, C., and Leonhard, K., AAA proteases of mitochondria: quality control of membrane proteins and regulatory functions during mitochondrial biogenesis. *Biochem Soc Trans* **2001,** *29* (Pt 4), 431-436.

(43) Leonhard, K., Guiard, B., Pellecchia, G., Tzagoloff, A., Neupert, W., and Langer, T., Membrane protein degradation by AAA proteases in mitochondria: extraction of substrates from either membrane surface. *Mol Cell* **2000,** *5* (4), 629-638.

(44) Leonhard, K., Herrmann, J. M., Stuart, R. A., Mannhaupt, G., Neupert, W., and Langer, T., AAA proteases with catalytic sites on opposite membrane surfaces comprise a proteolytic system for the ATP-dependent degradation of inner membrane proteins in mitochondria. *EMBO J* **1996,** *15* (16), 4218-4229.

(45) Cordova, J. C., Olivares, A. O., Shin, Y., Stinson, B. M., Calmat, S., Schmitz, K. R., Aubin-Tam, M. E., Baker, T. A., Lang, M. J., and Sauer, R. T., Stochastic but highly coordinated protein unfolding and translocation by the ClpXP proteolytic machine. *Cell* **2014,** *158* (3), 647-658.

(46) Rivas, G. and Minton, A. P., Macromolecular Crowding *In Vitro*, *In Vivo*, and In Between. *Trends in Biochemical Sciences* **2016,** *41* (11), 970-981.

(47) Herman, C., Thevenet, D., Bouloc, P., Walker, G. C., and D'Ari, R., Degradation of carboxy-terminal-tagged cytoplasmic proteins by the Escherichia coli protease HflB (FtsH). *Genes Dev* **1998,** *12* (9), 1348-1355.

(48) Okuno, T., Yamanaka, K., and Ogura, T., An AAA protease FtsH can initiate proteolysis from internal sites of a model substrate, apo-flavodoxin. *Genes to Cells* **2006,** *11* (3), 261-268.

(49) Wang, Y., Zhang, Y., and Ha, Y., Crystal structure of a rhomboid family intramembrane protease. *Nature* **2006,** *444* (7116), 179-180.

(50) Parsell, D. A., Silber, K. R., and Sauer, R. T., Carboxy-terminal determinants of intracellular protein degradation. *Genes Dev* **1990,** *4* (2), 277-286.

(51) Kihara, A., Akiyama, Y., and Ito, K., Different pathways for protein degradation by the FtsH/HflKC membrane-embedded protease complex: an implication from the interference by a mutant form of a new substrate protein, YccA. *J Mol Biol* **1998,** *279* (1), 175-188.

(52) Guo, R., Gaffney, K., Yang, Z., Kim, M., Sungsuwan, S., Huang, X., Hubbell, W. L., and Hong, H., Steric trapping reveals a cooperativity network in the intramembrane protease GlpG. *Nat Chem Biol* **2016,** *12* (5), 353-360.

(53) Min, D., Jefferson, R. E., Bowie, J. U., and Yoon, T. Y., Mapping the energy landscape for second-stage folding of a single membrane protein. *Nat Chem Biol* **2015,** *11* (12), 981-987.

(54) Paslawski, W., Lillelund, O. K., Kristensen, J. V., Schafer, N. P., Baker, R. P., Urban, S., and Otzen, D. E., Cooperative folding of a polytopic alpha-helical membrane protein involves a compact N-terminal nucleus and nonnative loops. *Proc Natl Acad Sci USA* **2015,** *112* (26), 7978-7983.

(55) Baker, R. P. and Urban, S., Architectural and thermodynamic principles underlying intramembrane protease function. *Nat. Chem. Biol.* **2012,** *8* (9), 759-768.

(56) Lu, W., Schafer, N. P., and Wolynes, P. G., Energy landscape underlying spontaneous insertion and folding of an alpha-helical transmembrane protein into a bilayer. *Nature Communications* **2018,** *9*.

(57) Cymer, F., von Heijne, G., and White, S. H., Mechanisms of integral membrane protein insertion and folding. *J Mol Biol* **2015,** *427* (5), 999-1022.

(58) Preiner, J., Janovjak, H., Rankl, C., Knaus, H., Cisneros, D. A., Kedrov, A., Kienberger, F., Muller, D. J., and Hinterdorfer, P., Free energy of membrane protein unfolding derived from single-molecule force measurements. *Biophys J* **2007,** *93* (3), 930-937.

(59) Waxman, L. and Goldberg, A. L., Protease La from Escherichia-Coli Hydrolyzes Atp and Proteins in a Linked Fashion. *Proceedings of the National Academy of Sciences of the United States of America-Biological Sciences* **1982,** *79* (16), 4883-4887.

(60) Martin, A., Baker, T. A., and Sauer, R. T., Protein unfolding by a AAA+ protease is dependent on ATP-hydrolysis rates and substrate energy landscapes. *Nat Struct Mol Biol* **2008,** *15* (2), 139-145.

(61) Baytshtok, V., Chen, J. J., Glynn, S. E., Nager, A. R., Grant, R. A., Baker, T. A., and Sauer, R. T., Covalently linked HslU hexamers support a probabilistic mechanism that links ATP hydrolysis to protein unfolding and translocation. *Journal of Biological Chemistry* **2017,** *292* (14), 5695-5704.

(62) Armstrong, J. K., Wenby, R. B., Meiselman, H. J., and Fisher, T. C., The hydrodynamic radii of macromolecules and their effect on red blood cell aggregation. *Biophysical Journal* **2004,** *87* (6), 4259-4270.

(63) Minton, A. P., Models for excluded volume interaction between an unfolded protein and rigid macromolecular cosolutes: Macromolecular crowding and protein stability revisited. *Biophysical Journal* **2005,** *88* (2), 971-985.

(64) Kuznetsova, I. M., Turoverov, K. K., and Uversky, V. N., What Macromolecular Crowding Can Do to a Protein. *International Journal of Molecular Sciences* **2014,** *15* (12), 23090-23140.

(65) Shi, X. Y., Wu, T., Cole, C. M., Devaraj, N. K., and Joseph, S., Optimization of ClpXP activity and protein synthesis in an E-coli extract-based cell-free expression system. *Scientific Reports* **2018,** *8*.

(66) Benaroudj, N. and Goldberg, A. L., PAN, the proteasome-activating nucleotidase from archaebacteria, is a protein-unfolding molecular chaperone. *Nat Cell Biol* **2000,** *2* (11), 833-839.

(67) Carvalho, P., Goder, V., and Rapoport, T. A., Distinct ubiquitin-ligase complexes define convergent pathways for the degradation of ER proteins. *Cell* **2006,** *126* (2), 361-373.

(68) Kihara, A., Akiyama, Y., and Ito, K., Dislocation of membrane proteins in FtsH-mediated proteolysis. *EMBO J* **1999,** *18* (11), 2970-2981.

(69) Wohlever, M. L., Mateja, A., McGilvray, P. T., Day, K. J., and Keenan, R. J., Msp1 Is a Membrane Protein Dislocase for Tail-Anchored Proteins. *Molecular Cell* **2017,** *67* (2), 194-+.

(70) Sanders, M. R., Findlay, H. E., and Booth, P. J., Lipid bilayer composition modulates the unfolding free energy of a knotted alpha-helical membrane protein. *Proc Natl Acad Sci U S A* **2018,** *115* (8), E1799-E1808.

(71) Chang, Y. C. and Bowie, J. U., Measuring membrane protein stability under native conditions. *Proc Natl Acad Sci U S A* **2014,** *111* (1), 219-224.

(72) Findlay, H. E., Rutherford, N. G., Henderson, P. J., and Booth, P. J., Unfolding free energy of a two-domain transmembrane sugar transport protein. *Proc Natl Acad Sci U S A* **2010,** *107* (43), 18451-18456.

(73) Harris, N. J., Findlay, H. E., Simms, J., Liu, X., and Booth, P. J., Relative domain folding and stability of a membrane transport protein. *J Mol Biol* **2014,** *426* (8), 1812-1825.

(74) Dong, Y. C., Zhang, S. W., Wu, Z. L., Li, X. M., Wang, W. L., Zhu, Y. A., Stoilova-McPhie, S., Lu, Y., Finley, D., and Mao, Y. D., Cryo-EM structures and dynamics of substrate-engaged human 26S proteasome. *Nature* **2019,** *565* (7737), 49-+.

(75) Majumder, P., Rudack, T., Beck, F., Danev, R., Pfeifer, G., Nagy, I., and Baumeister, W., Cryo-EM structures of the archaeal PAN-proteasome reveal an around-the-ring ATPase cycle. *Proceedings of the National Academy of Sciences of the United States of America* **2019,** *116* (2), 534-539.

(76) Hersch, G. L., Burton, R. E., Bolon, D. N., Baker, T. A., and Sauer, R. T., Asymmetric interactions of ATP with the AAA+ ClpX6 unfoldase: allosteric control of a protein machine. *Cell* **2005,** *121* (7), 1017-1027.

(77) Yaginuma, H., Kawai, S., Tabata, K. V., Tomiyama, K., Kakizuka, A., Komatsuzaki, T., Noji, H., and Imamura, H., Diversity in ATP concentrations in a single bacterial cell population revealed by quantitative single-cell imaging. *Sci Rep* **2014,** *4*, 6522.

(78) Peterson, C. N., Levchenko, I., Rabinowitz, J. D., Baker, T. A., and Silhavy, T. J., RpoS proteolysis is controlled directly by ATP levels in Escherichia coli. *Genes Dev* **2012,** *26* (6), 548-553.

(79) Linkerhagner, K. and Oelze, J., Cellular Atp Levels and Nitrogenase Switchoff Upon Oxygen Stress in Chemostat Cultures of Azotobacter-Vinelandii. *Journal of Bacteriology* **1995,** *177* (18), 5289-5293.

(80) Picard, M., McEwen, B. S., Epel, E. S., and Sandi, C., An energetic view of stress: Focus on mitochondria. *Frontiers in Neuroendocrinology* **2018,** *49*, 72-85.

(81) Tiwari, B. S., Belenghi, B., and Levine, A., Oxidative stress increased respiration and generation of reactive oxygen species, resulting in ATP depletion, opening of mitochondrial permeability transition, and programmed cell death. *Plant Physiology* **2002,** *128* (4), 1271-1281.

(82) Soini, J., Falschlehner, C., Mayer, C., Bohm, D., Weinel, S., Panula, J., Vasala, A., and Neubauer, P., Transient increase of ATP as a response to temperature up-shift in Escherichia coli. *Microbial Cell Factories* **2005,** *4*.

Chapter 5 Concluding remarks and future outlook

In my dissertation work, I addressed several key questions regarding the molecular mechanisms of MP degradation mediated by the membrane-integrated AAA+ protease FtsH.

In chapter 2, to study the degradation of MPs in a lipid bilayer environment, I successfully reconstituted the FtsH-mediated MP degradation for creating a model system to study this process quantitatively. The fluorophore-labeled stable helical membrane protein GlpG was tagged with known degradation markers, and then the degradation kinetics was precisely measured in real-time by monitoring the fluorescence change in the presence of an ATP regeneration system. The result was the first quantitative report on MP degradation, which led to the determination of the folding-degradation relationship of the MP.

In chapter 3, to further study the quantitative relationship between the folding and degradation relationship, the system created in chapter 2 and the steric trapping strategy developed by Hong's lab were employed. I discovered that FtsH has a substantial ability to actively unfold MP substrates, challenging the long-standing paradigm that FtsH cannot actively unfold a substrate due to its low unfoldase activity. The ATP cost and degradation rate of GlpG were similar to well-studied water-soluble proteins by the known robust AAA+ proteases such as ClpXP and ClpAP, highlighting the efficiency of FtsH in both unfolding and extracting its substrates from the membrane. The degradation of a single copy of GlpG was also quantified as the hydrolysis of 380-550 ATP molecules by FtsH. The stability and hydrophobicity of membrane proteins were also identified as the key factors that determine the degradation rate. These insights would provide general insights into

the MP degradation mediated by ATP-dependent proteolysis, which is a major process in ERAD in eukaryotic cells.

In chapter 4, I investigated how FtsH utilizes ATP hydrolysis to degrade MPs. I found a surprising result that FtsH has a unique nonlinear dependence between degradation rates and ATP hydrolysis rates. The nonlinearity is represented by a sigmoidal dependence between the two rates. The Hill analysis then explained this nonlinearity, which stems from the coupling of multiple ATP hydrolysis events. This behavior of FtsH is unique from other water-soluble AAA+ proteases such as ClpXP, HslUV, Lon, and proteasomes, which displays linear relationships between degradation rates and ATP hydrolysis rates. This nonlinearity further revealed that only 40-60% total ATP was consumed compared to the ATP consumption measured at maximal ATP hydrolysis rates determined in Chapter 3.

The knowledge obtained from this study including the degradation activity, the folding-degradation relationship and the ATP efficiency may be used to model the quality control network of MPs in the *E. coli* inner membranes, as done for the water-soluble proteins in the *E. coli* cytosol by the Gierash group in 2012. Also, the physical principles of MP degradation obtained from this study may be extended to the ATP-dependent degradation in ERAD, which is a major protein degradation pathway in eukaryotic cells. In ERAD, misfolded MPs are recognized by the ubiquitin ligase complexes in the ER membrane, dislocated by a membrane associated AAA+ enzyme, and finally targeted to the proteasome in the cytosol, which has a similar logic to FtsH-mediated degradation.

This study yields numerous novel problems that are awaiting to be solved. First, what is the rate-determining step in the degradation of MPs? Is it substrate unfolding or membrane dislocation? Which step requires more ATP hydrolysis? Second, how different types of AAA+ proteases compete for degrading MPs in the inner membranes of *E. coli* cells? Does the membrane-integrated FtsH have any advantages in recognizing MP substrates because of the colocalization effect? Third, is FtsH itself enough for the quality control of MPs, or does it work together with other ATP-independent proteases or molecular chaperones? Fourth, how many pulling events by AAA+ subunits are required to induce a single unfolding event? Does the unfolding occur in a single step or involve multiple steps? How many residues are pulled from the membrane at each event of ATP hydrolysis? These have been challenging questions to approach so far. The degradation system that has been developed in this study will serve as a useful platform to address these questions in the future.